

AN ABSTRACT OF THE THESIS OF

Cynthia T. McMurray for the degree of Doctor of Philosophy in
Biochemistry and Biophysics presented on April 30, 1987.

Title: THE BINDING OF ETHIDIUM BROMIDE TO CHROMATIN: MODEL FOR

CARCINOGEN INTERACTIONS

Redacted for privacy

Abstract approved: _____

Dr. K.E. van Holde

Five forms of chromatin, which represent the in vivo folded forms of nucleic acid, were isolated and used as the binding substrate for model intercalating compound, ethidium bromide. For all forms of chromatin, the affinity, location and structural effects of binding were examined. On the level of the nucleosome, the binding of ethidium caused a step-wise dissociation of nucleoprotein complex resulting in the initial release of one copy each of H2A and H2B before complete dissociation to free DNA. Dissociation was induced by the intercalation mode of ethidium binding, and was not due to electrostatic interactions or alternate binding modes. The binding of ethidium resulted in no major particle unfolding event prior to step-wise dissociation. Initial ethidium binding to the core particle occurred only at the end 25 bp of the core particle DNA, and occurred with very low affinity. Ethidium binding to the 11 nm fiber comprising polynucleosomes, free from H1 and non-histone chromosomal proteins, was characterized by high affinity, very similar to free

DNA. The initial binding events were localized within the linker DNA in preference to the folded nucleosomal DNA. In contrast, ethidium binding to the long chromatin form containing H1, the extended 30 nm fiber, displayed a 10-fold lower affinity than either free DNA or the 11 nm fiber. More extensive folding of the 30 nm fiber to its condensed form, induced by the addition of monocations, resulted in a 30-fold decrease in binding affinity of ethidium relative to free DNA. In conclusion, the structure of the chromatin has a large effect on the binding of intercalating compounds. Generally, intercalation into DNA does occur, but the placement of dye molecules appears to be governed by the accessibility of the DNA at the expense of bound histone proteins. The in vitro data were used to construct a model for the interaction of mutagens and carcinogens in vivo and to gain structural information about the native nucleoprotein complexes.

The Binding of Ethidium Bromide to Chromatin:
Model for Carcinogen Interactions

by

Cynthia T. McMurray

A THESIS

submitted to

Oregon State University

in partial fulfillment of
the requirements for the
degree of

Doctor of Philosophy

Completed April 30, 1987

Commencement June 1987

APPROVED:

Redacted for privacy

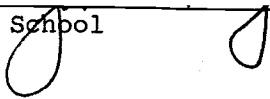
Professor of Biochemistry and Biophysics in charge of major

Redacted for privacy

Chairman of Department of Biochemistry and Biophysics

Redacted for privacy

Dean of Graduate School



Date thesis is presented April 30, 1987

Typed by Barbara Hanson for Cynthia T. McMurray

TABLE OF CONTENTS

	<u>Page</u>
INTRODUCTION	1
I. Aims	1
II. Background	2
III. Materials and Methods	12
A. Isolation of Purified Core Particles	12
1. Purification of Nuclei	12
2. Purification of Chromatin	14
B. Preparation of Nucleosomal-Sized DNA	19
1. Calf-Thymus DNA	19
2. Chicken Erythrocyte DNA	19
C. ^{31}P -NMR Studies	19
D. ^1H Nuclear Magnetic Resonance	20
E. Sedimentation Velocity	21
F. Circular Dichroism	22
G. Electron Microscopy	22
H. Thermal Melting	23
I. Electrophoresis	24
1. Type I: Native Core Particle Gels	24
2. Type II: Single-Stranded Gels	24
3. Type III: Laemmli Protein Gels; Coomassie-Stained	25
4. Type IV: Laemmli Gel; Silver Stain	25
5. 2-D Gel Electrophoresis	26
6. Low Ionic Strength Gel Electrophoresis	26
J. 5' End Labeling	27
K. Fluorescence Intensity Measurements (Steady-State)	28
L. Fluorescence Lifetime Measurements	29
M. Sucrose Gradient Centrifugation	31
N. Equilibrium Dialysis	32
O. UV-Visible-Absorbance Spectrophotometric Measurements	33
P. Photoaffinity Labeling of Core Particles and Histones with ^3H -8-Azido Ethidium Bromide	35
Q. Methidiumpropyl-EDTA-Fe(II) (MPE) Footprinting	37
R. Diffusion Coefficient Measurements by Dynamic Laser Light Scattering	38

	<u>Page</u>
CHAPTER I. CHARACTERIZATION OF A HOMOGENEOUS CORE PARTICLE PREPARATION ISOLATED FROM CHICKEN ERYTHROCYTES	58
Abstract	59
Introduction	60
Results	63
I. Electrophoresis	63
II. Circular Dichroism, Thermal Melting and ^{31}P -NMR of Core Particle Preparation	66
CHAPTER II. THE BINDING OF ETHIDIUM BROMIDE CAUSES DISSOCIATION OF THE NUCLEOSOME CORE PARTICLE	85
Abstract	86
Introduction	87
Results	90
I. Integrity of the Core Particle	90
II. The Binding of Ethidium Bromide to the Nucleosome Core Particle Results in Dissociation	91
III. Quantification of Dissociation	96
Discussion	100
CHAPTER III. A GEL ELECTROPHORETIC METHOD FOR QUANTIFYING MULTI-COMPONENT EQUILIBRIA	116
Abstract	117
Introduction	118
Results	121
I. Selection of a Gel System	121
II. Calibration of DNA Standards and Quantification of Amount the Dissociated DNA	123
III. Controls	125
Application	129
Discussion	133
CHAPTER IV. THE BINDING OF ETHIDIUM BROMIDE TO THE NUCLEOSOME CORE PARTICLE: INTERNAL AND EXTERNAL BINDING	157
Abstract	158
Introduction	159
Results	164
I. Binding to Protein	164
II. Binding to DNA	165
Discussion	177

	<u>Page</u>
CHAPTER V. THE BINDING OF ETHIDIUM TO THE NUCLEOSOME CORE PARTICLE: THE BINDING REACTION	197
Abstract	198
Introduction	199
Results	201
I. Binding Properties of Ethidium to Free DNA and to the Core Particle at Low Ionic Strength	201
II. Determination of f	212
III. The Temperature and Ionic Strength Dependence of Ethidium Binding to the Core Particle	213
IV. Conformational Changes: Unfolding Versus Step-Wise Dissociation	216
Discussion	226
CHAPTER VI. THE BINDING OF ETHIDIUM BROMIDE TO THE NUCLEOSOME CORE PARTICLE: THE DISSOCIATION REACTION	281
Abstract	282
Introduction	283
Results	285
I. Characterization of Dissociation	285
II. Temperature and Ionic Strength Dependence of Dissociation	287
Discussion	302
CHAPTER VII. HIGHER ORDER STRUCTURE AND CONCLUSION	340
Abstract	341
Introduction	342
Results	346
I. The Number of Base Pairs Protected by H1 and H5	346
II. Binding Studies	347
Discussion	352
Conclusion	354
BIBLIOGRAPHY	379

LIST OF FIGURES

	<u>Page</u>
Introduction	
Figure i.1	42
	Illustration of the complex of ethidium with dCpG.
Figure i.2	44
	Schematic illustration of the many orders of chromatin packaging.
Figure i.3	46
	Model for the nucleosomal organization of DNA in chromatin.
Figure i.4	48
	The flow chart of core particle preparation.
Figure i.5	50
	Results of the CM-sephadex removal of H1 and H5 and non-histone proteins from whole chicken erythrocyte chromatin.
Figure i.6	52
	Results of the polyacrylamide gel electrophoretic analysis of a representative test digestion for long monomer production.
Figure i.7	54
	Electron micrograph of the chicken erythrocyte core particle preparation.
Figure i.8	56
	Results of the polyacrylamide gel electrophoretic analysis of the trimming digestion to produce homogeneous core particles.
Chapter I	
Figure I.1	71
	Results of gel electrophoretic analysis for the nucleosome core particles and DNA isolated from the core particles.
Figure I.2	73
	Electron micrograph of the chicken erythrocyte core particle preparation.
Figure I.3	75
	Quantitation of double stranded internal cutting in particle preparation.

		<u>Page</u>
Figure I.4	Coomassie-stained SDS-15%-polyacrylamide gel electrophoretic analysis of the protein components of the core particle preparation and whole chicken erythrocyte chromatin.	77
Figure I.5	Silver stained SDS-15% polyacrylamide gel electrophoretic analysis of the protein components of the core particle preparation and whole chicken erythrocyte chromatin.	79
Figure I.6	U.V. and C.D. thermal melting profiles for chicken erythrocyte DNA and core particles.	81
Figure I.7	The proton-decoupled 101.2 MHz ^{31}P -NMR spectra at 30°C for the chicken erythrocyte core particle and ~200 BP calf thymus DNA.	83
Chapter II		
Figure II.1	Results of the gel electrophoretic component analysis for the nucleosome core particles and the corresponding DNA.	104
Figure II.2	Results of the polyacrylamide gel electrophoretic analysis of the core particle/ethidium bromide complexes over a range of input ratios.	106
Figure II.3	Time-dependence of the step-wise dissociation of the core particle by ethidium bromide at 30°C.	108
Figure II.4	Results of the two-dimensional gel electrophoretic analysis of the core particle/ethidium bromide complex at an input ratio of R=0.3.	110
Figure II.5	Results of the linear 5-20% sucrose gradient centrifugation of the ethidium bromide complexes with the nucleosome core particle and free DNA.	112
Figure II.6	Plot of % dissociation versus <u>bound</u> ratio for several core particle/ethidium bromide complexes.	114

Chapter III

Figure III.1	Results of the polyacrylamide gel electrophoretic analysis of the core particle complexes with ethidium bromide and bromophenol blue.	143
Figure III.2	Calibration of the linear intensity range of the DNA standards and film exposure time for the gel quantification method.	145
Figure III.3	Illustration of the quantitative gel electrophoretic method.	147
Figure III.4	The DNA concentration dependence of the ethidium-induced dissociation of the core particle.	149
Figure III.5	The sample volume dependence of dissociation for the intact core particle and a core particle/ethidium complex at $R = 0.3$ on native low cross-linking ratio polyacrylamide gels.	151
Figure III.6	Plot of % dissociation of the core particle versus the input ratio of ethidium bromide.	153
Figure III.7	Plot of % dissociation versus bound ratio of ethidium.	155

Chapter IV

Figure IV.1	Polyacrylamide gel electrophoretic analysis of the products of the ethidium-induced dissociation of the nucleosome core particle separated on sucrose gradients.	187
Figure IV.2	The plot of the number of ^3H -azido-ethidium bromide molecules covalently bound per core particle versus log input ratio.	189
Figure IV.3	The absorbance spectra of ethidium complexed with chicken erythrocyte free DNA, the core particle and polyvinylsulfate at $T = 23^\circ\text{C}$.	191
Figure IV.4	The plot of fluorescence intensity versus input ratio for complexes of ethidium bromide with chicken erythrocyte core particles and the corresponding free DNA in 10 mM Tris, pH 8.0, 0.1 mM EDTA at 20°C .	193

		<u>Page</u>
Figure IV.5	Examples of the measured scatter profile and of the fluorescence decay of ethidium complexes with core particle length DNA.	195
Chapter V		
Figure V.1	The Scatchard plot for the binding of ethidium bromide to the chicken erythrocyte core particle at 30°C.	241
Figure V.2A	Schematic representation of the method used to determine v_{core} .	243
Figure V.2B	The plot of % dissociation versus v_{core} .	245
Figure V.3	The corrected Scatchard plot for the binding of ethidium to the nucleosome core particle at 30°C.	247
Figure V.4A	The Scatchard plot for the binding of ethidium to the core particle and to free DNA at 30°C.	249
Figure V.4B	The plot of the free energy difference between the binding ethidium to free DNA and to the core particle at 30°C.	251
Figure V.5	Schematic design of the experimental procedure for determination of the location of ethidium binding sites on the nucleosome core particle.	253
Figure V.6	The results of the MPE cleavage reaction with the nucleosome core particle.	255
Figure V.7	The results of the cleavage reaction of MPE with the ^{32}P -5'-end-labeled core particles and the corresponding free DNA.	257
Figure V.8	The temperature dependence of the ethidium binding to the core particle.	259
Figure V.9	The van't Hoff plot for the binding of ethidium to the nucleosome core particle.	261
Figure V.10	The Scatchard plot of the $[Na^+]$ dependence of ethidium binding to the nucleosome core particle at 30°C.	263

		<u>Page</u>
Figure V.11	The $[Na^+]$ dependence of the intrinsic equilibrium constants for the binding of ethidium to the core particle and to free DNA at 30°C.	265
Figure V.12	The results of the polyacrylamide gel electrophoretic analysis of the core particle/ethidium complexes used in the diffusion constant measurements. The laser densitometer traces of lanes A-E.	267
Figure V.13	The plot of fluorescence anisotropy versus input ratio of complexes of ethidium with nucleosome core particle and for the corresponding free DNA in 10 mM Tris, pH = 8.0, 0.1 mM EDTA at 20°C.	269
Figure V.14	The plot of fluorescence anisotropy versus viscosity for the ethidium complexes with the nucleosome core particle in 10 mM Tris, pH = 8.0, 0.1 mM EDTA at 20°C.	271
Figure V.15	The Perrin plot for several complexes of ethidium with the nucleosome core particle.	273
Figure V.16	The scans of the fluorescence anisotropy decay for three ethidium/core particle complexes.	275
Figure V.17	Schematic representation of the model for ethidium binding to the core particle.	277
Figure V.18	A schematic diagram for the passing of a polymerase through a nucleosome.	279
 Chapter VI		
Figure VI.1	Schematic representation of the step-wise dissociation of the nucleosome core particle.	318
Figure VI.2	Time dependence of the ethidium-induced dissociation of the chicken erythrocyte core particle at 30°C in 10 mM Tris, pH 8.0, 0.1 mM EDTA.	320
Figure VI.3	Reversibility of the ethidium-induced dissociation of ^{32}P -5'-end-labeled core particles in 10 mM Tris, pH 8.0, 0.1 mM EDTA at 30°C.	322

		<u>Page</u>
Figure VI.4	The % dissociation versus bound ratio plots for the dissociation of the chicken erythrocyte core particle as a function of temperature.	324
Figure VI.5	van't Hoff plot of the ethidium-induced dissociation reaction of the nucleosome core particle in 10 mM Tris, pH 8.0, 0.1 mM EDTA.	326
Figure VI.6	Laser densitometer trace of the ^{32}P -end-labeled-core particle/ethidium complexes, $R = .25$, at various ionic strengths.	328
Figure VI.7	The % dissociation versus bound ratio plot for the dissociation of the chicken erythrocyte core particle as a function of ionic strength at $T = 30^\circ\text{C}$.	330
Figure VI.8	The Log K versus Log $[\text{Na}^+]$ plot for the dissociation of the chicken erythrocyte core particle several bound ratios.	332
Figure VI.9	Schematic mechanism for the condensation Na^+ upon ethidium-induced dissociation.	334
Figure VI.10	Schematic diagram for a thermodynamic cycle which describes both ethidium-induced dissociation and the formation of the core particle.	336
Figure VI.11	The van't Hoff plot of the DNA conformational change of the nucleosome core particle in 10 mM Tris, pH = 8.0, 0.1 m EDTA.	338
Chapter VII		
Figure VII.1	Results of the CM-sephadex removal of H1 and H5 and non-histone proteins from whole chicken erythrocyte chromatin.	363
Figure VII.2	The circular dichroism spectra from 250-300 nm for the core particle, a nucleosome dimer, long chromatin +H1 and long chromatin -H1.	365
Figure VII.3	The plot of molar ellipticity versus % free DNA from the various chromatin forms.	367

	<u>Page</u>
Figure VII.4 The Scatchard plot for the binding of ethidium to long chromatin -H1 generated from a spectrophotometric titration method.	369
Figure VII.5 The Scatchard plot for the binding of ethidium to long chromatin +H1 (LC+H1) generated from a spectrophotometric titration method.	371
Figure VII.6 The Scatchard plot for the binding of ethidium to the chicken erythrocyte free DNA, the core particle, long chromatin +H1 (LC+H1) and long chromatin -H1 generated from a spectrophotometric titration method.	373
Figure VII.7 Schematic representation of the looped chromatin domains in the interphase nucleus.	375
Figure VII.8 The tabulated probabilities of finding the dye molecules bound within different folded structures within the interphase nucleus.	377

LIST OF TABLES

	<u>Page</u>
Chapter II	
Table II.1	Calculated relative populations of octamer, hexamer, and free DNA for ethidium bromide ³² P-core particle complexes at 30°C.
	103
Chapter III	
Table III.1	Quantification of the ethidium-induced dissociation of the chicken erythrocyte core particle by the gel electrophoresis method.
	139
Table III.2	Ionic strength, polyacrylamide/agarose, glycerol content, and voltage dependence of ethidium-induced dissociation of the chicken erythrocyte core particle.
	140
Table III.3	Results of the v _{core} determination for the complex of ethidium bromide with the chicken erythrocyte core particle at T = 30°C.
	142
Chapter IV	
Table IV.1	Absorbance and fluorescence spectral properties of ethidium bromide (EB) complexes with DNA, the core particle (CP) and polyvinyl sulfate (PVS) at low ionic strength.
	179
Table IV.2	Comparison of the fraction bound and intensity ratios for ethidium bound to the core particle and the corresponding free DNA at 20°C.
	180
Table IV.3	Fluorescence lifetime measurements of ethidium bromide complexed with chicken erythrocyte core particles and the corresponding free DNA.
	181
Table IV.4	Effect of data collection conditions on the resolution of lifetime components of ethidium bromide complexes with free DNA and nucleosomes.
	183

		<u>Page</u>
Table IV.5	Multi-component analysis of ethidium bromide complexes with chicken erythrocyte core particle and free DNA from fluorescence intensity and fluorescence lifetime measurements combined.	184
Chapter V		
Table V.1	K, n and w computer-generated best-fit values for the binding of ethidium with free DNA and core particles at 30°C.	234
Table V.2	Temperature-dependence of ethidium binding to the nucleosome core particle.	235
Table V.3	Ionic strength dependence of ethidium binding to the nucleosome core particle.	236
Table V.4	The translational diffusion constants for native core particles and ethidium complexes	237
Table V.5	The average fluorescence lifetime of core particle/ethidium complexes as a function of viscosity.	239
Table V.6	Radii calculated from steady-state and lifetime anisotropy measurements for ethidium pre-dissociation complexes with the core particle.	240
Chapter VI		
Table VI.1	Temperature dependence of the K_{obs} , ΔG° and ΔS° for the ethidium-induced dissociation of the nucleosome core particle R = .23 complex.	314
Table VI.2	Ionic strength dependence of K_{obs} , ΔG° and v_c for the ethidium-induced association of the nucleosome core particle R = .13 complex at 30°C.	315
Table VI.3	Values for $C\psi_c$ and C calculated from the slope of the $[Na^+]$ -dependence of the observed equilibrium constant for the ethidium-induced dissociation reaction of the nucleosome core particle.	316
Table VI.4	Summary of thermodynamic parameters which govern the association/dissociation of the nucleosome core particle at 30°C.	317

Chapter VII

Table VII.1	Empirical relationship between % free DNA and molar ellipticity values at 272 nm for core particles, dimers, long chromatin -H and long chromatin +H ₁ .	360
Table VII.2	The results of the best fit for K, n and w for the binding of ethidium bromide to the nucleosome core particle, free DNA, long chromatin +H ₁ and long chromatin-H ₁ at 30°C.	361
Table VII.3	The calculated probability of finding intercalating dyes associated with various folded forms of chromatin according to biological models.	362

The Binding of Ethidium Bromide to Chromatin:

Model for Carcinogen Interactions

INTRODUCTION

I. Aims

Intercalation is a process by which flat, planar molecules insert between the base pairs of DNA (Fuller and Waring, 1964; Waring, 1970; Le Pecq and Paoletti, 1967; Lerman, 1961; Lerman, 1963; Lerman, 1964). The binding properties of intercalating molecules are of particular interest since compounds of this class include mutagens (Hajduk et al., 1978) chemotherapeutic agents (Meienhofer et al., 1972) and carcinogens (Remers, 1979). While extensive investigation has been undertaken to elucidate the sequence requirements, base pair specificity and binding properties of many intercalating dyes to free DNA, little is known concerning how chromatin structure modifies their binding or how dye binding affects the chromatin structure. This lack of knowledge is particularly surprising since the in vivo target of many carcinogens and mutagens appears to be DNA complexed into chromatin.

What factors affect the induction of chemically induced carcinogenesis via DNA-binding, intercalating compounds? It is the overall philosophy of this thesis that the ability of an intercalating molecule to initiate a carcinogenic response is directly related to its ability to bind DNA, and that the binding is governed by underlying physico-chemical principles which take into account the

accessibility, conformation and the degree of chromatin folding. In order to evaluate the physico-chemical principles which drive the binding reaction of intercalating carcinogens, we have studied in detail the binding of a model intercalating dye, ethidium bromide, to various forms of chromatin. The information gained from this study will be used to establish a thermodynamic model for predicting the binding site of intercalating chemical carcinogens in vivo. The specific aims of this thesis are as follows:

1. To prepare homogeneous preparations of chromatin forms and to carefully characterize each form in terms of nucleic acid size, protein components and conformation. The forms of chromatin prepared in this study include chicken erythrocyte core particles; long polynucleosomes, devoid of H1, H5 and non-histone chromosomal proteins; and long whole chromatin.
2. To examine any gross structural changes which occur upon the binding of the intercalating dye, ethidium bromide.
3. To analyze the binding properties of ethidium bromide to the various folded forms of nucleic acids.
4. To determine the site of binding of ethidium bromide to the different forms of chromatin.
5. To use the dye molecules as probes for the structure and conformation of the chromatin forms.

II. Background

Ethidium bromide is a polycyclic aromatic dye which binds by intercalation between the base pairs of DNA (Fuller and Waring, 1964;

Waring, 1970; Le Pecq and Paoletti, 1967; Lerman, 1961; Lerman, 1963; Lerman, 1964). The structure and primary binding modes of the dye are shown in Figure i.1. Very early studies demonstrated that the intercalation mode of binding was extremely sensitive to the tertiary structure of the nucleic acid substrate. Vinograd and Bauer (1968, 1970) first showed that the ethidium bromide displays higher affinity to supercoiled regions relative to linear, B-form DNA. Removal of the supercoils in the DNA via intercalation binding was accompanied by a negative free energy change which increased the association of the dye. Terrence et al. (1985) reported that equilibrium binding of ethidium to poly d(m⁵GC) at physiological ionic strength, conditions under which the copolymer was known to be in the B-form, was non-cooperative with an intermediate binding constant of $\sim 5.0-8.0 \times 10^5$. When the ionic strength was increased to 4.4 M, conditions under which the copolymer flips to the left-handed Z-form conformation, the highly cooperative ethidium binding was correlated with circular dichroism data to indicate a sequential Z to B-form transition wherever the dye bound. Since the dye was found clustered in only the B-form regions, the authors concluded that ethidium bromide binding was unfavorable to Z-form DNA. Finally, Le Pecq and Paoletti (1967) demonstrated that the binding of ethidium bromide to RNA, single-stranded nucleic acid, was greatly diminished relative to linear, duplex DNA or double stranded-RNA. Since both electrostatic and hydrophobic components comprise the total binding free energy of intercalated ethidium, denaturation of the double helix removed the hydrophobic pocket provided by the base pairs, eliminating the free energy due to the hydrophobic interaction.

Thus, the binding of intercalating molecules can be used to probe the structure of DNA, and the differential binding affinity of intercalating ligands to the different conformations of DNA in vitro can be used as a starting point to predict the DNA binding site of intercalating ligands in vivo. Modeled on the binding free energy to DNA, the probability of dye placement is ordered in the following way: $P_{\text{supercoiled}} > P_{\text{B-form}} > P_{\text{single-stranded}} > P_{\text{Z-form}}$. Consequently, we would predict the dye binding in greatest density to supercoiled regions of the genome and the exact distribution of dye binding sites governed by the probability of binding to the respective conformation. But in eukaryotes, little, if any, free DNA actually exists in the cell. Instead, the DNA is condensed into various levels of packaged structures, the most "simple" being a length of DNA associated with eight proteins. How, then, can we extrapolate the site preference for dye binding in simple systems to the complexities of the eucaryotic genome? Does the presence of chromatin structure and associated proteins alter the distribution of the dye? Does the level of chromatin packaging or the conformation of the DNA dictate the site of intercalation? Let us begin by examining the chromatin structures which are available as potential carcinogen binding sites.

The common denominator of all the folded levels and their most basic component is the genetic material, DNA. In the eucaryotic nucleus, DNA is folded into regularly repeating nucleo-protein units called nucleosomes (Richmond et al., 1984; van Holde, 1974; Olins and Olins, 1974; Noll, 1974; Hewish and Burgoyne, 1973). A detailed structural model is presented in Figure i.2. The nucleosome is a roughly spherical particle of dimensions 55Å by 110Å (Richmond et al.,

1984; Bentley et al., 1984) which results in a 7-fold condensation of the DNA, i.e., 7 lengths of DNA are folded per particle length. The nucleosome consists of a core length of DNA, 145 bp, which is supercoiled 1.75 times around a central core of basic histone proteins containing two copies each of H2a, H2b, H3 and H4. Each core particle unit is connected to adjacent particles by a variable length of free, linker DNA, usually 50-60 bp (Lewin, 1980). Under low ionic strength conditions, the polymerized chain of the core particles and linker DNA form the 11 nm fiber known as the "beads-on-a-string" form of chromatin shown in Figure i.3. The major features of the 11 nm fiber have been distinguished by nuclease digestion studies (Noll, 1973; Sollner-Webb et al., 1975; Whitlock and Simpson, 1976; Shaw et al., 1976) which have indicated that, independent of the source of the chromatin, random cleavage of the phosphodiester backbone of DNA with enzymes such as micrococcal nuclease and Dnase-1 resulted in the production of a resistant 145 bp intermediate in the degradation of the polynucleosomal chain to nucleotides. The particles were isolated by sucrose gradient centrifugation, and analysis of the protein component revealed that the intermediate was associated with the histone octamer. The slow digestion kinetics of the 145 bp intermediate suggested that the histones protected the inner, folded DNA and that the linker DNA remained relatively exposed.

The presence of the 11 nm fiber is normally observed only when chromatin is spread or dissolved in low ionic strength or in the presence of divalent cation chelators. In vivo, the bulk of chromatin is found in association with a fifth class of histone protein, H1, which allows the further condensation of the 11 nm polynucleosomal

fiber. H1 consists of a central globular protein domain and two random coil tails, one at each end of the C- and N-terminal portions of the molecule. The globular portion of the molecule forms tight contact points with the nucleosome at histone H2A (Nelson, 1980) and H3 (Bonner and Stedman, 1979) and secondary weaker binding sites at the N- and C-termini which are distributed along the whole length of the linker DNA in gaps that are free of core histones (Mirzabekov, 1980). X-ray crystallography (Finch and Klug, 1976, 1977) and neutron scattering (Pardon and Lilley, 1979) have established the position of H1 binding to be on the outside of the nucleosome at the entry and exit point of the linker DNA. The presence of H1 on the nucleosome enhances the thermal stability (Whitlock and Simpson, 1976), nuclease resistance (Simpson, 1978; Varshavsky et al., 1977; Varshavsky et al., 1976), and orders the entry/exit points of the linker DNA such that the strands enter and leave on the same tangent (Thoma et al., 1979). In the presence of 0.2-0.3 mM Mg^{++} or 5-7 mM monovalent cation concentration, H1 mediates the condensation of the loosely helical 11 nm fiber to the highly condensed 30 nm form (Thoma et al., 1979) (Figure I.3). Although little detail is known concerning involvement of H1 or the internal architecture of the 30 nm fiber, considerable agreement has been reached on the overall dimensions of the structure. This next higher order of chromatin folding results in the formation of a supercoiled "solenoid" with pitch of 11 nm, diameter of 30 nm and with approximately 6 nucleosomes per turn of the solenoid (Finch and Klug, 1976; McGhee et al., 1980, 1983; Butler and Thomas, 1980; Thomas and Butler, 1980; Campbell et al., 1978; Hollandt et al., 1979; Rattner and Hamkalo, 1978; Hamkalo and Rattner, 1980; Widom and Klug,

1986; Felsenfeld, 1986). The model in best agreement with all the available data (McGhee et al., 1983) proposes that the nucleosomes are radially arranged within the solenoid with parallel faces inclined at an angle of 20-30° to the long axis of the fiber. The linker DNA, in this model, is also assumed to be supercoiled. Formation of the 30 nm fiber allows the compaction of 40-50 lengths of DNA per solenoidal unit as determined in the mass per unit length measurements of chicken erythrocyte chromatin by neutron scattering (Suau et al., 1979). Thus, the 30 nm solenoid accounts for half the compaction observed for the DNA in the average interphase nucleus (packing ratio = 100).

The third and fourth levels of chromatin folding represent the packaging level of interphase chromatin and metaphase chromatin, respectively, and are also seen in Figure I.3. Both levels involve the folding of the 30 nm solenoid into loops (Benyajati and Worcel, 1976; Paulson and Laemmli, 1977) or domains (Igo-Klemenens and Zachau, 1978). The less compact interphase chromatin is thought to arise from the simple looping of the 30 nm fiber which compacts the DNA ~2-fold over the formation of the fiber itself, yielding a total packing ratio = ~100. Each loop or domain contains 35-100 kbp of DNA (Paulson and Laemmli, 1977; Stumph et al., 1982, 1983) and is thought to be anchored at the base by specific non-histone proteins to the basal lamina of the nuclear membrane (Berezney and Coffey, 1977; Bodner et al., 1983; Cook et al., 1980; McCready et al., 1982; Murray et al., 1979), usually viewed as a supporting structure. In the case of the metaphase chromatin, the helical interphase loops condense another 2-fold (packing ratio = ~500-1000) relative to interphase chromatin to form the chromosomes in metaphase. Through the electron microscopic

imaging of histone-depleted chromosomes, Paulson and Laemmli (1977) observed metaphase chromosomes tightly packed around a central scaffold of metalloprotein (Lebkowski and Laemmli, 1982a,b; Lewis and Laemmli, 1983). With the stabilization provided by the binding of metalloproteins, such additional folding has been postulated to occur by either the side-to-side association of 30 nm fibers (Langmore and Paulson, 1983a,b) or by the formation of a supersolenoid (Sedat and Manuelidis, 1978; Bak et al., 1979).

Examination of the hierarchical packaging of nuclear DNA reveals that each level of DNA folding results from the supercoiling of the next lower level of chromatin, mediated by the binding of divalent ions and one or many protein factors. If we can extrapolate the dye binding probability of intercalating dyes for free, uncomplexed DNA to the packaged forms found in the cell, would we expect intercalation dye binding to be favored to the highly condensed supercoiled regions of DNA or to the relaxed, accessible chromatin regions? Since the release of superhelical stress increases the binding free energy of intercalating compounds, we might predict that dye binding would be favored to metaphase chromatin. Yet, while higher order folding results from the supercoiling of chromatin chains, it is not clear that the eucaryotic genome is under superhelical tension. To address this question, Sinden et al. (1980) measured the number of covalent adducts formed between trimethyl-psoralen and Hela nuclear DNA. The nuclei were pre-treated with gamma-irradiation which results in single-stranded breaks in the phosphodiester backbone of the DNA, and allows relaxation of torsional stress, if present, in the genome. After the DNA had been nicked with radiation, the intercalating dye

was added and photoactivated with visible light to allow the formation of covalent adducts. Since intercalation is energetically favored in regions of torsional stress, the authors predicted that more psoralen adducts should be formed in the control nuclei (in the absence of irradiation), relative to the nicked nuclei, if torsional tension existed. The authors found that the level of adduct formation was independent of the number of single stranded nicks, and suggested that little or no unrestrained superhelical tension was present in the eucaryotic genome. While experiments of this type might indicate that superhelical tension in bulk eucaryotic chromatin is utilized only in the formation of nucleosomes, the low sensitivity of the experiments rendered them incapable of detecting small populations which might experience torsional stress, such as transcriptionally active domains. Superhelical stress has been implicated in the transcriptional activation of yeast mating type genes (Abraham et al., 1983), the 5S ribosomal genes of *Xenopus Laevis* (Reynolds and Gottesfeld, 1983; Ryoji and Worcel, 1983), the SV40 viral genes (Lucknik et al., 1982) and the chicken β -globin genes (Villponteau et al., 1984).

Prediction of where an intercalating molecule will bind in vivo is rendered even more difficult by the fact that chromosomal proteins and ions, essential for the folding process, compete for binding sites on the DNA lattice. Further, their association may present a steric and/or conformational block to dye binding, as is the case for macromolecules such as RNA polymerase (Huang and Huang, 1969; Huang et al., 1967). Does the presence of chromatin proteins and divalent ions present a barrier to the binding of intercalating dyes or does binding to a particular conformation of nucleic acid occur at the expense of

protein binding? From the data available on this point, little agreement has been reached. For example, analysis of the binding of ethidium bromide to the nucleosome has resulted in two opposing models. Wu et al. (1980) determined that the binding of ethidium bromide to the chicken erythrocyte core particle displayed negative cooperativity typical of neighbor exclusion binding seen for free DNA. Thus, the binding of the dye was greatest at very low ratios, and gradually decreased. The authors observed that, at low ratios of the dye to DNA, below $R = 0.75$, the binding affinity of ethidium to the core particle was an order of magnitude higher ($\sim 10^7$) than for DNA ($\sim 10^6$) in low ionic strength buffers. As more dye was added, the affinity of the dye for the core particles was exceeded by the affinity for DNA, and the authors showed that the binding of the dye proceeded without loss of the histone proteins as high as $R = 0.2$. Thus, in this model, the association of the histones to DNA resulted in increased affinity of the dye for its nucleic acid substrate. The initial high affinity of the dye to the core particles was attributed to the coupling of drug binding to the release of superhelical stress induced by the binding of the histones. Implicit in the argument was the assumption that the tight binding of histones produced the topological constraints required for a linking number relationship to hold. In contrast, Erard and co-workers (1979) demonstrated that the binding of ethidium bromide to the core particle was a positively cooperative process. Binding of the first molecules favored the binding of the next and, consequently, the affinity of the dye was lowest at very low ratios, but gradually increased below $R = 0.15$. In this model, the presence of the histone proteins reduced the affinity

of the dye to the nucleic acid substrate. The positive cooperativity was attributed to the availability of more binding sites through the gradual loosening of the steric block presented by the tight binding of the histone proteins.

There is overwhelming evidence to suggest that the target binding site for intercalating mutagens and carcinogens in vivo is DNA (Waring, 1981 and references therein; Wilson and Jones, 1981; DiMarco et al., 1975; Theologides et al., 1968), although DNA may not be the only binding site (Tritton and Lee, 1982; Yang et al., 1985; Nelson et al., 1984; Tewey et al., 1984). But what factors are most important in the induction of chemically induced carcinogenesis by intercalating compounds? Does accessibility or the conformation of the DNA dictate the site of intercalation? If accessibility is the most critical factor then, perhaps, other, less energetically favorable conformations, may dominate the intercalation probability order, if found in more accessible regions. The Z-form conformation (Nordheim and Rich, 1983; Reeves, 1984) has been indirectly associated with accessible, transcriptionally active regions of the genome. Additionally, an 11-12 bp, polymerase-associated, single-stranded region has been directly measured in procaryotes within the transcriptional "bubble", the unpaired region at the site of RNA synthesis (Siebenlist, 1979). A polymerase-induced transcriptional bubble is likely to occur in eucaryotes, as well.

Despite the availability of only limited information, it is clear that the relative importance of physical binding parameters and the factors which affect intercalation binding underlie a basis set of physico-chemical principles which dictate the placement of a dye

molecule within the eucaryotic genome. If the induction of carcinogenesis is related to the binding of intercalating carcinogens to DNA, then these same principles will be important in elucidating the ability of a dye to initiate a carcinogenic response. A thermodynamic understanding of how carcinogens bind to DNA can aid in establishing a fundamental relationship between chromatin structure and the mechanism of chemically-induced carcinogenesis by intercalating compounds, i.e., whether carcinogenesis results from the binding of intercalators to functionally significant chromatin domains or whether disruption of chromatin structure by intercalation induces altered function.

III. Materials and Methods

A. Isolation of purified core particles

1. Purification of nuclei

Chicken erythrocyte core particles were prepared by a modification of the procedure of Paton et al. (Paton, 1983; Lutter, 1978). In order to avoid nucleoprotein degradation which can occur upon total cellular lysis, the nuclei were first isolated from the cytoplasm of the cell, which is the major source of the degradative enzymes. All steps were performed at 0°C. A flow chart of the isolation procedure is outlined in Figure I.4.

The fresh blood of three (3) adult chickens was collected into a 1-liter beaker containing 1.5 ml of heparin (1000 u/ml) at 0°C. (The

final concentration of heparin was 10 u/ml.) The blood was next filtered through four layers of cheesecloth in order to remove feathers and debris. The erythrocytes were pelleted by centrifugation for five (5) minutes at 1000 g in a Sorvall RC-5B Refrigerated Superspeed Centrifuge with a GS-3 rotor. The red erythrocyte pellet was washed three consecutive times in a buffer which contained 15 mM Tris, pH 7.4, 15 mM NaCl, 15 mM β -mercaptoethanol, 60 mM KCl, 0.5 mM spermidine-HCl, 0.15 mM spermine-HCl, 0.34 M sucrose, 2 mM EDTA, 0.5 mM EGTA, and 0.1 mM PMSF (Buffer-1). The proteolytic inhibitor PMSF was added from a concentrated stock solution to all wash buffers just prior to use. The 100 mM PMSF stock solution was made by fresh dissolution of solid PMSF into isopropyl alcohol; addition of .01 volumes of the PMSF solution into the buffer yielded a final concentration of 0.1 mM and a final alcohol content of 2%. The wash buffers offered maximum stabilization of the nucleic acid while providing protection against proteolytic degradation. Polyamines, spermine and spermidine were used in lieu of divalent cations which can activate endonucleases (Ca^{++} and Mg^{++}). After each washing with Buffer-1, the supernatant was discarded and the pellet was resuspended with a stirring rod. The supernatant at the end of the third washing appeared clear and the pellet contained both white nuclei and unlysed red erythrocytes. The cells were further washed in Buffer-2 which was identical in composition to Buffer-1 but also contained 0.5% Nonidet P-40 (NP-40-Sigma Chemicals, St. Louis, Missouri), a nonionic detergent which dissociates the cellular membrane and cleans the surface of the nuclear membrane from cytoplasmic debris. The pellet was again washed three consecutive times in Buffer-2, collected by

centrifugation at 1000 g for five (5) minutes but was resuspended with a tissue-mizer. Speed variability was provided by attachment of the tissue-mizer to a rheostat. During Buffer-2 washings the superatant changes from red (lysis of the erythrocyte results in the presence of the heme group in solution) to colorless which indicated that most of the cytoplasmic debris had been removed. The nuclear pellet became increasingly white. Finally, the nuclei were washed in Buffer-3 which was identical to Buffer-1 but contained neither EDTA nor EGTA. Buffer-3 removes traces of the nonionic detergent and is a suitable medium for enzymatic digestion. Again the pellet was collected and resuspended in the same manner as with Buffer-2. After a total of nine washings (Buffer 1-2-3) the white nuclear pellet was checked for integrity by staining with ethidium bromide and examination under an Olympus C-01 Phase-Contrast Microscope. Microscopic examination showed regularly spherical nuclei free of cytoplasmic debris.

2. Purification of chromatin

The white nuclear pellet was resuspended in Buffer-3 with a tissue homogenizer in preparation for the initial enzymatic digestion. Ideally the DNA concentration for the digestion was 4.92×10^{-3} M BP which was determined by a spectrophotometric absorbance reading at 260 nm ($A_{260} = 65$). Since the nuclei were particulate and gave rise to much scatter, the samples for the spectrophotometric readings were made by diluting the nuclear suspension 1:200 into .1 M NaOH against a blank made in an analagous manner. The nuclei were initially digested in the following manner:

1. The suspension was allowed to reach thermal equilibrium at 37°C in a thermostat controlled H₂O bath.
2. Since micrococcal nuclease requires Ca⁺⁺ for its activation, the nuclear suspension was made 1 mM in Ca⁺⁺ by the addition of .01 volumes of .1 M CaCl₂.
3. From a stock solution of 30,000 units/ml of micrococcal nuclease (Worthington Biochemical Corp.), 45 units/ml of enzyme was added to the suspension and the digestion was allowed to proceed for 5 minutes at 37°C.
4. The reaction was stopped by making the suspension a final concentration of 2 mM EDTA by the addition of .01 volumes of a .2 M EDTA solution. The entire solution was chilled on ice to 10°C.

The nuclear pellet was centrifugation for 10 minutes at 8000 g and resuspended in 80 ml of 0.25 mM EDTA, pH = 8.0. The nuclei were lysed by gentle stirring for 1 hour at 4°C. The 0.25 mM EDTA solution was used as a lysis buffer because of its low ionic strength and its ability to chelate ions which stabilize the membrane. Any insoluble material was pelleted by centrifugation for 10 minutes at 8000 g and the opalescent supernatant of long soluble chromatin was decanted and saved. The average yield of chromatin from 3 adult chickens was 15,000-20,000 total A₂₆₀ units.

The chromatin from the lysis contained H-1 histone protein as well as an array of non-histone chromosomal proteins present as contamination. H1, H5 and non-histone proteins were next removed by a modification of the method of Libertini and Small (1980). The absorbance of the long soluble chromatin was determined. The chromatin solution was diluted with a Tris/NaCl solution so that the

final concentration of Tris was 10 mM, the final NaCl concentration was 0.35 M and the final DNA concentration was 3.79×10^{-3} M BP ($A_{260} = 50$). Finally, a cation-exchange resin, carboxymethyl Sephadex (CM-25) (Pharmacia or Sigma), was next added, slowly and with stirring, to 30 mg/ml. The exchange reaction was allowed to proceed for 3 hours with constant stirring and the resin was removed by centrifugation for 20-30 min at $8000 \times g$. As shown in Figure I.5, the CM-25 Sephadex exchange reaction removes both histones 1 and 5, as well as the other non-histone chromosomal proteins which were present. The relative low ionic strength condition used for the stripping process prevented sliding and/or dissociation of histone cones. After the stripping procedure (lane 2, Figure V), the long chromatin contained only the four core histones H2A, H2B, H3 and H4. The supernatant was carefully removed with a pasteur pipette and dialized into 10 mM Tris, pH 8.0, 0.1 mM EDTA (digestion buffer). The dialysate was further collected and concentrated to ca. 1.89×10^{-3} M BP ($A_{260} = 25$) with an Amicon Stirred-Cell Ultrafiltration Diaflo Apparatus using PM-50 membranes.

A second enzymatic digestion was specifically performed to optimize production of long monomer units, free from any subnucleosome nicking. A test digestion was performed and the best digestion time was determined which maximized long monomers and minimized internal nicking by the enzyme. The selected digestion time varied according to the length of the initial digestion and the activity of the enzyme. In order to determine the optimal time, the following procedure was followed:

1. 0.5 ml of the long chromatin was incubated at 37°C for 2

minutes which allowed thermal equilibrium.

2. 5 μ l of 0.1 M CaCl_2 was added to the chromatin solution.

3. 25 units (50 units/ml) of micrococcal nuclease were added to the chromatin solution and the digestion was allowed to proceed.

4. At time points 0, 1, 2, 3, 4, 5, 8, 10, 15 and 20 minutes aliquots of 50 μ l of the test digestion solution were withdrawn and pipeted into tubes which contained 5 μ l of .2 M EDTA, pH 7.0. The tubes were kept at 0°C in an ice bath to retard further digestion. The results of the test digestion were analyzed by denaturing SDS-urea-polyacrylamide electrophoresis. The results of a typical test digestion are shown in Figure I.6. Immediately upon addition of the enzyme (lane 1) the presence of a nucleosome repeating ladder was observed. Further digestion (lanes 2-11) produced increasing amounts of monomer and dimer units at the expense of the higher molecular weight oligomers. The selected digestion time varied from 3-5 minutes, but most frequently was 4 minutes. A full-scale batch digestion was performed according to the results of the test digestion.

The batch digest was centrifuged for 2 minutes at 8000 g, concentrated to 7.56×10^{-3} M BP ($A_{260} = 100$) by ultrafiltration on a Amicon PM-50 filter and ~3000 units were loaded onto Sephacryl S-400 (Pharmacia) gel filtration column with the following characteristics:

Bed volume	4200 ml
Exclusion volume	1275 ml
Flow Rate	1 ml/min
Length	5.5 ft

Diameter	2 inches
M.W. limits	proteins 1×10^4 - 1.5×10^6
For fractionation	polysaccharides 1×10^3 - 4×10^5
Maximum sample volume	200 ml
Average sample volume	75-100

The eluent was a buffer which contained .02 M NaCl, 5 mM Tris, pH 7.5, 2 mM EDTA and, at a flow rate of 1-2 ml/min, the monomer peak eluted at ~1500 ml. The length of this column afforded an increased ability to distinguish molecular weight differences and, thus, fractions containing the monomer (145 BP) and the dimers (350 BP) were well resolved. Figure I.7 displays the peak elution profile. Each 20 ml fraction was checked on a SDS-urea 6% polyacrylamide gel. The heterogeneous long monomer fractions from the column were pooled and concentrated to a final concentration of 1.89×10^{-3} M BP ($A_{260} = 25$) by ultrafiltration on an Amicon pm-50 membrane. A careful test digestion was performed on the long monomer fraction, which was identical to the second digestion, to produce the "trimmed" core particles. An optimal digestion time was determined to be the time point where the monomers were trimmed to 145 ± 3 BP and subnucleosomal nicking was at a minimum, usually 0.5 - 1.5 minutes. Figure I.8 shows the results of the trimming test digestion.

The "trimmed" mononucleosomes were concentrated to $A_{260} \approx 100$ by ultrafiltration (Amicon PM 50) and loaded on the Sephacryl column, as above. Fractions were analyzed by gel electrophoresis and the homogeneous core particles were pooled. The pooled core particles were concentrated by ultrafiltration to $A_{260} \approx 100$ (Amicon PM 50),

dialyzed into 10 mM Tris, 0.1 mM EDTA, pH 8.0, millipore filtered using a .22 u membrane and stored on ice. The typical yield from 150 ml blood was ~4000 A₂₆₀ units of core particles which corresponds to about 20% of the starting material.

B. Preparation of nucleosomal-sized DNA

1. Calf-thymus DNA

Sonicated 200 BP calf-thymus DNA was prepared as described in Wilson et al. (1981).

2. Chicken erythrocyte DNA

The DNA was extracted directly from the purified core particles by standard deproteinization and phenol extraction procedure described in Maniatis et al. (1982).

C. ³¹P-NMR studies

Fourier transform spectra were accumulated at 101.2 MHz on a JEOL GX NMR spectrometer with quadrature detection using 10 mm tubes. Spectra of 6000-8000 scans were obtained with fast Fourier transformation of 8192 time domain points, a 90° pulse, 1000 Hz spectral window, broad band proton decoupling, and a 10 second pulse repetition time which represented 5 x T₁. In most cases a 1-Hz broadening function (exponential filter) was applied to each free induction decay before Fourier transform. Temperature was maintained with a JEOL NM 5471 Variable Temperature Control and checked with a "³¹P-thermometer" (Gorenstein et al., 1982). DNA samples were

prepared by lyophilizing the appropriate volume of the stock DNA in 10 mM Tris, pH 8.0, .1 mM EDTA buffer and redissolving in 99.8% D₂O (Aldrich) to obtain a final DNA concentration of approximately $1-2 \times 10^{-2}$ M BP. An internal standard of .01% Trimethylphosphate (TMP) was used in all samples. All core particle samples were prepared by lyophilizing .3 ml of buffer and TMP and resuspending in an equal volume (.3 ml) of 99.8% D₂O. The stock core particles were diluted directly to the buffered D₂O to yield a DNA concentration of $1-2 \times 10^{-2}$ M BP/1 and 25% D₂O. The final 1.5 ml sample contained .01% trimethylphosphate as an internal standard.

³¹P-NMR curves were evaluated for best chemical shift and linewidth by use of a Lorentzian Least Squares Fitting Program. Values were based on the minimization of root mean square deviation sum for all points.

D. H¹ nuclear magnetic resonance

Fourier transform spectra were accumulated at 270 MHz from a JEOL GX 270 spectrometer with quadrature detection using 5 mm tubes. Spectral parameters were 20,000 scans of 8192 time domain points, 10,822 Hz spectral window and a .5 second pulse repetition time (.1 second pulse delay) for the Redfield 214 pulse sequence (Redfield and Kunz, 1979). A 4 Hz line-broadening was applied to each exponential decay before Fourier transform. DNA samples were dialyzed into 10 mM Tris, pH 8.0, 0.1 mM EDTA. An appropriate volume of the DNA solution was next lyophilized and redissolved in 0.5 ml H₂O and 50 μ l 99.8% D₂O to yield a final DNA concentration of 3.0×10^{-2} M/(bp)/(A₂₆₀ = 400)

and a 9% D₂O content. Each sample contained an internal standard of .01% 3-(trimethylsilyl) propionic acid (TSP) which was added solid to each tube. The core particles ($A_{260} \sim 100$) were dialyzed into 10 mM Tris, pH 8.0, 0.1 mM EDTA and the appropriate NaCl concentration. The dialyzed samples were concentrated further to a final concentration of 3×10^{-2} M bp ($A_{260} = 400$) by using an Amicon PM-50 membrane. A buffered D₂O:TSP solution was made by lyophilizing TSP with 10 mM Tris, pH 8.0, 0.1 mM EDTA, and then redissolving in 99.8% D₂O. Concentrated core particles were added directly to the buffered TSP such that the final concentration of internal standard was 0.01% 3-(trimethylsilyl) propionic acid and final D₂O content was 9%.

E. Sedimentation velocity

Core particles were sedimented at 40,000 rpm in a Beckman Model E ultracentrifuge equipped with a photoelectric scanner using either 12 mm or 30 mm cells. The concentrations of the core particles were either 6.0×10^{-5} M (BP) ($A_{260} = .8$) or 2.3×10^{-5} M (BP) ($A_{260} = .3$), respectively, depending on which cell length was chosen. The buffer used for all experiments was 10 mM Tris, pH 8.0, 0.1 mM EDTA, with the addition of .5% sucrose to stabilize the boundary. All experiments were usually maintained at $20^{\circ}\text{C} \pm 1^{\circ}\text{C}$. Sedimentation coefficients were corrected to $S_{20,w}$ using standard corrections for buffer density and viscosity and S calculations utilized a partial specific volume, \bar{v} , = $0.66 \text{ cm}^3/\text{g}$ (Olins et al., 1976).

F. Circular dichroism

All samples were prepared by dilution of a concentrated core particle stock in 10 mM Tris, pH 8.0, 0.1 mM EDTA into the same buffer such that the final DNA concentration was $5.3 - 6.0 \times 10^{-5}$ M BP ($A_{260} = .7 - .8$). The circular dichroism measurements were made on a Jasco J-41-A spectropolarimeter using a 1.0 cm cylindrical quartz cell. The temperature was controlled by a Lauda Circulating Constant Temperature Bath (Brinkman Instruments) in conjunction with a Cuvette Temperature Control Device (MDC). The temperature was checked during all experiments by an immersible probe connected to a YSI Model 425C Tele-thermometer. For each temperature point, the sample was scanned from 300 nm to 250 nm and a separate measurement was made at a fixed wavelength ($\lambda = 275$ nm). All measurements were made at a sensitivity of 0.5 millidegree/cm, a time constant of 4 seconds and a slit width of 1.4 μ m. The baseline was recorded after every two temperature points and at the end of the experiment. The resulting curves were corrected for any baseline drift.

G. Electron microscopy

Samples were prepared by dialysis into .25 mM EDTA, pH 8.0 and dilution into the same buffer to a final concentration range of $1-5 \times 10^{-4}$ M ($A_{260} \approx 1-3$). The samples were absorbed onto carbon supports which were positively charged by plasma (glow) discharge for 30-60 seconds in a vacuum of 50 μ m Hg. The carbon support films were produced by evaporating carbon from a baked electron gun onto freshly

cleaved mica at a vacuum below 5×10^{-6} torr. The films were floated off on distilled water and allowed to settle down on to 500-mesh copper grids. The 5 μ l specimen was dropped onto the carbon support and immediately dipped into a Eastman-Kodak photoflow solution made with 3 drops Kodak photo-flow-200, 1 drop pH 10.0 buffer diluted to 50 ml with distilled water. The photo flow solution minimized surface tension during drying which can result in distortion. The excess photoflow solution was drawn off with filter paper and allowed to air dry before staining. One 5 μ l drop of 0.1% uranyl acetate stain which had been millipored through a .22 μ membrane was placed onto the grid for 30 seconds, drained off with filter paper and allowed to air dry. The grids were examined in a Siemens Elmiskop 102 microscope at 100,000 magnification with an accelerating voltage of 100 K volts. An E.F. Fullam carbon grating replica grid was used for magnification calibration.

H. Thermal melting

The core particle samples were extensively dialized into 10 mM Tris, pH 8.0, .1 mM EDTA. The samples dialized into 10 mM Tris, pH 8.0, 0.1 mM EDTA were diluted directly into the same buffer. In all cases the DNA concentration was $\sim 5 \times 10^{-5}$ M ($A_{260} = .3$). The temperature was increased at a rate of 0.5°/minute which was monitored by an immersible probe connected to a digital temperature display attachment in a Cary 219 Spectrophotometer (Varian). Temperature regulation was achieved by an ET-3 Programmable Temperature Control Unit (Neslab) in conjunction with a Neslab Circulating Temperature

Bath. Absorbance changes were monitored at 260 nm on the Cary 219 interfaced with an Apple II plus microcomputer. Transition midpoints were taken as maxima of the first derivative plot.

I. Electrophoresis

1. Type I: Native core particle gels.

Native core particle gels were used to analyze the nucleosome core particles and resulting DNA for size integrity and the presence of double stranded nicking. DNA analysis was performed by polyacrylamide gel electrophoresis on 1.0 mm thick slab minigels (Idea Scientific, Corvallis, OR). These gels were composed of 3.5% (acrylamide: bis-acrylamide; 20:1) in 40 mM Tris, pH 7.2, 20 mM NaOAc, 1 mM EDTA, prepared by the method of Kovacic (1977). Purified chicken erythrocyte core particle samples were mixed 1:1 with sample buffer consisting of 20% glycerol in 10 mM Tris, pH 8.0; 0.1 mM EDTA. The final glycerol composition was 10%. DNA samples were extracted directly from core particle stocks by standard procedures reported in Maniatis (1982). The DNA was mixed 1:1 with the same (2X) sample buffer used for the core particle with the addition of .02% bromophenol blue. The DNA size markers used for Type I and II gels were Cfo-I generated restriction fragments from PBr 322. Minigels were run at 10 v/cm for 1-2 hours at 4°C. Gels were stained for 15 minutes with 1 µg/ml solution of ethidium bromide in H₂O and photographed with Polaroid Type 55 film.

2. Type II: Single-stranded gels.

Polyacrylamide electrophoresis under denaturing conditions was

also used to determine size distribution to assay for and the presence of single stranded nicking. Samples were analyzed on 6% (0.8 mm) polyacrylamide minislabs (acrylamide:bisacrylamide 29:1) containing 5M urea, 2% SDS, 0.09 M Tris, pH 8.33, 0.09 M Boric Acid, 2.5 mM EDTA, prepared by the method of Paton et al. (1983). Core particle DNA was isolated as in the Type I gel and mixed 1:1 with 2 x sample buffer containing 10 M urea, 1% SDS, 0.2 x TBE (running buffer), .02% bromophenol blue. The samples were boiled for 1 minute and allowed to cool on ice before loading. For good resolution, the individual wells were flushed with TBE running buffer (.09 M Tris, pH 8.33, .09 M Boric Acid, 2.5 mM EDTA) just prior to loading to remove excess urea which leaked out of the gel. DNA markers (see Type I) were mixed with core particle DNA in 30% DMSO before boiling to avoid renaturation of the fragments. Minigels were run at 15-20 v/cm for 1-2 hours at 4°C. Gels were stained for 15 minutes with 1 µg/ml solution of ethidium bromide in H₂O and photographed with Polaroid Type 55 film.

3. Type III: Laemmli protein gel; Coomassie-stained.

The protein composition of the purified core particles was analyzed on standard Laemmli gels (Laemmli, 1970). The 0.5 mm Minislab gels were 18% acrylamide (acrylamide:bisacrylamide, 30:.8), with a 6% stacking gel. Gels were run at 15-20 v/cm for 1 hour at 4°C and stained with Coomassie Blue (Weber and Osborn, 1969). All other details were identical to the Laemmli procedure (Laemmli, 1970).

4. Type IV: Laemmli gel; silver stain.

Type III gels, after Coomassie staining, were silver stained exactly by the procedure of Wray et al. (1981).

5. 2-D Gel Electrophoresis.

Core particle/ethidium bromide complexes were analyzed in the first dimension on native core particle gels exactly as described in Type I gel electrophoresis. The core particle DNA concentration has usually 8.0×10^{-4} M BP. After ethidium staining, each band was cut from the native gel and soaked for 5 minutes in O'Farrell's buffer (O'Farrell, 1975). The soaked bands were placed flush against the top of a NaDodSO₄-polyacrylamide protein gel prepared exactly as described in Laemmli, 1970. Each protein gel was composed of a 6% stacking gel and a 15% separating gel and was stained with Coomassie blue. The running and staining procedures were described in Laemmli, 1970. The resulting protein bands were scanned with a Zeineh Soft Laser Scanning Densitometer Model SL-504-XL interfaced to an Apple-C microcomputer. Integration was done by cutting and weighing the respective peaks.

6. Low ionic strength gel electrophoresis.

a. Varshavsky type nucleoprotein gels. Low ionic strength vertical slab polyacrylamide gels for deoxyribonucleoprotein were slightly modified from the procedure described in Varshavsky et al. (1976; 1978). Vertical slab minigels were 1.0 mm thick, 10 cm long and contained 5% polyacrylamide (acrylamide: bisacrylamide ratio = 30:1), 0.5 mM EGTA, 1 mM EDTA, 10 mM Tris, pH = 8.0. Gels were electrophoresed for 7-10 hours at 150 volts (15 volts/cm). The electrode buffer was identical to the gel buffer. Gels were stained for 10 minutes with 1 µg/ml ethidium bromide in water. All other details of sample conditions and loading are as described in Type I native gel.

b. 0.5% Agarose. Low ionic strength vertical slab polyacrylamide gels were made as described in Todd and Garrard (1977). Vertical slab minigels were 1.0 mm thick, 10 cm long and contained 2.5% polyacrylamide (acrylamide: bisacrylamide ratio = 20:1), 0.5% agarose, 3.2 mM sodium acetate, 0.32 mM EDTA, 6.4 mM Tris, pH = 8.0. Gels were electrophoresed for 1 hour at 150 volts (15 volts/cm). The electrode buffer was identical to the gel buffer. Gels were stained for 10 minutes with 1 µg/ml ethidium bromide in water. All other details of sample conditions and loading are as described in Type I native gel.

c. 30% glycerol gels. Low ionic strength vertical slab polyacrylamide gels were made as described in Todd and Garrard (1979) and Albright et al. (1980). Vertical slab minigels were 1.0 mm thick, 10 cm long and contained 3.5% polyacrylamide (acrylamide: bisacrylamide ratio = 20:1), 0.5% agarose, 30% glycerol, 3.2 mM sodium acetate, 0.32 mM EDTA, 6.4 mM Tris, pH = 8.0. Gels were electrophoresed for 7-10 hours at 150 volts (15 volts/cm). The electrode buffer was identical to the gel buffer. Gels were stained for 10 minutes with 1 µg/ml ethidium bromide in water. All other details of sample conditions and loading are as described in Type I native gel with the exception that the sample buffer also contained 30% glycerol or sucrose.

J. 5' End Labeling.

Core particles at 9.5×10^{-4} M (BP) ($A_{260} \sim 12.5$) were labeled at their 5' DNA termini by incubation for 1 hour at 37°C with 3.0 µM

[γ - ^{32}P]-ATP (3000 Ci/mmol) (NEN), 7 units of T4 polynucleotide kinase (BRL, Bethesda, MD), in a buffer which contained 70 mM Tris, pH 7.6, 3 mM MgCl₂, and 5 mM DTT. Low Mg⁺⁺ concentration was used to avoid dissociation of the core particles. The reaction volume was 10 μl .

The end labeled stocks were diluted 1:600 with unlabeled core particles for every dissociation experiment. The specific activity of the resulting solutions was 2 cps/ μl . A sample volume of 5-15 μl was loaded into each well for scanning and the film was usually exposed for 15-24 hours. For calibration purposes, a separate 3.5% native polyacrylamide gel was developed simultaneously with each experiment which contained lanes with a series increasing volumes (1-20 μl) of control (R = 0) core particles. Each lane was scanned and a plot of intensity versus μl was constructed. All data were collected within the linear response range of the film determined by the control gel.

K. Fluorescence Intensity Measurements (Steady-State).

Fluorescence Intensity and anisotropy measurements were made on a computer interfaced fluorescence spectrometer (Ayres et al., 1974). Ethidium Bromide was excited at a wavelength of 510 nm from a Hg-Xe arc isolated through two grating monochrometers and polarized with a double Glan-Taylor prism polarizer. Emission was detected at both propagation and polarization directions at right angles to the exciting light. Emission was monitored at 585 nm isolated by a grating monochromater after passage through a double Glan-Taylor prism polarizer oriented either parallel (F_{\parallel}) or perpendicular (F_{\perp}) to the excitation polarizer. Stray excitation light was removed with a

Corning 0-54 cut-off filter (less than 1% transmission below 300 nm). A sensitivity correction (Ayres et al., 1974) was made for differential light transmission in the two polarization modes. After correction, fluorescence intensity was computed as $F = F_{\parallel} + 2F_{\perp}$ and anisotropy was calculated as $A = (F_{\parallel} - F_{\perp})/F$. Temperature was maintained at 20°C. The viscosity was varied by increasing the sucrose concentration. Solutions were made in 10 mM Tris, pH 8.0, 0.1 mM EDTA with either 10%, 20%, 30%, 40% or 50% sucrose.

L. Fluorescence Lifetime Measurements.

Decay measurements were made on the monophoton decay instrument described by Small et al. (1984) with the following changes. 1) The dye laser was operated with Rhodamine 575 (Exciton) in ethylene glycol. 2) The dye laser was pumped by the frequency doubled output (532 nm) of a mode-locked Spectra Physics series 3000 Neodymium:YAG laser. 3) Interactive mode was not used. 4) Hamamatsu R1564U microchannel plate photomultipliers were used. Initially, measurements were done with a triple-plate tube operated at -3800 V. Due to eventual failure of this tube, later measurements were made on a dual-plate tube operated at -4000 V. 5) For either photomultiplier, the output signal was sent to a LeCroy model VV101ATS amplifier. The amplifier output was split to provide the timing signal and a signal to be used for energy windowing. The latter signal was amplified and shaped through an Ortec 474 timing filter amplifier using a 500 ns integrated time constant (in place of the Ortec 113 preamplifier). 6) In some experiments, the stop signal for the time-to-amplitude

converter (TAC) was provided by the cavity dumper "Sync-out" signal via an Ortec 416A gate and delay generator.

The excitation wavelength was at 550 or 555 nm as indicated. Emission was collected through a broadband interference filter followed by a 3 mm Corning CS 3-73 cutoff filter. This combination has a maximum transmittance of 29% centered at 593 nm and a halfwidth of 15 nm, tailing to the red. Temperature was maintained at 22°C. The buffer was 10 mM Tris/HCl (pH 8), 0.1 mM EDTA, and NaCl as indicated. Analysis of the data was done on a PDP 11/34 computer (Digital Equipment Corp.) using the method of moments (Isenberg and Dyson, 1969) with moment index displacement, MD (Isenberg, 1973; Small and Isenberg, 1976; Small and Isenberg, 1977) and lambda invariance plots (Isenberg and Small, 1982). The program used, and a booklet describing the method and its use in detail, are available from Enoch Small, Oregon State University. The data were also analyzed by Least Squares Iterative Reconvolution using a program developed by the laboratory of Bruce Hudson at University of Oregon, Eugene, Oregon. All data were collected in 1024 channels at 0.1856 nsec/channel. Total counts in the measured scatter profiles were generally about 12×10^6 ($7-13 \times 10^6$) and the decays usually contained about 33×10^6 counts.

Because of the very narrow scatter profile, it was necessary to use a procedure which we term shift-summing for the least squares analyses. In shift-summing, both the scatter profile and the decay are shifted one channel to the right and summed to the unshifted data [i.e., $a'(i) = a(i) + a(i-1)$]. The problem which this step corrects can best be understood by calculating the Simpson's integral of the data

equivalent for a delta function (which the scatter profiles resemble). The result is an approximation to a step function (the true integral) onto which is superimposed an oscillation. Simpson's integration is used in the iterative reconvolution for Least Squares analysis, and when the scatter profile is very narrow it results in a similar oscillation which dominates the reduced chi-square. Shift-summing corrects this problem without significant effect on the statistics with respect to random noise (i.e., the reduced chi-square still approaches 1.0 for a good fit). The effect of non-random error (such as a wrong model, scatter contamination of the decay, "bumps" on the data, etc.) on the reduced chi-square are enhanced considerably by shift-summing as can be shown easily by applying the approach to data in which the scatter profile is relatively broad. Thus, if normally a reduced chi-square below 1.5 is usually considered acceptable, then for shift-summed data a considerably higher cutoff value should be accepted. It is significant that this emphasis of non-random over random error by shift-summing resembles the effect of increasing the total number of counts in the dataset.

M. Sucrose Gradient Centrifugation.

Ethidium complexes with the core particle and free DNA were analyzed on 5-20% linear sucrose gradients buffered with 10 mM Tris, pH 8.0, 0.1 mM EDTA. The 5% and 20% buffered sucrose solutions were chilled on ice to 0°C, mixed in a homemade gradient mixer and used immediately. The gradients were checked for linearity by refractive index. Core particle or DNA solutions were always 7.6×10^{-4} M BP

($A_{260} = 10$). Core particle stocks were always added last to diluted ethidium bromide solutions. Because of the high DNA concentrations used, aggregation occurred at intermediate and high dye/BP ratios. Since this aggregation was time dependent, samples were centrifuged immediately after mixing. The samples of 0.5 ml were layered on to the top of the gradients and centrifuged in a Beckman SW40 rotor at 26,000 rpm for 24-30 hours. Each gradient was fractionated into 0.5 ml fractions with an Isco Model 185 Density Gradient Fractionator. The gradients were pushed through a u.v. monitor using a 50% sucrose density bed. The peaks were monitored by an Isco VA-5 Absorbance/Fluorescence Monitor Chart Recorder attached to the fractionator. The flow rate was 3.0 ml/min and the chart speed was 60 cm/hr, therefore 1 cm = 3 ml of the gradient. The absorbance was calibrated by an absorbance standard check which is provided by the instrument. Chart recorder settings were sensitivity = 2.0 and a pen response time of 2.5 seconds.

N. Equilibrium Dialysis.

Equilibrium dialysis experiments were performed in a home-made, three-chambered plexiglass apparatus designed by W.D. Wilson and W. Germon at Georgia State University. Each block contained 8 separate cells holding 8.4 ml per chamber. The central chamber contained the buffer plus ethidium bromide; thus, every sample was measured in duplicate. The buffer used for all experiments was 10 mM Tris, 0.1 mM EDTA, pH 8.0. The core particle concentration was 3.8×10^{-5} M BP. Ethidium bromide was added to the central chamber and allowed to

equilibrate for 2-4 days at 30°C while gently shaking. The concentration of free ethidium bromide was determined directly by measuring the absorbance of the central chamber at 480 nm and dividing by the extinction coefficient of free ethidium bromide, $5750 \text{ M}^{-1}\text{cm}^{-1}$ (Waring, 1970). The concentration of bound dye was calculated by subtraction of the free dye concentration from the total concentration of added ethidium bromide. Division of the free and bound concentrations of ethidium bromide with the total concentration of added ethidium bromide yielded the respective fractions. Each chamber containing core particles was analyzed for dissociated DNA.

O. UV-Visible-Absorbance Spectrophotometric Measurements.

Absorbance measurements in the UV-visible region were made on a Cary 219 spectrophotometer interfaced to an Apple IIe microcomputer or a Cary 2200 spectrophotometer. Cell holders were thermostated by using Neslab or Haake circulating water baths. Wavelength scans and extinction coefficient measurements were made in cells from 1- to 10-cm path length at the wavelength or wavelength range appropriate for the compound being investigated. Extinction coefficients of compounds bound to DNA were determined at the same wavelength as the extinction coefficient measurements of the free compound, but a large molar excess of DNA was present ($[\text{DNA-P}]/[\text{compound}] > 100$). The Cary 219 spectrophotometer was also used in spectrophotometric binding studies. To remove some of the random error, for each absorbance measurement in the absence or presence of DNA, the microcomputer calculated the average of 100 acquired absorbance readings at the

preselected wavelength for the compound under study. These averaged absorbance values were converted by the microcomputer to v (moles of compound bound per mole of DNA base pairs) and free ligand concentrations using the free and bound extinction coefficients for the compound by equations (i.1) and (i.2). At the end of a titration, the computer plotted the digitalized data which were in the fraction-bound range 0.2-0.8. Any binding results outside of this range are subject to large systematic errors as a result of experimental errors in extinction coefficients. The computer then calculated nonlinear least-squares best fit K , n , and ω values from the site-exclusion method of McGhee and von Hippel (1974) as defined in equation (i.3).

$$\text{Fraction bound} = \frac{\epsilon_{\text{Free}} - \epsilon_{\text{APP}}}{\epsilon_{\text{F}} - \epsilon_{\text{B}}} \quad (\text{i.1})$$

$$[\text{Bound}] = F_{\text{B}} \times [\text{Ligand}]_{\text{T}} \quad (\text{i.2})$$

$$v/C = K(1-nv) \times \left[\frac{(2\omega-1)(1-nv) + (v-R)}{2(\omega-1)(1-nv)} \right]^{n-1} \left[\frac{1-(n+1)v+R}{2(1-nv)} \right]^2 \quad (\text{i.3})$$

where

$$R = \left[(1-(n+1)v)^2 + 4 \omega v(1-nv) \right]^{1/2}$$

Where v is the moles of ligand per polymer base pair, c is the free dye concentration, K is the intrinsic equilibrium constant, n is the number of base pairs excluded per binding site and ω is the

cooperativity parameter which represents the equilibrium constant for transfer of a bound ligand molecule from an isolated to a singly contiguous site.

P. Photoaffinity labeling of core particles and histones with ^3H -8-azido ethidium bromide.

^3H -8-azido ethidium bromide (8-AZEB) was synthesized by the method of Graves et al., 1977, and kindly provided by L.W. Yielding. All 8-AZEB stocks were dissolved in H_2O and checked for impurities or degradation by TLC and absorbance in the 700-350 nm range. Individual core particle/8-AZEB samples were mixed such that the final ratio of dye to DNA BP varied from 0-0.4. All samples were mixed under photographic safe lights using red filters. The 118 μl samples were equilibrated on ice for 10 minutes prior to photoactivation and were kept on ice during the photoactivation procedure. Samples were photolyzed for 10 minutes by exposure to unfiltered light from a Sylvania Daylite Bulb. The concentration of the core particle DNA in each sample was 1.5×10^{-3} M (BP). After photoactivation the samples were ethanol precipitated 3 times to remove all non-covalently bound drug. The precipitated samples were redissolved in SDS sample buffer, without boiling, (Laemmli, 1970) and the protein components were analyzed on a 0.8 mm 15% SDS-protein gel with a 6% stacking (Laemmli, 1970). The gels were run at 60 mA, constant current, with cooling at 21°C . The protein bands were stained with Coomassie blue as described in Laemmli, 1970. All four histone bands at each ratio were cut from the gel and extracted by shaking overnight at 37°C in 10 ml of

Scintillation Buffer containing 10% protosol-econophor in H₂O. The level of radioactivity in each sample was detected by scintillation.

The percentage (%) of 8-AZEB which formed covalent bonds with the histone octamer was calculated by equation (1.4).

$$\% \text{ Adducts} = \frac{\text{Sample Counts} - \text{Dark Control Counts}}{\text{Total Input Counts, corrected for temperature}} \times 100 \quad (1.4)$$

Where the dark control was a sample with a dye to BP ratio of 0.1 which was not photoactivated, but otherwise went through the entire procedure. The number of covalent bonds formed by ³H-8-azido-ethidium bromide to the histone octamer was calculated from the % of remaining dye by equation (1.5).

$$\# \text{ adducts per octamer} = (\% \text{ remaining lable})(\text{Input Ratio})(145) \quad (1.5)$$

For NMR samples, since the DNA concentrations were very high (1.3×10^{-2} M (BP)), the photoactivation procedure was slightly modified. An appropriate volume of 8-azido-ethidium bromide was lyophilized to dryness under red-filtered light. The DNA was added directly to the dried dye and redissolved to form the complexes. All DNA solutions were buffered in Pipes 20 which contained 10 mM pipes, .2 M NaCl, pH 7.0, 1 mM EDTA. The individual complexes were poured into a 50 ml beaker to form a thin surface on the bottom so that the solution was maximally exposed to the light. Each beaker was immersed in ice and vigorously shaken during photoactivation. After activation the samples were ethanol precipitated 3 times and redissolved in Pipes

20 for measurements.

Q. Methidiumpropyl-EDTA•Fe(II) (MPE) footprinting.

Purified MPE was kindly provided by P.B. Dervan and MPE footprinting was performed as described in Dervan et al., 1984. MPE (1.0 mg/ml) stock solutions in H₂O were stored frozen and dilute 1:1 with 1.0×10^{-3} M Fe(NH₄)₂(SO₄)₂•6H₂O solution. The MPE/Fe solution was immediately diluted to 10 ml with 10 mM Tris, pH 8.0, 0.1 mM EDTA. The final MPE working solution was 7.0×10^{-6} M. MPE complexes with DNA or core particles ranged from input ratios of 0 to 0.2 in order to stay within the pre-dissociation binding limits. Solutions were usually 3 ml and the core particles were always added just prior to the addition of DTT. The cleavage reaction was started by diluting a 30 mM DTT stock 1:10 into the core particle/MPE complexes such that the final concentration of DTT was 3 mM. The cleavage reaction was allowed to proceed for 3 hours at 23°C and was stopped with the addition of EDTA to 20 mM. The core particles were deproteinized with pronase (1 mg/ml) for 1 hour at 37°C and the core particle DNA was purified by phenol extraction and ethanol precipitation (Maniatis, 1982). The purified DNA was analyzed by 7% native polyacrylamide gel electrophoresis (Maniatis et al., 1975). In some cases ³²P-5'-end labeled core particles were added to the reaction. In these cases, the gels were dried and exposed to autoradiographic film overnight, 16-20 hours.

R. Diffusion Coefficient Measurements by Dynamic Laser Light Scattering

Diffusion measurements were made on a Spectral Physics 171 Argon ion laser tuned to the 514.5 nm blue-green intensity band. All measurements were made in the transverse mode called the TEM₀₀. An etalon was inserted into the laser cavity in an attempt to obtain light of a single longitudinal mode. Etalon insertion resulted in the removal of several longitudinal modes, however, because the etalon and the cavity were not temperature stabilized, some switching between modes occurred during the experiment. Thus, the etalon alignment was periodically adjusted to maximize power output and to minimize destructive interference within the beam. The power output was kept constant at 200 mW. The laser was set to autoregulate the power output by splitting the beam and monitoring the intensity of an output beam fraction. By observing the counts per second registered on the photomultiplier tube, we found that the autoregulation mode held intensity fluctuations of the output beam to $>200 \text{ mW} \pm 80 \text{ mW}$, i.e., $>4\%$ power fluctuation. The beam was focused directly on the sample cell by use of a focusing lens which retained the original polarization of the beam. The scattered light was attenuated with a pinhole aperture and then focused onto the photomultiplier tube with a second lens. We adjusted the placement of the photomultiplier tube so that it lay at the focal plane of the second lens. Adjustments were made by maximizing the counts/sec of the scattered light.

The sample cuvet was contained in an optically clear water bath of 100 ml with the temperature controlled by a Haake circulating constant

temperature bath. Temperature was monitored with a Hg thermometer immersed in the bath. Fluctuations in temperature during an experiment were monitored by an immersible thermistor attached to a digital voltmeter so that fluctuations of $\pm 0.01^\circ\text{C}$ could be detected. The typical temperature fluctuation during an experiment was $< 0.03^\circ\text{C}$. All measurements were made between 19.3°C and 20.3°C . All measurements were made between 19.3°C and 20.3°C .

Data were collected and analyzed with a Langly-Ford CD24 correlator. A second order cumulative analysis was performed over 64 channels using an average value of 16 additional channels as the uncorrelated background. The 16 additional channels were separated from the 64 channels by a delay time of 1024 channels. The autocorrelation function is defined by (Chu, 1974)

$$|g^1(t)| = \int_0^\infty e^{-\Gamma t} G(\Gamma) d\Gamma \quad (\text{i.4})$$

where $\Gamma = [4\pi\pi/\lambda \sin \theta/2]^2 \times D$, $|g^1(t)|$ is the autocorrelation function for a polydisperse system, $G(\Gamma)d\Gamma$ is the fraction of scattered light intensity from the molecules with correlation decay constants between Γ and $d\Gamma$, D is the translational diffusion coefficient, π is the refractive index, λ is the wavelength and θ is the angle of scatter.

The following conditions were utilized for the calculations:

$$\int_0^\infty G(\Gamma) d\Gamma = 1 \text{ and} \quad (\text{i.5})$$

$$\int_0^\infty \Gamma G(\Gamma) d\Gamma \equiv \bar{\Gamma} \quad (\text{i.6})$$

Expansion and integration of $e^{-\Gamma\tau}$ in a Taylor's series about $\bar{\Gamma}$, including only the first and second order terms, yields

$$|g^1(t)| = e^{-\Gamma\tau} \{1 + 1/2!(\mu_2/\bar{\Gamma})(\Gamma\tau)^2\} \quad (i.7)$$

where the second moment of Γ is defined as

$$\mu_2 = \int_0^\infty (\Gamma - \bar{\Gamma})G(\Gamma)d\Gamma \quad (i.8)$$

The mean autocorrelation function decay constant, $\bar{\Gamma}$, and the z-average diffusion coefficient can be calculated from Eq. i.7, where, $\mu_2/\bar{\Gamma} = [(D_2)_z - (D_z)^2]/(D_z)^2$, the z-average normalized variance of the D distribution. The $\mu_2/\bar{\Gamma}$ term is called the "quality parameter" because it describes how well the autocorrelation function in Eq. i.7 conforms to a single exponential. We empirically determined that a $\mu_2/\bar{\Gamma} < 0.2$ indicated a good fit to a single exponential.

Data had to satisfy two criteria before acceptance. (i) The number of counts per channel had to be $< .15$ to insure the validity of the Poisson statistics, and (ii) the ratio of the average value of the uncorrelated background calculated from the 16 channels and as p^2/n had to fall between .995-1.005. This ratio was extremely sensitive to fluctuations in beam intensity.

All core particle samples were dialyzed into 10 mM Tris, pH 8.0, 0.1 mM EDTA. The core particle concentration was always 3.8×10^{-4} M bp. Aliquots of concentrated ethidium bromide solutions were added to attain the indicated ratio. Samples were filtered through a Millex 0.22 μ filter to remove dust before adding dye. The samples were not

filtered after the addition of dye since the filter absorbed ethidium and altered the ratio. The homogeneity of the sample and freedom from error due to dust particle was indicated by the invariance of D_z with scattering angle from 120°C to 60°C . All results were corrected for viscosity and temperature differences.

Figure i.1. Illustration of the complex of ethidium with dCpG.

A) The crystal structure of the ethidium/dCpG complex is viewed approximately parallel to the planes of the G:C base pairs and ethidium molecule. The dCpG base pairs and sugar-phosphate backbone are drawn in dark solid lines. Intercalative ethidium (1) and stacked ethidium (2) modes of binding are drawn in open lines. Hydrogen bonding between guanine and cytosine pairs is indicated with broken lines (taken from Jain, S.C. et al., J. Mol. Biol., 1977, 114, 317-331). B) The structure of ethidium viewed perpendicular to the plane of the dye.

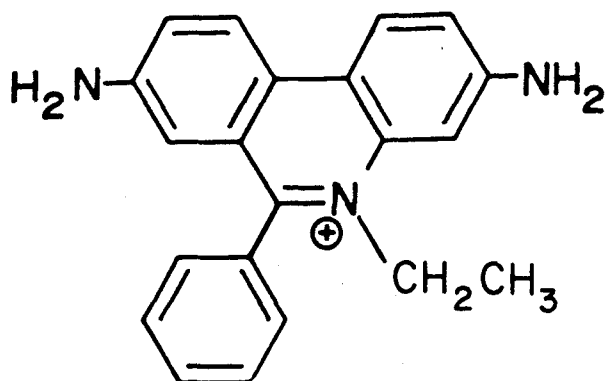
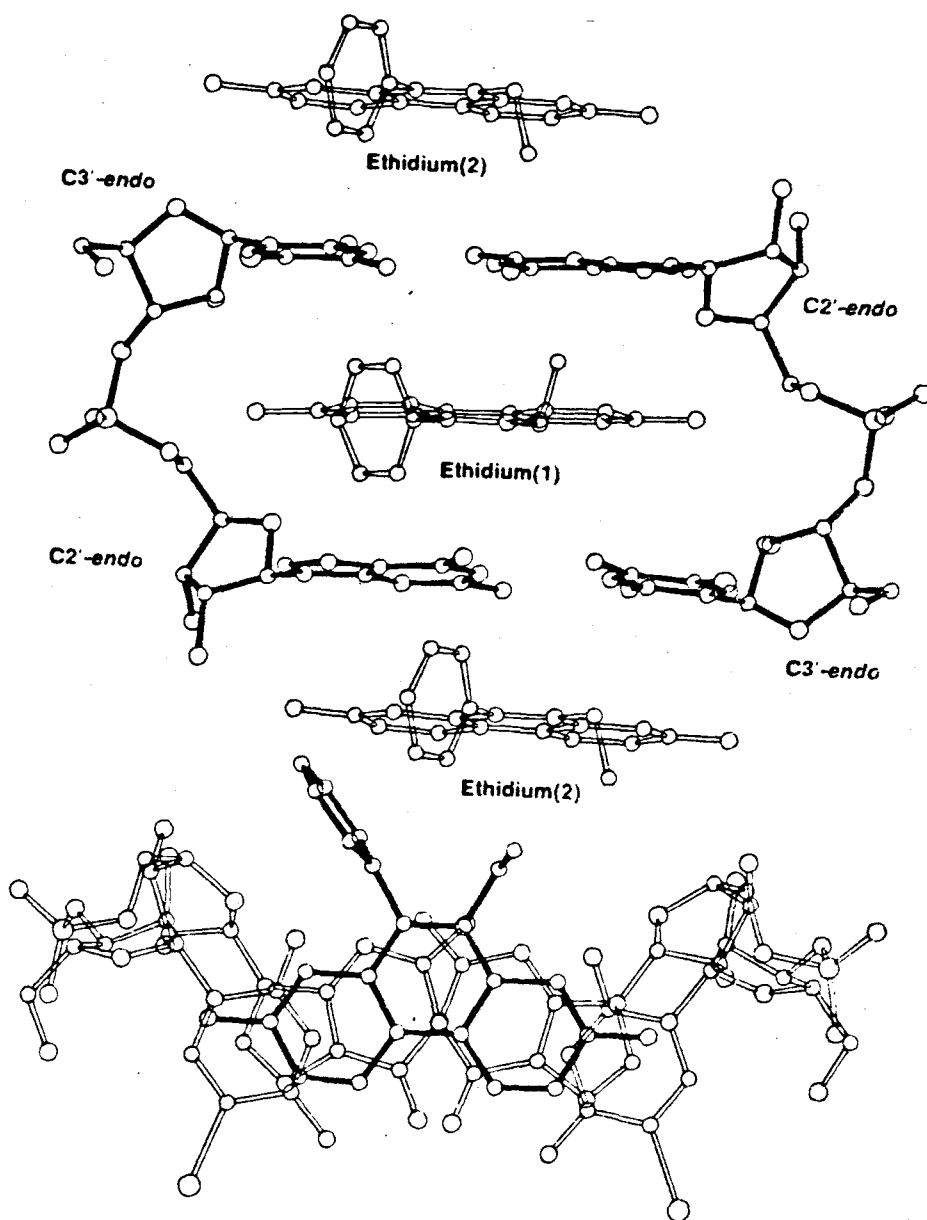


Figure i.1

Figure i.2. Schematic illustration of the many orders of chromatin packaging. Each level of supercoiling is drawn from postulated models which are thought to give rise to the highly condensed metaphase chromosome (taken from Alberts, B., Bray, D., Lewis, J., Raff, M., Roberts, K., Watson, J.D., Molecular Biology of the Cell, p. 399).

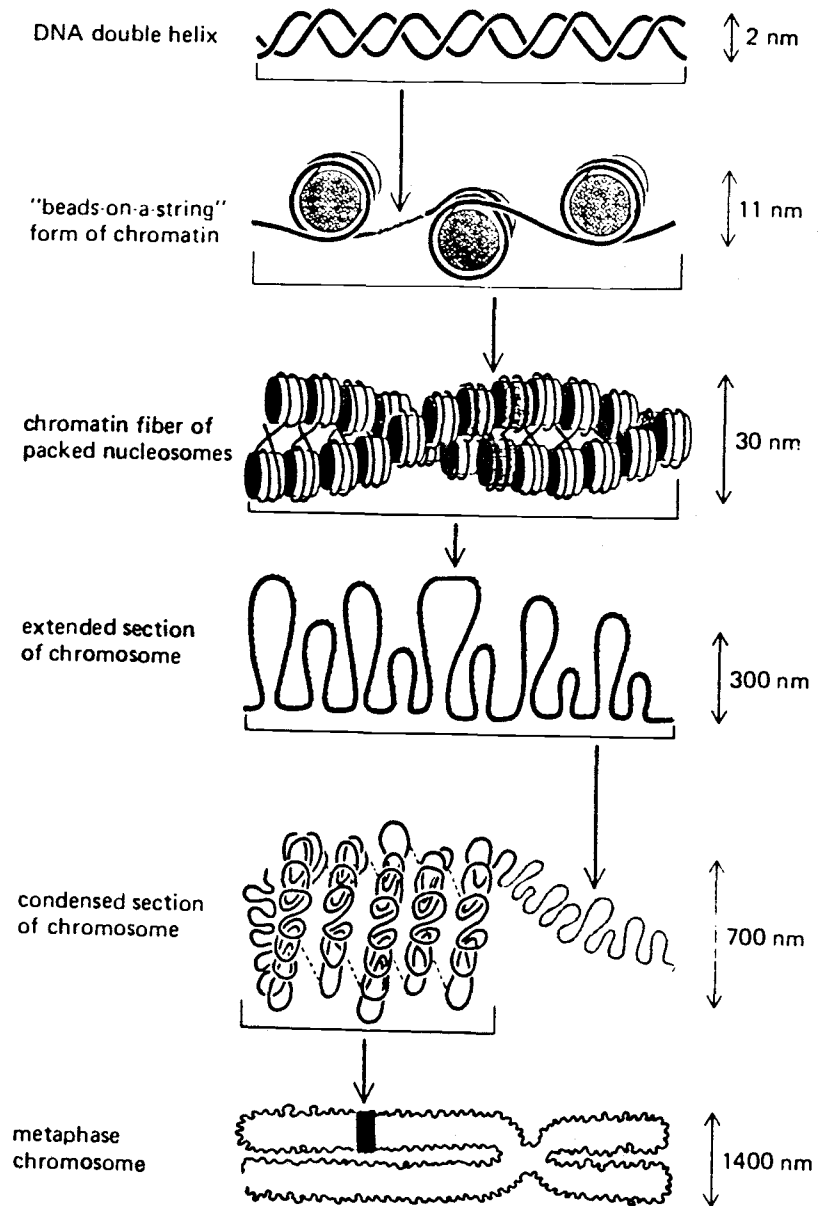


Figure i.2

Figure i.3. Model for the nucleosomal organization of DNA in chromatin (Taken from Isenberg, 1979). The DNA double-helix is supercoiled around the nucleosomal core formed of two tetramers each of one molecule of histones H2A, H2B, H3 and H4. The 11 x 5.5 nm nucleosome contains 1.75 superhelical turns of DNA with a pitch of 2.8 nm and an average of 140 base pairs. The basic N-terminal domains of the histones at the surface interact with the DNA thus providing a local protection against DNase I attack (sites 30, 60, 80 and 110). Other, non-protected sites are easily cleaved (sites 10, 20, 40, 50 and 130). The preferential cleavage at base numbers which are multiples of 10 results from the fact that the DNA helix contains 10 base pairs per helical turn and thus each strand rises to the nucleosome surface every 10 nucleotides. The bands on the DNA denote this distance of ten base pairs for one of the two DNA strands.

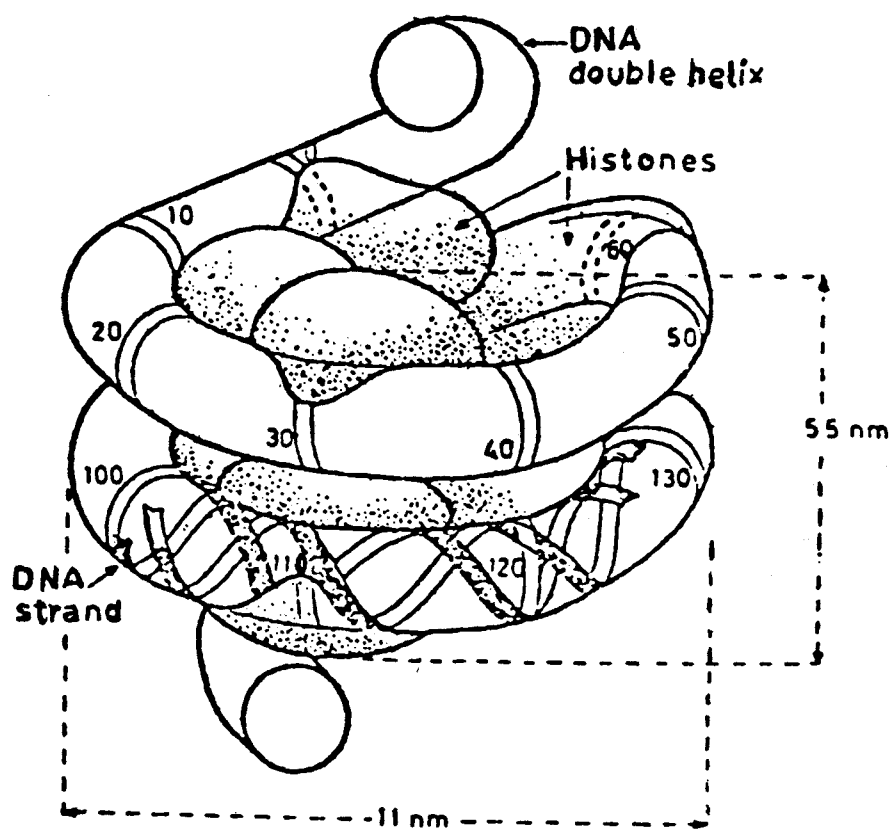


Figure i.3

Figure i.4. The flow chart of core particle preparation.

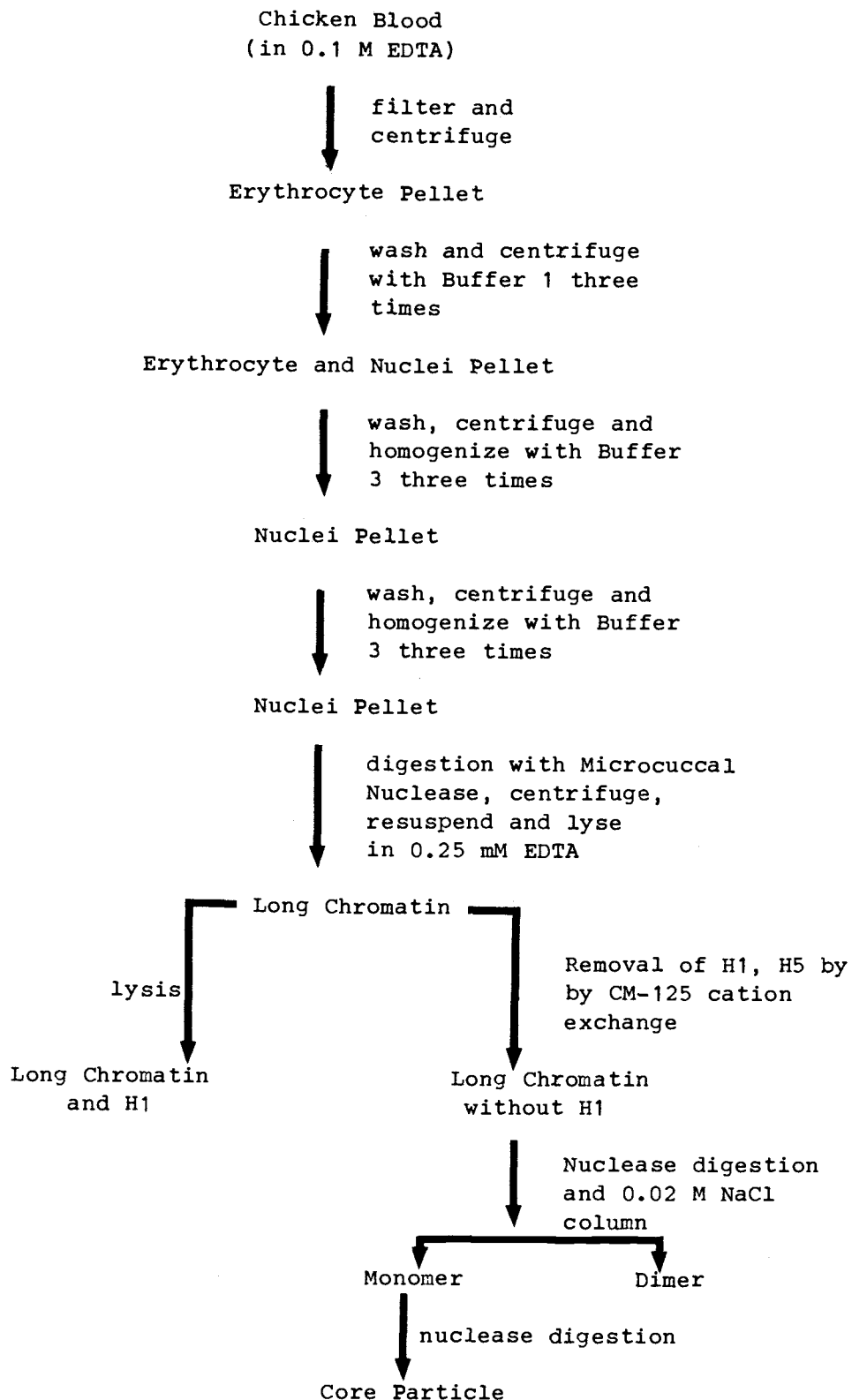
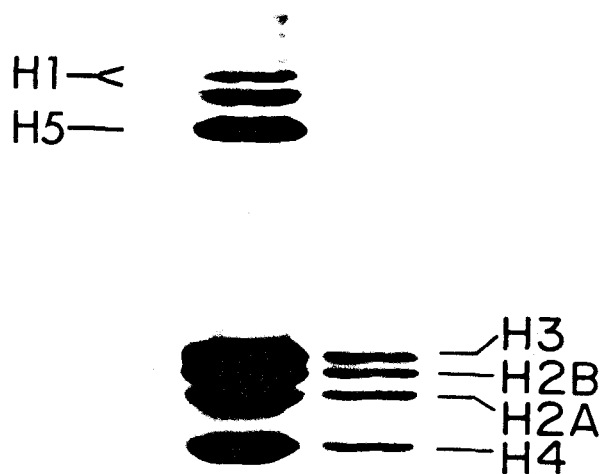


Figure i.4

Figure i.5. Results of the CM-sephadex removal of H1 and H5 and non-histone proteins from whole chicken erythrocyte chromatin.

Laemmli SDS - 15% polyacrylamide gel electrophoresis results of the CM-Sephadex treated chromatin (lane 2) and untreated chicken erythrocyte chromatin (lane 1). Polyacrylamide gels were 0.8 mm thick containing 15% polyacrylamide (acrylamide: bisacrylamide 30:.8) in the separating gel and 6% acrylamide in the stacking gel. Lane 2 contains 1.0 μ g of total protein from our preparation. Lane 1 represented 3.12 μ g of chicken erythrocyte whole chromatin. Samples from a core particle solution ($A_{260} = 1.0$) in 10 mM Tris, .1 mM EDTA, pH 8.0 were boiled in Laemmli (1970) SDS sample buffer for 1 minute, cooled on ice and loaded onto an Idea Scientific minigel apparatus. Gel electrophoresis was performed at 4°C at 15 v/cm for 1 hour. The gels were stained overnight with 0.25% Coomassie blue and destained in methanol:acetic acid according to the procedure of Laemmli (1970).



1 2

Figure i.5

Figure i.6. Results of the polyacrylamide gel electrophoretic analysis of a representative test digestion for long monomer production. Lanes 1-11 represent time point digestion intervals of 0, 1, 2, 3, 4, 5, 6, 8, 10, 15 and 20 minutes, respectively. Long stripped chromatin was digested with 50 u/ml of micrococcal nuclease. The digestion buffer was 10 mM Tris, pH 8.0, 0.1 mM EDTA and the chromatin concentration was 1.9×10^{-3} M BP ($A_{260} = 25$). The test digestion volume was 1 ml and the temperature was 37°C. The digestion was stopped at each time point by addition of EDTA to a final concentration of 2.5 mM. M, D and T refer to monomer, dimer and trimer, respectively. Samples were analyzed on a SDS-urea-6% polyacrylamide single-stranded gel. Gels were 1.0 mm thick and 10 ug were loaded into each well.



Figure i.6

Figure i.7. Electron micrograph of the chicken erythrocyte core particle preparation. Core particles were dialyzed into 0.25 mM EDTA, pH 8.0 and diluted to a final concentration of $1.0-5.0 \times 10^{-4}$ M BP ($A_{260} = 1-3$). The samples were absorbed onto carbon support films on copper grids. The grids were examined in a Siemens Elmiskop 102 microscope at 100,000 magnification with an accelerating voltage of 100 K volts.

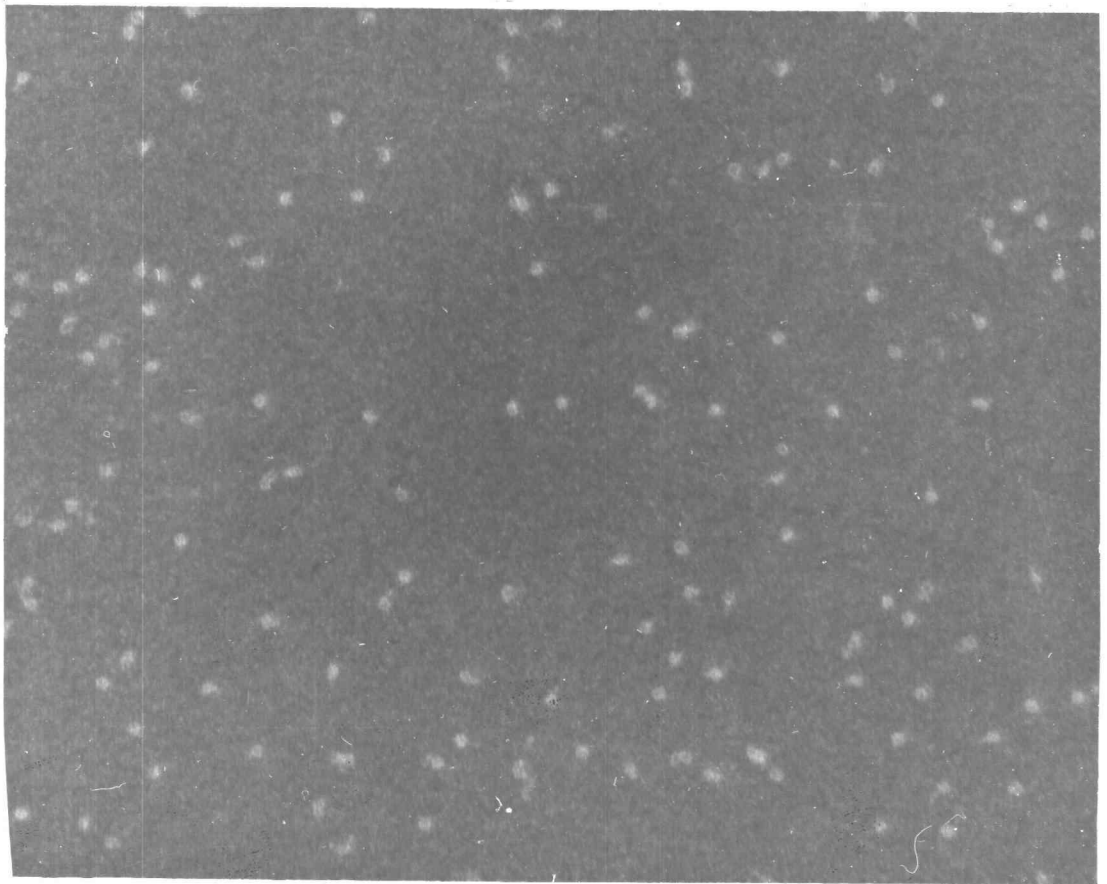


Figure i.7

Figure i.8. Results of the polyacrylamide gel electrophoretic analysis of the trimming digestion to produce homogeneous core particles. Lanes 1-12 represent digestion times of 0, 15s, 30s, 45s, 1 m, 1.5 m, 2.0 m, 7.5 m, 3.0 m, 3.5 m, 5.0 m and 0 min, respectively. Long monomer units were digested with 45 u/ml of micrococcal nuclease. The digestion buffer was 20 mM NaCl, 5 mM Tris, pH 7.5, 2 mM EDTA and the monomer concentration ranged from 3.8×10^{-4} - 7.6×10^{-4} M BP ($A_{260} = 5-10$). The test digestion volume was 1 ml and the temperature was 37°C. The digestion was stopped at each time point by addition of a .25 M EDTA solution to a final concentration of 2.5 mM. The samples were analyzed on an SDS-urea-6% polyacrylamide single-stranded gel. The gels were 0.8 mm thick and 10 ug were loaded into each well.



Figure i.8

CHAPTER I. CHARACTERIZATION OF A HOMOGENEOUS CORE PARTICLE

PREPARATION ISOLATED FROM CHICKEN ERYTHROCYTES

ABSTRACT

We report the detailed physical characterization of highly homogeneous, trimmed core particles isolated from chicken erythrocytes. The core particles were purified by a new method, modified from the procedure of Lutter (1978), that we specifically designed for homogeneity. The resulting particles were tested for homogeneity, protein content and physical integrity by five different physical techniques and four types of gel electrophoretic methods. The core particle DNA length population was determined to be 95% of 145 ± 3 bp, 2% between 130-145 bp, 2% at 110 bp and <1% at 80 bp. Analysis of protein content indicated that our preparation contained >99% the four histone proteins H2A, H2B, H3 and H4. Our preparation lacked any trace of H1 or H5 and <2% non-histone protein contaminants. The core particles displayed a sedimentation coefficient of 10.8 S, a molar ellipticity value at 284 nm of 1200 ± 200 (deg/cm²mole), a biphasic thermal melting curve with thermal melting midpoints in 10 mM Tris, pH 8.0, >1 mM EDTA of 73°C and 78°C and ³¹P-NMR parameters characteristic of a homogeneous preparation.

INTRODUCTION

The DNA of eucaryotic organisms is organized into various levels of packaged structures, the most basic of which is the nucleosome core particle (McGhee and Felsenfeld, 1980). The core particle is defined as 145 bp of DNA wrapped around an octamer of histone proteins comprised of two copies each of histones H2A, H2B, H3 and H4. The binding of the histones to DNA to form the nucleosome structure results in a complex which has fundamentally different properties than free DNA. The nucleosome differs from free DNA in its conformation (Cowman and Fasman, 1978; Simpson and Shindo, 1979; Shindo et al., 1980), solubility (Komaiko and Felsenfeld, 1985; Ausio et al., 1986; Perry and Chalkley, 1982) and response to ionic strength changes (Yager and van Holde, 1984; Ausio et al., 1984; Cotton and Hamkalo, 1981; Stacks and Schumaker, 1979), among others.

Because the properties of the nucleosome differ significantly from free DNA, it is not surprising that these differences are reflected in the ligand binding properties of the two forms of nucleic acid (Wu et al., 1980; Cahires et al., 1982; Erard et al., 1979). First, the association of the positively charged histones and the negatively charged phosphates in the DNA backbone results in some degree of charge neutralization within the complex (Doenecke, 1977; Girardet and Lawrence, 1979; McGhee and Felsenfeld, 1980). Thus, the reduced charge density may affect the binding properties of charged ligands. Second, the association of histones with DNA in the nucleosome results in a decreased number of bp/turn in the DNA helix from 10.4 bp/turn (winding angle = $35.2^\circ/\text{bp}$) found in free DNA to 10.2 bp/turn (winding

angle = $34.2^\circ/\text{bp}$) found in the nucleosome (Levitt, 1978; Lutter, 1979; Baase and Johnson, 1979; Lutter and Klug, 1982). Thus, changes in the conformational angle and differences in the interphosphate charge distance may contribute to the way a particular ligand binds to the Dna in the nucleosome complex relative to free DNA. Finally, the physical presence of the histones may present a steric block to the binding of ligands (Marishuge and Bonner, 1966; Noll, 1974). Thus, the energetics of maintaining nucleosome formation and the availability of binding sites may also affect the ability of ligands to bind to the nucleosome relative of free DNA.

Chromatin, at its most basic level, is formed from the polymeric repeat of folded, histone-associated nucleosomal DNA joined by a segment of free, linker DNA. The dynamics of the nucleosome structure is important since it is this levels which is involved in important biological processes such as transcription. In the many attempts over the years to understand the structure and function of chromatin, much confusion and error has arisen because little care was taken to define the starting material in terms of protein-associated portions of DNA and free linker portions, which have different properties. It has been suggested that discrepancies in data concerning dye binding (Wu et al., 1980; Erard et al., 1979) and salt folding transitions (Schlessinger et al., 1982; Uberbacher et al., 1983) of nucleosomes may be due to poorly prepared starting materials which contain mixtures of folded and free forms of nucleic acid. In this report, we describe a new method of core particle purification which yields an extremely homogeneous preparation, 145 ± 3 bp, free from contamination with linker DNA. The integrity of the particles are tested by five

different physical methods and four types of gel electrophoresis to insure the purity of the final product. The method was used to prepare the starting material for all subsequent studies.

RESULTS

I. Electrophoresis

Native polyacrylamide gel electrophoresis (Type I) (Figure I.1) of the native core particle (lanes 2-6) and corresponding DNA extracted from the core particles (lanes 8-12) showed an extremely homogeneous preparation which lacked both high molecular weight contamination and any significant subnucleosomal nicking. To demonstrate the discrete size of the core particle, lanes 8-12 were loaded with increasing amounts of DNA such that lane 12 represented a DNA content greater than 10 times the linear intensity range of the gel. The DNA isolated from the core particle, in all lanes, migrated as a single tight band. Plots of log molecular weight versus relative mobility (not shown) of the marker DNA fragments were used to determine the molecular weight distribution of the core particle preparation. The relative mobility of the upper and lower edges of the core particle long DNA band indicated that the core length ranged from 143 to 147 BP, and is therefore taken as 145 ± 2 BP. The preparation shown in Figure I.1 displayed no trace of dimer or higher molecular weight oligomer present in any lane. The integrity of the intact core particle, which has reduced mobility relative to the free DNA, also migrated as a single tight band. In addition, lanes 2-6 display no trace of free dissociated DNA or short oligomers running below the native band. The integrity of the intact core particle was confirmed by sedimentation velocity analysis which determined the sedimentation coefficient of the intact cores in 10 mM Tris, pH 8.0, 0.1 mM EDTA to be $10.8 \pm .2$ S

at 20°C. These results are in excellent agreement with previous studies (see Table I.1). Further, electron micrographs (Figure I.2) of our core particle preparation in 0.25 mM EDTA, pH 8.0, revealed a core particle preparation which contained no free DNA component and spherical particles free from DNA linker "tails".

Because our preparation method included three enzymatic digestions, we assayed for the presence of subnucleosomal DNA nicking, a possible source of error for physical studies. The % nicking for both double and single stranded nicks was determined, respectively, by analysis on native (Type I) and single-stranded (Type II) SDS-urea-polyacrylamide gel electrophoresis (Type II). The method and results are shown for double-stranded nicking in Figure I.3. Increasing amounts of DNA from the preparation shown in Figure I.1 were loaded in lanes 7-12 until detectable amounts subnucleosomal nicking were observed. The nicked DNA bands were then scanned with a Laser scanning densitometer and the total area was determined by cutting and weighing the respective peaks. Each area was converted to grams by extrapolation of the nicked peak areas to the calibration curve plotted from the DNA standards observed in lanes 1-5. The areas of the known DNA standards were also determined by the scanning and weighing procedure. The percentage of nicked material was calculated directly from the ratio of nicked material to DNA loaded on the gel. By the gel quantitation method (Figure I.3) we determined that 93% of our core particle preparation homogeneously distributed between 143-147 BP. Approximately 5% of the core particles displayed intensity below the main core particle band between 130-143 BP. This region was difficult to analyze; some of the intensity is probably the

result of band diffusion since the sub-nucleosomal bands were only visible at high gel loadings. If we suppose that all the 130-140 BP intensity is the result of double-stranded cutting then our preparation is 93% homogeneous in length; if we attribute this region to diffusion then our preparation is 98% homogeneous in length. Taking the average of these two values we report that our preparation consists of core particles, 95% of which are 145 ± 2 BP. In addition, we observed ~2% regular double stranded cutting of the nucleosomes at ~110 BP and a minor band (<1%) at ~80 BP. No additional sub-nucleosomal nicking was observed when the core particles were analyzed on single-stranded gels.

Analysis of protein on standard Laemmli (1970) gels (Figure I.4) demonstrated that our preparation was extremely pure, lacking both H1, H5 and any significant amounts of non-histone proteins. Figure I.4 shows the protein component of increasing amounts of the particle preparation stained with Coomassie Blue (sensitive to μg level of protein). At the μg level, the core histones appear equimolar and no trace of contaminating protein is observed in any sample lane (lanes A, B, C, D, E, F range from 0.25 μg to 5.0 μg total protein). Whole, unstripped chicken erythrocyte chromatin, present in every other lane, shows 3.12 μg of total protein for comparison. Detection at the nanogram level by a more sensitive silver staining technique of the histone proteins (Figure I.5) clearly demonstrates the complete absence of either H1 or H5 and the integrity of the core inner histones. We did observe, at this sensitivity, the presence of trace amounts of contaminating protein in Lanes 5, 7 and 9 shown in Figure I.5. Quantitation of the contaminating bands, however, revealed that

the % non-histone bands was <.2% determined by scanning and weighing calibration analogues to the method used for the DNA.

II. Circular Dichroism, Thermal Melting and ^{31}P -NMR of Core Particle Preparation.

To confirm that our core particles were pure and intact, we measured the circular dichroism spectrum and the thermal melting profiles of the core particles. The circular dichroism spectrum in the region from 300 nm to 260 nm, displayed the characteristics features of the native nucleosomes: a small negative peak at ~295 nm, a double peak exhibiting a maximum of $1400 \pm 200 \text{ deg. cm}^2 \cdot \text{dmole}^{-1}$ at 282.4 nm and a zero crossover-point at ~270 nm. Midpoints of the thermal melting profiles (Table I.1, Figure I.6) in 10 mM Tris, 0.1 mM EDTA, pH 8.0 were 73° and 78°C, respectively, for the two melting phases, in excellent agreement with previously reported results (see Table I.1). Finally, we measured the ^{31}P -NMR spectral characteristics of the nucleosome core particle. ^{31}P -NMR best fit values for calf thymus DNA, chicken erythrocyte DNA and chicken erythrocyte core particles are listed in Table I.2. Each spectrum was evaluated by a least squares Lorentzian fitting program which determined best values by minimizing the sum of the root mean square deviation for all points from a theoretical Lorentzian distribution. Each value for the chemical shift, linewidth at peak half-height and peak intensity is the average of at least three separate experiments which represent separate batch isolations to insure that the results were independent of any particular preparation or experiment. We have found that

incomplete enzymatic digestion of long stripped chromatin to yield monomer nucleosomes retaining some amount of free DNA linker can alter the values for the ^{31}P -NMR parameters obtained. Similarly, incomplete removal of H1, H5 and other non-histone chromosomal proteins can also yield erroneous results. The measurements reported in this manuscript reflect the ^{31}P -NMR spectral parameters for highly homogeneous trimmed core particles, 145 ± 3 BP. The error limits for each measurement were $\delta = \pm .03$ ppm, $\nu^{1/2} = \pm 1$ Hz, $T_1 \pm .01$ second and T_2 values $= \pm 5$ msec.

The 101 MHz, proton decoupled ^{31}P -NMR spectra of calf thymus DNA, chicken erythrocyte DNA and the chicken erythrocyte core particle are shown in Figure I.7. Both the calf thymus DNA and the chicken erythrocyte DNA gave rise to a single symmetric signal which fit well to a single Lorentzian distribution. For both types of native nucleosome-sized DNA, the chemical shift was close to -4.3 ppm and, for each, the observed linewidths exhibited the relatively large values expected for random-sequence native polymers. The slightly larger linewidth observed for calf thymus DNA relative to chicken erythrocyte DNA can be attributed to length heterogeneity. The sonicated calf thymus DNA consisted of a range of molecular weights with 67% of the sample between 170-210 BP. Both DNA types have the same base composition (57% AT, 43% G-C (Marmur and Doty, 1962)) and both exhibit spin-lattice relaxation times (T_1) of ~ 2.2 seconds.

The ^{31}P -NMR spectra for the chicken erythrocyte core particle at 30°C also gave rise to a single symmetric peak which fit well to a single Lorentzian distribution. Comparison of Figure I.7 and Table I.2 reveals three distinct differences between the ^{31}P -NMR spectral

parameters for free DNA and the core particles. First, the chemical shift value for the nucleosome (-4.47 ppm) was found 0.2 ppm upfield relative to free DNA (-4.27 ppm). This difference has been previously observed (Shindo et al., 1980). We find the upfield shift due to histone octamer binding to be a reproducible and important characteristic of the core particle structure. Second, the linewidth increases ~30% (4 Hz) from 13.5 Hz to 17-18 Hz at 30°C. Finally, the T_1 value increases from 2.15 seconds for free DNA to 2.8 seconds when the DNA is bound to the histone octamer to form the nucleosomal structure. The chemical shift, linewidth and symmetric shape of the ^{31}P -NMR signal for the core particle were in excellent agreement with previously reported data (Shindo, 1980) and indicated that our preparation was intact and homogeneous.

We determined, by the above criteria, that our preparation was of excellent quality and suitable for physical studies.

Table I.1

Physical Characterization of the Chicken Erythrocyte Core Particle
in 10 mM Tris, pH 8.0, 0.1 mM EDTA

Technique	Value	Supporting References ^a
<u>Sedimentation Velocity</u> ($S_{20,w}$)	10.8S ^b	1
<u>(U.V.) Thermal Melting</u>	Phase I 73°C ^c Phase II 78°C	2
<u>Circular Dichroism</u> $\lambda=284$ nm	1200 \pm 200 deg. cm ² mole	3
<u>Electrophoresis</u>		
(Type I,II) Size Distribution	145 \pm 2 BP	
(Type I) Integrity	Homogeneous	
(Type I,II) Nicking ds (I) ss (II)	<1%	
(Type III,IV) Protein	equimolar core histones 0.2% other no H1, H5	

a. References reported by first author only.

b. S = Svedberg units = 10⁻¹³ seconds

c. Midpoints for the first phase were taken as the 1st derivative of absorbance vs. temperature curve.

1. (Kovacic, 1977; Yager, 1984; Ausio, 1984)
2. (McGhee, 1980; Simpson, 1979; Weischet, 1978)
3. (Cowman, 1978; Watanabe, 1981; Weischet, 1978)

Table I.2

³¹P-NMR (24.15 MHz) Parameter Best Fit Values for Calf Thymus DNA, Chicken Erythrocyte DNA and Chicken Erythrocyte Core Particles at Two Temperatures

Sample ^a	Length in Base Pairs	T°C	# Peaks	δ^b	$\nu_{1/2}^c$	T ₁ ^d
Calf Thymus DNA	~200 BP	30°	1	-4.3	16	2.2
Chicken Erythrocyte DNA	145±2	30	1	-4.27	13.5	2.15
Chicken Erythrocyte Core Particle	145±2	30	1	-4.46	17.3	2.80
		50	1	-4.42	15.4	2.80

a The buffer for the calf thymus DNA was 10 mM Tris, .1 mM EDTA pH 8.0, 0.1 M NaCl. All other measurements were made in 10 mM Tris, 0.1 mM EDTA, pH 8.0. The addition of NaCl to the DNA buffer at 50°C was necessary to avoid denaturation of the DNA helix at this temperature. We justify this Na⁺ addition since the addition of NaCl has no observable effect on the ³¹P-NMR chemical shift, linewidth or T₁ value measured for free DNA ().

b Chemical shifts were measured in ppm upfield relative to TMP internal standard as described in material and methods.

c Linewidth measurements were made at peak half height and expressed in Hz.

d T₁ value expressed in seconds.

Figure I.1. Results of gel electrophoretic analysis for the nucleosome core particles and DNA isolated from the core particles. Polyacrylamide gels were 1.0 mm thick containing 3.5% polyacrylamide (acrylamide: bisacrylamide 20:1). Lanes marked M contain molecular weight markers from CfoI cut PBr322. From top to bottom, the fragment sizes are 393, 348 + 337 + 332, 270, 259, 206, 190, 174, 153 + 152 + 151, 141, 132 + 131, 109, 103, 100, 93, 83, 75 + 67 + 62 + 60. Lanes 6-10 contain the native core particle in 10% glycerol, 10 mM Tris, pH 8.0, 0.1 mM EDTA. No dye marker was added to the native core particle. Amounts of core loadings from lanes 6-10 were 30, 50, 75, 85, 100 ng. Lanes 5-1 contain the DNA isolated directly from the core particles. The DNA, in standard Laemmli (1970) sample buffer, was loaded in amounts of 10, 40, 75, 250, 625 ng. Gel electrophoresis was performed at 4°C at 10 v/cm for ~50 minutes. The gels were stained for 20 minutes with 1 µg/ml ethidium bromide.

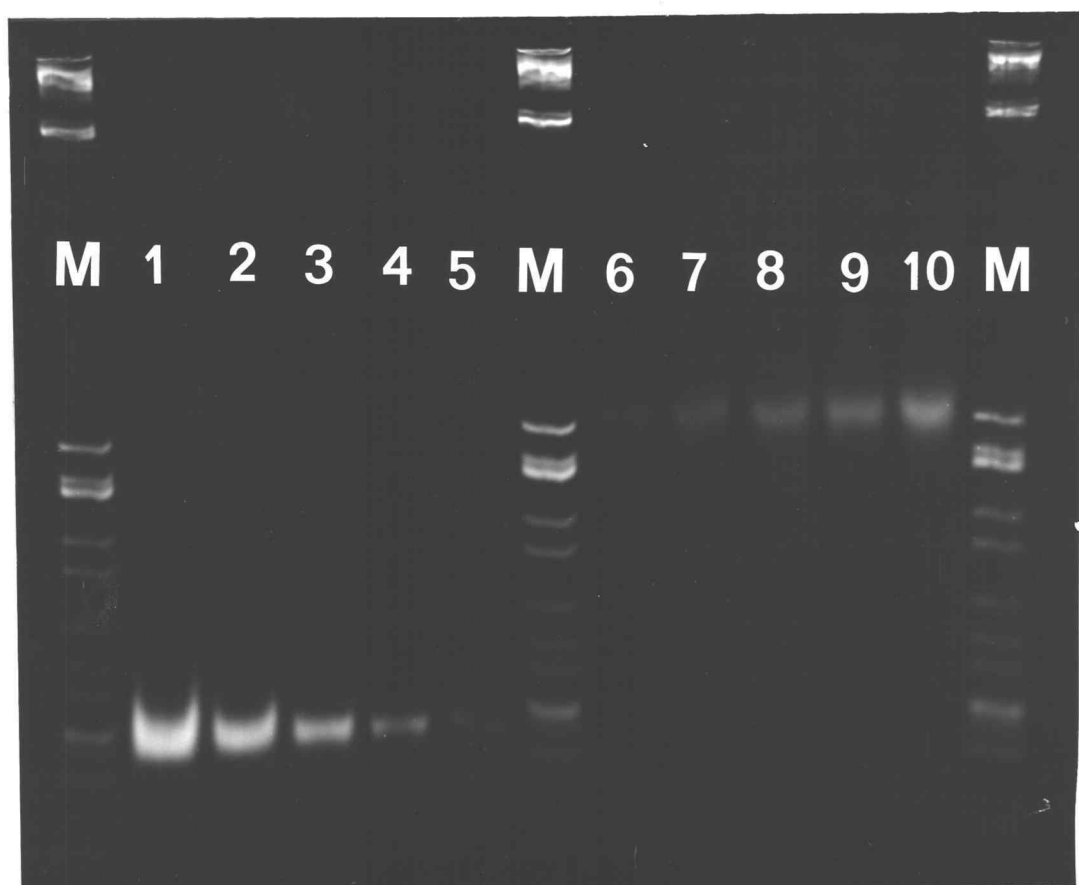


Figure I.1

Figure I.2. Electron micrograph of the chicken erythrocyte core particle preparation. Core particles were dialyzed into 0.25 mM EDTA, pH 8.0 and diluted to a final concentration of $1.0-5.0 \times 10^{-4}$ M bp ($A_{260} = 1-3$). The samples were absorbed onto carbon support films on copper grids. The grids were examined in a Siemens Elmiskop 102 microscope at 100,000 magnification with an accelerating voltage of 100 K volts.



Figure I.2

Figure I.3. Quantitation of double stranded internal cutting in particle preparation. Lanes 1-5 contain 5, 10, 15, 20 and 25 ng of DNA standards. Each standard was scanned with a laser densitometer and the area was integrated. A calibration curve of area versus ng was constructed from the standards. Lanes 7-12 contain 30, 50, 80, 100, 150 and 208 ng of core particle preparation. All sub-nucleosomal sized bands were scanned and integrated. The percentage of double-stranded cutting was determined from the ratio of the nicked material to the total amount of DNA loaded onto the gel.

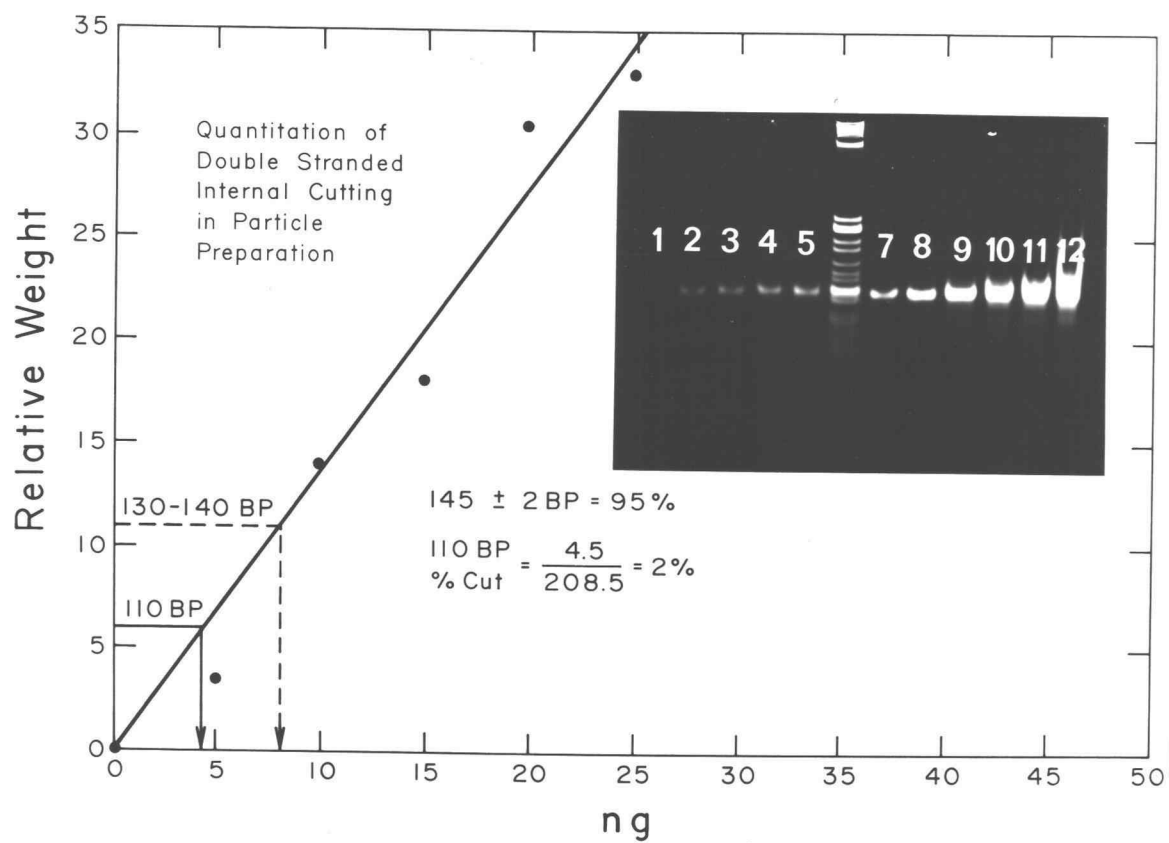
Figure I.3

Figure I.4. Coomassie-stained SDS-15%-polyacrylamide gel electrophoretic analysis of the protein components of the core particle preparation and whole chicken erythrocyte chromatin. Polyacrylamide gels were 0.8 mm thick containing 15% polyacrylamide (acrylamide: bisacrylamide 30:.8) in the separating gel and 6% acrylamide in the stacking gel. Lanes 1, 3, 5, 7, 9, 11 and 13 are successive increments of core particles containing 0.25 μ g, .50 μ g, 1.0 μ g, 2.0 μ g, 3.0 μ l and 5.0 μ g total protein. Lanes 2, 4, 6, 8, 10, 12 and 14 represent 3.12 μ g each of chicken erythrocyte whole chromatin. Samples from a core particle solution ($A_{260} = 1.0$) in 10 mM Tris, .1 mM EDTA, pH 8.0 were boiled in SDS sample buffer for 1 minute, cooled on ice and loaded onto an Idea Scientific minigel apparatus. Gel electrophoresis was performed at 4°C at 15 v/cm for 1 hour. The gels were stained with Coomassie blue according to the procedure of Laemmli (1970).

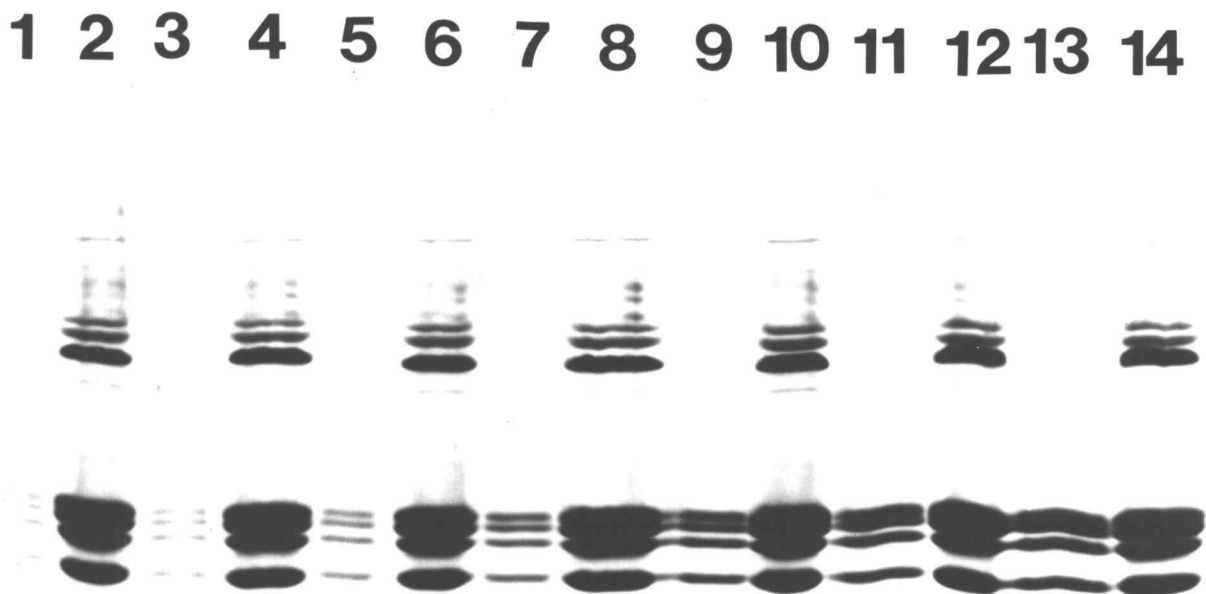


Figure I.4

Figure 1.5. Silver stained SDS-15% polyacrylamide gel electrophoretic analysis of the protein components of the core particle preparation and whole chicken erythrocyte chromatin. Gel is identical to Figure XIV except that it was silver-stained by the method of Wray et al. (1981).

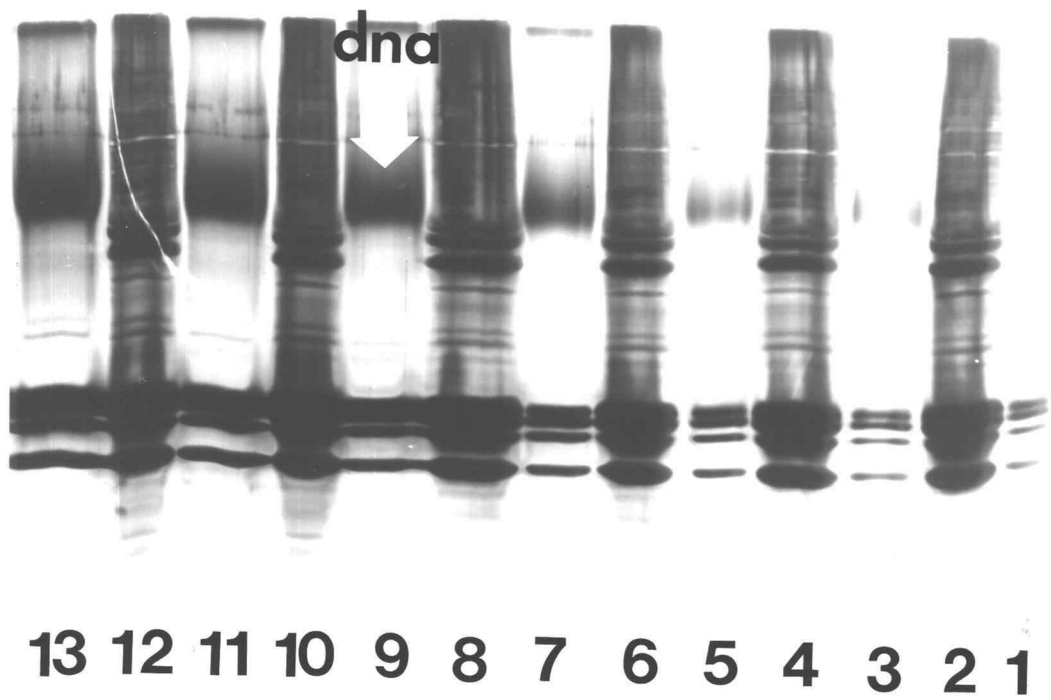


Figure I.5

Figure I.6. U.V. and C.D. thermal melting profiles for chicken erythrocyte DNA and core particles. The melting profiles were monitored by both U.V. absorbance change at 260 nm and molar ellipticity (C.D.) changes at 275 nm: (O) U.V. melting profile for chicken erythrocyte DNA, (O) U.V. profile for chicken erythrocyte core particles, (Δ) circular dichroism profile for the core particles. The buffer used for all experiments was 10 mM Tris, pH 8.0, 0.1 mM EDTA, and the concentration used for U.V. and C.D. melting was, respectively, 2.2×10^{-5} M (bp) ($A_{260} = .3$) and 5.3×10^{-5} M (bp) ($A_{260} = 0.7$). All measurements made in rectangular or cylindrical 1 cm quartz cell.

Figure I.6

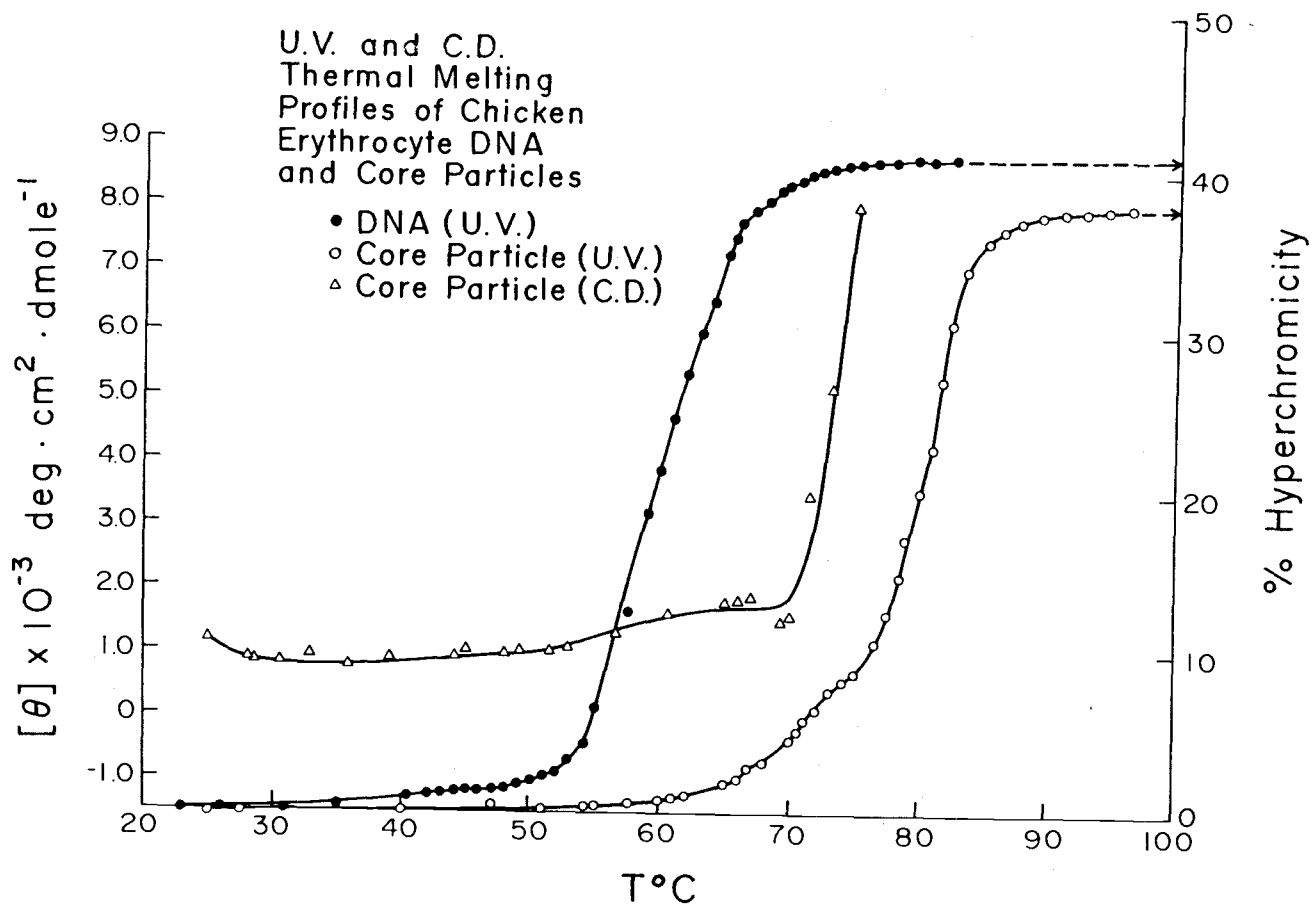


Figure I.7. The proton-decoupled 101.2 MHz ^{31}P -NMR spectra at 30°C for the chicken erythrocyte core particle and ~200 BP calf thymus DNA. A 0.5 ml sample in 5 mm tubes contained $1-2 \times 10^{-2}$ M phosphates ($A_{260} = 75-125$) was dialyzed into 10 mM Tris, pH 8.0, 0.1 mM EDTA. Spectra of 6000-8000 scans were obtained by fast Fourier transformation of 8192 time domain points, a 90° pulse, 1000 Hz spectral window, a 1 Hz exponential filter broadening and a 10 or 12 second pulse repetition time.

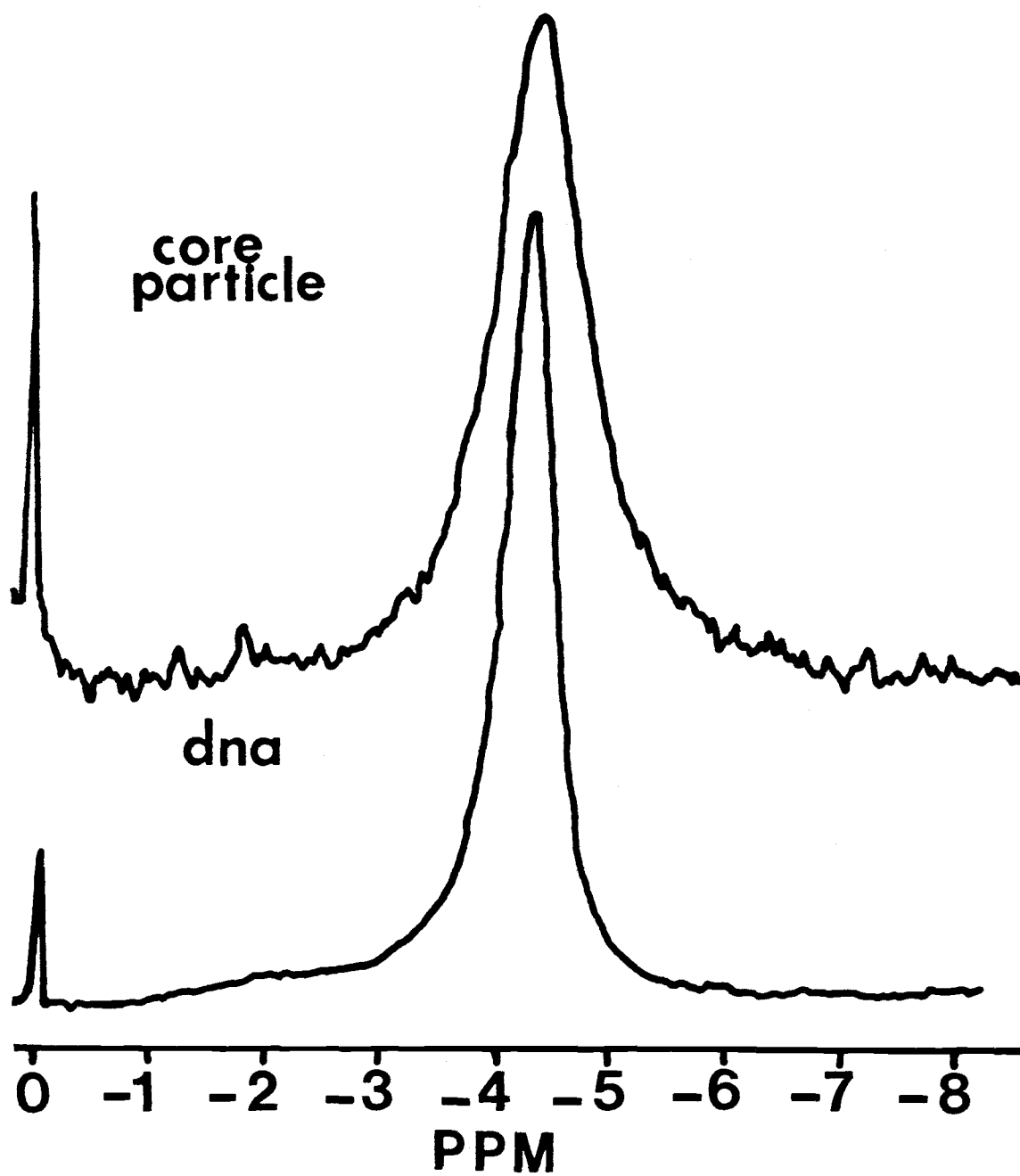


Figure I.7

CHAPTER II. THE BINDING OF ETHIDIUM BROMIDE CAUSES
DISSOCIATION OF THE NUCLEOSOME CORE PARTICLE

ABSTRACT

We have studied the interaction of ethidium bromide with the chicken erythrocyte core particle. The binding of ethidium bromide to the nucleosome core particle results in a step-wise dissociation of the core particle structure which involves the initial release of one copy each of H2A and H2B. Quantification of the dissociated DNA reveals that a critical amount of drug is required for the dissociation. Above the critical value, the dissociation is both time-dependent and reversible. Under the low ionic strength conditions used for these studies, dissociation was independent of DNA concentration and, therefore depended only on the amount of bound ethidium.

INTRODUCTION

Ethidium bromide is a polycyclic aromatic dye which binds by intercalation between the base pairs (BP) of DNA (Fuller and Waring, 1964; Waring, 1970; LePecq and Paoletti, 1967; Lerman, 1961, 1963, 1964). The binding properties of intercalating molecules are of particular interest since compounds of this class include mutagens (Hajuk, 1978), chemotherapeutic agents (Meienhofer and Antherton, 1977; Remers, 1979; Wilson and Jones, 1981) and carcinogens (Waring, 1981). Ethidium bromide binding to free DNA appears to follow the neighbor exclusion model (Crothers, 1968; McGhee and von Hippel, 1974) which predicts that binding of one dye molecule conformationally forbids binding at the adjacent site. Thus, at saturation, the number of sites excluded by each ligand is two. Ethidium bromide displays little base pair specificity (Müller and Crothers, 1975), but does prefer to bind at purine-pyrimidine (5'-3') sequences (Reinhardt and Krugh, 1978; Kastrup et al., 1978). Binding affinity of this dye to DNA is moderate, ranging from $\sim 10^4$ - 10^6 M⁻¹ depending on the ionic conditions (Quadrifoglio et al., 1974; Jones et al., 1980).

While extensive investigation has been undertaken to elucidate the base pair specificity and sequence requirements of many intercalating dyes to free DNA (Wilson and Jones, 1982; Waring, 1972), little is known about how chromatin structure modifies their binding, or how the binding affects chromatin structure. This is particularly surprising since the in vivo target of many mutagens and carcinogens appears to be nucleic acid, complexed into chromatin. At the level of the 30 nm fiber, ethidium bromide promotes the release of histone H-1 (Fenske et

al., 1975), an important packaging protein. Thus, ethidium binding has the potential to disrupt higher order structure. At the level of the 11 nm fiber, the binding of ethidium bromide derivatives (Cartwright et al., 1983) has indicated that the linker segment is preferentially bound relative to the nucleosome. This binding preference for the linker region, however, conflicts with the binding analysis of ethidium bromide to the nucleosome (Wu et al., 1980) which has indicated that the affinity to the nucleosomal form of the DNA is 10-fold greater relative to free DNA. In general, little agreement has been reached concerning dye binding affinity, cooperativity and structural consequences of intercalation (Wu et al., 1980; Erard et al., 1979) to the core particle.

Recently, ethidium bromide, its derivatives and other intercalating agents have been used to investigate the motional dynamics of the core particle (Wang et al., 1982; Hurley, 1982), to analyze nucleosome phasing in active genes (Benezra et al., 1986) and to identify torsional stress in the procaryotic and eucaryotic genomes (Sinden et al., 1980; Pettijohn and Pfenninger, 1980). In order to evaluate the results of such experiments, a clear understanding of the properties and the effects of intercalation on the nucleosome structure must be established.

We have studied the interaction of ethidium bromide with carefully prepared chicken erythrocyte core particles. The highly homogeneous preparation represents only the folded form of the nucleic acid, free from contamination with lengths of linker DNA (which has different properties). In this initial study, we report that a major structural

consequence of binding ethidium bromide to the core particle is a time-dependent dissociation.

RESULTS

I. Integrity of the Core Particle

Polyacrylamide gel electrophoresis (Figure II.1; A) of the native core particle (lane 1) and DNA extracted from the core particles (lane 3) showed an extremely homogeneous preparation which lacked both high molecular weight contamination and any significant subnucleosomal nicking. The DNA isolated from the core particle (lane 3), migrated as a single tight band. Plots of log molecular weight versus relative mobility (not shown) of the marker DNA fragments were used to determine the molecular weight distribution of the core particle preparation. The plot indicated that the core length ranged from 142 to 148 BP, and is therefore taken as 145 ± 3 BP. Our preparation displayed no trace of dimer or higher molecular weight oligomer. In addition, lane 1 displays no trace of free dissociated DNA or significant subnucleosomal fragments. The integrity of our core particle preparation was confirmed by sedimentation velocity and electron microscopy. Sedimentation velocity analysis determined the sedimentation coefficient of the intact cores in 10 mM Tris, pH 8.0, 0.1 mM EDTA to be 10.8 ± 0.2 S at 20°C, in excellent agreement with previous studies (Weischet et al., 1978; Tatchell, 1978). Electron micrographs of our core particle preparation in 0.25 mM EDTA, pH 8.0, revealed a core particle preparation which contained only spherical particles free from contamination with free DNA (Figure I.2).

Analysis of protein on standard Laemmli gels (Figure II.1; B), stained with Coomassie blue, demonstrated that our preparation (Lane

2) was extremely pure, lacking any significant amounts of non-histone proteins. We detected neither a trace of H1 or H5 nor degradation of any of the inner core histones H2A, H2B, H3 or H4. More sensitive staining of the protein gel with silver (not shown) confirmed the integrity of our inner core histones, but revealed minor contamination of H1, H5 and several non-histone protein bands. However, none of these minor bands is visible with Coomassie blue staining, and densitometer-trace calibration indicated that each of these bands were present at less than 0.2%. The circular dichroism spectrum displayed the characteristic features of native nucleosomes: a small negative peak at ~295 nm, a double peak exhibiting a maximum ellipticity of $1400 \pm 200 \text{ deg} \cdot \text{cm}^2 \cdot \text{mole}^{-1}$ at 282.4 nm and a zero crossover-point at ~270 nm. Inflection points of the thermal melting profiles in 10 mM Tris, 0.1 mM EDTA, pH 8.0, were in excellent agreement with previously reported results (Weischet, 1978; McGhee and Felsenfeld, 1980).

II. The Binding of Ethidium Bromide to the Nucleosome Core Particle

Results in Dissociation

Initial study of the effects of ethidium bromide on the core particles utilized gel electrophoresis. Examination of Figure II.1 shows that the native core particle and free DNA are well separated by low percentage polyacrylamide gel electrophoresis. The core particle band on these gels co-migrated with the 393 BP (Cfo cut pBR322) DNA marker. Detection of structural changes was monitored by altered mobility on a gel of the intact core particle band. Figure II.2 shows the results of the electrophoretic analysis. Lanes 1-12 represent

increasing input ratios of ethidium bromide to core particle bp, equilibrated for 15 hours after mixing. In the absence of drug (lane 1), we observed only a single band (band 1) which migrated near the 404 BP (Hpa II cut pBR322) marker DNA band as expected for the intact core particle. Increasing the input ratio to $R = 0.1-0.2$ (lanes 3,4) resulted in the appearance of a second, faster migrating band (band-2) which migrated between the 404 bp and 309 bp DNA marker bands. The presence of band-2 was observed at ratios above 0.10 and persisted even at high dye to BP ratios as high as ~ 1.0 . At input ratios above 0.2, we identified a third form (band-3) which co-migrated with deproteinized nucleosome-sized chicken erythrocyte DNA standards (lane 3; figure II.1A). Band-3 was tentatively assigned as free DNA. Between input ratios of 0.1-2.0 (lanes 3-12), the intensity of band-3 increased at the expense of both bands 1 and 2 until, at a ratio of 2.0, it was the major component. Thus, the gel analysis indicated that two structurally different forms resulted from binding of ethidium bromide to the core particle. One of those forms appeared to be free DNA.

The intensities of both band-2 and band-3 were enhanced when the samples were allowed to equilibrate at 30°C for longer periods of time. Figure II.3 displays the results of the electrophoretic analysis of a core particle/ethidium bromide complex, $R = 0.5$, separated at two times after mixing. Lane A represents the $R = 0.5$ complex immediately after mixing (time = 0 hours). The mixing plus the loading time was ~ 1 minute. The laser densitometer trace of Lane A revealed that most of the intensity for the complex was seen in band-1. A small amount ($\sim 7\%$) of intensity was also observed in

band-3. At time = 36 hours, however, the intensity distribution had changed significantly. Most distinctly, laser densitometer tracing of lane B revealed the presence of the intermediate, band-2, which was absent immediately after mixing. Additionally, we observed that the amount of free DNA increased, with increasing time. At time = 36 hours, the intensity of band-3 increased from 7% at time = 0 to 25%, representing a 3-4 fold increase. At 36 hours, it was also clear that band-2 and band-3 arose at the expense of the intact core structure (band-1) since the appearance of these bands was concomitant with a decrease in the intensity of band-1. At all ratios measured between 0.05 and 1.0, increased levels of band-2 and band-3 were seen relative to the time = 0 case. Upon equilibration at low ratios, band-2 was observed to form prior to any intensity in band-3. We concluded from the electrophoretic analysis that the binding of ethidium bromide to the intact core particle resulted in a time-dependent dissociation of the native structure to free DNA, first proceeding through at least one intermediate form.

Conclusive identification of bands 1, 2 and 3 is shown by 2-dimensional polyacrylamide gel electrophoretic analyses in Figure II.4. In the first dimension, a core particle/ethidium bromide complex, $R_I=0.3$, was separated on a 3.5% native core particle gel. As seen in Figure II.4, we observed bands 1, 2 and 3 in exact agreement with Figure II.2. Each band was cut from the gel and analyzed in the second dimension on an SDS-15% polyacrylamide standard protein gel (O'Farrell, 1975). Densitometer tracings of each protein band are included in the figure. As expected from its mobility on the gel, band-1 displayed the full complement of all four histone proteins in

equimolar quantities. Comparison with Fig. II.1 verified that this band represented the native core particle which contained 145 ± 2 BP of DNA and the histone octamer. Similarly, we identified band-3 as free chicken erythrocyte DNA. Two-dimensional analysis revealed that band-3, in the first dimension, migrated in an identical manner with purified nucleosomal chicken erythrocyte DNA (lane D; Figure II.3) and we observed no protein component (dimension 2) associated with this band. Finally, band-2 was identified as a DNA/histone complex which contained only 6 of the 8 histones. This form shall be referred to as the hexamer. In the second dimension protein analysis for band-2, all four histone proteins were present; however, histones H2A and H2B were clearly depleted. Laser densitometer tracing and integration of the protein peak areas showed the ratio of H2A+H2B area relative to H3+H4 area was equal to 0.5, indicating that only one H2A, H2B dimer was present in band-2. Thus, prior to complete dissociation, one copy each of histones H2A and H2B appears to be lost.

We conducted extensive controls on the gel system that we used. The amount of ethidium-induced dissociation was tested by varying the sample load, concentration, ionic strength, glycerol content and voltage. In all cases we determined that both the presence and degree of dissociation were not an artifact of the electrophoresis method. However, to further insure that dissociation was not gel-dependent, we analyzed the core particle-ethidium complexes by sucrose gradient centrifugation. As shown in Figure II.5, the sucrose gradient results are in excellent agreement with the gel electrophoresis results. Sucrose gradient analysis, again, showed the presence of only three distinct peaks. Scan 1 (peak-1) represents the native core particle

structure with no dye bound ($R_T=0$). In order to correlate each peak in the sucrose gradient with the gel electrophoresis results, we separated each gradient into 0.5 ml fractions and analyzed each fraction for both DNA and protein content. The results of the DNA gel electrophoresis corresponding to the central fraction of each peak (peaks numbered 1-4) can be seen at the bottom of Figure II.5. Peak #1, which had the fastest migration rate on the sucrose gradient, co-migrated with the 393 BP CFO cut pBr322 and was, therefore, assigned as the native core particle. Analysis for the protein component of peak #1 confirmed that all 4 histones were present in equimolar ratios (not shown). As we increased the ratio of ethidium to DNA base pair to 0.1, we observed the appearance of a second, more slowly migrating, component, peak #2. As seen in Figure II.5, the mobility of this peak was identical to the intermediate band seen in Figures II.2-II.4. Again, protein analysis in standard Laemmli gels (1970) confirmed that only 6 of the eight histone proteins were associated with DNA in this peak and the missing proteins were one copy each of H2A and H2B. Peak #2 was assigned as the hexamer. Finally, above a bound ratio of $v = 0.130$ (input ratio = 0.20), we observed increasing area in peak #3 until at $v = 0.35$ (input ratio = 2.0), peak #3 was the sole component on the gradient. As expected, the DNA corresponding to this peak co-migrated with free nucleosome-sized DNA on both the native polyacrylamide gels (3 and 4 bottom, Figure II.5) and on the sucrose gradients (top, Figure II.5). Peak #3 was assigned to be free 145 ± 3 BP DNA. The peak labeled "eth" in Figure II.5 was determined to be free ethidium. This peak was a red band on the top of the sucrose gradients and contained

neither a DNA nor a protein component. Ethidium has absorbance intensity at 280 nm, the monitor wavelength.

Ethidium bromide complexes with the core particles are prone to aggregation under suitable conditions. Aggregation is favored at high DNA concentrations ($> 7.8 \times 10^{-5}$ M BP) and is particularly apparent at high dye to BP ratios and higher ionic strength. We emphasize that both the hexamer and free DNA, bands-2 and 3, occur in the total absence of aggregation. However, quantification was limited to specific conditions. For the low ionic strength sucrose gradients, where the DNA concentration was very high ($4.0-8.0 \times 10^{-4}$ M BP), aggregation was observed at input ratios above 0.3. No aggregation was observed below this ratio. For the equilibrium dialysis and gel electrophoresis experiments, where the DNA concentration was usually low ($\sim 4 \times 10^{-5}$ M BP), no aggregation was observed in solution at any input ratio of ethidium bromide. However, when the complexes were analyzed by gel electrophoresis, aggregation could be detected at the top of the lane above $R_I = 0.5$ due to increasing amounts of free histone. Therefore, we have limited our quantitative analysis only to regions where no aggregation was observed on the gel, i.e., to DNA concentrations of $3.8-7.8 \times 10^{-5}$ M (A_{260} 0.5-1.0) and drug input ratios ranging from 0-0.5.

III. Quantification of Dissociation.

On an ethidium bromide-stained gel, the fluorescence intensity of an ethidium bromide complex with free DNA was usually greater than the corresponding complex with the core particle. As a consequence,

quantitative assessment of the amount of DNA produced at a particular ratio of dye could never be calculated from the fractional intensities of the three bands. We, therefore, quantified the amount of free DNA over a range of input ratios between 0-0.5 by two different electrophoretic methods. Method I involved a series of 6 accurately determined DNA standards which were electrophoresed through each gel. All standards, which migrated as tight bands, were scanned with a laser scanning densitometer and the area was determined by cutting and weighing the respective peaks. We next constructed a plot of peak area versus ng DNA from the peak intensities of the DNA standards. In the remaining lanes, quantitative volumes of ethidium bromide core particle complexes were loaded onto the gel. Since the DNA is well separated from the intact core particle and the hexamer, we could easily scan the free DNA band which appeared at each input ratio of ethidium bromide. The unknown amount of dissociated DNA was scanned and the area integrated by the same cutting and weighing procedure used for the standards. The integrated area of the unknown sample was determined by extrapolation to standard curve. The fraction of core particles which had dissociated was calculated by the ratio of free DNA to the known amount of core particle DNA loaded onto the gel. All measurements were made within the linear response ranges of both the film and the instrument systems used. The actual samples used in these experiments were taken from the sample cell in a three-chambered equilibrium dialysis apparatus. Thus, for every input ratio, we could directly determine the fraction of dye actually bound. Method II involved the use of end-labeled core particles. ^{32}P -5'-end-labeled core particles were mixed with unlabeled core particles at all input

ratios of ethidium bromide. The ethidium bromide/core particle complexes were separated on native gels and the gels were exposed to film. The autoradiograms were scanned with the laser densitometer and the relative population of each band could be directly determined by its fractional intensity. The results of a typical experiment are listed in Table II.1. We again emphasize that only ratios below 0.5 were quantified due to aggregation which occurred at higher ratios. We note that the total intensity is relatively constant in this range of input ratios and that the percentage population of the hexamer ranges from 7-17%. Since the end-labeling procedure produced a small amount of free DNA, the actual amount of ethidium-induced DNA was calculated by subtracting the amount of free DNA in the $R = 0$ lane from the total % free DNA calculated at each ratio.

The results of the % free DNA calculated from both methods are shown in Figure II.6. Figure II.6 shows the plot of % dissociation versus ratio of moles dye bound per moles BP (v). The amount of dissociation appeared to be dependent on the bound ratio of dye in a smooth, but non-linear manner. Extrapolation of the curve to zero dissociation indicated dissociation did not occur at the lowest level of ethidium bromide binding, but rather that a critical amount of the compound was required to be bound before dissociation began. This value, called v_c , was empirically determined to be $v = 0.06$. Below this ratio, we observed no dissociation by the gel electrophoresis method. Since the core particle length is defined as 145 BP of DNA, a $v = 0.06$ indicated that $\sim 9 \pm 1$ ethidium molecules were involved in the pre-dissociation binding. If we assume that ethidium bromide follows the neighbor exclusion principle, then we conclude that

pre-dissociation binding involves $\sim 17 \pm 2$ BP of core particle DNA. Above $R = 0.35$, dissociation was extremely sensitive to further addition of ethidium bromide. Extrapolation of the curve towards increasing bound ratio suggested that dissociation asymptotically approaches completion at about $R = 0.35$. Data were not analyzed at higher ratios because of aggregation at the top of the gel (see above).

DISCUSSION

We have carefully prepared homogeneous chicken erythrocyte core particles, free from contamination with linker DNA. When ethidium bromide, an intercalating dye, is allowed to form a complex with the folded, nucleosomal DNA, the result is a step-wise dissociation. We have demonstrated this dissociation by both gel electrophoresis and sucrose gradient centrifugation. We have also observed the dissociation in the analytical ultracentrifuge, but these results are more difficult to interpret due to the presence of free dye. Dissociation, at least at low concentrations, is fully reversible and, therefore, represents an equilibrium process.

The dissociation proceeds through at least one intermediate form, a particle containing 145 BP DNA and a histone hexamer. Since this particle is detected prior to any amount of dissociated DNA, we conclude that the initial loss of one copy each of H2A and H2B is an obligatory step in the dissociation process. If other intermediates are formed, such as one containing a histone tetramer, these structures are not kinetically stable for we have not been able to detect them on the time scale of our experiments. Extrapolation of the percent dissociation versus bound ratio curve (Figure II.6) to zero dissociation indicated that $\sim 9 \pm 1$ ($v = 0.06$) ethidium bromide molecules were the critical number required to be bound for dissociation to begin. In our estimation of v_C , we have made the assumption that the fractional population (f) of the core particles which binds the dye is 1.0. If the $f < 1.0$, then the correct value of v_C is v_C/f . If we assume that ethidium bromide follows neighbor

exclusion binding when bound to the core particle and that $f = 1.0$, then $\sim 17 \pm 2$ BP are involved in the pre-dissociation binding. This value is very close to the putative binding site of an H2A•H2B dimer (Richmond et al., 1984). This value is also close to a theoretically predicted (20 BP) number of sites available for initial binding of ethidium bromide to the core particle native structure (Schmitz, 1982). The approach of the percent dissociation curve to a limiting bound ratio also suggests that a limited number of sites are available for ethidium bromide binding to the intact structure.

The intercalation binding of ethidium bromide to free DNA has several effects. First, it unwinds the DNA helix by 26° (Wang, 1974). Thus, after ethidium binding, the normal plane to the base pairs are separated by 10° instead of the 36° found in the B-helix (Dickerson, 1983). Ethidium bromide intercalation induces changes in sugar pucker, glycosidic torsional angle and phosphodiester torsional angles in DNA and RNA (Tsai et al., 1977; Jain et al., 1977; Sobell, 1977). Thus, both the winding angle and conformation change as the result of complex formation. These changes produce a slight bending of the DNA helix towards the major groove (Sobell, 1977). In general, intercalation of planar molecules causes lengthening and stiffening of the helix (Lerman, 1961). If these effects hold for the core particle, it is not surprising that dissociation occurs. We conclude that stiffening of the helix accompanied by changes in the winding angle due to a minimum level of ethidium bromide binding prohibit the ability of DNA to bend around the histone octamer. We have observed that the binding of daunorubicin, an intercalator with quite different binding geometry and unwinding angle (12°) (Jones et al., 1980;

Fritzsche et al., 1982; Quigley, 1980) also induces dissociation of the core particle. The level of dissociation is increased relative to that caused by ethidium bromide (C. T. McMurray, unpublished results). Thus, dissociation may be an effect common to the intercalation mechanism. However, the exact process probably involves the sum of winding, conformational and steric factors which govern the binding ability of the DNA to the protein core. Therefore, each intercalator probably represents a slightly different case.

We suggest a few experimental consequences of dissociation. First, since dissociation leads to the presence of free DNA, which binds ethidium with a different affinity than do nucleosomes, binding isotherms must be corrected for the levels of free DNA present. To our knowledge, dissociation has never been considered in constructing Scatchard plots for ethidium binding to nucleosome complexes. Second, investigators attempting to measure motional dynamics of the core particle via an intercalating molecule, must exercise caution in describing the type of complex they are measuring. Since partial release of histones is produced, even at low ratios of dye to BP, such studies may reflect only the dynamics of a free DNA/ethidium complex tethered at one end, or even free DNA. Finally, the use of ethidium bromide to relax supercoils and to determine the linking number for nucleoprotein systems will require proof that nucleosome structure is maintained. It should be noted, however, that our results cannot necessarily be extrapolated to the effects of ethidium binding to long chromatin.

Table II.1

Calculated relative populations of octamer, hexamer, and free DNA
for ethidium bromide ^{32}P -core particle complexes at 30°C

Input ratio ^a	% octamer ^b	% hexamer	% DNA	Total area ^c
0	95	-	5	80.8
0.05	94	-	6	84.3
0.10	94	+ ^d	6	87.5
0.20	83	10	7	80.3
0.25	72	17	11	88.8
0.30	73	17	10	84.1
0.35	69	10	20	91.0
0.40	70	7	23	84.6

^aInput ratio = moles added ethidium bromide/moles DNA BP

^b% = (peak area/total area) x 100

^cTotal area = total area of scanned lane from autoradiogram of ^{32}P -labeled core particles at indicated ratios

^d+ indicates the presence of a hexamer band. Hexamer was detected as a slight shoulder on the octamer peak, but was not resolved enough to quantify.

Figure II.1. Results of the gel electrophoretic component analysis for the nucleosome core particles and the corresponding DNA.

A. Results of gel electrophoretic analysis for the nucleosome core particles (lane 1) and DNA isolated from the core particles (lane 3). Polyacrylamide gels were 1.0 mm thick containing 3.5% polyacrylamide (acrylamide: bisacrylamide 20:1). Lane 2 contains DNA molecular weight markers from CfoI cut pBr322. Lane 1 shows 30 ng of the native core particle in 10% glycerol, 10 mM Tris, pH 8.0, 0.1 mM EDTA. Lane 3 contains 50 ng of the DNA isolated directly from the core particles in standard Laemmli (1970) sample buffer. Gel electrophoresis was performed at 4°C at 10 v/cm for ~50 minutes. The gels were stained for 20 minutes with 1 µg/ml ethidium bromide.

B. Laemmli NaDodSO₄-15% polyacrylamide gel electrophoresis of the core (lane 2) and untreated chicken erythrocyte chromatin (lane 1). Polyacrylamide gels were 0.8 mm thick containing 15% polyacrylamide (acrylamide: bisacrylamide 30:.8) in the separating gel and 6% acrylamide in the stacking gel. Lane 2 contains 1.0 µg of total protein from our preparation. Lane 1 represented 3.12 µg of chicken erythrocyte whole chromatin. Samples from a core particle solution ($A_{260} = 1.0$) in 10 mM Tris, .1 mM EDTA, pH 8.0 were boiled in Laemmli (1970) NaDodSO₄ sample buffer for 1 minute, cooled on ice and loaded onto an Idea Scientific minigel apparatus. Gel electrophoresis was performed at 4°C at 15 v/cm for 1 hour. The gels were stained overnight with 0.25% Coomassie blue and destained in methanol:acetic acid according to the procedure of Laemmli (1970).

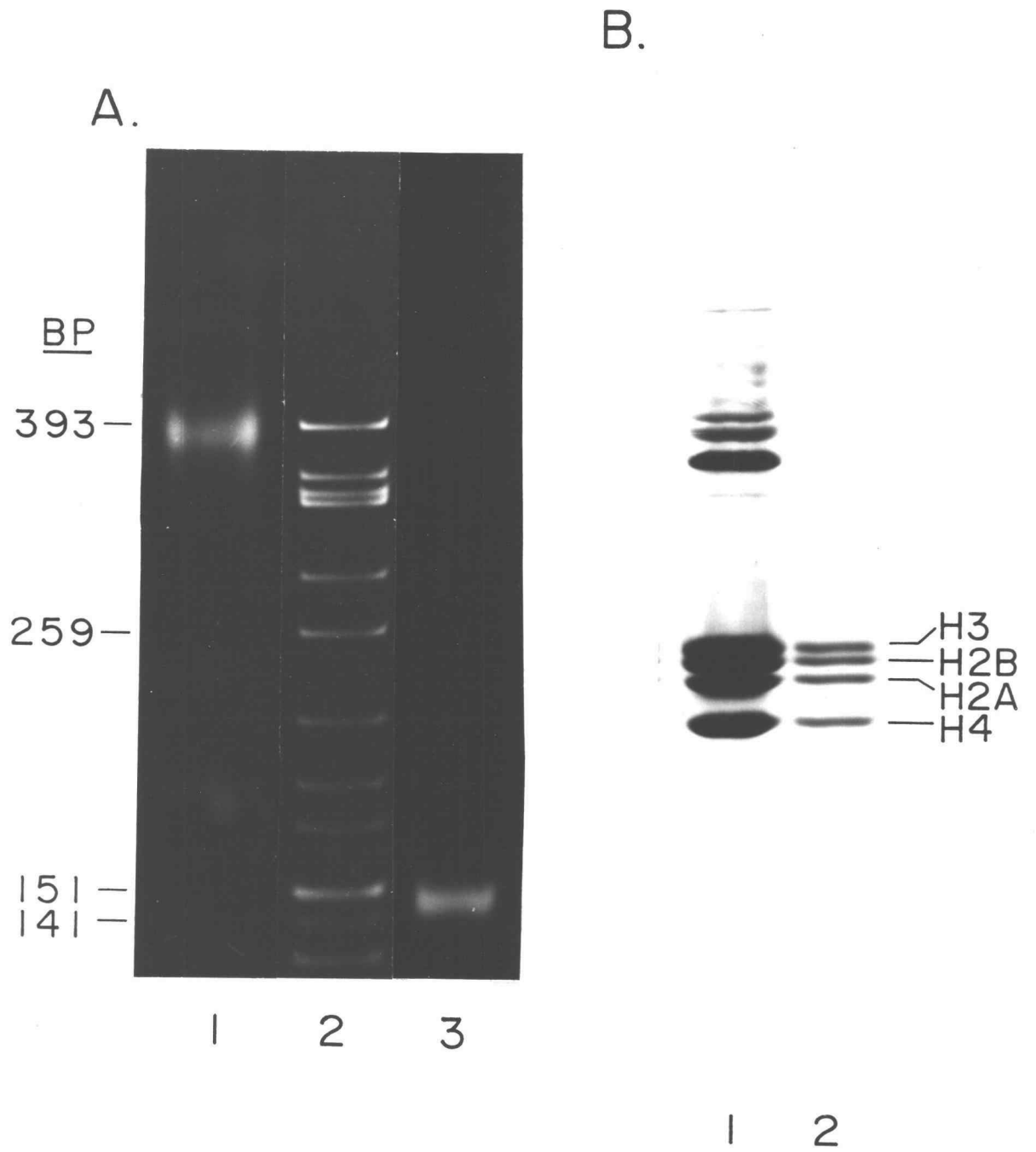


Figure II.1

Figure II.2. Results of the polyacrylamide gel electrophoretic analysis of the core particle/ethidium bromide complexes over a range of input ratios. Complexes were analyzed 15 hours after mixing. 1) R = 0; 2) R = 0.05; 3) R = 0.1; 4) R = 0.2; 5) R = 0.3; 6) R = 0.4; 7) R = 0.45; 8) R = 0.5; 9) R = 0.75; 10) R = 1.0; 11) R = 1.5; 12) R = 2.0, where R = moles added ethidium bromide per BP. Lanes marked M indicate Hpa II cut pBr322 DNA molecular weight markers. Bands 1, 2 and 3 represent the three products formed from the binding of ethidium bromide to the core particle and are discussed in the text. Each lane represents 250 ng of DNA. Complexes were analyzed on 1.0 mm, 3.5% native polyacrylamide gels (acrylamide: bisacrylamide, 20:1). Core particle DNA concentration was 3.8×10^{-5} BP and the buffer used for all samples was 10 mM Tris, pH 8.0, 0.1 mM EDTA. Gel electrophoresis was performed at 4°C at 10 v/cm for 50 minutes. The gels were stained for 10 minutes with 1 µg/ml ethidium bromide in H₂O.

Figure II.2

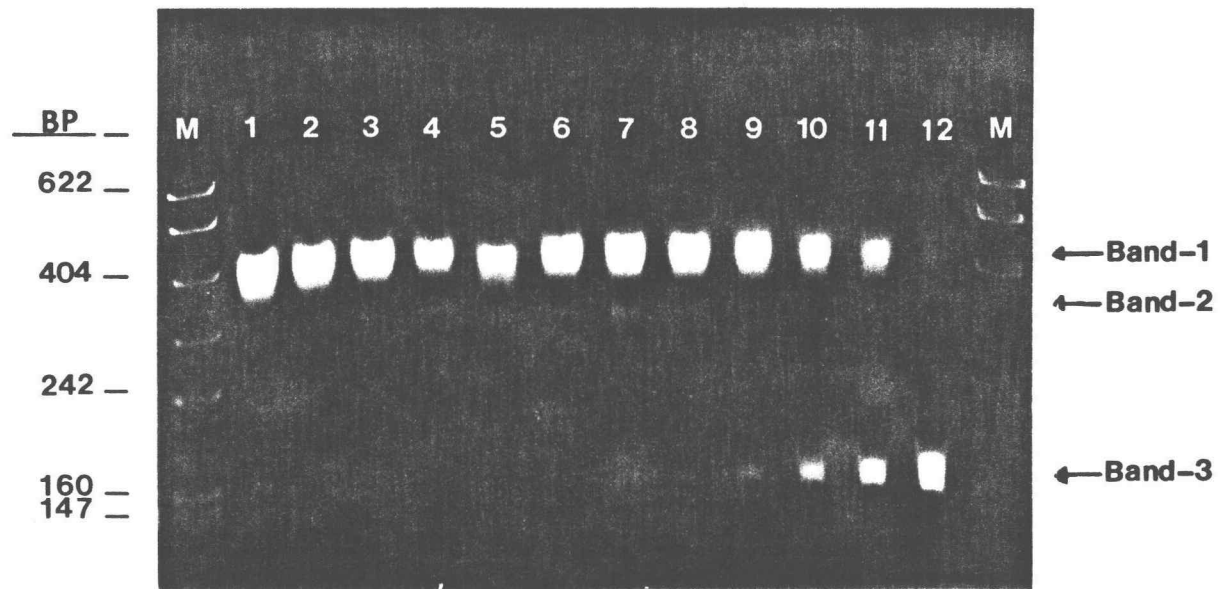


Figure II.3. Time-dependence of the step-wise dissociation of the core particle by ethidium bromide at 30°C. Top: At an input ratio of 0.5, the core particle/ethidium bromide complex was analyzed by 3.5% polyacrylamide gel electrophoresis. Lane A (time = 0) represents the core particle complex analyzed immediately after mixing (the mixing and loading time was ~1 minute). Lane B (time = 36 hours) represents the core particle/ethidium bromide complex equilibrated for 36 hours after mixing. M and D refer to CFO cut pBR322 DNA molecular weight markers and deproteinized 145 ± 3 BP chicken erythrocyte DNA standards, respectively. Bottom: laser densitometer tracing of lanes A and B.

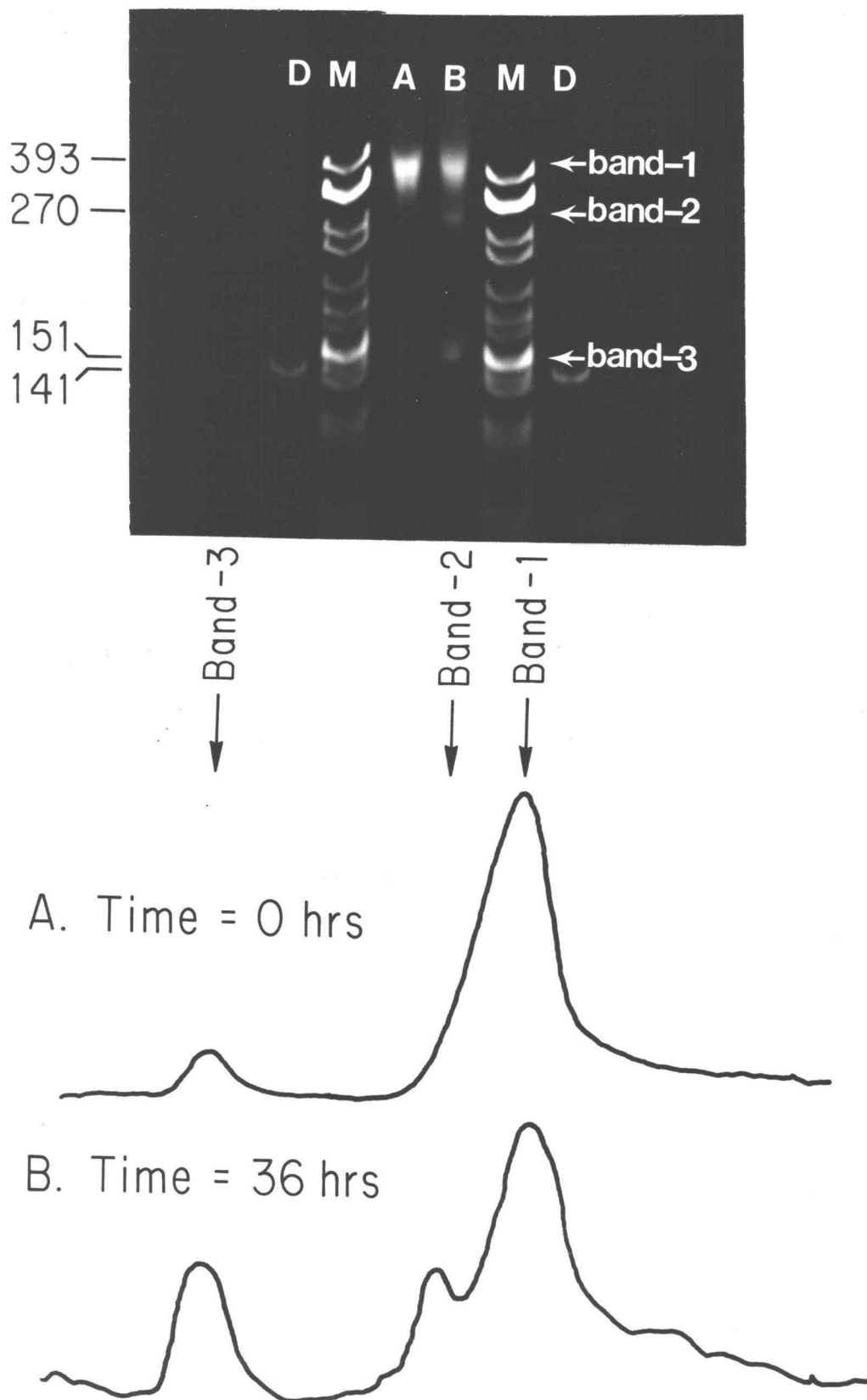


Figure II.3

Figure II.4. Results of the two-dimensional gel electrophoretic analysis of the core particle/ethidium bromide complex at an input ratio of $R=0.3$. The core particle complex was analyzed in the first dimension on a 1 mm, 3.5% native polyacrylamide gel (acrylamide:bisacrylamide 20:1). Gel conditions are identical as described in Figure XVIII. Band 1 is the intact core particle; Band 2 is the hexamer; Band 3 is free DNA. Each band was cut from the first dimension gel and sealed with agarose onto the top of a second dimension NaDodSO₄-polyacrylamide Laemmli (1970) protein gel. The protein gel was composed of a 15% separating gel and a 6% stacking gel. The excised bands were soaked for 5 minutes in O'Farrell's buffer (O'Farrell, 1975) before sealing onto the protein gel. Running conditions for the protein gel were as described in (Laemmli, 1970). The resulting protein bands were scanned with a Laser densitometer and the peak areas were integrated by a cutting and weighing procedure.

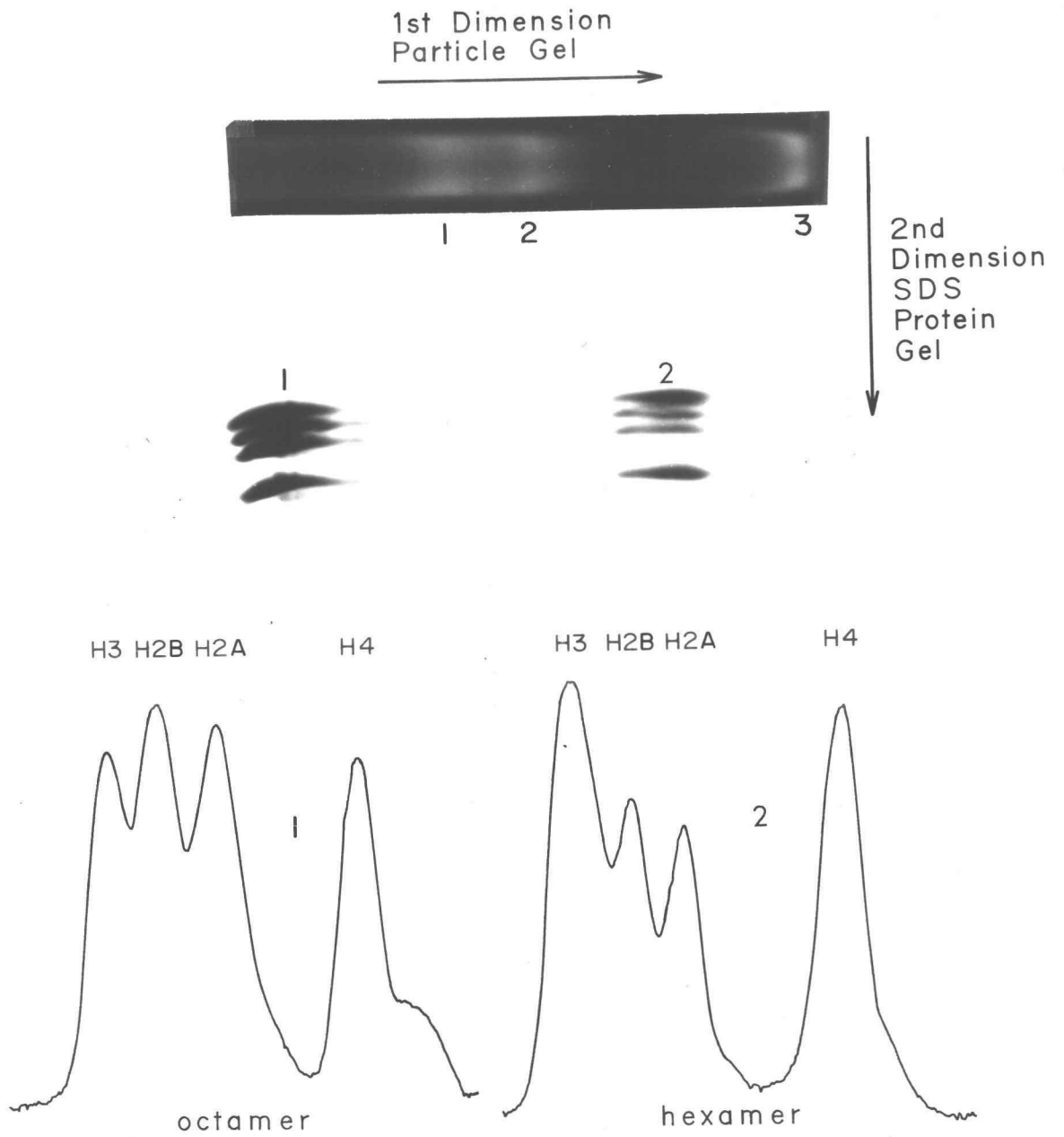


Figure II.4

Figure II.5. Results of the linear 5-20% sucrose gradient centrifugation of the ethidium bromide complexes with the nucleosome core particle and free DNA. Time = 0 indicates that the samples were loaded immediately after mixing and the arrow indicates the direction of migration. The v = moles ethidium bromide bound/mole BP; R = moles ethidium bromide added/mole BP. Top: $v=0$, $R=0$; $v=.072$, $R=0.1$; $v=.13$, $R=.20$; $v=.19$, $R=0.5$; $v=.35$, $R=2.0$. Peaks 1-4 correspond to the bands on the gel found at the bottom of the figure. Peak-1 is the intact core particle, peak-2 is the hexamer, peak-3 is ethidium-induced, dissociated free DNA and peak-4 is a free DNA/ethidium complex. The peak marked "eth" is free ethidium bromide found at the top of the gradient. Sucrose gradients and core particle stocks were buffered with 10 mM Tris, pH 8.0, 0.1 mM EDTA. The concentration of the core particle samples was 7.8×10^{-4} M BP ($A_{260}=10$). Gradients were centrifuged for 24-30 hours at 25,000 rpm in a Beckman SW40 rotor at 4°C.

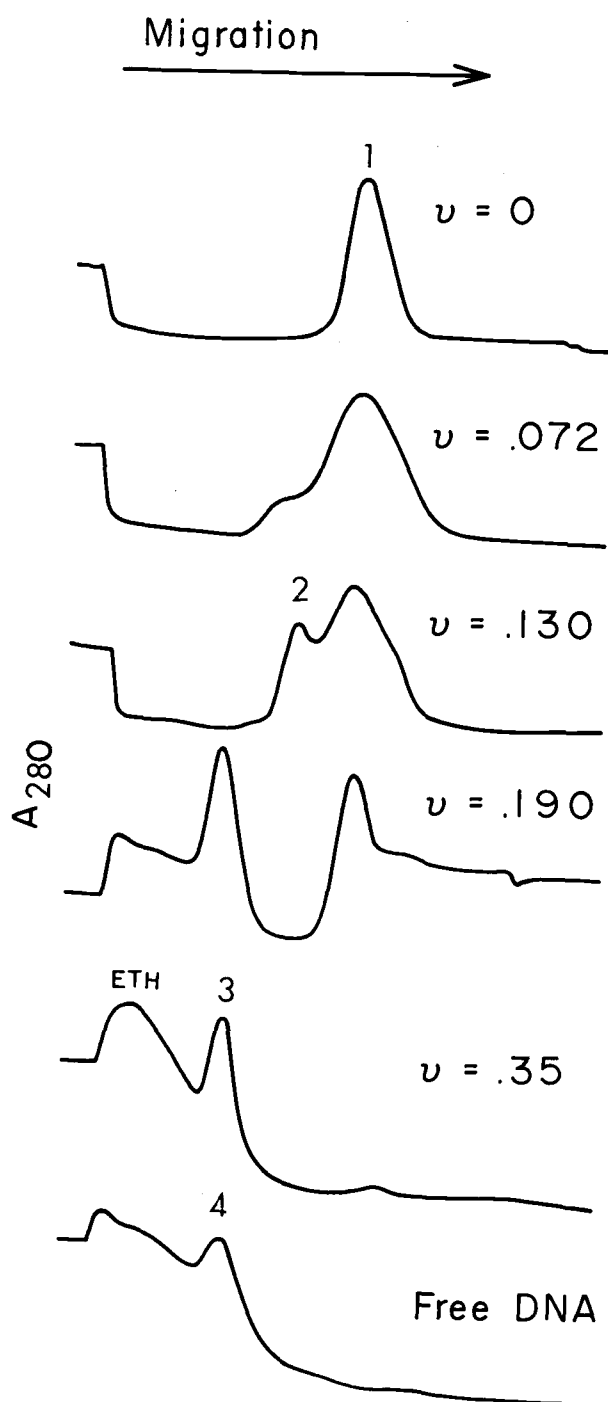


Figure II.5

Figure II.6. Plot of % dissociation versus bound ratio for several core particle/ethidium bromide complexes: (●) data obtained by Method I, ethidium-stained DNA calibration; (▲) data obtained by Method II, scanning of ^{32}P -end labeled core particles. The core particle concentration used for all measurements was 3.8×10^{-5} M BP. The buffer used for all measurements was 10 mM Tris, pH 8.0, 0.1 mM EDTA. The fraction of bound dye was determined for each sample by equilibrium dialysis as described in the Methods section.

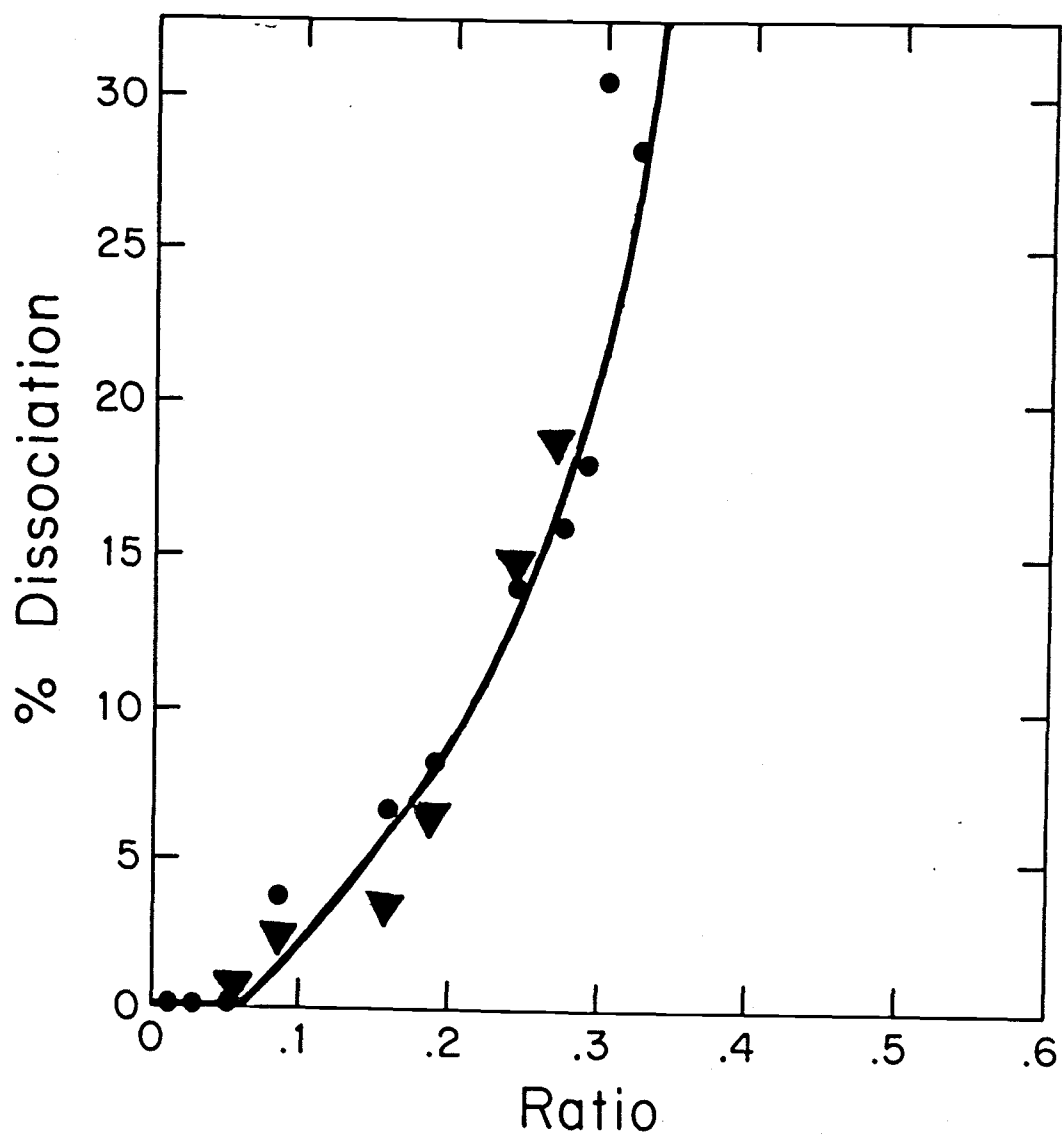


Figure II.6

Chapter III. A GEL ELECTROPHORETIC METHOD FOR

QUANTIFYING MULTI-COMPONENT EQUILIBRIA

ABSTRACT

We outline an electrophoretic method which we have used to reliably and accurately determine the level of free DNA that was dissociated from an intact DNA/protein complex. The method is rapid, sensitive and can be used as a general method to calculate multi-component binding equilibria for DNA, RNA, protein or DNA, RNA/protein complexes, where the components are often found in small quantities or the equilibria between components is not easily measured by other techniques. In this report, the amount of free DNA produced from the dissociation of the nucleosome core particle by the intercalating dye, ethidium bromide, was quantified from the integrated fluorescence intensities of a series of DNA standards. We have tested the method as a function of core particle DNA concentration, sample volume, ionic strength, glycerol content and voltage to insure that the gel method itself did not cause dissociation of the complexes. While we have used fluorescence intensity of ethidium-stained DNA bands as the standard curve for the method, the intensity of radio-labeled standard bands from autoradiography film will work equally well. We have applied the method to determine the amount of ethidium bromide bound only to the core particle at every input ratio of the dye, in the presence of another binding substrate, free DNA.

INTRODUCTION

Many biological processes are critically dependent on the association or dissociation of protein-protein or protein-nucleic acid complexes (Pabo and Sauer, 1984; von Hippel et al., 1984; Lewin, 1983). For example, in prokaryotes, the association of repressor molecules (such as the lac repressor) with the operator DNA blocks the transcription of polycistronic genes (Miller and Reznikoff, 1978; Jacob and Monod, 1961). If the binding of the repressor is too weak or too strong, the repressor function and cell metabolism are seriously impaired. In mammals, the oxygen binding ability of the blood is dependent on the association of the α - and β -subunits in hemoglobin (Perutz, 1970, 1978; Gelin and Karplus, 1977). Mutations which affect the binding affinity of these protein subunits often result in genetic disorders such as sickle cell anemia (Edelstein, S.J., 1975; Maniatis, T., 1980; Orkin and Kazazian, 1984). Thus, frequently, it is of interest to determine the binding constants and component equilibria which are involved in the formation or dissociation of biological complexes and it is useful to have methods which can measure such equilibria.

Recently, we have shown that the binding of a critical level of ethidium bromide, an intercalating dye, causes dissociation of the nucleosome structure to free DNA and histone proteins. The affinity of intercalating molecules for different forms of chromatin and to free DNA is of interest because it is thought to be the physico-chemical basis which governs the location of intercalating, chemical carcinogens within the genome. Since the binding constant of

ethidium bromide to free DNA was found to be higher than to nucleosome core particles (Erard et al., 1979; McMurray, unpublished results), it became necessary to determine how the dye was distributed in a multi-component equilibrium between free DNA and the core particles. The need to determine the distribution of the dye presented a second problem: since the dye itself caused the dissociation, how much free DNA was present at a particular input ratio of dye? Because the nucleosome and free DNA have similar absorption and emission properties, we were unable to determine the amount of free, dissociated DNA through the use of spectroscopic techniques which utilized those properties to distinguish between the two forms of nucleic acid. In addition, we were unable to quantify the amount of free DNA produced from the binding of ethidium by gentle separation techniques, such as sucrose gradients or columns, since the presence of the aromatic dye strongly absorbs light in the U.V. region. However, since the core particle and free DNA had different electrophoretic mobilities, the two forms of nucleic acid were well separated by polyacrylamide gel electrophoresis. In this report, we outline an electrophoretic method which we have used to reliably and accurately determine the level of dissociated DNA in our complexes. We have tested the method as a function of core particle DNA concentration, sample volume, ionic strength, glycerol content and voltage to insure that the gel method itself did not cause dissociation of the complexes. Additionally, we have applied the method to determine the amount of ethidium bromide bound only to the core particle at every input ratio of the dye, in the presence of another binding substrate, free DNA. We feel that the gel method is

generally useful as a technique for calculating biological equilibria involving proteins, RNA and DNA, where the components are often found in small quantities and the equilibria between components is not easily measured by other techniques.

RESULTS

I. Selection of a gel system.

Figure III.1A shows the effect of binding ethidium bromide at increasing ratios on the nucleosome core particle. The binding and intercalation of ethidium results in the step-wise dissociation of the core particle to free DNA, passing through one intermediate form (McMurray and van Holde, 1986). The intermediate has been identified as the hexamer, a particle containing 145 bp of DNA and only six of the eight histone proteins, missing 1 copy each of H2A and H2B (Figure 1C). The intact core particle, the hexamer and free DNA are seen in Figure III.1A as band-1, 2 and 3, respectively. In our system, we were interested in the dissociation process; thus, we wanted to resolve the intact histone/DNA complex in the nucleosome from the free ethidium-induced dissociated DNA component (145 bp). Since our DNA length was small and the intact nucleosome differed in both shape and charge from free DNA, we selected a low percentage polyacrylamide gel system which utilized a low acrylamide/bis-acrylamide crosslinking ratio. The lowered crosslinking ratio allowed the complex to remain intact while the use of the polyacrylamide afforded the necessary degree of resolution. Figure III.1A shows the relative mobilities of the intact complex and free DNA on Tris-buffered 3.5% polyacrylamide, 1.0 mm minigel with an acrylamide/bis-acrylamide crosslinking ratio of 20:1. The 145 bp DNA migrated as a single tight band which co-migrated between the 141 bp and 151 bp Cfo-restricted pBr322 DNA marker bands. The intact core particle band which had reduced

mobility relative to the free DNA migrated as a single tight band near the 393 bp DNA marker band. The moderate ionic strength of the gel ($\text{Na}^+ = 40 \text{ mM}$) resulted in no observable dissociation of the intact complex and afforded excellent resolution between the two forms of the nucleic acid. The core particle band and free DNA are well resolved by two other gel systems which we examined, but found to be more difficult to use. The low ionic strength agarose/polyacrylamide gels described by Garrard (1977) resulted in good resolution, required short running times but the matrix congealed very quickly. When pouring a series of vertical slab minigels, gels were often discarded because the gel matrix congealed before the combs were properly placed. The low ionic strength glycerol-containing polyacrylamide gels described by Garrard (1979) or Albright et al. (1980) also yielded good resolution, but we found these gels relatively difficult to work with and required long periods to run (7-10 hours). Neither of the low ionic strength gel methods produced better results than the use of simple, native low cross-linking ratio gels which we used. Regardless of the type of gel, we did find that a critical factor in maintaining the integrity of the nucleo-protein complex was the presence or absence of tracking dye. At the concentration of bromophenol blue used in standard sample tracking buffers (.25%), the effect of including bromophenol blue directly to the sample caused the loss of histone protein which resulted in the formation of a band with faster mobility than the intact core particle. Analysis of the protein component also identified this band as the hexamer (Figure III.1C). This loss of histone proteins was especially apparent in the non-glycerol containing gels. To avoid the effects of adding

bromophenol blue, samples prepared for electrophoresis were always diluted with tris-buffered 20% glycerol, and tracking dye was always loaded into a separate well to monitor the gel mobility.

II. Calibration of DNA standards and quantification of the amount of dissociated DNA.

The amount of free DNA produced from the dissociation of the nucleosome core particle by the intercalating dye, ethidium bromide, was quantified from the integrated fluorescence intensities of a series of DNA standards. Because it was necessary to determine the intensities with extreme accuracy, the DNA standards were first used to calibrate the linear response range for the set of experimental conditions, i.e., the intensity range of the standards, the particular filter type used and the exposure time of the film. We electrophoresed a series of DNA standards, ranging from 5 nanograms to 10 micrograms, on the native gel system which we used. The gels were stained with ethidium bromide, photographed with a 3 minute exposure time and the negatives were traced with a laser-scanning densitometer. The integrated area of each standard was determined by cutting and weighing the respective peaks. The results of the calibration are shown in Figures III.2. For Type 55 Polaroid film with a red filter, the plot of integrated area versus ng of DNA indicated that the linear response range of the film corresponded to the fluorescence intensity produced from DNA standards in the 5-35 ng range. As shown in Figure III.2A, the areas above the 35 ng standards (seen as broken line) were not proportional to the amount of DNA present in the band. Thus, only

standards from 5-30 ng were used for quantitative purposes. Since it was the most intense, we used the 30 ng DNA band to determine the linear range of exposure time for the film. The integrated area from film exposure times, ranging from 30 seconds to 10 minutes, were plotted versus time in Figure III.2B. We determined that above 3 minutes (broken line), the film became saturated and no longer fairly represented the amount of DNA present in the band. For all quantification of dissociated DNA, an exposure time of 2.5 minutes was generally used.

To determine the amount of free DNA produced from the core particles at every input ratio of ethidium bromide, we extrapolated the amount of dissociated DNA in the sample to a standard curve constructed from the integrated area of six accurately determined DNA standards. Figure III.3A shows the results of a typical gel electrophoresis experiment and Figure III.3B schematically depicts the quantification method. On every gel, lanes 1-6 contained the DNA standards of 30, 25, 20, 15, 10 and 5 ng. All standards, which migrated as tight bands, were scanned with a laser densitometer and the integrated area was determined by cutting and weighing the respective peaks. Simple least squares linear regression analysis of the six standards yielded the best-fit equation, which was used to determine the unknown dissociated DNA in the samples. We always included at least six standard points in the area versus ng plot to insure the statistical significance of the fitted equation. In the remaining lanes on the gel, quantitative volumes of core particle/ethidium complexes were loaded and separated. The unknown amount of DNA present in every sample was scanned and the integrated

area was determined by the same cutting and weighing procedure that was used for the DNA standards; the areas of dissociated DNA were converted to ng DNA through the use of the standard curve. The fraction of core particles which had dissociated was calculated by the ratio of free DNA in the sample to the known amount of core particle DNA loaded onto the gel. From the 30 ng linear intensity limit, we were able to estimate the amount of sample to load into each well for a particular input ratio. If initial experiments indicated that the fractional dissociation (f) in a sample was 0.30, then the amount loaded into a lane was maximally 30 ng/ f . Usually, at least two different sample volumes of the same input ratio were loaded onto every gel and the average dissociation value from these loadings were reported per experiment. The results from three such experiments, which utilized three different preparations of core particles, are shown in Table III.1. When the average value of several loadings were reported per experiment, the results were reproducible with a standard deviation of 1%-3%.

III. Controls.

To insure that the dissociation which we observed was induced by the binding of ethidium and not an artifact of the gel, we conducted extensive controls on the gel system that we used. We quantified the % dissociation of the core particle at various input ratios of ethidium bromide as a function of sample concentration, sample load, glycerol content in the gel, gel ionic strength and voltage. The results are summarized in Figures III.4 - III.5 and in Table III.2.

A. Concentration dependence. Figure III.4 shows the laser trace of a dissociated DNA band from the core particle/ethidium complex, at input ratio $R = 0.4$, as a function of sample concentration. Various amounts of core particle stock were added to ethidium bromide solutions such that the final concentration of core particle DNA ranged from 3.8×10^{-5} M (bp) to 7.6×10^{-4} M (bp), a 20-fold range in concentration ($A_{260} = 0.5-10$). As can be seen in Figure III.4, the amount of dissociation is close to 15% at or below a concentration of 7.8×10^{-5} M (bp). Above this concentration, however, the amount of dissociation which we detect on the gel is nearly tripled, but remains constant at all higher DNA concentrations that we tested. We concluded from this control that concentration did have an effect on the amount of dissociated DNA in a complex way. Either a DNA-mediated mechanism for dissociation occurred at concentrations above 7.8×10^{-5} M or the gel artifactually produced dissociation at high concentrations of core particle complexes. Since the level of dissociation was higher at high DNA concentrations, but remained constant over a range of those concentrations, we concluded that the electrophoretic method could induce artifactual dissociation at high concentration of the complex and, consequently, the core particle/ethidium complexes were analyzed only at or below a concentration of 7.8×10^{-5} M (bp).

B. Sample volume dependence. Figure III.5 shows the effect of varying the sample volume for the intact core particle and a core particle/ethidium complex, input ratio of $R = 0.4$, at constant core particle DNA concentration (7.8×10^{-5} M) on a 1.0 mm polyacrylamide

minigel. For the intact core particle, loading volumes from 0.5 to 8 μ l resulted in no observable amount of free DNA (Figure III.5A). We were unable to detect any dissociated DNA band at any volume tested from 0.5-20 μ l. Similarly, for the core particle/ethidium bromide complex, varying the sample load from 0.5-8.0 μ l had no effect on the amount of free, dissociated DNA found at any ratio tested. Figure III.5B shows the results for the complex at a ratio of $R = 0.4$. As can be seen in the figure, the integrated area of the scanned DNA band is linearly related to the sample volume loaded into the well. The area of the 8.0 μ l load is almost exactly 8 X's the area found in the 1.0 μ l load. We concluded that the amount of dissociation detected on the gel for both the intact core particle and the core particle/ethidium complexes were independent of the sample volume loaded onto the gel.

C. Dependence of dissociation on gel ionic strength, glycerol content and running voltage. The core particle/ethidium complexes were further tested as a function of the gel matrix conditions and the gel running conditions to insure that no dissociation was artifactually produced as a function of the gel conditions. The results are summarized in Table III.2. We have found that neither the presence nor the extent of dissociation was affected by any of the conditions which we tested at any ratio. The same amount of ethidium-induced dissociation of the core particle was detected independent of gel ionic strength from 4-50 mM. We tested 4 types of low ionic strength polyacrylamide gels which varied in cross-linking ratio, % acrylamide, the presence of glycerol and the presence of agarose. In all cases, the same amount of ethidium-induced

dissociation resulted, independent of the gel type. In addition, the extent of dissociation was not affected by increasing the ionic strength of the gel to 40 mM. Finally, we detected no voltage dependence on the amount of ethidium-induced dissociation of the core particle. We measured the amount of ethidium-induced dissociation at 50, 100, 150 and 300 volts (5, 10, 15 and 30 volts/cm) with no observable difference in dissociation levels. In some cases, (data not shown) the gels were started at low voltage (~50 V) until the bands had entered the gel and completed at a running voltage of 150-250. In all cases, no effect of voltage on the ethidium-induced dissociation was observed. We concluded from the controls that the gel method itself caused no artifactual dissociation of the core particle/ethidium complexes and that the method could be used to calculate accurate levels of free DNA and equilibrium constants for the ethidium-induced dissociation process.

APPLICATION

Correction of the % dissociation versus bound ratio curve for the amount of ethidium bromide bound to the free DNA. The results of the % dissociation versus input ratio (Table III.1), as determined from the gel quantification method, are plotted in Figure III.6. Above the critical ratio of $v = .06$, the dissociation appears to be linearly related to the concentration of dye up to 0.45. To determine the actual bound ratio, samples were taken from the sample chamber of an equilibrium dialysis apparatus. Thus, for every input ratio of ethidium bromide, we could directly determine the concentration of free dye (C_F) by measuring the absorbance of the buffer chamber. The C_F was converted to moles, and the total moles of bound dye $m_B(\text{total})$ was determined by

$$m_F = C_F \times \text{cell volume (buffer + sample)} \quad (3.1)$$

$$m_B(\text{total}) = m_I - m_F \quad (3.2)$$

(B = bound, I = input, F = free)

Alternatively, spectrophotometric titrations were used to calculate $m_B(\text{total})$. In this case, the extinction coefficient in the presence of the nucleic acid, E_{app} , was measured by absorbance and the fraction of total bound dye (F_B) was calculated by

$$F_B = (E_{free} - E_{app}) / (E_{free} - E_{bound}). \quad (3.4)$$

The total moles of bound dye, $m_B(\text{total})$, was calculated by

$$m_B = F_B \times m_I. \quad (3.5)$$

In both cases the bound ratio was calculated by

$$v_B = m_B(\text{total}) / \text{moles DNA bp.} \quad (3.6)$$

While the % dissociation values and bound ratios were accurately measured, the bound ratios calculated directly from spectroscopic measurements represented the sum of the ethidium bound to all forms nucleic acid present in solution. Since the ethidium binding to the intact core particle produced two other forms of nucleic acid, the hexamer and free DNA, any dye bound to the free DNA after dissociation did not contribute to the dissociation of the intact core particles. Thus, it became necessary to measure the distribution of the bound dye at every input ratio, i.e., the number of moles bound to the core particle, called $m_B(\text{core})$, and the number of moles bound to the free DNA, $m_B(\text{DNA})$. Since we were interested in the dissociation process, the $m_B(\text{core})$ values which we measured were defined as the sum of the hexamer and the intact particle. The values for v_{core} and $m_B(\text{core})$ were determined by the method shown in Figure III.7A.

Since the binding of ethidium bromide to free DNA is initially 100 times stronger than to the intact core particle (see Chapter 5), we made the assumption that the dye would preferentially bind to free DNA, when present, even if the dye was initially bound to the core particle. Thus, based on the measured binding constant ($K_{\text{DNA}} = 1.0 \times$

10^6 ; $K_{\text{core}} = 2.2 \times 10^4$), we reasoned that a good approximation of the number of moles of DNA-bound ethidium could be determined by measuring the amount of dye bound to the dissociated DNA in the absence of the core particle. Using the % dissociation values from the gel quantification method, we determined the concentration of free DNA at every input ratio of ethidium bromide. We, next, made an independent series of DNA solutions which corresponded to the dissociated free DNA concentration measured in every sample and added the total moles of ethidium bromide at that input ratio. The absorbance was measured and we calculated the apparent extinction coefficient in every DNA sample. The fraction of bound ethidium to DNA, $F_B(\text{DNA})$, was calculated as in equation 3.4, and the moles of dye bound to the DNA component alone was calculated by

$$m_B(\text{DNA}) = [F_B(\text{DNA}) - (V_C)(F_B(\text{DNA}))] \times m_{\text{bound}}(\text{total}). \quad (3.7)$$

Since the critical ratio of dye bound to the DNA component was present when the DNA was still an intact particle, this value was subtracted from the $m_B(\text{DNA})$ expression. Finally, the $m_B(\text{core})$ was calculated by

$$m_B(\text{core}) = m_B(\text{total}) - m_B(\text{DNA}). \quad (3.8)$$

The plot of dissociation versus V_{bound} (Figure III.7B; A) and the corrected V_{core} (Figure III.7B; B) are shown in Figure 7B and listed in Table III.3. In contrast to Figure III.6, the % dissociation of the core particles appears related to the bound ratio in a smooth but

non-linear manner. In both bound ratio plots, the curves asymptotically approach a limiting ratio of ethidium bromide, suggesting that only a limited number of sites in the intact structure are available for binding. For the total bound ratio (A), the curve approaches infinite slope at $R = 0.35$. In the corrected plot, v_{core} (B), the value is more accurately determined to be $R = 0.23$. The corrected values of v_{core} were used in further analysis to calculate ethidium-induced dissociation constants for the core particle and the association constants of ethidium bromide to the core particle, corrected for the presence of free DNA (see Chapter 5).

DISCUSSION

We have described a gel electrophoresis method which we have used to quantitatively determine the levels of free DNA that were dissociated from an intact DNA/protein complex. The method is rapid, sensitive and can be used to calculate multi-component binding equilibria for DNA, RNA, protein or DNA, RNA/protein complexes providing the correct gel system is used and the equilibrium is not perturbed during the separation process. The success of the method depends only on three criteria: the selection of an appropriate gel system which can resolve the components, usage of the linear intensity range of the photographic system and good analytical technique. While, in this report, we have used fluorescence intensity of ethidium-stained DNA bands as the standard curve for the method, the intensity of radio-labeled standard bands from autoradiography film, will work equally well. The use of gel electrophoresis to determine binding constants and binding equilibria has several advantages.

1. Sensitivity. The use of common gel detection methods, such as ethidium bromide staining, autoradiography, silver staining, Coomassie blue staining, etc., allows the detection of small quantities of material. Thus, gel electrophoresis can be used to detect the components and to calculate the equilibria in biological complexes for which the components are frequently present only in small amounts. Since the lower limit of the detection method for both DNA and proteins is usually the sub-nanogram level, the gel electrophoresis method has the potential for quantifying biological equilibria in vivo, without the necessity to isolate or purify the components. The

method can also be used for in vitro experiments where very high sample concentrations are required. We have used the gel method to analyze the association state of DNA/protein complexes present in samples used for experiments such as light scattering or nuclear magnetic resonance. Since physical techniques always measure an average parameter value for the sample, the accuracy of the physical measurement is dependent on the homogeneity of the sample. Especially in the case of reversible biological complexes, it is important to establish the state (aggregation, dissociation, etc.) of the complex as a function of a particular experimental condition (ionic strength effects, ligand binding experiments, etc.). Thus, in most cases, it is necessary to combine the physical measurement of a complex with a technique capable of resolving the components of the complex so that a correlation can be drawn between the state of the sample population and changes in the measured physical parameter. The gel electrophoresis method is sensitive to a wide range of sample concentrations and potentially has no upper limit range, providing the sample is analyzed on the gel under conditions which do not cause artifacts.

When measuring the association or dissociation of a biological complex, the gel electrophoresis method is sensitive in another way. In our system, because a sample volume is selected such that the fluorescence intensity of the band of interest is always in the 5-30 ng linear range, the detection of even a miniscule amount of dissociation had the same signal as a large amount of dissociation. Few techniques have this advantage. Thus, the gel method is capable of detecting components with large association constants or small

dissociation constants. This sort of sensitivity is particularly useful in fitting cooperative binding curves which depend critically on the ability to detect low levels of components.

2. Versatile. In addition to using common staining techniques such as ethidium bromide, the method can be used equally well with radiolabeled material. When using labeled material, however, the activity of the standards should correspond to a known concentration range of the standard and the specific activity of the standard and the unknowns must be identical. For radio-labeled material, the calibration of the autoradiographic film and exposure time will be the same as those shown in Figure 2. Since all radiolabeled components will have equal intensity, the maximum unknown sample volume will be the same as the most intense standard.

3. Rapid, reliable, easy to use. In our system, we used only simple native gels which retained the association properties of the native nucleoprotein complex. This type of gel is easy to make, easy to use and requires only short running periods. We disfavor the use of glycerol containing gels for measuring equilibrium constants and the levels of associating/dissociating components since the addition of glycerol changes the dielectric constant of the medium and may change the association/dissociation properties of biological complexes. Finally, because the series of standards are applied to every gel, the standards serve as an internal control. Since the results of any individual experiment are always compared internally, slight changes in the conditions (such as variation in exposure time) have no effect on the quality of the data, as long as, the linear range is maintained.

4. Useful for biological complexes where the equilibria cannot be monitored by other methods. Since the electrophoretic method exploits mobility as the detection parameter, it can be useful in the measurement of biological complexes when the association or dissociation cannot be monitored by spectral changes. In our case, the dissociation of the core particle complex to free DNA results in small spectral changes, but could not be monitored spectroscopically due to interference from the bound ligand. In addition, while the calculation of equilibrium constants from absorbance or fluorescence changes is relatively easy process, many reversible complexes do not give rise to observable spectral changes. Since a macromolecular component, associating or dissociating from a complex, frequently differs in shape and molecular weight from the complex, the gel method, while more time-consuming than spectroscopy, is a reliable way to obtain equilibrium information in the absence of other techniques.

5. Uses standard laboratory equipment, inexpensive. The gel electrophoresis method uses standard electrophoretic apparatus and scanning devices, present in any biochemical laboratory. Therefore, no special equipment or supplies are necessary to use the technique. Since sensitive staining methods for both DNA and proteins are now available, in many cases, the method can be used without the expense and health hazard of radiolabeled material, if preferred.

The method has its difficulties.

1. The gel electrophoresis method depends critically on analytical skill. All steps in the process, the addition of the dye, determination of the dye and the DNA concentration, loading of the samples, loading of the standards, etc., must be done precisely. On a

single gel, an average of 15 precise measurements must be made and the analysis of binding curves over a range of ligand concentrations requires the analysis of many such gels. Initially, a series of gels must be analyzed to determine the extent of the association or dissociation of the biological complex, before the final stages of the analysis can begin. If the intensities of the DNA standards do not form a good line, the gel is discarded. If the bands are not sharp enough or run in a way which is not easily scanned, the gel is not used. Every series of measurement must be repeated several times. Thus, while the running and analysis of a single gel is a relatively rapid and easy process, the analysis of a complete binding experiment is a long process.

2. If a particular staining detection method is used, only the component used as the standard can be quantified in the unknown samples. In our system, neither the intact core particles (band-1) nor the hexamer (band-2) had the same staining intensity with ethidium bromide as did free DNA. Thus, we could not quantify the levels of these components in the same experiment. This problem can be circumvented by the use of more than one type of standard or by carefully calculating an intensity correction factor for the other bands. If component X stains with a constant 85% of the intensity of the standard, then the amount of unknown X can be determined from the standard line by extrapolating the integrated area of X to ng and dividing by the fractional correction factor, i.e., $ng/.85$. Alternatively, the use of radiolabeled DNA, RNA or protein can circumvent the problem of differential staining intensity.

As a final comment, since every biological complex may have

different properties, no assumptions can be made as to the stability of the complex on the gel. Thus, the voltage, ionic strength, and other appropriate controls must be determined for each new type of complex quantified by the method.

Table III.1

Quantification of the Ethidium-Induced Dissociation of the
Chicken Erythrocyte Core Particle by the Gel Electrophoresis Method

Input Ratio ^a	Trial #1	Trial #2	Trial #3	Dissociation AVG
0	0	0	0	0
.05	1%	0	0	0.3% ± .7%
.10	1%	3%	2%	2.0 ± 1%
.20	2%	3%	3%	2.7% ± 1%
.25	4%	-	5%	4.5% ± 0.5%
.30	7%	6.5%	7%	7.0% ± 0.5%
.35	15%			15%
.40	18%	15%	15%	16% ± 2%
.45	20%	16%	18%	18% ± 2%

^a Input Ratio = $\frac{\text{moles ethidium bromide}}{\text{moles DNA bp}}$

Table III.2

Ionic Strength, Polyacrylamide/Agarose, Glycerol Content,
and Voltage Dependence of Ethidium-Induced Dissociation
of the Chicken Erythrocyte Core Particle

Condition ^a	Reference ^b	% Dissociation		
		R=0 ^c	R=0.3	R=0.45
1. Polyacrylamide = 2.5% C.L. ^d Ratio = 20:1 [Na ⁺] = 7.0 mM Voltage = 150 Agarose = 0.5%	(1)	0	7.0	18
2. Polyacrylamide = 3.5% C.L. Ratio = (20:1) [Na ⁺] = 7.0 mM Voltage = 150 Agarose = 0.5% Glycerol = 30%	(2)			
3. Polyacrylamide = 5% C.L. Ratio = (30:1) [Na ⁺] = 7.0 mM Voltage = 150	(3)	0	6.7	15%
4. Polyacrylamide = 3.5% C.L. Ratio = (20:1) [Na ⁺] = 5 mM Voltage = 150	(4)	0	6.5	16.5%
5. Polyacrylamide = 3.5% C.L. Ratio = (20:1) [Na ⁺] = 40 mM Voltage = 150	(5)	0	7.8	17.8
6. Polyacrylamide = 3.5% C.L. Ratio = (20:1) [Na ⁺] = 40 mM Voltage = 50	(5)	0	8.0	16%
7. Polyacrylamide = 3.5% C.L. Ratio = (20:1) [Na ⁺] = 40 mM Voltage = 300	(5)	0	7.4	16%

^a Core particle and ethidium sample buffer was always 10 mM Tris, pH 8.0, 0.1 mM EDTA. The core particle concentration was 4.0-7.0 x 10⁻⁵ M (BP) and all experiments were performed at 30°C.

Table III.2 (continued)

^b References: (1) Todd and Garrard, 1977; (2) Todd and Garrard, 1979; Albright et al., 1980; (3) Varshavsky et al., 1976, 1978; (4) Kovacic and van Holde, 1977; (5) this work.

^c R = Input Ratio = moles added ethidium bromide/mole DNA BP.

Table III.3

Results of the v_{core} Determination for the Complex of Ethidium Bromide with the Chicken Erythrocyte Core Particle at $T = 30^\circ\text{C}$

Input Ratio (R) ^a	v_{TOTAL} ^b	v_{core} ^c	v_{DNA}	%D
0	0	0	0	ND ^d
.02	.017	.02	0	ND
.04	.039	.04	0	ND
.06	.047	--		De
.08	.067	.06	.025	1%
.10	.088	.06	.037	2%
.15	.13	.08	.05	3%
.20	.16	.12	.04	5%
.25	--	--	--	7%
.30	.19	.15	.04	8%
.35	.25	.17	.08	14%
.40	.28	.19	.09	16%
.45	.29	.20	.09	18%

a. Input Ratio (R) = moles added ethidium bromide/mole BP. Core Particles and ethidium bromide solutions were in 10 mM Tris, pH 8.0, 0.1 mM EDTA. The core particle DNA concentration was $4.0\text{--}7.0 \times 10^{-5}$ M (BP) and all experiments were performed at 30°C .

b. v_{TOTAL} = moles bound ethidium/mole BP.

c. v_{core} = moles bound ethidium/mole BP (other than free DNA).

d. ND = not detectable.

e. D = detectable. At very heavy loading of the complex, small free DNA band intensity was sometimes detected. The quantified amount of free DNA was within experimental error of 0%; $0.3\% \pm 0.5\%$.

Figure III.1. Results of the polyacrylamide gel electrophoretic analysis of the core particle complexes with ethidium bromide and bromophenol blue. (A) Results of the polyacrylamide gel electrophoretic analysis of the core particle/ethidium bromide complexes over a range of input ratios. Complexes were analyzed 15 hours after mixing. 1) $R = 0$; 2) $R = 0.05$; 3) $R = 0.1$; 4) $R = 0.2$; 5) $R = 0.3$; 6) $R = 0.4$; 7) $R = 0.45$; 8) $R = 0.5$; 9) $R = 0.75$; 10) $R = 1.0$; 11) $R = 1.5$; 12) $R = 2.0$, where R = moles added ethidium bromide per BP. Lanes marked M indicate HpaII cut pBr322 DNA molecular weight markers. Bands 1, 2 and 3 represent the intact core particle, the hexamer and free DNA respectively. Each lane represents 250 ng of DNA. Complexes were analyzed on 1.0 mm, 3.5% native polyacrylamide gels (acrylamide:bisacrylamide, 20:1). Core particle DNA concentration was 3.8×10^{-5} BP and the buffer used for all samples was 10 mM Tris, pH 8.0, 0.1 mM EDTA. Gel electrophoresis was performed at 4°C at 10 v/cm for 50 minutes. The gels were stained for 10 minutes with 1 µg/ml ethidium bromide in H₂O. (B) The effect of adding 0.25% bromophenol blue at a 1:1 ratio to intact core particles. 1) 200 ng; 2) 50 ng. Core particle concentration was 7.5×10^{-5} M (BP). The buffer and gel conditions are as in (A). Lane marked M indicate Hae III restricted pBr322 DNA molecular weight markers. Lane marked D indicates 145 ± 3 BP free DNA isolated from the core particles. Bands 1 and 2 are the intact core particle and the hexamer. (C) Laser densitometer trace of the protein component of band 2, seen both in 1A and 1B.

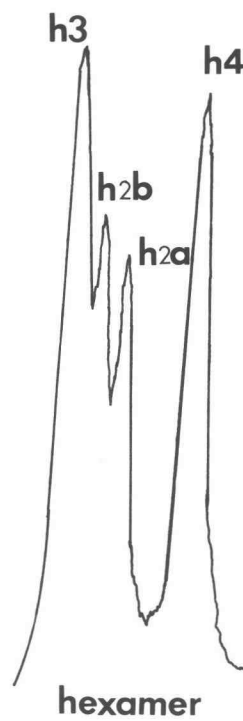
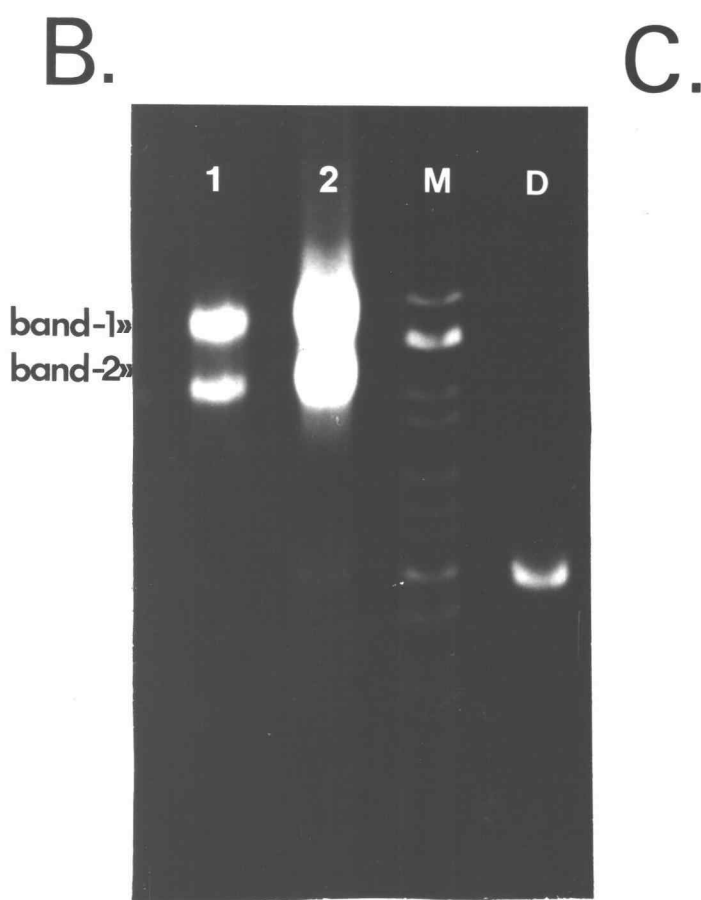
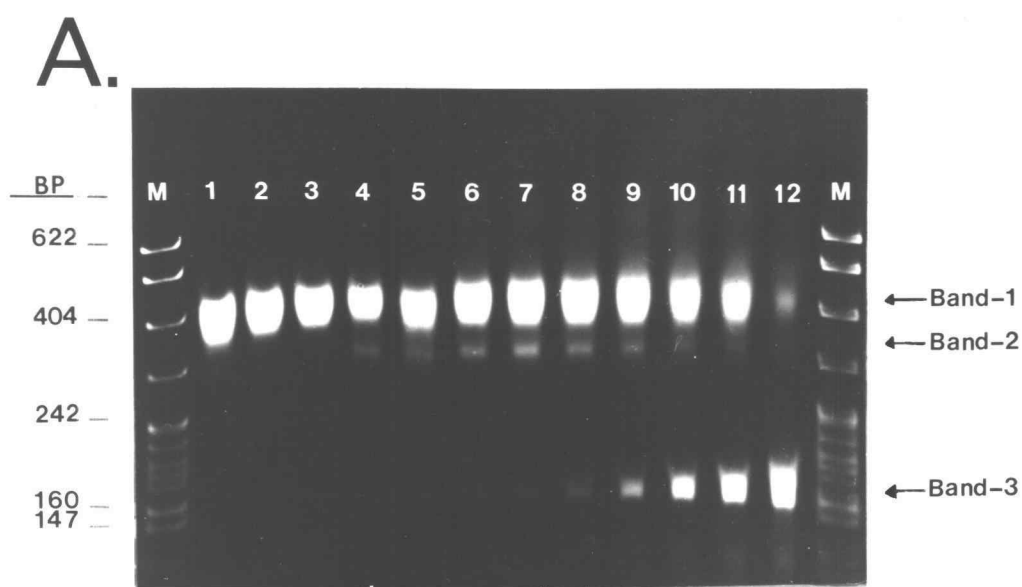


Figure III.1

Figure III.2. Calibration of the linear intensity range of the DNA standards and film exposure time for the gel quantification method.

(A) Plot of integrated area from the fluorescence intensity of the DNA standards versus ng of DNA at a 3 minute exposure time. (B) Plot of integrated area from the fluorescence intensity of a 30 ng DNA standard versus film exposure time. In all experiments, the DNA was diluted into 20% glycerol buffered with 10 mM Tris, pH 8.0, 0.1 mM EDTA. Gel were stained for 10 minutes with 1 μ g/ml ethidium bromide in water and photographed with type 55 Polaroid film using a red filter.

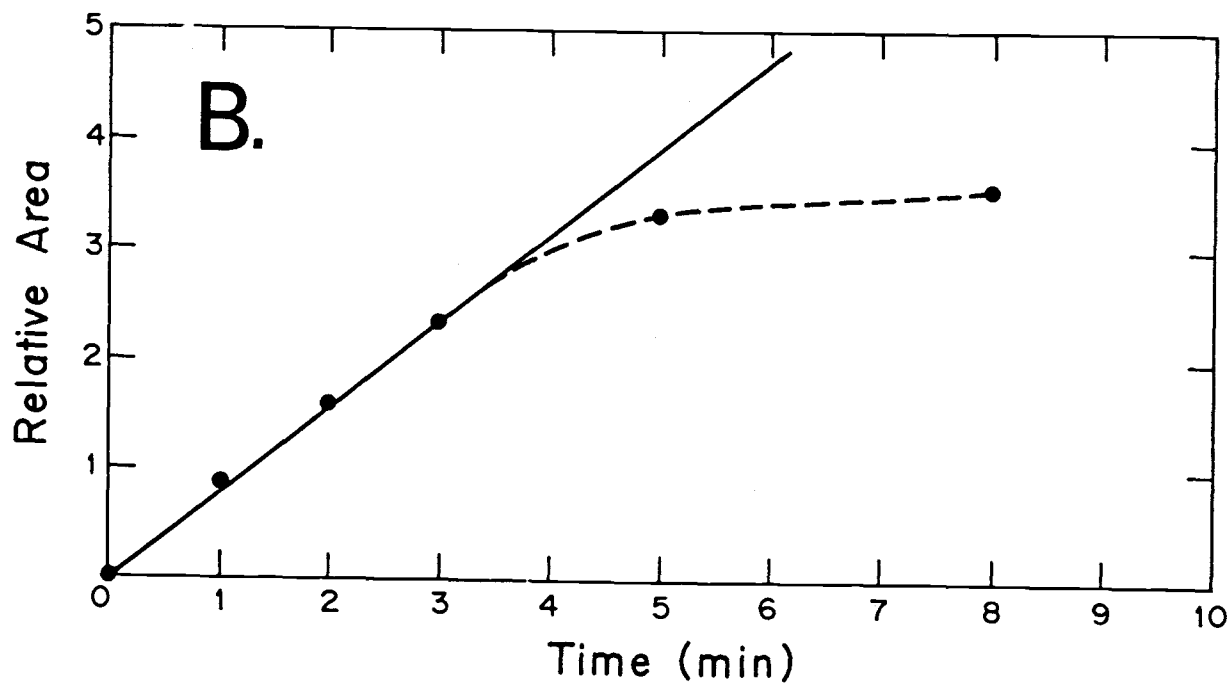
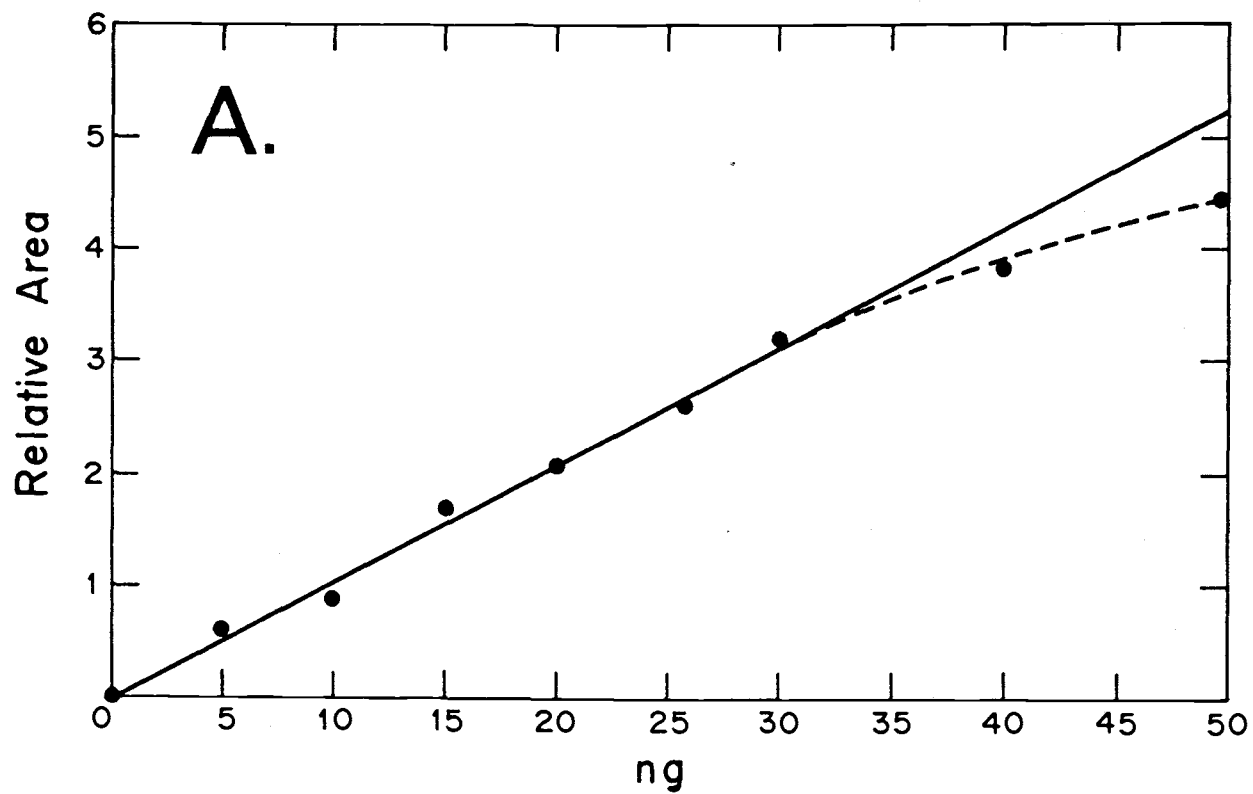


Figure III.2

Figure III.3. Illustration of the quantitative gel electrophoretic method. (A) Schematic representation of the gel electrophoresis method used to quantify the amount of dissociated DNA present at any ratio of ethidium bromide. Each point () represents the integrated intensity of 5, 10, 15, 20, 25 and 30 ng DNA standards. The resulting line is the best fit to all points by linear regression analysis. Unknown DNA band intensities (---) can be interpolated to yield the amount of free DNA present at any point. (B) Example of a typical 3.5% polyacrylamide native gel of DNA standards and core particle complex unknowns. Lanes 1-6 are the DNA standards. 1) 30 ng, 2) 25 ng, 3) 20 ng, 4) 15 ng, 5) 10 ng, 6) 5 ng. Lane marked M = Cfo/cut pBr322 DNA molecular weight standards. Lanes 7-12 are the core particle/ethidium complexes. 7) R = .10, 5 μ l sample volume, 8) R = .10, 10 μ l sample volume, 9) R = .20, 5 μ l sample volume, 10) R = .20, 10 μ l sample volume, 11) R = .30, 5 μ l sample volume, 12) R = .30, sample volume. All core particle samples were 3.8×10^{-5} M BP. The buffer was 10 mM Tris, pH 8.0, 0.1 mM EDTA. The experiment was performed at 30°C.

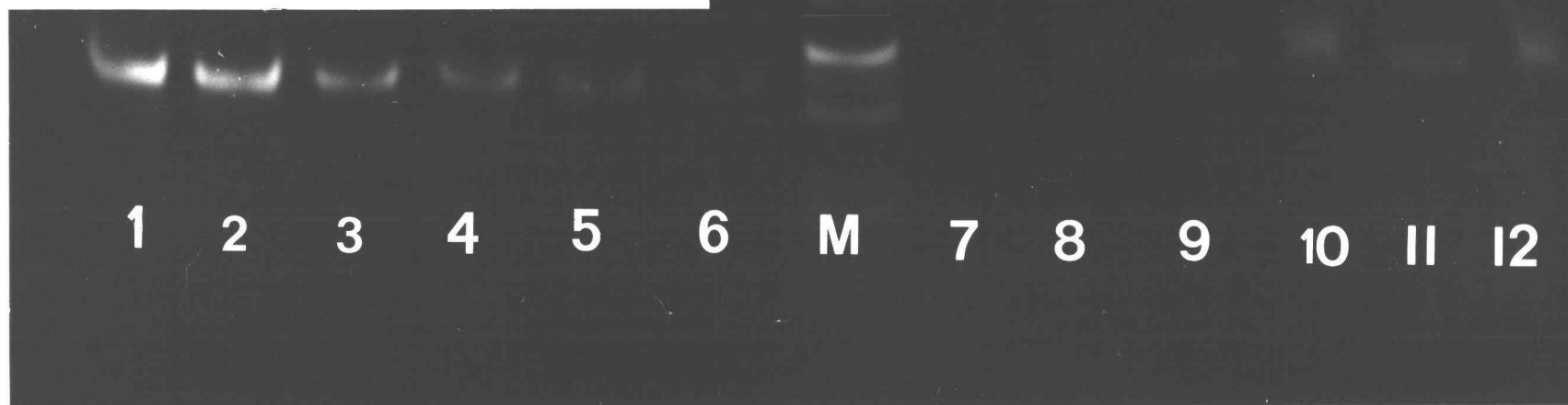
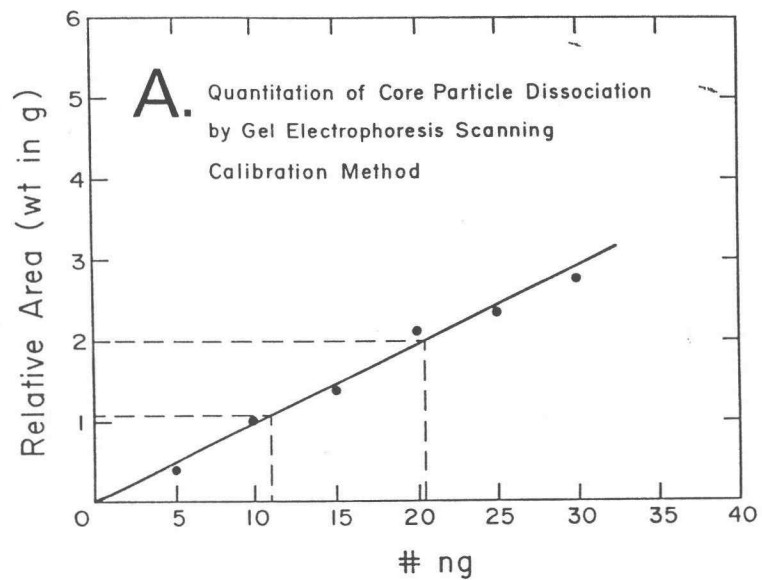
B.

Figure III.3

Figure III.4. The DNA concentration dependence of the ethidium-induced dissociation of the core particle. Each scan represents the dissociated free DNA from a core particle/ethidium complex at $R = 0.4$ which varied in DNA concentration. (A) $A_{260} = 0.5$, $[CP] = 3.8 \times 10^{-5}$ M (BP); (B) $A_{260} = 1.0$, $[CP] = 7.6 \times 10^{-5}$ M (BP); (C) $A_{260} = 3.0$, $[CP] = 2.3 \times 10^{-4}$ M (BP); (D) $A_{260} = 5.0$, $[CP] = 3.8 \times 10^{-4}$ M (BP); (E) $A_{260} = 10.0$, $[CP] = 7.6 \times 10^{-4}$ M (BP). The buffer used for all experiments was 10 mM Tris, pH = 8.0, 0.1 mM EDTA. The free DNA was separated from the intact core particles or 3.5% polyacrylamide gels. The running conditions for the gels are as described in Figure III.1.

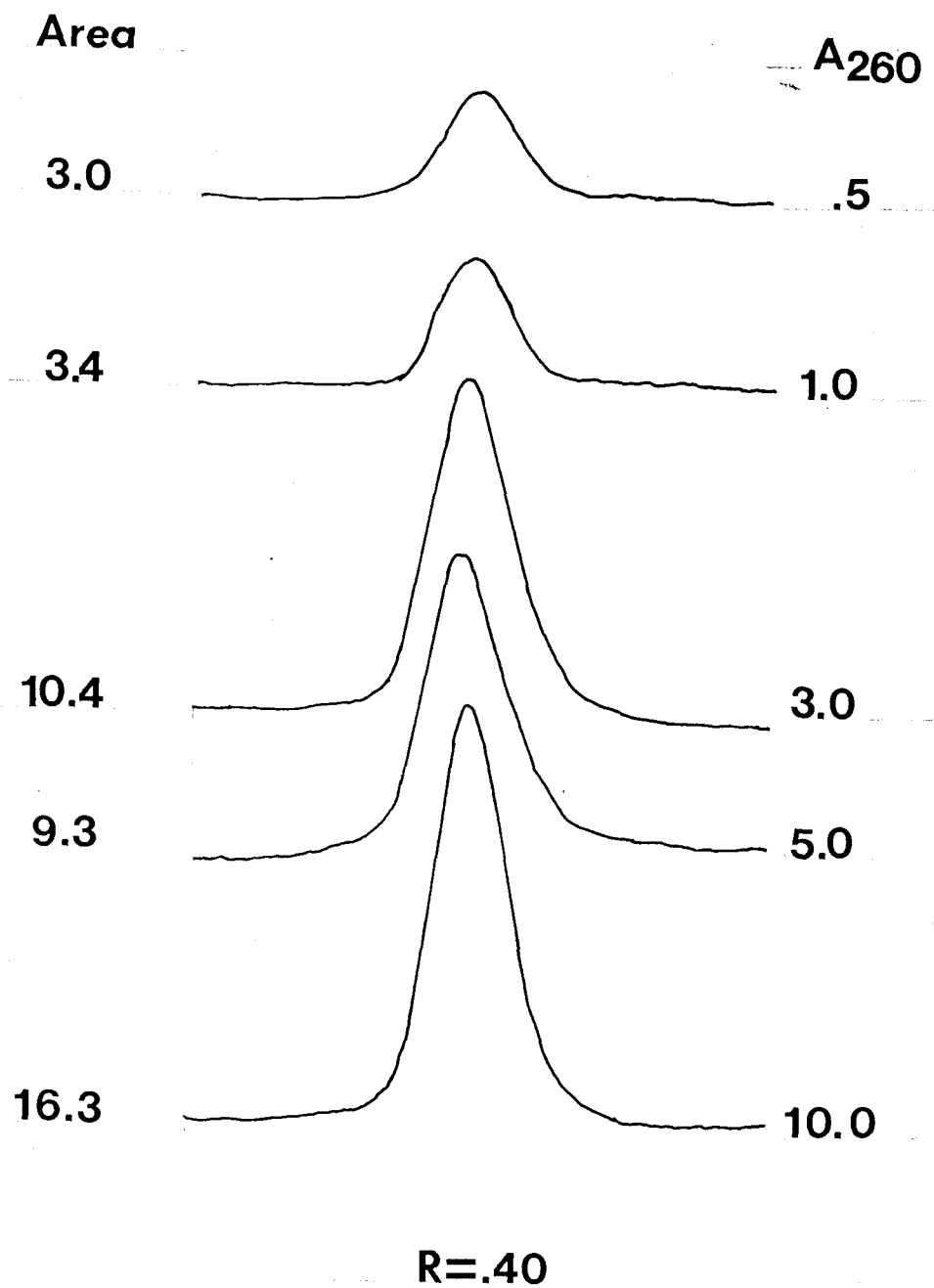


Figure III.4

Figure III.5. The sample volume dependence of dissociation for the intact core particle and a core particle/ethidium complex at $R = 0.3$ on native low cross-linking ratio polyacrylamide gels. (A) The sample volume dependence of dissociation for the intact core particle. Lanes 1-7 are: 1) 0.5 μl ; 2) 1.0 μl ; 3) 1.5 μl ; 4) 3.0 μl ; 5) 5.0 μl ; 6) 10.0 μl ; 7) 15.0 μl . The concentration of the sample was 33 ng/ μl . The sample was equilibrated at 30°C in 10 mM Tris, pH = 8.0, 0.1 mM EDTA. Lanes marked D and M are 145 bp nucleosomal DNA standards and Hae III-restricted pBr322 DNA marker bands, respectively. (B) The sample volume dependence of a core particle/ethidium complex at $R = 0.3$. Lanes 1-6 are: 1) 0.5 μl ; 2) 1.0 μl ; 3) 2.0 μl ; 4) 3.0 μl ; 5) 5.0 μl ; 6) 8.0 μl . The concentration of the sample was 70 ng/ μl . The sample was equilibrated at 30°C in 10 mM Tris, pH = 8.0, 0.1 mM EDTA. Lanes marked D and M are 145 bp nucleosomal DNA standards and the Hae III-restricted pBr322 DNA marker bands, respectively. The samples were analyzed on 3.5% polyacrylamide gels at 4°C with running conditions as described in Figure 1. Bottom: Laser densitometer trace of the dissociated DNA band in (B) lanes 1-6. The integrated area of the peaks was determined by cutting and weighing the bands. The peak area and sample load are indicated.

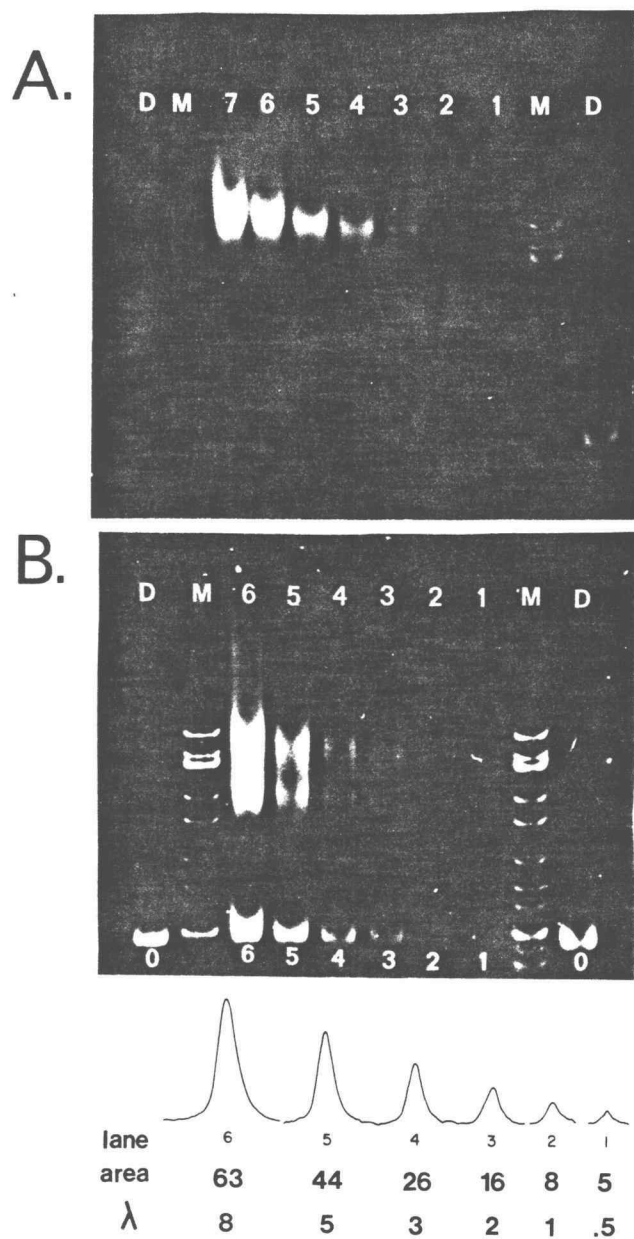


Figure III.5

Figure III.6. Plot of % dissociation of the core particles versus the input ratio of ethidium bromide. Dissociation was measured by the gel electrophoretic method as described in text. The input ratio is defined as moles added ethidium bromide/moles DNA base pairs. All measurements made at 30°C in 10 mM Tris, pH = 8.0, 0.1 mM EDTA. The concentration of the core particle solution was 7.0×10^{-5} M BP.

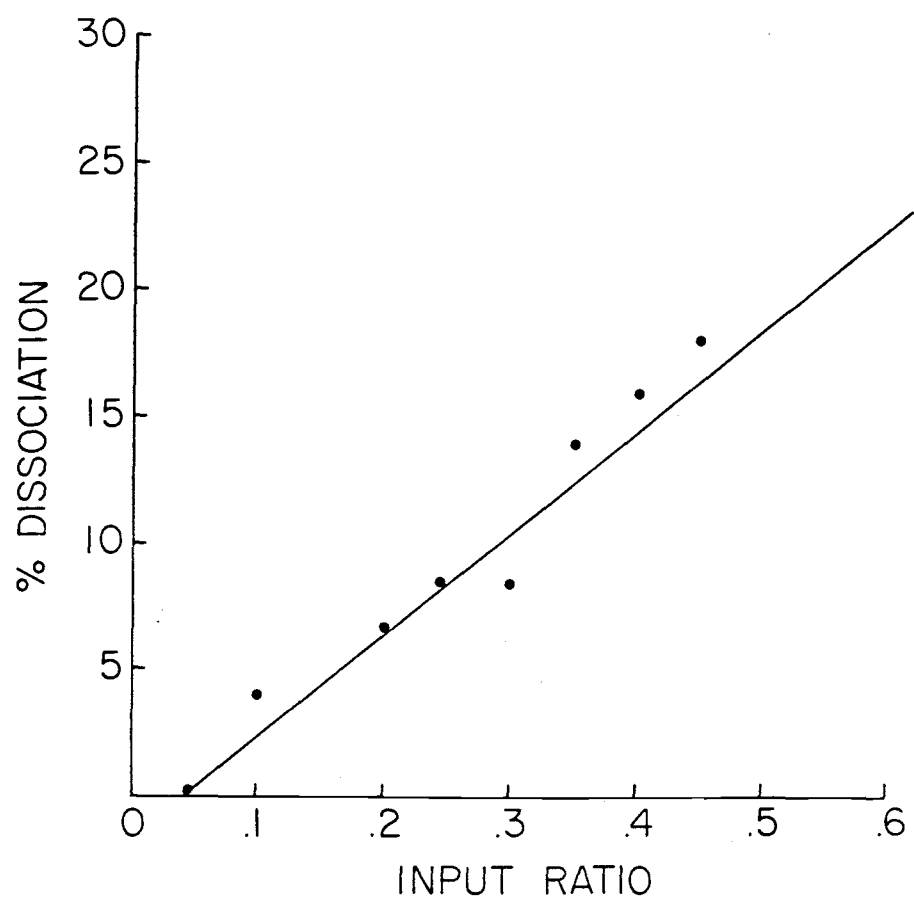


Figure III.6

Figure III.7. Plot of % dissociation versus bound ratio of ethidium.

A. The schematic diagram for the method used to determine V_{core} . B. Plot of % dissociation versus bound ratio of ethidium. (A) Plot of % dissociation versus total bound ratio (V) of ethidium. (B) Plot of % dissociation versus ratio of ethidium bound to only the undissociated core particles, V_{core} . The level of dissociation was determined by the gel electrophoretic method as described in the text. The bound ratio is defined as $V = \text{moles bound ethidium} / \text{moles DNA BP}$. All measurements were made at 30°C in 10 mM Tris, pH = 8.0, 0.1 mM EDTA. The concentration of the core particle solution was 7.0×10^{-5} M BP.

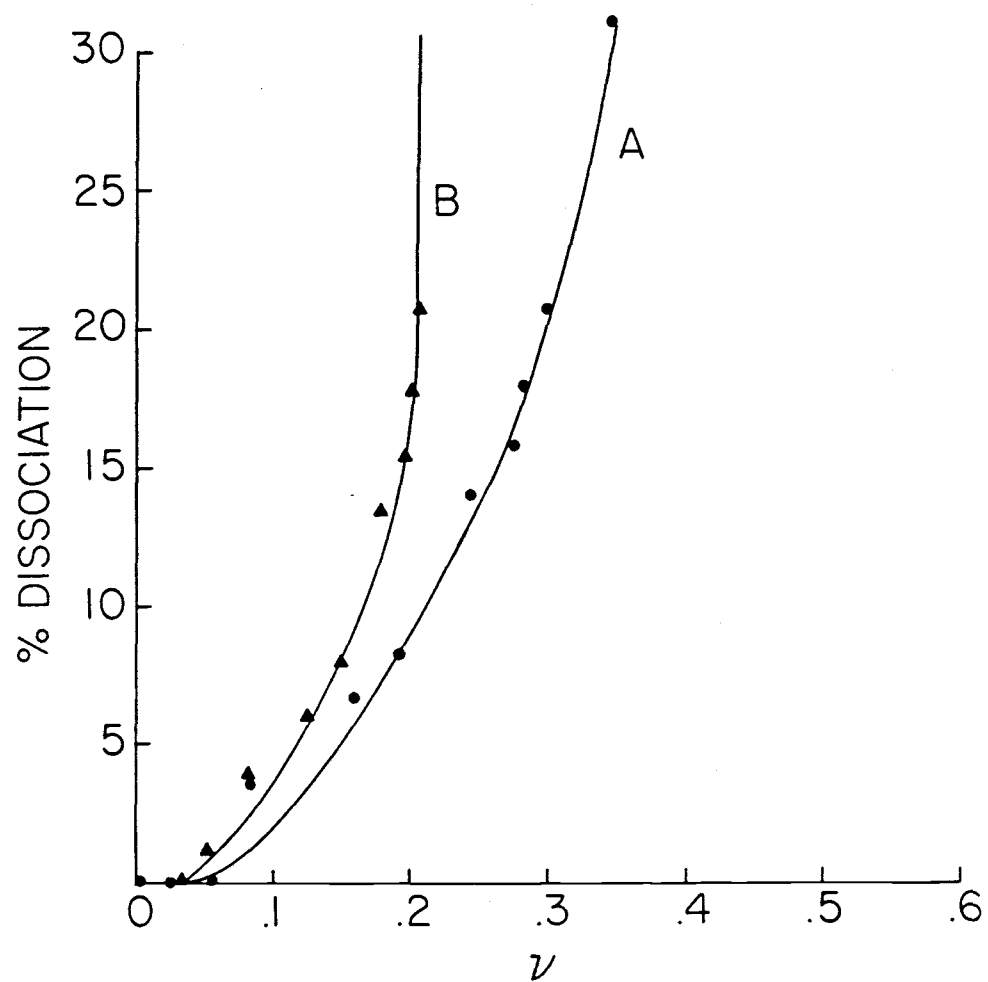


Figure III.7

CHAPTER IV. THE BINDING OF ETHIDIUM BROMIDE TO THE NUCLEOSOME

CORE PARTICLE: INTERNAL AND EXTERNAL BINDING

ABSTRACT

We have previously reported that the binding of ethidium bromide to the nucleosome core particle results in a step-wise dissociation of the structure which involves the initial release of one copy each of H2A and H2B (McMurray and van Holde, 1986). In this report, we examine the absorbance and fluorescence properties of intercalated and outside bound forms of ethidium bromide. From these properties, we have examined the extent of external, electrostatic binding of the dye versus internal, intercalative binding to the core particle, free from contamination with linker DNA. We have established that dissociation is induced by the intercalation mode of binding to DNA within the core particle, and not by non-specific binding to the histones or alternate, non-intercalative binding to DNA. The covalent binding of ³H-8-azido-ethidium to the core particle clearly shows that < 1.0 adducts are formed per histone octamer over a wide range of input ratios. Simultaneously, analysis of fluorescence intensity increments and fluorescence lifetime data from bound ethidium complexes demonstrate extensive intercalation binding. Combined analysis from both fluorescence intensity and fluorescence lifetime data revealed that dissociation began when ~17 bp of DNA are bound by intercalation and << 1.0 non-intercalated ion-pair was formed per core particle. We evaluate the contribution of both modes to the ethidium-induced dissociation process.

INTRODUCTION

The association of polycyclic, planar molecules with deoxyribonucleic acids (DNA) has been correlated with a wide range of biological effects including mutagenesis, carcinogenesis and antimicrobial action (Waring, 1981; Wilson and Jones, 1981, 1982). The most well-characterized binding mode which is associated with this type of molecule is intercalation, the insertion of the planar portion of a molecule between the base pairs of DNA (Lerman, 1961, 1963, 1964). Classical intercalation binding to DNA is characterized by a lengthening and stiffening of the DNA double helix, a decrease in the winding angle between adjacent base pairs and a decreased mass per unit length of the DNA rod (Lerman, 1961, 1964; Cohen and Eisenberg, 1969; Saucier et al., 1971; Waring, 1972; Bauer and Vinograd, 1974). To exploit these characteristics, experimentally, the effect of intercalation can be detected by measuring the large changes in the sedimentation, viscometric and diffusion properties of the DNA/dye complex relative to free DNA. Intercalation binding is stabilized by both an electrostatic component, if the dye is charged, and a non-electrostatic component which involves the formation of specific hydrogen bonding and the hydrophobic association of the ring system.

While intercalation may be the major binding mode of planar molecules to DNA, many cationic compounds which contain fused ring systems bind strongly to DNA by mechanisms other than intercalation. At high ratios dye to DNA, when the intercalation sites are largely saturated, cationic dyes can cooperatively bind by a DNA-mediated self-association mechanism (LePecq and Paoletti, 1962, 1967; Blake and

Peacocke, 1968; Cannon et al., 1975; Chaires et al., 1982). We will refer to this mode as the outside stacked configuration. In contrast to intercalation, the outside stacking of planar dye molecules results in little change in the hydrodynamic properties of the DNA/dye complex (Bradley and Wolf, 1959). Since much of the stabilization for the stacked aggregate is provided through the electrostatic interaction of the dye with the anionic phosphate backbone of DNA, this mechanism is much weaker than intercalation and is easily disrupted by increasing the ionic strength of the solution (Bradley and Wolf, 1959; LePecq and Paoletti, 1967). Under low ionic strength conditions, outside stacking of dye molecules can interfere with interpretation of binding data and can lead to curvature in Scatchard plots (Bloomfield et al., 1974).

If hydrogen bonding potentials are large enough, a dye molecule, capable of intercalation, can prefer to bind to the base pairs within the grooves of the DNA, enhanced by the electrostatic interaction with the phosphates (Muller, W., Crothers, D.M. and Waring, M.J., 1973, *Eur. J. Biochem.*, 39, 223. We shall refer to this mode as groove binding. In this case, the hydrogen bonding is usually quite specific, and the dyes will bind as monomers. Hydrophobic interactions stabilize groove binding, in addition to electrostatic and hydrogen bonding components. Binding of this type also results in only small changes, at best, in the hydrodynamic properties of the complex, but is not as sensitive to changes in ionic strength as outside stacking. Finally, a third external, non-intercalated state can occur when the conformation of the nucleic acid is not favorable for intercalative binding or when the dye is sterically restrained

from binding by intercalation. In this case, the dye binding will be stabilized through purely electrostatic interactions of the cation to the phosphate backbone of DNA (Davidson et al., 1977a,b).

Consequently, we shall refer to this mode as electrostatic binding.

In contrast to outside stacking, the electrostatic binding is not dependent on the concentration of the dye and can occur even at very low ratios of dye to DNA base pair. Like outside stacking, electrostatic binding induces negligible changes in the hydrodynamic properties of the dye/DNA complex, and is extremely sensitive to ionic strength. Electrostatic binding is favored under low ionic strength conditions and is essentially abolished at intermediate to high ionic strengths.

The intercalative binding and stacking of planar dye molecules to free DNA and RNA have been directly observed by X-ray crystallography for several compounds (Fuller and Waring, 1985; Sobell et al., 1977; Jain et al., 1977; Reddy et al., 1979; Sakore et al., 1977; Jain et al., 1979; Quigley et al., 1980). Further, intercalation has been shown to be the primary binding mode to free DNA under a range of ionic strength conditions (Jones et al., 1980; Wilson and Lopp, 1979). Consequently, non-specific, external binding of intercalating dyes to DNA is usually considered an artifact or problem in the study of the intercalation mode. But do intercalating dyes bind in the same manner when DNA is wrapped around the histone octamer to form the nucleosome structure? The nucleosome differs from free DNA in its charge/mass ratio (Donecke, 1977; Mirzabekov and Rich, 1979; Girardet and Lawrence, 1979; McGhee and Felsenfeld, 1980), its average twist angle (Fasman, 1977; Simpson and Shindo, 1979; Klug and Lutter, 1982) and

its solubility properties (Perry and Chalkley, 1982; Komaiko and Felsenfeld, 1985; Ausio, 1986). Additionally, the presence of the histone octamer may present a barrier to the intercalation of the dye. While for free DNA, the problem of external binding is easily circumvented through the utilization of a near physiological ionic strength environment (Bloomfield, 1974; Tanford, 1970), high ionic strengths destabilize the DNA/histone complex inducing dissociation and aggregation (Ausio et al., 1984; Yager et al., 1984; Cotton and Hamkalo, 1981; Stacks and Schumaker, 1979; Lilley et al., 1979). However, the necessary utilization of low ionic strength conditions favors the electrostatic binding mode of cationic intercalating dyes and, simultaneously, increases the binding affinity of the histone octamer. Thus, the conditions employed in the study of nucleoprotein systems optimize the possibility for external binding modes, if they occur. While intercalation binding to polymeric chromatin has been the subject of many low ionic strength studies (Lawrence and Louis, 1972; Angerer and Moudrianakis, 1972; Lurquin and Seligy, 1972; Williams et al., 1972; Angerer et al., 1974; Lapeyre and Bekhor, 1974; Erard et al., 1979; Hurley et al., 1982), few studies of chromatin have adequately distinguished between the binding properties of intercalating dyes to the relatively free, linker DNA versus the histone-associated portions. Additionally, a large number of these reports involved chromatin prepared in a manner that denatured the proteins. Reports of dye binding with the putative "core particle", have frequently utilized preparations contaminated with various lengths of linker DNA (Wu et al., 1980), which binds the dye differently (Wu et al., 1980; Erard et al., 1979). It has not been

established whether low ratios of dye bound to such core particles are bound to folded, histone-associated DNA or to the linker tails of the nucleosome. Although most of these studies have utilized low ionic strength conditions, the possibility of alternative binding modes has been largely ignored. In short, while it is clear that intercalation occurs to free DNA and within the linker DNA of chromatin, it is not clear, after years of study, that planar dye molecules are able to bind by intercalation to the histone-associated DNA.

We have prepared highly homogeneous, trimmed core particles which are (95-98%) 145 ± 3 bp in length. In studying their properties with intercalating dyes, we have recently reported that the binding of ethidium bromide to the nucleosome core particle results in a step-wise dissociation of the structure which involves the initial release of one copy each of H2A and H2B (McMurray and van Holde, 1986). Since ethidium induces a dissociation of the core particle, it is essential for development of a binding model to determine if this dissociation is the result of intercalation events or an external electrostatic association of the dye. In this report, we examine the absorbance and fluorescence properties of intercalated and outside bound forms of ethidium bromide. From these properties, we have examined the extent of external, electrostatic binding of the dye versus internal, intercalative binding to the core particle, free from contamination with linker DNA, and from the contribution of both modes to the ethidium-induced dissociation process.

RESULTS

Ethidium bromide binding to the nucleosome core particle, results in a step-wise dissociation of the structure which involves the initial release of one copy each of H2A and H2B (McMurray and van Holde, 1986). The products of the dissociation can be resolved on sucrose gradients and are shown in Figure IV.1. Bands 1, 2 and 3 represent each step of the ethidium-induced dissociation process: the intact core particle, the hexamer and free DNA, respectively. Because ethidium is capable of forming an external association with the core particle through an electrostatic interaction with the DNA phosphate or of forming a hydrophobic association with the histone protein, we wanted to establish the nature of the binding mode which induced the dissociation equilibrium. Initial studies were aimed towards distinguishing whether the primary target for ethidium binding was to DNA or to protein.

I. Binding to Protein

To evaluate the extent of non-intercalative binding of ethidium bromide to the protein component of the core particle, we measured the amount of ^3H -label retained by the histones from the covalent binding of an ethidium derivative, ^3H -8-azido-ethidium bromide (^3H -8-AzEB). (An initial characterization of the binding of 8-azido-ethidium to free DNA is provided in the Appendix.) The ^3H -8-AzEB has binding properties and geometry similar to the parent compound (Bolton and

Kearns, 1977; Graves et al., 1981; Yielding et al., 1983; Laugaa et al., 1983), but contains an azido group which, upon activation by light, will form "zero-length" covalent bond with the nearest reactive group. The formation of the covalent bond occurs via the formation of a nitrene radical produced by the light-induced decomposition of the azido group. We added increasing ratios of 3H-8-AzEB to individual core particle solutions. The complexes were photoactivated for 10 minutes with unfiltered visible light and ethanol precipitated to remove any non-covalently bound dye. Each sample was diluted 1:1 in Laemmli (1970) SDS sample buffer, gently heated to 37°C and separated on 15%-SDS-polyacrylamide gels. All four histone protein bands were cut from the gel, extracted at 37°C by shaking overnight in a scintillation mixture and the retained label was measured by scintillation counting. The results of the covalent adduct formation experiment are shown in Figure IV.2. The plot of adducts formed per histone octamer versus input ratio revealed that, at all ratios measured, little of the dye is associated with the histone protein component. At even the highest ratio measured, less than one covalent adduct was formed per two histone octamers. We concluded from these experiments that significant binding of the dye to the histones did not occur and, consequently, that the primary binding site for ethidium bromide to the core particle was the DNA component.

II. Binding to DNA.

A. Absorbance Measurements. To evaluate the binding of ethidium bromide to the DNA component of the core particle at low ionic

strength, we analyzed the absorbance properties of ethidium bromide in its free form, as well as the dye complexed with free DNA, the core particles and to polyvinylsulfate in 10 mM Tris, pH = 8.0, 0.1 mM EDTA (TE). The inclusion of PVS as a binding substrate for ethidium bromide provided information on the spectral properties of the external, electrostatic binding mode of the dye alone. Since polyvinylsulfate (PVS) has a single negatively charged group and no planar ring moiety, the binding of ethidium bromide can occur only through an electrostatic association, unmixed with either intercalation modes or hydrophobic stacking modes. The spectrophotometric analyses, in the visible range from 650 nm to 350 nm, of the complexes formed between ethidium bromide and free DNA, the core particle and PVS are shown in Figure IV.3 A, B and C. For free DNA (Figure IV.3A), the titration of small volumes of concentrated DNA solutions resulted in a progressive hypochromic shift of the spectra and a reduced extinction coefficient of the fully bound complex (curve 10; Figure IV.3A) relative to the free dye (curve 1, Figure IV.3A). The reduction in extinction coefficient was accompanied by a 40 nm shift of the maximum absorbance wavelength from 480 nm to 520 nm. The data are summarized in Table IV.1. If the dye molecule has only one free and one bound form, the spectra for the complexes should overlap at one or more points, called the isosbestic point(s), where the free and bound forms display the same extinction coefficient. The complex of ethidium with free DNA at all ratios of dye displayed distinct isosbestic points (IB) at 513 nm and 388 nm, suggesting that, under low ionic strength conditions (in TE buffer), no intermediate forms of bound dye were present in solution. The spectrophotometric absorbance

results for the core particle (Figure IV.3C) were similar to those obtained with free DNA. The titration of concentrated core particles, at constant ethidium bromide concentration, also resulted in reduced extinction coefficient (curve 10; Figure IV.3C) relative to the free dye (curve 1; Figure IV.3C), a shifted absorbance maximum from 480 nm to 520 nm and the presence of isosbestic points at 388 and 517 nm. The shape of the spectra, absorbance maxima and the extinction coefficients for totally bound ethidium to both free DNA and to the core particle were identical (see Table IV.1), differing only in the longer wavelength isosbestic point. The IB for the core particle was shifted to longer wavelengths (red-shifted) by 4 nm relative to free DNA. The presence of a distinct isosbestic point for the core particle at low ionic strength also suggested that only two forms of the dye were present in solution, free and bound, with no intermediate forms.

While the existence of an isosbestic points for both free DNA and the core particle is a good indication of a two state model, it is not proof of only two binding forms. The validity of the apparent two-state model relies on the knowledge that no intermediate form has the same absorbance properties as either the bound or the free state. Inspection of Figure IV.3B reveals that the external, electrostatic binding of ethidium bromide to PVS shows binding properties very similar to both free DNA and the core particle. The absorption spectrum of ethidium bound to PVS was shifted to longer wavelengths (~30 nm) relative to the free dye and distinct isosbestic points were observed at 393 nm and 513 nm, identical to the ethidium/free DNA complex. The absorbance properties of ethidium/PVS were identical when measured in water or TE but were extremely sensitive to higher

levels of ionic strength. Increasing the ionic strength to 0.2 M NaCl completely abolished the reduced extinction coefficient and wavelength shift characteristics of the PVS/EB complex. Consequently, purely electrostatic binding of ethidium bromide was eliminated by increasing the ionic strength, and the absorbance spectrum for the PVS/EB complex at 0.2 M NaCl resembled that of the free dye. As previously reported (LePecq and Paoletti, 1967), we were unable to obtain the fully bound form of EB to PVS, at low ionic strength, due to the release of condensed Na⁺ from PVS upon EB binding. Increasing the ionic strength to 0.2 M resulted in no changes in the absorbance properties of ethidium complexed to either free DNA or to the core particle. We concluded from these studies that the absorbance properties of ethidium bromide did not distinguish between intercalative and electrostatic binding modes under our buffer conditions. Consequently, absorbance measurements could not be used as proof of intercalation.

B. Fluorescence Intensity Measurements. Since the absorbance properties of ethidium in its intercalated state and electrostatically bound state were similar, we measured the fluorescence intensity properties of ethidium bound to free DNA, the core particles and to PVS. In agreement with other studies (LePecq and Paoletti, 1967; Wu et al., 1980), the fluorescence emission maxima for free ethidium and ethidium bound to both the core particles and free DNA were found at 606 nm. Consequently, we were able to measure all ethidium complexes at the same wavelength. Because large fluorescence intensity enhancement had been observed for ethidium bromide when intercalated into free DNA and into t-RNA (Olmstead and Kearns, 1977; Bolton and

Kearns, 1978; Wu et al., 1980), we measured the fluorescence intensity ratio of fully bound ethidium (I_B) to the same concentration of free dye (I_F) for ethidium complexed to free DNA or to core particles. The ratio of the bound to free fluorescence intensity was calculated for both nucleic acid complexes and was compared to the intensity ratio measured for the EB/PVS complexes. For the nucleic acids, a first approximation of the intensity of the fully bound dye was measured as the fluorescence intensity of ethidium in the presence of 100-fold excess of nucleic acid, i.e., an input ratio of $R = .01$. Since this is well below the critical ratio for ethidium-induced dissociation, we may assume that in the core particle experiments, all of the dye is bound to the particles. The observed values for the I_B/I_F ratio were 28 for free DNA and 19 for the core particles. Using these values, we calculated the fraction bound of the added dye by

$$f_B = I - I_0 / (V-1)I_F \quad (4.1)$$

where I is the total fluorescence intensity in the presence of nucleic acid, I_0 is the fluorescence intensity in the absence of nucleic acid and V is the observed intensity ratio measured at 100-fold excess nucleic acid. However, since the fraction bound of the added dye was always less than 1.0, the correct I_B/I_F values were recalculated by dividing the observed I_B/I_F by the fraction bound. The new I_B/I_F value was used to recalculate the fraction bound (Eq. 4.1), and the calculation was iterated until the I_B/I_F ratio converged to a single value. The corrected I_B/I_F values results are listed in Table IV.1. For both nucleic acids, the fluorescence intensity of the fully bound

form of the dye was >20 times the intensity of the same concentration of free dye. For free DNA, the I_B/I_F value was determined to be 29; the I_B/I_F value for the core particle was 21.1. The I_B/I_F values listed in Table IV.1 for free DNA and the core particles were calculated from the input ratio which yielded the largest f_B . Interestingly, the I_B/I_F value for the core particles did not have the largest I_B/I_F at the lowest ratios that we measured ($R = .001$), but increased as more dye was bound. The core particle/EB complex displayed the largest I_B/I_F value near $R_I = 0.1$, while the value for free DNA was highest near $R_I = .01$. These results indicated that ethidium bound to the core particles in a positively cooperative manner. (The cooperative aspects of ethidium binding will be analyzed in Chapter V). In contrast to the nucleic acid complexes, the fluorescence intensity of the electrostatic binding mode, gauged by the EB/PVS complex, was quenched relative to the free form of the dye. The I_B/I_F values ranged from 1.0-0.5 depending on the concentration of added dye. At $R = .01$, the I_B/I_F was 1.0. Increasing the input ratio of dye to PVS resulted in a loss of fluorescence intensity and a decrease in the I_B/I_F value to 0.5 at $R = .10$. Thus, pure electrostatic binding of ethidium did not give rise to any fluorescence intensity enhancement and, consequently, fluorescence intensity measurements, in the absence of quenching effects, monitored intercalation binding alone.

Direct measurement of the fluorescence intensity ratio for the intercalated and electrostatic binding modes of ethidium allowed a detailed analysis of the fluorescence intensity versus input ratio curve for ethidium binding to free DNA and to the core particle shown

in Figure IV.4. For the free DNA, the fluorescence intensity of the ethidium complex increased linearly with increasing ratio of added dye below $R = 0.2$. Large fluorescence intensity increments were apparent up to ratios of 0.35, but, in this range, the intensity versus input ratio relationship became non-linear. Using the I_B/I_F values listed in Table IV.1, we calculated the fraction bound of added ethidium and I_B/I_F for each point in the curve. The results are listed in Table IV.2. Comparison of the fraction bound, I_B/I_F values in Table IV.2 and the fluorescence intensity measurements in Figure IV.4 reveals that the loss of linearity is entirely due to the progressive saturation of intercalation sites, since division of I_B/I_F by the fraction bound yields a constant, 29. Above $R = 0.35$, the slope of the fluorescence intensity versus ratio plot of the ethidium complex with free DNA decreased until, finally, above $R = 0.4$, the intensity was strongly quenched. Examination of Table IV.2 reveals that at $R = 0.4$, the fraction bound increases very slowly. Because the intercalation sites are largely saturated at this point, quenching is attributed to the increasing contribution of the external binding configurations which occurs only at high dye concentrations. Both electrostatic and outside stacking binding modes of the dye result in more solvent exposure, energy transfer and, consequently, the loss of fluorescence intensity relative to intercalation binding.

The fluorescence intensity versus input ratio of the core particle/ethidium complexes also displayed large intensity increments with increasing concentration of dye, but differed from free DNA in three ways. First, the fluorescence intensity of the EB/core particle complexes was less than for EB/DNA complexes at all input ratios

measured. Second, the intensity versus ratio plot deviated from linearity at lower ratio and to a greater extent than the plot for free DNA. Finally, we observed no quenching effect for EB/core particle complexes as high as $R = 0.9$. Examination of Table IV.2 reveals that the lowered intensity of the core particle complexes is entirely due to a smaller fraction bound of total added dye. As observed for free DNA, the I_B/I_F value, corrected for the fraction bound, was constant at 21.1. After $R = .1$, the fraction of intercalated dye molecules for core particle complexes begins to decrease more rapidly than for free DNA, resulting in an intensity versus input ratio curve of smaller slope. The lack of intensity increase above $R = 0.4$ indicates that little intercalation occurs in this range of input ratios; however, high input ratios of dye resulted in no detectable fluorescence intensity quenching. These data suggest that, as a consequence of histone association, binding of ethidium does not occur to core particles at input ratios as high as $R = 0.9$.

C. Fluorescence Lifetime Measurements. Large fluorescence intensity increments provided evidence that intercalation binding of ethidium did occur to both free DNA and to highly trimmed core particles, devoid of DNA tails. However, since intensity measurements were not sensitive to external binding modes, we could not confirm that external electrostatic binding was absent from EB/core particle complexes or that intercalation binding induced dissociation of the core particle structure. We, therefore, measured the average fluorescence lifetime of ethidium bromide complexed to both free DNA, to core particles and to PVS at $R = .01$. The results are listed in Table IV.1. For free DNA and for core particles, the average

fluorescence lifetimes of the ethidium complex were 22.4 nsec and 21.8 nsec, respectively, in good agreement with previous studies. In contrast the fluorescence lifetime of electrostatically bound ethidium, measured in the EB/PVS complex, was only 4-5 nsec. Thus, like fluorescence intensity measurements, the fluorescence lifetime of ethidium distinguished between the intercalated and electrostatically bound ethidium binding modes with one useful difference. While fluorescence intensity measurements were sensitive only to the number of intercalated ethidium molecules, fluorescence lifetime measurements were sensitive to the number of intercalated and externally bound dye molecules. Additionally, the lifetime of each bound state was significantly resolved from the lifetime of free ethidium, 1.6 nsec. Thus, we were able to measure the extent of externally bound ethidium by the difference in bound molecules calculated from the two techniques.

To evaluate the total fraction, f_T , of bound dye molecules, we first measured the fluorescence lifetimes of ethidium over a range of input ratios in free DNA and in core particle complexes. The best fit to the decay data was obtained on the premise that, at any input ratio, a fraction of the free ethidium molecules would be present. Therefore, the lifetime of free ethidium in buffer, 1.6 nsec, was used as a Cheng-Eisenfeld filter (Cheng and Eisenfeld, 1979) in all analyses. The Cheng-Eisenfeld filter requires the computer to use the 1.6 nsec lifetime in fitting the decay data. Filtering out the contribution of the free ethidium in this manner reduced the complexity of the analysis by decreasing the number of parameters. Figure IV.5A shows an example of the fluorescence decay data obtained;

for each decay, a total of 20×10^6 data points were collected. Figure IV.5B shows the deviation plot for a typical analysis, demonstrating the narrow scatter profile obtained. In all cases the half-width of the scatter profile was less than 0.15 nsec. The data were analyzed by both method of moments and least squares analysis in which one lifetime was kept constant at 1.6 nsec. In all cases, the conclusions derived from both methods were equivalent.

The results of the fluorescence lifetime measurements are listed in Table IV.3. For free DNA at $R = .01$, under our experimental conditions, the best fit to the decay data indicated that the fluorescence decay curve comprised two components, in addition to free ethidium. The longest lifetime component (t_1) was 24 nsec; the second component (t_2) displayed a somewhat shorter lifetime of 17 nsec. The % population of each component was 80% and 14%, respectively. The average fluorescence lifetime, calculated from these components, was in excellent agreement with previously reported values for single-component resolution fits to the decay curve, usually obtained with far fewer data points (Paoletti et al., 1977; Olmsted and Kearns, 1977; Wahl et al., 1970; Thomas and Schurr, 1983). The use of the Cheng-Eisenfeld filter had no effect on the value of the average fluorescence lifetime or the fraction bound as seen in Table IV.4. A multiple long lifetime result appears to characterize the intercalated state of the ethidium since multiple long-lifetime components were observed even at low ratios where fluorescence intensity measurements have indicated that all the dye is bound by intercalation. Additionally, a multiple component fit to the decay data is obtained when ethidium is complexed to DNA or to core

particles, independent of ionic strength, base composition or length of the DNA. The results for the fluorescence lifetime analysis for the complex of ethidium with high molecular weight chicken erythrocyte DNA, poly dAT•poly dAT at low ionic strength and with DNA at various ionic strengths are also listed in Table IV.3. Increasing the input ratio from $R = .01 - .08$ resulted in no change in the value for fluorescence lifetimes or the relative population of the individual components. However, above $R = .10$, we observed a steady decrease in the average lifetime which was characterized by a decreased t_1 , an increased t_2 and a large increase in the amount of free ethidium. The results of the fluorescence lifetime for the core particle over a range of input ratios were quite similar to those with free DNA with only minor differences. Most notably, the average lifetime for ethidium complexed to the core particle was consistently lower than for the corresponding free DNA. Additionally, the average lifetime appeared resistant to decrease between $R = .10 - .20$, in contrast to free DNA.

Using the lifetime data and comparing them to the fluorescence intensity measurements, we calculated the number of external ion-pairs formed between the ethidium cation and the DNA phosphates. Making no assumptions about the mode of binding, we calculated the total bound dye by summing the populations of any component with a lifetime longer than free ethidium. The fractional population of total bound dye was termed f_T . Since the length of the free DNA and the core particle DNA is 145 bp, the number of bound ethidium molecules per core particle was calculated by

$$S_T = E_T = f_T \times R \text{ (eth/bp)} \times 145 \text{ bp} \quad (4.2)$$

The number of bound ethidium molecules is equal to the number of binding sites, S_T . Similarly, the number of intercalation sites, S_I , was calculated from fluorescence intensity measurements in the same manner. Finally, the number of externally bound sites per core particle was determined by

$$S_E = S_T - S_I \quad (4.3)$$

Since S_E , the number of external binding sites per core particle, is expressed in base pairs and ethidium is a monocation, the number of ion-pairs formed per core particle between the dye was $S_E/2$. The results are listed in Table IV.5. The analysis reveals that, for free DNA under low ionic strength conditions, the number of ion-pairs formed between ethidium and the DNA phosphates per core particle ranged from 1-8 with the maximum number observed at a high input ratio of $R = 1.0$. For the core particles, the number of ion-pairs ranges from 1 to 9. At $R = .30$, conditions under which we detected 8-9% dissociation, only 6 phosphate charges (2% of the total charges in the nucleosome) are neutralized by external, electrostatic association of ethidium. At $R = 1.0$, conditions under which we detected 50% dissociation, only 9 phosphate charges (3.1% of the total charges in the nucleosome) were neutralized by external electrostatic binding. We concluded that the external binding of ethidium bromide occurred to an equal extent to both free DNA and to core particles. Additionally, we concluded that the small fraction of charge neutralization of the core particle, at even high input ratios, would not be likely in itself to induce dissociation of the DNA/histone complex.

DISCUSSION

We had previously demonstrated that the dissociation of the core particle occurs as the result of binding ethidium bromide (McMurray and van Holde, 1986). The kinetics and reversibility of the ethidium-induced dissociation reaction reveal that the process is a time-dependent equilibrium. Kinetic measurements demonstrated that under our low ionic strength conditions, dissociation is slow, taking 15-24 hours to reach completion. In this report, we have established that dissociation is induced by the intercalation mode of ethidium-binding to DNA, and not by non-specific binding to the histones or alternate, non-intercalative binding to DNA. The covalent binding of ^3H -8-azido-ethidium to the core particle clearly shows that < 1.0 adducts are formed per histone octamer over a wide range of input ratios. Simultaneously, the large intensity increments observed during fluorescence intensity measurements and the long fluorescence lifetime of bound ethidium demonstrated that extensive intercalation binding was occurring. Taken together, we concluded that ethidium was binding by intercalation to DNA. Combined analysis from both fluorescence intensity and fluorescence lifetime data revealed that significant electrostatic binding of ethidium occurred only at input ratios > 1.0 , while dissociation occurred at even low input ratios of the dye. In 10 mM Tris, pH 8.0, 0.1 mM EDTA, dissociation began when ~ 17 bp of DNA are bound by intercalation and $\ll 1.0$ non-intercalated ion-pair was formed per core particle. Additionally, the large increases in dissociation with small increases in added dye did not correlate with the resulting number of external ion-pairs formed. We

conclude that, under our buffer conditions of 10 mM Tris, pH = 8.0, 0.1 mM EDTA, ethidium does bind primarily by intercalation to the highly trimmed core particle DNA, and it is this mode which induced dissociation of the histone proteins.

Table IV.1

Absorbance and Fluorescence Spectral Properties of
Ethidium Bromide (EB) Complexed with DNA, the Core
Particle (CP) and Polyvinyl Sulfate (PVS)
at Low Ionic Strength

	DNA/EB	CP/EB	PVS/EB	Free
<u>Absorbance^a</u>				
λ_{\max} (nm)	520	520	N.D.	480 nm
shift (nm)	40	40	(30-40)	--
ϵ_{\max} ($M^{-1}cm^{-1}$)	2300	2300	N.D.	5750
Isosbestic Point (nm)	513 388	517 388	513 393	--
<u>Fluorescence^b</u>				
$\lambda_{\max}^{\text{emission}}$ (nm)	606	606	--	606
I_B/I_F	29.1	21.1	0.5-1.0	1.0
τ_F (avg) ^c	22.4	21.8	4.0	1.6

a. The core particles for the absorbance measurements were titrated into a solution of ethidium bromide which ranged from $3-7 \times 10^{-4}$ M. Details of the conditions are as stated in Figure IV.5.

b. Fluorescence intensity of the ethidium complexes were excited at 550 nm and emission was monitored at 593 nm. The core particle concentration was 7.8×10^{-5} M bp. The temperature was 20°C.

c. $\tau_F \text{ avg} = \sum (\% \text{ population}) (\tau_i) \div \sum (\% \text{ population})$

Table IV.2

Comparison of the Fraction Bound and Intensity Ratios for Ethidium Bound
to the Core Particle and the Corresponding Free DNA at 20°C

R ^a	f _B ^b	DNA		R ^a	f _B ^b	Core Particle	
		I _B /I _F ^c	(I _B /I _F)/f _B			I _B /I _F ^c	(I _B /I _F)/f _B
.006	.88	25.5	28.9	.001	.56	12.2	21.7
.013	.96	25.8	26.9	.006	.82	17.5	21.3
.026	.88	25.7	29.2	.027	.88	18.6	21.1
.047	.86	25.2	29.3	.05	.91	19.2	21.0
.098	.84	24.5	29.1	.11	.86	17.7	20.6
.130	.83	24.2	29.1	.15	.83	17.7	21.3
.170	.81	23.6	29.1	.18	.79	17.0	21.5
.20	.79	23.2	29.3	.24	.80	14.0	21.3
.27	.77	22.7	29.4	.30	.69	14.8	21.4
.33	.72	21.2	29.4	.37	.62	13.5	21.8
.47	.58	17.2	29.5	.50	.52	11.3	21.7

- a. R = input ratio = moles dye added/mole DNA base pair. The buffer used in all experiments was 10 mM Tris, pH 8.0, 0.1 mM EDTA. The core particle concentration was 4.0×10^{-5} M bp; the DNA concentration was 7.8×10^{-5} M bp.
- b. f_B = fraction of the added dye which was bound by the nucleic acid = $(I - I_0)/(V - 1)I_F$
- c. (I_B/I_F) is the ratio of the fluorescence intensity of the ethidium bound in the presence of nucleic acid to the intensity of the identical concentration of dye, if it were free.

Table IV.3

Fluorescence Lifetime Measurements of Ethidium Bromide Complexed with Chicken Erythrocyte Core Particles and the Corresponding Free DNA.^a

Buffer	R_I^b	$\tau(\text{DNA})^c$	$\tau(\text{AVG})_D^d$	% Population	S_B^e	$\tau(\text{CORE})$	$\tau(\text{AVG})_C$	% Population	S_B
10 mM Tris, pH 8.0 0.1 mM EDTA	.01	24.3	22.4	72.5	1.0	23.0	21.8	79.9	1.2
		17.2		26.5	.6	15.0		14.1	0.2
		1.6		2.0		1.6		6.0	--
	.032	24.2	22.2	68.2	3.2	22.6	21.5	84.0	3.7
		17.3		27.8	1.2	15.4		16.0	0.7
		1.6		4.0	--	1.6		0	
	.10	22.9	21.8	88.2	12.0	21.6	20.5	80.8	11.7
		12.2		9.8	1.3	13.9		13.2	0.2
		1.6		2.0	--	1.6		6.0	--
	.32	18.9	16.6	64.5	30.0	19.6	18.7	81.0	37.6
		13.6		32.5	15.0	11.0		10.0	4.6
		1.6		4.0	--	1.6		9.0	--
	1.0	19.2	17.4	58.1	84.1	17.2	16.6	33.6	48.7
		13.8		30.0	43.5	11.2		6.4	9.3
		1.6		22.0	--	1.6		60.0	--
HMW DNA ^f	.032	24.5	22.4	67.2			--		
		17.4		28.8		--		--	
		1.6		4.0					
p(dA•T) ^g	.032	25.3	24.5	87.4			--		
		15.2		7.6		--		--	
		1.6		5.0					

Table IV.3 (continued)

Buffer	R_I^b	$\tau(\text{DNA})^c$	$\tau(\text{AVG})_D^d$	% Population	S_B^e	$\tau(\text{CORE})$	$\tau(\text{AVG})_C$	% Population	S_B
10 mM Tris, pH 8.0 0.1 mM EDTA + .05 M NaCl	.032	25.3 19.5 5.9	22.1			22.0 14.8 1.6		63.7 13.0 23.3	
10 mM Tris, pH 8.0 .4 M NaCl	.032					23.0 15.7 1.6		47.3 13.0 39.7	

a. The length of the DNA and the core particles was 145 ± 2 BP. For all measurements the DNA concentration was 4.5×10^{-5} M (BP); the core particle concentration was 4.2×10^{-5} M (BP). Measurements were made at either 550 nm or 555 nm excitation wavelength, and emission was monitored at 593 nm.

b. $R = \frac{\text{moles ethidium}}{\text{DNA (BP)}}$

c. τ units are nanoseconds. Lifetime data were analyzed using a Cheng-Eisenfeld filter of 1.6 ns (the lifetime of free ethidium bromide).

d. $\tau(\text{AVG}) = \frac{\sum_i (\% \text{ population})(\tau_i)}{\sum_i (\% \text{ population})_i}$

e. S_B = the number of BP sites bound by ligand; $S_B = (R)(\% \text{ Pop})(145)$

f. HMW DNA = high molecular weight chicken erythrocyte DNA mw $\sim 10^6$

g. p(dA•T) = alternating A•T copolymer ~ 1000 BP

Table IV.4

Effect of Data Collection Conditions on the Resolution of Lifetime
Components of Ethidium Bromide Complexes with Free DNA and Nucleosomes

Counts	Ratio	τ (DNA)	% Pop	τ AVG	τ (CORE)	% Pop	τ AVG
5×10^3	.03	22.4	100	22.4	21.4	100	21.4
	.10	21.8	100	21.8	20.5	100	20.5
20×10^6	.03	22.4	100	22.4	21.9 5.0	88 12	21.5
	.10	21.8	100	21.8	21.1 5.0	98 2	20.5
20×10^6 + filter	.03	24.4	71	22.2	22.6	82	21.5
		17.3	29		15.4	12	
		1.6	4		1.6	6	
	.10	22.9	88.2	21.8	19.6	80.8	20.5
		12.2	9.8		11.0	13.2	
		1.6	2.0		1.6	6.0	

Table IV.5

Multi-Component Analysis of Ethidium Bromide Complexes with Chicken Erythrocyte
Core Particle and Free DNA from Fluorescence Intensity and Fluorescence Lifetime Measurements Combined

Sample ^a	A. Fluorescence Intensity				B. Fluorescence Lifetime Analysis					
	R _{APP} ^b	f _B ^c	v ^d	S _I ^e	f _T	S _B ^f	S _E ^g	S _E /2 ⁱ	%D ^h	
DNA					(.72)	(1.0)				
[Na ⁺]=.005 M	.013	.99	.013	1.9	.99	1.6	0.3	.15	--	
					(.27)	(.6)				
					(.68)	(3.2)				
	.033	.93	.030	4.4	.96	4.4	0		--	
					(.28)	(1.2)				
					(.88)	(12.0)				
	.098	.87	.085	12.3	.98	13.3	1.0	.50	--	
					(.10)	(1.3)				
					(.65)	(30.2)				
	.34	.75	.26	37.7	.98	45.5	7.8	4.0	--	
					(.33)	(15.3)				
					(.58)	(37.8)				
	1.0	.45	.45	65.3	.88	81.0	15.7	7.8	--	
					(.30)	(43.5)				
Core					(.80)	(1.2)				
[Na ⁺]=.005 M	.006	.82	.005	0.71	.94	1.4	0.7		0	
					(.14)	(.2)				

Table IV.5 (continued)

Sample ^a	A. Fluorescence Intensity				B. Fluorescence Lifetime Analysis					
	R _{APP} ^b	f _B ^c	v ^d	S _I ^e	f _T	S _B ^f	S _E ^g	ion ⁱ pairs	%D ^h	
	.027	.88	.024	3.4	(.84) .94 (.16)	(3.9) 4.6 (.7)	1.2	.6	0	
	.10	.83	.083	12.0	(.81) .94 (.13)	(11.7) 11.9 (.2)	0		3	
	.30	.69	.21	30.0	(.81) .91 (.10)	(37.6) 42.2 (4.6)	12.2	6.1	9	
	.50 1.0	.52 .28	.26 .28	37.7 40.6	(.34) .40 (.06)	(49.3) 58.0 (8.7)	18	9	50	
[Na ⁺]=.15 M	.032	--	--	--	(.45) .58 (.13)	(2.1) 3.6 (0.6)	--		--	

a. All DNA and core particle samples were dialyzed into 10 mM Tris, pH 8.0, 0.1 mM EDTA. The [Na⁺] concentration at this pH is .005. Other concentrations of NaCl are indicated. The concentration of DNA or core particle was 4.3-4.5x10⁻⁵ M (BP).

Table IV.5 (continued)

- b. $R_I = \text{input ratio} = \frac{\text{moles ethidium added}}{\text{mole BP}}$
- c. $f_B = \text{fraction bound} = (I - I_0)/(V-1)I_F$ where I is the fluorescence intensity in the presence of nucleic acid; I_0 is the fluorescence intensity in the absence of nucleic acid and V is the ratio of the bound to free intensity.
- d. $v = \text{bound ratio} = \frac{\text{moles ethidium bound}}{\text{mole BP}}$
- e. $S_I = \text{sites (BP) bound by intercalation} = v \times 145 \text{ BP}$
- f. $S_B = \text{sites bound; sum of the intercalation sites and non-intercalative sites}$
- g. $S_E = \text{sites bound by a non-intercalation mode} = S_B - S_I$
- h. $\%D = \text{the percent dissociation determined for the input ratio}$
- i. $\text{ion-pairs} = (S_B - S_T)/2$

Figure IV.1. Polyacrylamide gel electrophoretic analysis of the products of the ethidium-induced dissociation of the nucleosome core particle separated on sucrose gradients. Core particle/EB complexes were isolated on 5-20% linear sucrose gradients, and each resolved peak in the gradient was analyzed on a 1.0 mm thick, 3.5% native polyacrylamide gel. A. Band-1, the intact core particle: 145 bp DNA and histone octamer; B. Band-2, the hexamer: 145 bp DNA and six of the eight histone proteins, missing one copy each of H2A and H2B; C. Band-3, free DNA: produced by ethidium-induced dissociation of the core particles; D. Free DNA/EB complex. The buffer used for core particle solutions and sucrose gradient analysis was 10 mM Tris, pH 8.0, 0.1 mM EDTA. The core particle concentration was 7.5×10^{-4} M BP.

Figure IV.1

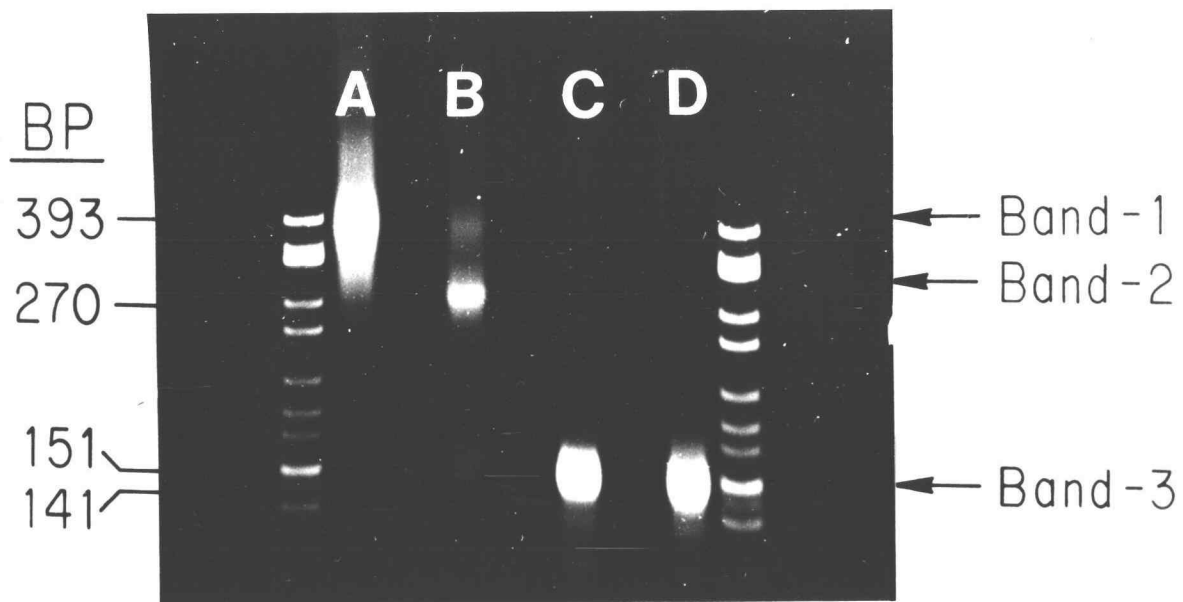


Figure IV.2. The plot of the number of ^3H -azido-ethidium bromide molecules covalently bound per core particle versus log input ratio. ^3H -azido-ethidium was photoactivated with visible light as described in text. The total protein component was separated by SDS-15%-polyacrylamide gel electrophoresis. The labeled protein was extracted and the amount of ^3H -label was detected by scintillation. The concentration of the core particle samples was 1.5×10^{-3} M bp and the temperature was 23°C . The buffer used in all experiments was 10 mM Tris, pH = 8.0, 0.1 mM EDTA.

Figure IV.2

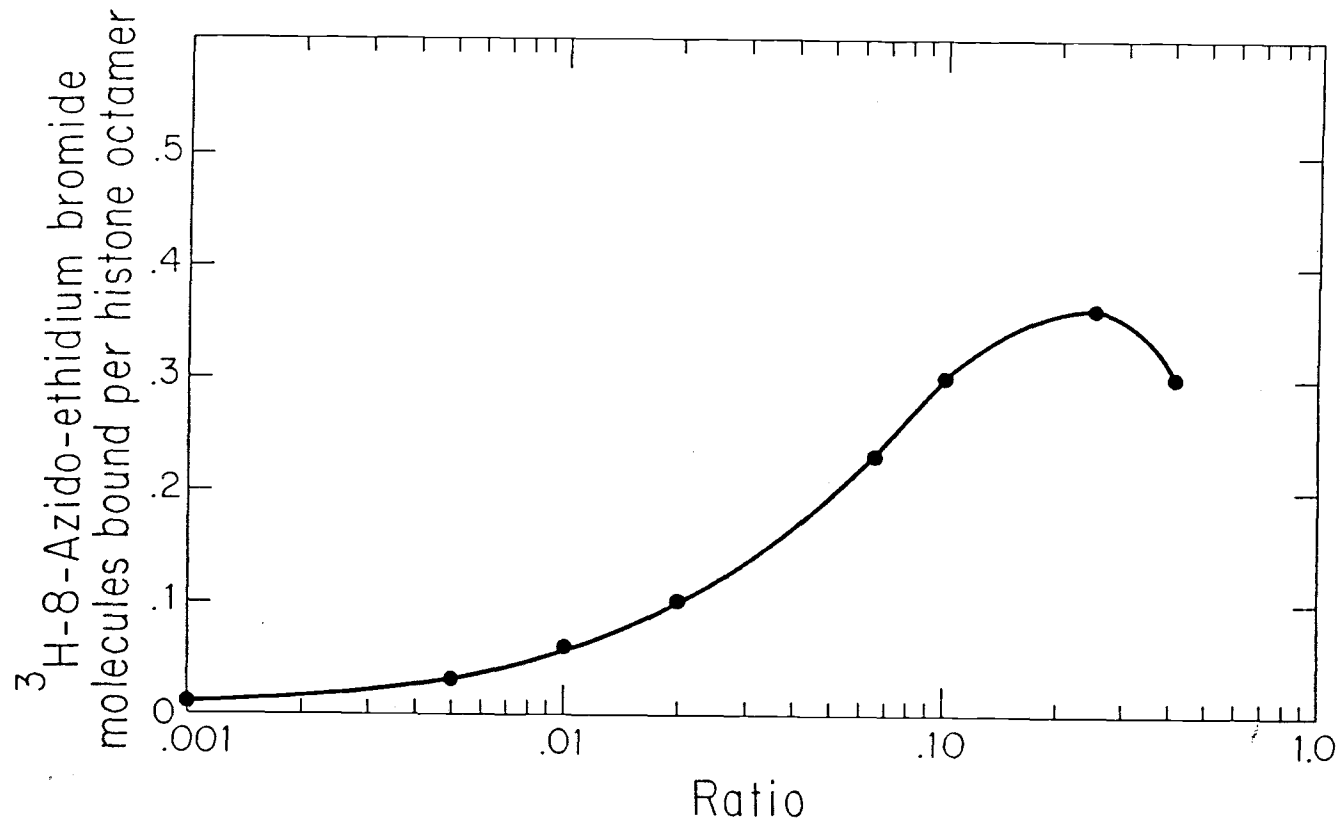


Figure IV.3. The absorbance spectra of ethidium complexed with chicken erythrocyte free DNA, the core particle and polyvinylsulfate at $T = 23^{\circ}\text{C}$. (A) Absorbance spectra for DNA/ethidium complexes: (1) free ethidium, $158 \times 10^{-4} \text{ M}$ (2) $R = 24$ (3) $R = 7.8$ (4) $R = 3.9$ (5) $R = 2.6$ (6) $R = 1.9$ (7) $R = 1.6$ (8) $R = 1.2$ (9) $R = 0.9$ (10) $R = 0.7$ (11) $R = 0.67$; (B) Absorbance spectra for the polyvinylsulfate/ethidium complexes: (1) free ethidium, $1.28 \times 10^{-4} \text{ M}$ (2) $R = 6.25$ (3) $R = 3.1$ (4) $R = 2.0$ (5) $R = 1.54$ (6) $R = 1.25$ (7) $R = .98$ (8) $R = .78$ (9) $R = .64$; (C) Absorbance spectra for the core particle/ethidium complexes: (1) free ethidium, $1.59 \times 10^{-4} \text{ M}$ (2) $R = 9.7$ (3) $R = 3.8$ (4) $R = 2.0$ (5) $R = 1.4$ (6) $R = .85$ (7) $R = .61$ (8) $R = .48$ (9) $R = .42$ (10) $R = .35$ (11) $R = .31$. All spectra were obtained by titration of concentrated nucleic acid or polyvinylsulfate stocks into a constant concentration of ethidium bromide. Spectra were obtained by measuring the absorbance in a quartz cell with a 1 cm path length. The buffer used for all experiments was 10 mM Tris, pH 8.0, 0.1 mM EDTA.

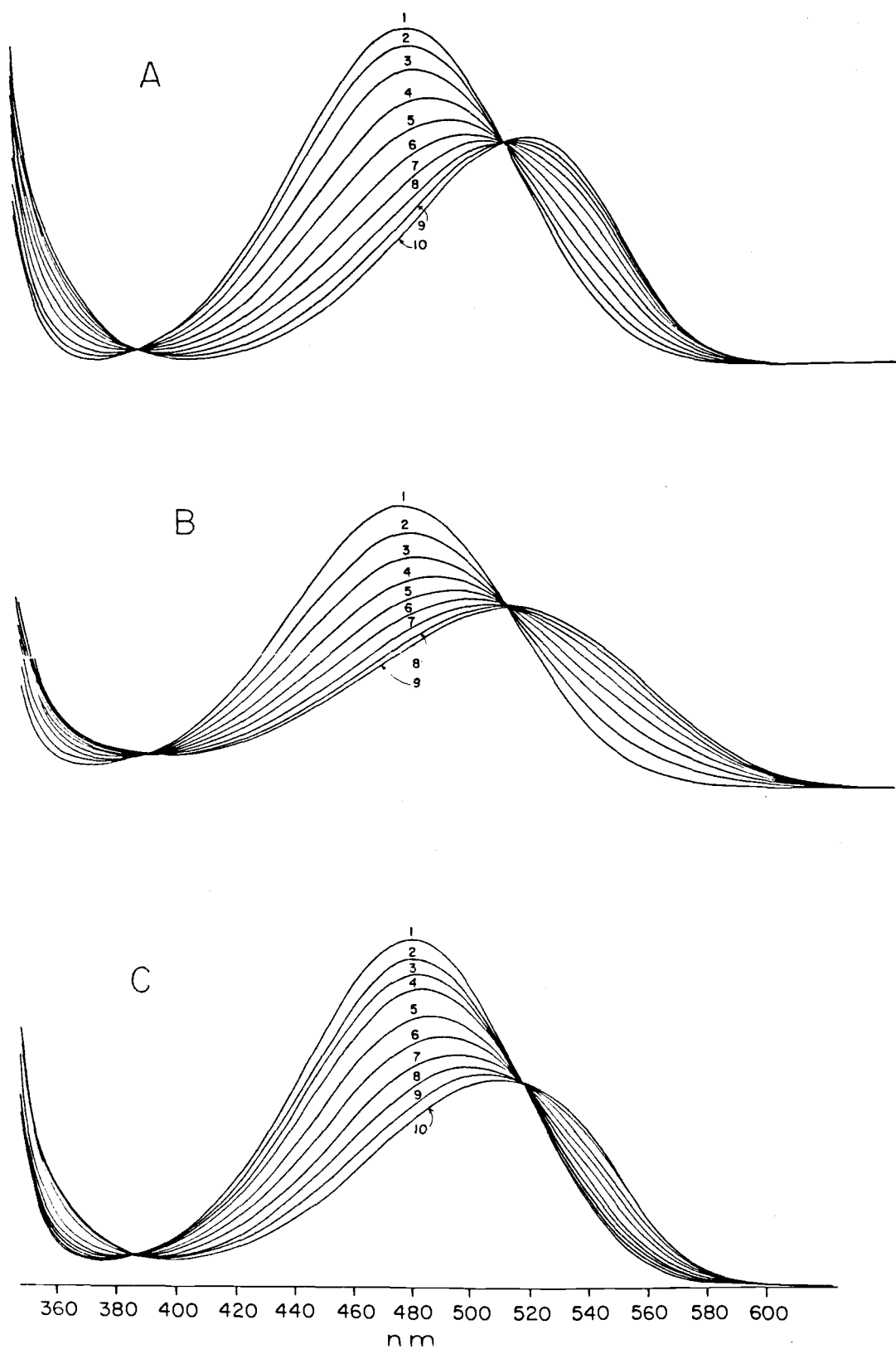


Figure IV.3

Figure IV.4. The plot of fluorescence intensity versus input ratio for complexes of ethidium bromide with chicken erythrocyte core particles and the corresponding free DNA in 10 mM Tris, pH 8.0, 0.1 mM EDTA at 20°C. () free DNA; () core particles measured immediately after mixing; () core particles measured after 72 hours. The excitation wavelength was 550 nm and emission was monitored at 593 nm. I_F is the fluorescence intensity in the presence of nucleic acid and I_0 is the fluorescence intensity of the buffer. R is the input ratio of ethidium bromide = moles ethidium added/mole DNA base pair. The inset corresponds to the boxed region in lower left corner. The core particle concentration was 4.0×10^{-5} M bp; DNA concentration was 7.8×10^{-5} M bp.

Figure IV.4

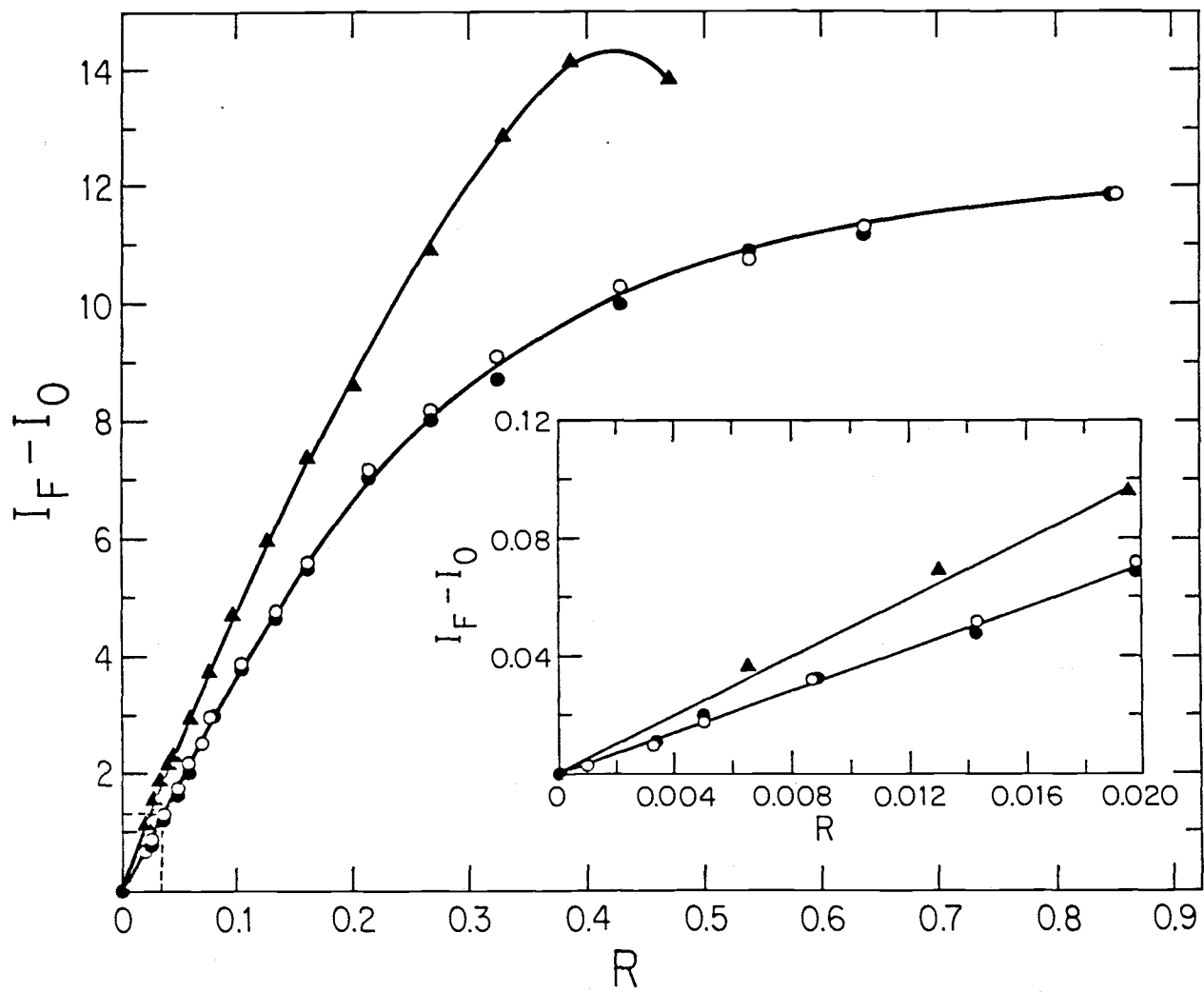


Figure IV.5. Examples of the measured scatter profile and of the fluorescence decay (labeled F) of ethidium complexed with core particle length DNA. (A) The fluorescence decay data, labeled F; (B) The deviation plot. These data were obtained with $R = 1$ using the triple-plate photomultiplier. The DNA base pair and total ethidium concentrations were 4.5×10^{-5} M. Excitation was at 550 nm. Deviation (weighted residual) plot obtained by Least Squares Iterative Reconvolution analysis of the data in (A).

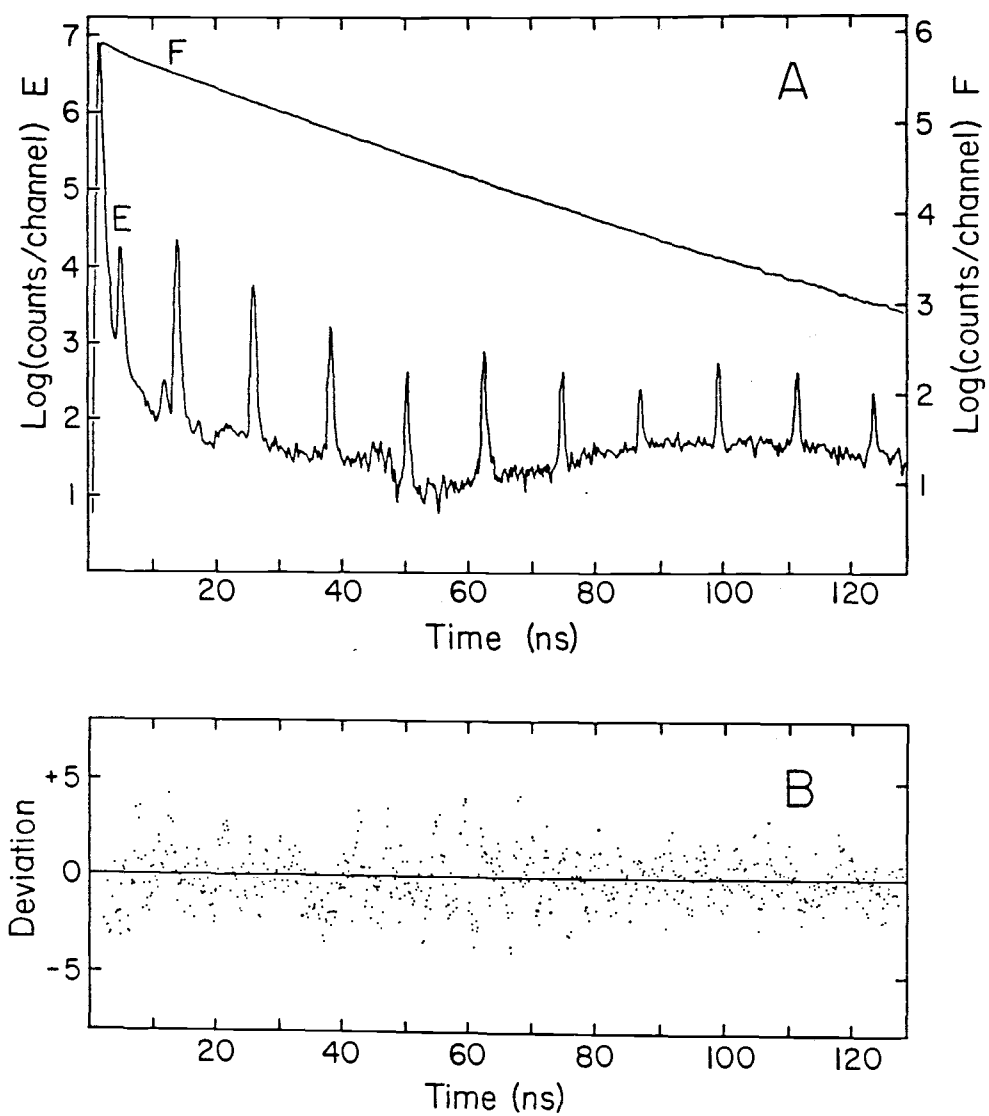


Figure IV.5

Chapter V. THE BINDING OF ETHIDIUM TO THE NUCLEOSOME

CORE PARTICLE: THE BINDING REACTION

ABSTRACT

We have carefully examined the binding properties of the dye, ethidium bromide, to the nucleosome core particle and free DNA. The binding curves for the core particle are corrected for the presence of free DNA due to dissociation of the core particle structure (McMurray and van Holde, 1986). The corrected curves reveal that the binding of ethidium to the core particles is a highly cooperative process with a very low intrinsic binding constant of $K = 2.2 \times 10^4 \text{ M}^{-1}$. Through the use of MPE footprinting, we have shown that the initial sites of ethidium binding are restricted to only the ends of the core particle DNA. The temperature and ionic strength dependence of the binding reaction were also examined. The results indicate that the initial binding of ethidium to the core particle is independent of both temperature and ionic strength. However, as binding progresses, it becomes both temperature and ionic strength sensitive. We discuss a number of consequences of these results. Additionally, based on the unwinding effect produced by the binding of ethidium, we propose a model for the unfolding of the core particle during transcription.

INTRODUCTION

Outside of control regions, it has become increasingly evident that histones remain bound to transcriptionally active or competent genes, even though the nucleosomal conformation may be altered in such regions (Cartwright et al., 1982; Weisbrod, S., 1982; Lewin, B., 1980; Mathis et al., 1980). The presence of histone in transcriptionally active regions must be reconciled with the observation of Lilley et al. (1979) that eukaryotic polymerase binds, but does not initiate transcription on intact nucleosomes. Instead, these authors found that transcription occurred only on dissociated or partially unfolded nucleosomal DNA. Thus, some mechanism must exist for core particle "disruption" at the moment of the passing of RNA-polymerase.

We have used the unwinding effects produced by an intercalating dye ethidium bromide as a model for RNA polymerase interactions. However, the dye binding properties, and the effects of dye binding on nucleosome structure were controversial. Analysis of the binding of ethidium bromide to the nucleosome has resulted in two opposing models. Wu et al. (1980) reported that the binding of ethidium bromide to the chicken erythrocyte core particle displayed negative cooperativity typical of the neighbor exclusion binding seen for free DNA. Thus, the binding of the dye was greatest at very low ratios, and gradually decreased. The authors observed that, at low input ratios (R) of the dye, below $R = 0.75$, the binding affinity of ethidium to the core particle was an order of magnitude higher ($\sim 10^7$) than for DNA ($\sim 10^6$) in low ionic strength buffers. As more dye was added, the affinity of the dye for the core particles was exceeded by

the affinity for DNA, and these authors claimed that the binding of the dye resulted in an overall unfolding of the core particle structure without loss of the histone proteins as high as $R = 0.2$. In this model, the association of the histones to DNA resulted in increased affinity of the dye for its nucleic acid substrate. The initial high affinity of the dye to the core particles was attributed to the coupling of drug binding to the release of superhelical stress induced by the binding of the histones. Implicit in the argument was the assumption that the tight binding of histones produced the topological constraints required for a linking number relationship to hold. In contrast, Erard and co-workers (1979) reported that the binding of ethidium bromide to the core particle was a positively cooperative process. Binding of the first molecules favored the binding of the next and, consequently, the affinity of the dye was lowest at very low ratios, but gradually increased below $R = 0.15$. In this model, the presence of the histone proteins reduced the affinity of the dye to the nucleic acid substrate. The positive cooperativity was attributed to the availability of more binding sites through the gradual loosening of the steric block presented by the tight binding of the histones.

We have carefully examined the binding properties of ethidium bromide to the nucleosome core particle. We find the dye binding is a highly cooperative process which results in the step-wise dissociation of structure. Additionally we have examined the temperature and ionic strength dependence of the binding reaction and the location of the ethidium binding sites. Based on the binding properties of ethidium, we propose and present evidence for a mechanism of core particle disruption.

RESULTS

I. Binding Properties of Ethidium to Free DNA and to the Core

Particle at Low Ionic Strength

The absorbance spectrum for ethidium bromide fully bound to both free DNA and the core particles in 10 mM Tris, pH = 8.0, 0.1 mM EDTA (TE) displayed in a reduced extinction coefficient $2300 \text{ M}^{-1}\text{cm}^{-1}$ for both nucleic acid forms. The absorbance maximum for the two complexes was shifted 40 nm to longer wavelengths, from 480 nm to 520 nm, relative to the free dye, and ethidium bound to both forms of nucleic acid displayed distinct isosbestic points, suggesting that only two states of the dye, free and bound, were present in solution (see Chapter 4). The measured extinction coefficients for the free and fully bound dye were used to generate Scatchard plots (Scatchard, 1949) for the binding of ethidium bromide to the core particle under various temperature and ionic strength conditions. The results for the binding of ethidium bromide to the chicken erythrocyte core particle at 30°C in TE are shown in Figure V.1. To insure the correctness of the binding parameters, the binding curve was calculated from absorbance measurements in two different types of experiments. The closed circles represents the observed binding constants generated from a spectrophotometric titration. Assuming that the extinction coefficient in the presence of nucleic acid, E_{app} , is a linear function of the bound dye, the absorbance for the complex was measured at 480 nm (where the maximum change occurred) and the extinction coefficients for the free, $5750 \text{ M}^{-1}\text{cm}^{-1}$, and the bound,

2300 M⁻¹cm⁻¹, forms of the dye were used to convert the absorbance measurements to Scatchard plots. In this case, the fraction of bound dye is calculated by

$$F_{\text{bound}} = E_{\text{free}} - E_{\text{app}}/E_{\text{free}} - E_{\text{bound}} \quad (5.1)$$

The concentrations of bound and free dye, as well as the ratio of bound dye were calculated by

$$C_{\text{bound}} = F_{\text{bound}} \times C_{\text{total}} \quad (5.2)$$

$$C_{\text{free}} = C_{\text{total}} - C_{\text{bound}} \quad \text{and} \quad (5.3)$$

$$V_{\text{bound}} = C_{\text{bound}}/[\text{DNA}] \quad (5.4)$$

The open circles were generated by equilibrium dialysis measurements where the concentration of free dye, C_{free} , is directly measured by the absorbance in the buffer cell of a three chambered equilibrium dialysis apparatus. The C_{F} was converted to moles, and the total moles of bound dye $m_{\text{B}}(\text{total})$ was determined by

$$m_{\text{F}} = C_{\text{F}} \times \text{cell volume (buffer + sample)} \quad (5.5)$$

$$m_{\text{B}}(\text{total}) = m_{\text{I}} - m_{\text{F}} \quad (5.6)$$

$$(B = \text{bound}, I = \text{input}, F = \text{free}) \quad \text{and}$$

$$V_{\text{bound}} = m_{\text{B}}(\text{total})/\text{sample volume} \quad (5.7)$$

The observed binding constants, $V_{\text{bound}}/C_{\text{free}}$, from both spectrophotometric binding and equilibrium dialysis were superimposable and agreed well with a previously reported binding curve generated from a third type of binding experiment calculated from fluorescence intensity measurements (Erard et al., 1979). Recently, however, we have shown that the binding of ethidium bromide, above a critical level, induces dissociation of the core particle into free DNA and histones (McMurray and van Holde, 1986). Thus, to generate the correct binding curve for the core particle, it was necessary to correct the core particle Scatchard plot for the amount of dye bound to the free DNA component. The correction involved the determination of the amount of free, dissociated DNA at every input ratio of dye and, ultimately, the number of moles of dye bound only to the core particle, $m_B(\text{core})$, at that ratio. The method is schematically shown in Figure VI.2A and described in detail in Chapter 3. Since the association of ethidium bromide to free DNA was initially 100 times stronger than to the intact core particle (Table V.1), we made the assumption that the dye would preferentially bind to free DNA, when present. Thus, we approximated the number of moles of DNA-bound ethidium by measuring the amount of dye bound to the dissociated DNA in the absence of the core particle. Using the % dissociation values from the gel quantification method (Chapter 3), we determined the concentration of free DNA at every input ratio of ethidium bromide. Next, we made an independent series of DNA solutions which corresponded to the dissociated free DNA concentration measured in every sample and added the total moles of ethidium bromide at that input ratio. The absorbance was measured and we calculated the

apparent extinction coefficient in every DNA sample. The fraction of bound ethidium to DNA, $F_B(\text{DNA})$, was calculated as in equation 5.1, and the moles of dye bound to the DNA component alone was calculated by

$$m_B(\text{DNA}) = [F_B(\text{DNA}) - (V_C(F_B(\text{DNA}))) \times m_{\text{bound}}(\text{total}) \quad (5.8)$$

Since the critical ratio of dye bound to the DNA component was present when the DNA was still an intact particle, this value was subtracted from the $m_B(\text{DNA})$ expression. Finally, the $m_B(\text{core})$ was calculated by

$$m_B(\text{core}) = m_B(\text{total}) - m_B(\text{DNA}) \quad (5.9)$$

The plot of % dissociation versus v_{core} is shown in Figure V.2B.

The dissociation of the core particles appears highly dependent on v_{core} in a smooth but non-linear manner, and asymptotically approaches infinite slope a limiting ratio at $R = 0.23$. Correction for the binding of ethidium to free DNA resulted in a reduction in the extrapolated value for zero dissociation to $v_C = .03$. This value represents the amount of dye which must be bound per core particle for dissociation to occur. Previously, we had determined that the critical ratio for dissociation was $v_C = .06$ (Chapter 2 and McMurray and van Holde (1986)). However, as described below, we measured the parameter f , the fraction of core particles which bind ethidium prior to dissociation, and calculated this value to be 0.5. Since $f < 1.0$, v_C must be v_C/f . Thus, the critical ratio remained unchanged at $v_C = .06$. The corrected values of v_{core} were used to construct the

Scatchard plot for the association of ethidium bromide to the core particle, corrected for the presence of free DNA. The results are shown in Figure V.3. The binding isotherm of ethidium bromide to the core particle is characterized by a highly positive slope which reached a maximum between $v = .08 - .10$. The cooperative initial slope in the binding curve corresponds to the region in the dissociation curve where we detect no dissociation. Additionally, the critical value is near the region in the binding curve where the curve reached a plateau. We concluded from these results that the rest of the uncorrected curve is due to the binding of ethidium to dissociated DNA.

The data plotted in Figure V.2 and V.3 were fitted to theoretical expressions for the McGhee and von Hippel (1974) conditional probability model of excluded site binding. The intrinsic binding constant, K , was determined from the apparent (observed) binding constant, v/C , using

$$v/C = K (1 - nv) \times \quad (5.10)$$

$$\frac{(2w - 1)(1 - nv) + (v - R)}{2(w - 1)(1 - nv)} n^{-1} \frac{1 - (n+1)v + R}{2(1 - nv)}$$

$$R = [(1 - (n + 1)v)^2 + 4 wv (1 - nv)]^{1/2}$$

where v is the moles of dye bound per polymer base pair, C is the free dye concentration, n is the number of base pairs excluded per dye molecule upon binding and w is the cooperativity parameter which represents the equilibrium constant for the transfer of a dye molecule

from an isolated site to a singly contiguous site. The values for K , n and w were calculated from Eq. 5.10 from a non-linear least squares fitting program by minimizing the sum of the root mean square for all experimental points. Since the cooperative shape of the uncorrected curve did not fit well at both high and low ratios to a single theoretical curve, we broke the curve into two regions which were fit separately. The first region (A) included only the points which in the initial positive slope, up to but not including, the maximum. The second region, B, included only points after the maximum. The K , n , w best-fit results for the spectrophotometric titration of ethidium to the core particle in both regions are listed in Table V.1. Interestingly, both the binding curve, corrected for ethidium bound to free DNA, and region A in the uncorrected curve fit well to a theoretical curve characterized by a low intrinsic binding constant, $2.2 \times 10^4 \text{ M}^{-1}$, and a large cooperative transition, $w = 143$. The points in region B fit best to a theoretical curve with higher intrinsic affinity, $2.5 \times 10^5 \text{ M}^{-1}$, and very little cooperativity, $w = .3$, similar in shape to the free DNA curve.

The uncorrected isotherm for the binding of ethidium bromide to the core particle was directly compared to free DNA in Figure V.4. Comparison of curves A and B in Figure V.4A reveals that the manner in which the two types of nucleic acid bind ethidium bromide is quite different. For free DNA, curve A, the binding of the dye displays slight negative cooperativity, $w = 0.3$, typical of exclusion binding. The curvature in the Scatchard plot arises from a statistical effect of fewer available binding sites as the dye saturates the DNA lattice. Consequently, the maximum affinity for the dye is observed at low

ratios of dye to bp, and gradually decreases. In contrast to free DNA, the shape of the curve B indicates that the binding of ethidium bromide to the core particle in TE buffer displays a large positive cooperativity, $w = 143$. Thus, binding of the first dye molecules to DNA in the core particle favors the binding of the next molecule, and, consequently, the binding affinity of the dye at very low ratios is at a minimum. Comparison of the intrinsic binding constants for ethidium bromide to the core particle, $K_A = 2.2 \times 10^4$, and to free DNA, $K_A = 1.1 \times 10^6$, reveals that the binding affinity of the first few ethidium molecules to free DNA is roughly 100-fold greater than to the core particle. The free energy difference between the binding of ethidium binding to free DNA and to the core particle, calculated from the observed binding constants (v/C), is plotted in Figure V.4B. At the very lowest ratio, the binding of ethidium to free DNA is favored by 3.5 kcal/mole over binding to the core particle. As the level of dye is increased, the energy difference of ethidium binding to the two forms decreases exponentially until it is essentially the same at or above a ratio of 0.1.

In addition to the large differences in binding constant and cooperativity between the two forms of nucleic acid, comparison of the fitted values in Table V.1 indicated that the number of base pairs excluded by the dye is much larger when bound to the core particle ($n = 7.0$) than when bound to free, random sequence DNA ($n = 2.4$). Was this observation correct at face value? In the McGhee and von Hippel analysis, the value of n is obtained by the reciprocal of the x-intercept value at saturating levels of the ligand, with the assumption that, at least initially, the entire lattice is available

for binding. Thus, the apparent number of sites excluded by the dye, obtained in a particular experiment represents only an average value for the lattice. If the assumption of random binding does not hold, then the correct value for n relies on the boundary conditions imposed by the binding substrate. For the core particle, the possibility that the histones presented an obstacle to dye binding led the consideration of two binding models which could both account for the $n = 7.0$ observation. The first possibility was a model based on random access of the dye. In this case, the histones presented no steric block to dye binding and the dye was able to bind anywhere on the lattice. The large n value for the core particle (7.0) relative to free DNA (2.0) could arise, then, from a conformational effect of histone binding, the combined effect of the dye binding to the histone/DNA complex being one dye binding site per 7 base pairs. The second possibility was regional binding. In this case, only particular region(s) on the lattice are actually available for dye binding due to histone binding, and since only a fraction of lattice (f) is available, the true value for n would be nf .

To distinguish between these two cases, we devised the following experiment which is schematically illustrated in Figure V.5. We monitored the binding of a derivative of ethidium bromide, methidiumpropyl-EDTA-Fe(II)(MPE) (Hertzberg and Dervan, 1982) to 5'-³²P-end-labeled core particles within the pre-dissociation range of input ratios. MPE has binding properties quite similar to ethidium, but contains the metal chelator, EDTA, tethered to the intercalator portion of the molecule. Upon reduction with agents such as dithiothreitol (DTT), MPE cleaves one strand of the DNA at or very

close to the binding site of the dye molecule. Since we knew that the length of the DNA is 145 bp, we predicted that random binding of MPE should result in the immediate breakdown of the DNA into a series of small DNA oligonucleotides as shown in Figure V.5B. Since the core particles comprise random sequence DNA, we should observe a smear of staining intensity with the eventual disappearance of the DNA band at high ratios, i.e., when the oligonucleotides were very small. On the other hand, if the binding were regional, we should observe discrete DNA bands whose length should indicate the region of dye binding. Figures V.5A and C illustrate examples of regional binding to one (A) or both ends (C) of the core particle. The core particles were complexed with MPE, and, after activation with DTT, the core particles were deproteinized to remove the histones. The resulting purified DNA was digested with S1 nuclease to create a double stranded cut (if necessary) and, finally, the DNA fragments were separated by 7% polyacrylamide gel electrophoresis. Analyses of the cleavage products of the MPE reaction detected by ethidium staining were utilized to determine the binding site of the dye and to distinguish between random versus regional binding.

The results of the MPE cleavage reaction of free DNA (lanes 1-4) and the core particles (lanes 5-10) are shown in Figure V.6. For both free DNA (lanes 1 and 2) and the core particles (lanes 5 and 6), we included two control lanes, $R = 0$. The DNA in the lanes 1 and 5 were directly extracted from the intact core particles or DNA without exposure to any of the reaction conditions. This control will be referred to as the untreated control lane. Lanes 2 and 6 represent the mock control reaction, i.e., the DNA went through all the reaction

steps minus the dye. For both the free DNA and the core particle, the amount of DNA present in the mock control was always less than the untreated control. Thus, while the reaction conditions did not degrade the DNA, they did cause increased solubility of the MPE/nucleic acid complex in phenol resulting in a loss of intensity of the $R = 0$ band relative to the untreated control. Consequently, integrated area in the presence of dye was always compared to the mock experiment. At $R = .02$, we observed immediate degradation of the free DNA indicated by loss of intensity of the intact band accompanied by an intensity smear below the intact band. At $R = .06$, all the free DNA was cleaved into small oligonucleotides and, as expected, all intensity was lost from the gel. Thus, for free DNA, the results from the MPE cleavage reaction clearly indicated random binding of the dye. In contrast, MPE cleavage of the core particles resulted in the appearance of discrete bands which were shortened in length relative to the mock reaction control (lane 6). The laser densitometer trace of the core particle DNA bands are shown in Figure V.6A. Increasing input ratios of MPE to the DNA in the core particle (from .02 - .20), resulted in the loss of intensity in the intact 145 bp position with a concomitant increase in intensity in the region between 145 - 120 bp. The intensity appeared to be distributed in at least three peaks, one centered at 135 bp and one centered at 120 bp with some intensity remaining in the intact, $R = 0$ band reduced by a few base pairs (140 - 142 bp). Over the entire ratio range, the total intensity in all lanes remained constant. Thus, MPE cleavage of the DNA within the intact core particle resulted in the loss of up to 25 bp. Since fragments of length = 120 bp could not be generated by cutting within

the center of the core particle, the cleavage pattern demonstrated that the ethidium binding sites on the core particle occurred only at the ends of the core particle under pre-dissociation conditions.

While fragment lengths, generated by the MPE-cleavage reaction, unambiguously identified the core particle ends as the site of binding for ethidium, the end-binding reaction could result from two different mechanisms. First, the dye could bind to only one end. In this case, we would conclude that MPE cleaves 20 bp at a single end of the core particle. If MPE bound to both ends, we would conclude that dye binding cleaves ~10 bp from two ends. These mechanisms are schematically depicted in Figure V.6A and C. To elucidate which of these two possibilities was correct, we monitored the fate of the terminal 5'-³²P-label attached to both ends of the core particle. Dye binding to only one end would be confirmed if the intensity of the end-labeled band was reduced by one-half with a reduction in the length of the fragment. On the other hand, if dye binding occurred to both ends, we would expect to observe gradual disappearance of the zero band intensity, accompanied by no reduction in fragment length. The results of these experiments, shown in Figure V.7, confirm that dye binding occurs to both ends of the core particle. At R=0 (Figure V.7(B) lane 2, all the intensity resides in the 145 bp band of the intact deproteinized core particle. As the ratio of dye to base pair is increased, we observed the gradual reduction in intensity of band intensity and no reduction in band length. Comparison of the laser densitometer trace of band intensities from gel autoradiography with the band intensities from ethidium staining of the gel in Figure V.7C indicates that a large portion of the DNA from R = .02 - .20, is near

to the zero band length, reduced by only a few base pairs. We predict that while binding occurs at both ends of the core particle, binding is preferred to one side.

II. Determination of f

The ^{32}P -end-label results were also used to determine f , the fraction of core particles which actually bind ethidium prior to dissociation occurred (McMurray and van Holde, 1986). We had previously determined this value by extrapolation of the % dissociation versus bound ratio to zero % dissociation, and determined its value to be $v_C = .06$. The critical ratio of dye was initially estimated under the assumption that $f = 1.0$, i.e., that all core particles bound dye below the critical value. However, the highly positive cooperativity, characteristic of ethidium binding to the core particle, indicated that f might be less than 1.0. Therefore, we directly measured the f from the results of the MPE experiment. Since MPE binding and cleavage of a ^{32}P -end labeled core particle results in the disappearance of its intensity, f can be measured from the total band intensity remaining after cleavage with MPE at the critical value. The fractional remaining intensity (f) at each input ratio is listed in Figure V.7C. The critical bound ratio, $v = .03$, corresponds to an input ratio close to $R = .04$. Since only half of the ^{32}P -end-label is retained after MPE cleavage, f is equal to 0.5. Since $f < 1.0$, then the correct critical ratio is v_C/f (McMurray and van Holde, 1986). We conclude that v_C remains unchanged at .06, i.e., 8-9 ethidium molecules are required for dissociation. However, the

results reveal important new aspects of the dissociation mechanism. At low ionic strength, dissociation is also a highly cooperative process with some core particles dissociating before others bind any dye at all.

III. The Temperature and Ionic Strength Dependence of Ethidium

Binding to the Core Particle

A. Temperature Dependence

The temperature dependence of ethidium binding reaction to the core particle is shown in Figure VI.8. As described earlier, each curve was divided into two regions, A and B, where region A corresponded to points which occurred before the cooperative maximum, and region B corresponded to points which occurred after the cooperative maximum. We assume from our analysis of the ethidium binding to the core particle seen in Figures V.1 and V.3 that region A represents binding to the intact core particle structure and region B represents binding to dissociated, core particle DNA. The observed equilibrium constants, v/C , were fit according to Eq. 5.10 for both regions, and the results are listed in Table VI.2. For region A points, increasing the temperature from 10-50°C resulted in no change in the intrinsic binding constant but did result in a large decrease in the cooperativity from $w = 124$ to $w = 29$ and a decrease in n from $n = 9.0$ to $n = 6.0$. From 30°C to 40°C, near physiological temperatures, the binding isotherms of ethidium to the core particle were almost superimposeable. For region B points, increasing the temperature from

10°C to 50°C resulted in a decreased binding constant, from 3.8×10^5 to $1.8 \times 10^5 \text{ M}^{-1}$, but we observed little change in either the cooperativity or the value of n which changed from $n = 3.1$ to $n = 2.6$.

We did not observe any temperature dependence of the observed equilibrium constant for the region A points. Therefore, the observed equilibrium constants from only region B in Figure VI.8 and Table VI.2 were plotted in Figure V.9 according to the van't Hoff equation

$$\ln K = \frac{\Delta H^\circ}{RT} + \frac{\Delta S^\circ}{R} \quad (5.11)$$

where ΔH° and ΔS° represent the observed enthalpy and entropy changes, respectively for the ethidium binding reaction. The plot of $\ln K$ versus $1/T$ in Figure V.9 indicated that the ΔH° was not constant over the measured temperature range, but varied depending on the temperature range. Therefore, we separated the line into three regions and, calculated the ΔH° from each slope. The ΔH_A° , calculated from the region A points (37°C-50°C), was -6.8 kcal/mole, very close to the ΔH° value for ethidium-binding to free DNA (Quadrifoglio et al., 1975). Between 30-40°C in region B, the observed equilibrium constant was independent of temperature, i.e., $\Delta H_B^\circ = 0$. The ΔH_C° calculated from the slope of the 20°C-30°C points was -8.2 kcal/mole. The average ΔH° , calculated from the slopes of regions A and C, was -7.5 kcal/mole.

B. Ionic Strength Dependence

The profiles for the binding of ethidium bromide to the core

particle under various ionic strength conditions are shown in Figure V.10. Each curve was calculated from absorbance measurements in two different types of experiments. The closed symbols represent the observed binding constants generated from a spectrophotometric titration while the open symbols represent binding constants generated from equilibrium dialysis measurements. As before, each curve was divided into two regions, A and B, where region A corresponded to points which occurred before the cooperative maximum, and region B corresponded to points which occurred after the cooperative maximum. The observed equilibrium constants, v/C , were fit according to Eq. 5.10 for both regions, and the results are listed in Table VI.3. The most striking observation is that, for all region A points, the intrinsic equilibrium constants were independent of ionic strength. Instead, increasing the ionic strength from 10 to 55 mM resulted in a continuous decrease in cooperativity from 143 to 2.5 and a concomitant decrease in the apparent n value. For the region B points, we observed a 10-fold decrease in the equilibrium constant from $2.7 \times 10^5 \text{ M}^{-1}$ to $2.2 \times 10^4 \text{ M}^{-1}$ upon increasing the $[\text{Na}^+]$ from 5 mM to 55 mM. The decrease in the equilibrium constant was accompanied by no change in the n value and little change in the cooperativity parameter. The binding curve at 55 mM $[\text{Na}^+]$ was not divided into two regions.

The intrinsic binding constants for the region A and the region B points were plotted versus $[\text{Na}^+]$ in Figure V.11. For charged polymers, the dependence of the observed equilibrium constants on counter-ion concentration (Record et al., 1978) is described by

$$\frac{\partial \log K_{\text{obs}}}{\partial \log [\text{Na}^+]} = -m'\psi \quad (5.12)$$

where m' depends on the number of ion pairs found in the DNA/ligand complex and ψ is the number of thermodynamically associated counterions per phosphate charge, found to be 0.88 for free B-form DNA (Record et al., 1976, 1978). Thus, from the slope of the $\log K$ versus $\log [Na^+]$ plot (Figure V.11), we can determine ψ_{core} or m' , the electrostatic contact points made between the cationic dye and DNA in the nucleosome. The results indicate that, at low ratios in region A, ethidium binding is independent of ionic strength. Thus, the binding of ethidium to the core particles, at least initially, does not appear to have a significant electrostatic component to the binding free energy. In contrast, the region B points displayed a distinct Na^+ dependence with a slope, $m'\psi$, equal to 1.1. Therefore we calculated m' and ψ for only the region B points. Since $m'\psi$ was a constant, we could not directly extract a value for ψ (core) and we were forced to estimate its value. Thus, if we assume that ethidium forms one ion-pair per base pair, then $m' = 1.0$ and $\psi = 1.1$. If we assume that ψ for the core particle is close to the value for free DNA, i.e., $\psi = .88$, then $m' = 1.25$. In either case both $m'\psi$ and ψ are close to the value found for free DNA (see Figure V.11).

IV. Conformational Changes: Unfolding Versus Step-Wise Dissociation

A. Translational Diffusion Constants

To determine if the binding of ethidium to the core particle resulted in an unfolding step prior to histone dissociation, we measured the translational diffusion constants for control DNA histone

complexes in their native state and for several complexes of ethidium bound to the core particle. The results of the diffusion measurements for the core particle/ethidium complexes uncorrected and corrected for the presence of free DNA and hexamer forms, are listed in Table V.4. For the intact native particle, i.e., DNA complexed with one histone octamer, the measured diffusion constants was found to be 3.8×10^{-7} cm²/sec in excellent agreement with previously reported values (Bloomfield et al., 1974). Upon the addition of ethidium, we observed little change, within experimental error, in the observed diffusion constants below the critical value, $R = .06$. Further increases in the input ratio of dye to base pair above the critical value resulted in a steady decrease in the diffusion constant from 3.6×10^{-7} cm²/sec at $R = .09$ to 3.2×10^{-7} cm²/sec at $R = .15$. Thus, uncorrected for the presence of free DNA, the observed diffusion constants for the core particle/ethidium complexes indicated that a conformational change occurred within the core particle, upon binding of ethidium, which resulted in an increased frictional coefficient for the complex.

In order to correct the diffusion constants for the presence of free DNA and hexameric forms of the nucleosome, we quantified the amount of these forms present in every input ratio sample used for the diffusion measurements. Each core particle/ethidium complex was analyzed by the previously described gel electrophoretic method (McMurray and van Holde, 1986). The results of the gel analysis are presented in Figure V.12. For both the $R = 0$ (not shown) and the $R = .03$ (lane 1) complexes, the core particle appeared to migrate as a single complex with mobility similar to the 404 bp molecular weight marker. We observed no significant amounts of either hexamer or of

free DNA in either sample. As the input ratio of dye to base pair was increased to $R = .06$, near the critical value we begin to see the presence of a small amounts of both free DNA and the hexameric form of the core particle. The laser densitometer traces of these bands are seen in Figure V.12B, and quantification of the amounts of octamer (intact), hexamer and free DNA for all samples are listed in Table V.4. At an input ratio of $.06$, we observed 6.6% hexamer and 6.7% free DNA. Correction of the Z-average diffusion coefficient for both these forms indicates that the octameric form of the core particle had a diffusion constant which was unchanged, within experimental error, from the uncomplexed form of the core particle. Further increases in the input ratio of the dye to $R = .15$ resulted in increased levels of both free DNA and the hexamer (see Table V.4). However, at all input ratios of dye which we measured, correction of the diffusion constant for the presence of these forms resulted in little change in the diffusion constant of the intact complex relative to the uncomplexed form. Thus, the apparent decrease in the observed diffusion coefficient was due to the presence of the products of an ethidium-induced step-wise dissociation of the core particle and not due to any ethidium-induced unfolding of the complex. The results are most easily compared by calculating the hydrated radius of the core particle/ethidium complexes from the diffusion constants. Since, by definition, $D_{20,w}^0 = RT/Nf$, where R is the gas constant, T is the temperature, N is Avogadro's number and f is the translational frictional coefficient, f may be directly calculated by rearrangement of the diffusion expression, assuming a shape for the complex. The solution of the 7\AA crystal structure of the core particle and its

known dimensions (Richmond et al., 1984) make such a shape prediction possible. If we model the core particle as an oblate ellipsoid, the frictional coefficient of the core particle complexes may be related to the equivalent radius of the particle by

$$f = 6\eta\pi r_h F \quad (5.13)$$

$$r_h = f/6\eta\pi F \quad (5.14)$$

where r_h is the hydrated equivalent radius of the particle and F is the Perrin shape factor. Using an F of 1.04 for an oblate ellipsoid (Cantor and Schimmel, 1980), we calculated the radii of all the core particle/ethidium complexes, listed in Table V.4. For the intact core particle, the calculated radius was 55Å, in excellent agreement with the results of the X-ray crystal structure of the core particle (Richmond et al., 1984). Increasing the input ratio of dye to DNA bp, resulted in little change in the corrected radius of the core particle/ethidium complex. At $R = .15$, the radius, calculated from the corrected diffusion constant of the complex, was 57Å. Thus, the results suggest a slight tendency for the core particle to attain a shape which has a larger frictional coefficient relative to the intact core particle, differing by only 2Å in radius. While all the corrected radii were within experimental error of the radius of the intact particle, we believe that this increase in the spherical radius of the core particle might indicate a small but real change in shape. Since we have used the diffusion constant calculated from the native hexamer in the absence of ethidium for the correction, it is likely

that the hexamer particle in the presence of ethidium might be slightly altered in its shape relative to its native form. If the diffusion constant for the ethidium complex with the hexamer is smaller than we calculated, the diffusion constant for the octamer form will also be smaller. Thus, while the diffusion measurements clearly indicate that no major unfolding of the octamer core particle takes place prior to dissociation, a small elongation of the particle may occur. We calculate that this unfolding event could result in a radius change of no more than 2-5Å.

B. Fluorescence Anisotropy Measurements

To confirm the results of the diffusion measurements, we measured both the steady-state fluorescence anisotropy and the lifetime of the fluorescence anisotropy for the native core particle and the core particle/ethidium complexes. Because maximum fluorescence intensity of an excited ethidium occurs only when the transition dipole is oriented parallel to the incident light, the anisotropy of fluorescence gives information about the rotation of the bound ethidium between excitation and emission. Thus, a change in the anisotropy can be related to changes in the rotational relaxation time of bound ethidium, and the relaxation time can be related to the size and shape of the substrate to which the ethidium is bound. The results of the steady-state fluorescence anisotropy measurements as a function of input ratio are shown in Figure V.13. The coefficient of anisotropy for the core particle and free DNA, extrapolated to zero bound dye, are .23 and .28, respectively, in excellent agreement with

previous results (Paoletti, 1971; Angerer et al., 1974; Paoletti et al., 1977); Wu et al., 1980). Upon the addition of dye, the anisotropy for the core particle decreases very rapidly but eventually becomes comparable to that of free DNA. The higher intrinsic anisotropy found for the core particle suggests that the core particle is a less flexible molecule than is free DNA, and the higher fluorescence anisotropy at low ratios of dye suggests that dye molecules bound to the core particle experience less rotational freedom relative to free DNA. Rapid depolarization of ethidium when bound to the core particle has been previously ascribed to energy transfer between bound dye molecules within the Forster distance for ethidium of 5 bp (Paoletti and LePecq, 1971; Paoletti et al., 1977; Wu et al., 1980). We also observe a rapid decrease in anisotropy of the core particle/ethidium complexes, and our results with the MPE cleavage reaction, localizing the site of binding to the ends of the core particle, confirm the clustering of the dye molecules within the Förster distance.

We used the fluorescence depolarization of ethidium bound to the core particle as a function of increasing viscosity to calculate the radii of the core particle/ethidium complexes for several input ratios of dye, and compared to the radius calculated for the intact octamer. The results of the viscosity dependence of steady-state fluorescence anisotropy for several complexes of ethidium are shown in Figure V.14. At all input ratios that we measured, the anisotropy of ethidium bound to the core particle displayed a distinct viscosity dependence: at constant ethidium, increasing the viscosity resulted in a decrease in the anisotropy. Concomitantly, on the identical samples, we measured the fluorescence lifetime at each viscosity point. The results of the

lifetime measurements are listed in Table V.6. The data in Figure V.14 and the average lifetime in Table V.6 were used to construct the Perrin plot shown in Figure V.15. According to the Perrin relationship,

$$1/A = 1/A_0 (1 + t_F/t) \quad (5.15)$$

where A is the observed anisotropy, A_0 is the intrinsic anisotropy, t_F is the fluorescence lifetime and t is the rotational relaxation time. Since,

$$t = \frac{v_m \pi}{kT} \quad (5.16)$$

Equation 5.15 reduces to

$$1/A = 1/A_0 (1 + \frac{t_F kT}{v_m \pi}) \quad (5.17)$$

where A, A_0 and t_F are defined as before, k is Boltzmann constant, T is the temperature, π is the viscosity of the solvent and v_m is the molecular volume. Because the core particle is approximately spherical, the slope of the anisotropy versus t/π curve is equal to $t_F k/A_0 v_m$. The radius can be calculated from v_m , the molecular volume, by assuming that $v_m = 4/3 \pi R^3$. We have calculated the radius for the spherical model of core particle/ethidium complexes in the pre-dissociation range of input ratios. The results of the calculations are shown in Table V.6. Listed in the table are the

composition of the samples, i.e., % octamer, hexamer and free DNA which we quantified by gel electrophoresis. Because we did not have any information about the viscosity dependence of the fluorescence anisotropy for DNA or for hexamers, we did not attempt to correct $R(\text{\AA})$ for the composition of the sample. At $R = .02$, conditions under which we detected no dissociated DNA, our calculations indicated that the radius of the core particle 43\AA . Further increase in the input ratio of the dye resulted in a decrease in the radius from 43\AA to 41\AA , a decrease in the intrinsic anisotropy and an increase in the amounts of hexamer and of free DNA. The radius at $R = .04$, prior to the appearance of any free DNA, was changed by only 2\AA , identical to the change seen in the diffusion measurements. While the relative change in the hydrated radius, measured by fluorescence anisotropy, paralleled the change measured by diffusion, the actual calculated radius was 8\AA smaller. The smaller value of the calculated radius is explained by the fact that the steady-state experiment measures the average of the fluorescence relaxation times. Since the overall ethidium anisotropy will monitor base motions, as well as internal torsional motions, the average of these relaxation times will tend to shorten t_C . A shorter t_C will result in an increased slope, and an increase in the slope will decrease v_m . Resolution of the relaxation times in the decay measurements discussed below, confirms this explanation. Thus, while the actual radii calculated from the Perrin plot were not good absolute numbers, the results of both the Perrin and the diffusion analyses suggest that the change in the observed radius is small. The observed $2\text{-}3\text{\AA}$ change is consistent with the

increased population of the hexamers which we observe, but inconsistent with an overall unfolding of the core particle structure.

Finally the radius of the core particle/ethidium complexes were measured by the decay of the fluorescence anisotropy. The results for the anisotropy decay for three core particle/ethidium complexes are shown in Figure V.16. The decay tracings indicate that a small increase in the rotational correlation time, t_C , occurs with increasing ratio of dye from $1.33 \times 10^{-7}s$ to $1.40 \times 10^{-7}s$. Each t_C was obtained from the slope of the line at the end of the decay curve so that we were measuring only the long lifetime decay due to overall tumbling of the core particle. The increase in t_C is accompanied by a small change in the intrinsic anisotropy determined by extrapolation to time = 0 in the decay curve. The radii calculated for two complexes and the composition of the samples are shown in Table V.6. The radii of the core particle/ethidium complexes were calculated by

$$t_C = V_h \pi / kT \quad (5.17)$$

and $V_h = t_C kT / \pi \quad (5.18)$

where $V_h = 4/3 \pi R^3$. The results again indicate that only a small change in the calculated radius of the ethidium complex with the core particle is observed prior to the appearance of free DNA and hexamers. At $R = .02$, radius if the complex is 51\AA . Increasing the input ratio to $R = .04$, increases the radius to 52\AA . We conclude from the above experiments that no major unfolding of the octamer core particle takes

place prior to dissociation. The measurements indicate that the hexamer/ethidium complex may be slightly elongated relative to the intact core particle, but the elongation results in a radius change of no more than 2-4Å, within experimental error of the intact octamer.

DISCUSSION

We have carefully examined the binding curves of ethidium bromide to the nucleosome core particles under low ionic strength conditions, accounting for ethidium-induced dissociation. The corrected binding curve revealed that dye binding to the core particle is a highly cooperative process, $w = 143$, confirming the results of Erard et al. (1979), which is characterized by a low intrinsic binding affinity, $2.2 \times 10^4 \text{ M}^{-1}$. Correction of the ethidium binding curve for the amount of dye bound to the dissociated free DNA, indicated that only the region A points, i.e., those points which occurred before the cooperative maximum, truly measured binding of ethidium to the core particle. The rest of the curve represented ethidium binding to free, dissociated DNA. Consistent with the highly cooperative binding, MPE footprinting analysis revealed that the ethidium binding sites were not distributed in a random fashion around the core particle, but instead were clustered near the ends. Approximately 25 bp of DNA were involved with the end-binding reaction. The end-label experiments revealed that both ends of the core particle became bound with dye below the critical ratio. However, comparison of the end-label results with the ethidium staining intensity revealed that ~40% of the MPE-cleavage products had a DNA length within a few base pairs of the intact 145 bp DNA length. The results suggested that while dye binding occurs to both ends, dye binding is favored to one side of the particle.

Analysis of region A points indicates that the binding affinity of ethidium to the core particle appears to be independent of both

temperature and ionic strength, while region B points were found to vary with temperature and ionic strength. Correction of the binding curves for dissociated DNA reveals that region B points reflected only dye binding to dissociated DNA. (The temperature and ionic-strength dependence of the % dissociation curves versus bound ratio for ethidium-binding to the core particle are shown in Chapter VI). Comparison of the % dissociation curves and the binding curves indicated that increases in % dissociation correspond to the "tailing" of the binding curves. Thus, the intrinsic low affinity of the dye for the core particle DNA, independent of salt or temperature, suggests that, at least initially, dye binding to the core particle is structurally prohibited. The structural feature must be related to the critical value, which is itself independent of temperature and ionic strength. Since the critical ratio involves the end-binding of ethidium, we conclude that the interior must be initially inaccessible to the dye.

The real effects of increasing temperature and ionic strength on the binding of ethidium to the core particle are reflected in the n and w values listed in Tables V.2 and V.3. Under low ionic strength conditions, increasing the temperature from 20-50°C results in a decrease in the n value from 9.0 to 7.0. Since the MPE experiments have revealed that n , measured from the Scatchard plot for ethidium binding to the core particle, represents the fraction of base pairs available as ethidium binding sites, a decrease in n suggests that more end-sites become available as the temperature is increased. Consequently, the "need" to bind cooperatively, reflected in w , decreases. The same effects are seen with increasing ionic strength,

but to a larger extent. We interpret the initial temperature independence of ethidium binding to suggest that binding of the dye molecules to the ends of the core particle is entropically driven. The entropic process probably involves the release of the DNA ends from association with the histone proteins, a charged macromolecule, and the subsequent replacement of the histones with the condensation of counterions, or with an increased level of hydration. We interpret the ionic strength independence of ethidium binding to suggest that, initially, the dye cannot insert itself between the base pairs in such a way that the quaternary ammonium ion makes contact with the negative phosphate. Consequently, electrostatic stabilization must occur only after dissociation takes place.

The independence of intrinsic ethidium binding on temperature and ionic strength suggest three important consequences. First, since initial ethidium binding to the core is independent of temperature, the van't Hoff plot for the binding of ethidium to the core particle is largely due to the binding of ethidium to dissociated DNA. Thus, the ΔH° value primarily reflects the ethidium/DNA enthalpy. However, below 30°C the extent of dissociation is low. Thus, the ΔH° calculated from the slope of the low temperature points, prior to the plateau region in Figure V.9, probably reflects more correctly ethidium binding to the ends of the core particle. Similarly, the ionic-strength independence of ethidium binding to the core particle renders the $\log K_{\text{obs}}$ versus $\log \text{Na}^+$ plot an ineffective method for determination of the condensation properties of the nucleosome. Again, since the ionic strength dependence of binding occurs in the region where extensive dissociation occurs, the slope of such a plot measures the

condensation properties of a DNA/ethidium complex. Finally, because the temperature and ionic strength dependence of the core particle and free DNA differ considerably, attempts to measure intercalator interactions with nucleoprotein complexes cannot be treated as free DNA with only a fraction of its base pairs available for binding. The binding properties of the core particle and free DNA differ in ligand affinity, accessibility and cooperativity. As a direct result of these differences, measurement of ligand binding to long chromatin or to nucleosomes comprised of core DNA and free linker moieties, must account for a multi-component equilibria and dissociation effects, if they occur.

Finally, we have established that the intercalation binding of dyes to the nucleosomal DNA does not induce a major unfolding of the core particle structure. After correction for the composition of the samples, three independent measurements indicate that the radius of the ethidium bound octamer, in the absence of dissociation, is very similar, within 2-4Å, of the radius of the native particle in the absence of dye. We point out that hydrodynamic measurements, uncorrected for step-wise dissociation, will lead to the conclusion that large changes in radius accompanies the formation of the core particle/ethidium complex. However, the observed increase in radius will result from the averaged radii of octamer, hexamer and free DNA forms. If dissociation occurs in long chromatin forms or nucleosomes containing a large portion of linker, then hydrodynamic measurements of these complexes will also require correction for the dissociation effect.

We propose the following model of ethidium binding to the core

particle, schematically represented in Figure V.17. The core particle, especially near physiological temperature and ionic strength conditions, appears to be a highly stable complex. Consequently, the initial affinity of the dye for the core particle DNA is low. The exact nature of the intrinsic unfavorable interaction of the dye with intercalation site is unknown but probably arises from a combination of conditions. First, the base pair opening motions within the helix may be suppressed due to histone association. The high intrinsic fluorescence anisotropy of the core particle suggests that the internal flexibility of the core particles DNA is decreased relative to free DNA. Since it is likely that the binding of ethidium requires the opening motion of the DNA base pairs to enter the intercalation site, a reduction in the open/closed equilibrium constant may decrease the availability of binding sites. We predict that the initial binding event may display slow kinetics.

The salt and temperature independence of ethidium binding suggests that ethidium is structurally inhibited from binding to the core particle, and that the first bound ethidium molecules cannot make electrostatic contact with the DNA phosphate. One possibility is that the histone tails bind in the core particle minor groove, the ethidium entry point, and initially block ethidium binding. The presence of histone tails would also tend to neutralize the negative charge of the DNA phosphate. While Weintraub and van Lente (1974) have shown that the presence of the histone tails does not appear to be necessary for the folding of the DNA, the absence of the histone tails results in a two-fold increase in nuclease cleavage susceptibility of the core particle DNA (Whitlock and Simpson, 1976). Their presence also results

in a reduced circular dichroism spectra ellipticity between 270-290 nm. Thus, the histone tails bind to the core particle and confer protection to the core particle DNA. We suggest that the initial low affinity for the binding of ethidium to the core particle may reflect the need to "unbind" histone tails which block the minor groove. Since fewer histone contacts are made at the ends of the core particle (Mirzabekov, 1980), the ends of the core particle will be more flexible and end binding would be predicted as the favored reaction.

Once ethidium has gained entry, the geometry of the compact particle is disrupted. The binding of one ethidium enhances the binding affinity for the next molecule, as long as the dye binds vicinally. The binding of the dye molecules also unwinds and stiffens the helix at the ethidium binding site. Since the DNA must be flexible to fold around the core particle, the binding of ethidium induces the dissociation of the histones, and the loss of histones results in the appearance of new binding sites. The initial binding of dye molecules results in a stiff, ethidium-bound tail which peels off the particle, accounting for the slight change in radius of the intact particle. Since only the inner-most histones, H3 and H4 are required for folding the particle (Camerini-Otero and Felsenfeld, 1977), dissociation occurs only after the loss of H2A and H2B. Only one copy of H2A and H2B is lost because the highly cooperative nature of ethidium binding to the core particle favors directional binding, i.e., the binding is greatly preferred to the side where more dye binding has occurred, destabilizing H3 and H4 interactions. Thus, while the core particle is initially a symmetric molecule, random initial binding events dictate some preferred direction.

A. Transcriptional Model

We propose that the binding of ethidium (unwinding angle of 26°) and its structural effects can be used as an in vitro model system for studying the effects of polymerase unwinding on nucleosome structure. The binding and initiation of DNA-dependent RNA polymerase results in the unwinding of 12 base pairs (BP) of DNA in the transcription "bubble", the unpaired region at the RNA-synthesis site. Within the bubble, the base pairs are totally unpaired, and the DNA may be thought to have an unwinding angle of 0° in this region. In eukaryotes, the situation is much more complicated since the DNA is packaged into nucleosomes. Consequently, we propose that three steps induced by ethidium binding also occur during transcription: the loss of one copy of H2A and H2B, transient dissociation of the histones during polymerase passing and reassociation of the intact structure. These events are depicted in Figure V.18. The binding of RNA-polymerase or some auxilliary protein induces the loss of H2A and H2B. Since both DNA and H2A, H2B are charged, the histones do not diffuse away, but remain in proximity of their original site. The loss of H2A and H2B requires the binding of the critical number of base pairs, 16-17 bp of DNA. This value is reasonably close to the number of base pairs unwound by polymerase, 11-12 bp. Additionally, upon isolating nucleosomes from transcriptionally active genes, Rhodes and Bauer (1983) found that the majority of the polymerase/nucleosome complexes were in the form of the hexamer, missing one copy each of H2A and H2B. Lilley et al. (1979) also made the observation that transcription occurred, in vitro, only on dissociated or partially

unfolded core particles. Finally, directional binding allows the processive passing of polymerase, and upon completion of transcription through the core particle DNA, the nucleosome reassociate.

Table V.1

K, n and w Computer-Generated Best-Fit Values for the Binding
of Ethidium with Free DNA and Core Particles at 30°C

Sample ^a	K(m ⁻¹)	n	w
Chicken Erythrocyte DNA (145 ± 3 BP)	1.2 x 10 ⁶	2.4	0.3
Chicken Erythrocyte Core Particles (Region A)	2.2 x 10 ⁴	7.0	143
Chicken Erythrocyte Core Particles (Region B)	2.7 x 10 ⁵	2.3	.4

- a. All experiments were conducted at 30°C in 10 mM Tris, pH 8.0, 0.1 mM EDTA (TE) buffer. All constants are defined in DNA base pairs and calculated by non-linear least squares fits using Equation 5.10.

Table V.2

Temperature-Dependence of Ethidium Binding
to the Nucleosome Core Particle^a

Sample	T°C	Region ^b	K(m ⁻¹) ^c	n ^d	w ^e
Core Particle	20	A	2.4 x 10 ⁴	9.0	130
	30	A	2.2 x 10 ⁴	7.4	143
	37	A	2.2 x 10 ⁴	5.8	14.0
	50	A	2.3 x 10 ⁴	6.7	29.4
	20	B	3.8 x 10 ⁵	3.1	.3
	30	B	2.7 x 10 ⁵	2.8	.4
	37	B	2.8 x 10 ⁵	2.6	.4
	50	B	1.8 x 10 ⁵	2.7	.7

- a. Core particle concentration was $3.8 \times 10^{-5} \text{ M}^{-1}$. The buffer in all experiments was 10 mM Tris, pH 8.0, 0.1 mM EDTA.
- b. Region A comprised points prior to the maximum in Figure V. Region B comprised points after the maximum in Figure V.
- c. K is the intrinsic binding constant of ethidium bromide to the core particle, defined in Eq. 5.10.
- d. n = the number of sites excluded by the dye.
- e. w is the cooperativity or clustering parameter and represents the equilibrium constant for moving an isolated dye to a singly bound site.

Table V.3

Ionic Strength Dependence of Ethidium Binding
to the Nucleosome Core Particle^a

Sample	[Na ⁺]	Region	K(M ⁻¹)	n	w
Core Particle	5 mM	A	2.2×10^4	7.0	143
	10 mM	A	4.0×10^4	6.0	29
	20 mM	A	2.0×10^4	2.6	16.5
	55 mM	A	2.2×10^4	2.4	2.5
	5 mM	B	2.7×10^5	2.6	.4
	10 mM	B	1.5×10^5	2.5	.4
	20 mM	B	7.5×10^4	2.4	.7
	55 mM	B	2.2×10^4	2.4	2.5

a. All sample conditions and definitions are as in Table V.2.

Table V.4

The Translational Diffusion Constants for Native
Core Particles and Ethidium Complexes

Sample ^a	Observed ^b $D_{20,w}^{\circ}(\text{cm}^2/\text{sec})$	Observed ^c $R(\text{\AA})$	Composition ^d			Corrected ^e $D_{20,w}^{\circ}(\text{cm}^2/\text{sec})$	Corrected ^f $R(\text{\AA})$
			%O	%H	%D		
Native Octamer	3.8×10^{-7}	55	100	--	--	--	--
Native Hexamer	3.2×10^{-7}	--	--	100	--	--	--
Free DNA	3.0×10^{-7}	--	--	--	100	--	--
Core Particle/EB Complexes							
R = 0	$3.8 \times 10^{-7} \pm .05$	55	100	--	--	3.8×10^{-7}	55
R = .03	$3.9 \times 10^{-7} \pm .05$	54	100	--	--	3.9×10^{-7}	54
R = .06	$3.8 \times 10^{-7} \pm .10$	55	86	6.6	6.7	3.9×10^{-7}	54
R = .09	$3.6 \times 10^{-7} \pm .20$	55	83	6.2	12.5	3.9×10^{-7}	55
R = .12	$3.3 \times 10^{-7} \pm .05$	64	73	11.1	15.9	3.4×10^{-7}	60
R = .15	$3.2 \times 10^{-7} \pm .15$	66	67	12.1	21.0	3.4×10^{-7}	60

Table V.4 (continued)

- a. All samples were measured at $20^{\circ}\text{C} \pm 1^{\circ}\text{C}$. The buffer used in all experiments was 10 mM Tris, pH 8.0, 0.1 mM EDTA and the concentration of the core particle and free DNA samples was 3.8×10^{-4} mbp ($A_{260} = 5.0$). The $D^{\circ}_{20,w}$ for the hexamer was calculated from the sedimentation coefficient (9.2 x) of the purified form reported in Read et al., 1985. The diffusion constant was calculated from the sedimentation coefficient by $D = SRT/m(1-v\rho)$ where s = the sedimentation coefficient, R = gas constant, T is the temperature, M is the anhydrous molecular weight, v is the partial specific volume of the core particle and ρ is the density of the solvent. The core particle ethidium complexes were made by the addition of ethidium to the core particle solutions. R = input ratio = moles added dye/DNA bp.
- b. Observed $D^{\circ}_{20,w}$ was the uncorrected diffusion constant = RT/Nf where R and T are defined as before, N is Avagadro's number and f is the frictional coefficient.
- c. Observed R is the radius calculated for the sample from the observed $D^{\circ}_{20,w}$. Since $D = RT/Nf$ and $f = 6\pi\eta r_h F$, $r_h = f/6\pi\eta F$ where D , R , T , N and f are defined as before and F is the Perrin shape factor = f oblate ellipsoid/ f sphere.
- d. Composition is the percentage population of intact octamer, the hexamer and free DNA present in each sample.
- e. Corrected $D^{\circ}_{20,w}$ is the $D^{\circ}_{20,w}$ for the intact octamer form after correction for the composition of the sample. Corrected $D^{\circ}_{20,w}$ ($D^{\circ}_{20,w}$ (observed) - ($f_H D_H$) - ($f_D D_D$)) $\div f_O$ where $f_{O,H,D}$ are the fractional population of the octamer, the hexamer and free DNA respectively and $D_{H,D}$ are the diffusion coefficients for the hexamer and free DNA.
- f. Corrected $R(\text{\AA})$ is the radius of the octamer calculated from the corrected diffusion constant for the intact core particle.

Table V.5

The Average Fluorescence Lifetime^a of Core Particle/Ethidium Complexes^b as a Function of Viscosity^c

% Sucrose	n	R = .02	R = .06	R = .10	R = .15
0	1.002	21.7	20.9	21.4	20.6
10	1.333	21.6	20.9	20.7	19.8
20	1.941	20.4	20.3	19.8	18.3
30	3.181	19.7	19.0	18.7	17.9
40	6.150	18.6	17.6	16.8	17.0
50	15.40	16.3	16.3	18.4	16.1

- a. The average fluorescence lifetime $\tau_{avg} = \sum_i (\% \text{ population}) (\tau_i) \div \sum_i (\% \text{ population})_i$. Excitation was at 555 nm and excitation was monitored at 593 nm. τ units are nanosecond.
- b. The length of the core particles was 145 ± 3 bp. For all measurements the DNA concentration was 4.5×10^{-5} mbp.
- c. Viscosity was increased by the addition of sucrose. Sucrose was added to the basic buffer of 10 mM Tris, pH 8.0, 0.1 mM EDTA. The 0% sucrose was the buffer in the absence of sucrose.

Table V.6

Radii Calculated from Steady-State and Lifetime Anisotropy
Measurements for Ethidium Pre-dissociation Complexes
with the Core Particle

Perrin Analysis	Observed A_0	Observed $R(\text{\AA})$	Composition		
			%O	%H	%D
$R = .02$.29	43 \AA	99	1.0	--
$R = .04$.28	42 \AA	96	4.0	--
$R = .06$.25	41 \AA	87	6.0	7.0
Fluorescence Anisotropy Decay	$\tau_c(s)$	Observed $R(\text{\AA})$	Composition		
			%O	%H	%D
$R = .005$	1.34×10^{-7}	51 \AA	100	--	--
$R = .06$	1.44×10^{-7}	52 \AA	98	2.0	--

Figure V.1. The Scatchard plot for the binding of ethidium bromide to the chicken erythrocyte core particle at 30°C. The (●) represented the results from the spectrophotometric titration and (○) represent the results from equilibrium dialysis measurements. All data were analyzed by the McGhee and von Hippel conditional probability binding model (McGhee and van Hippel, 1974). v/C is the observed binding constant, v is the ratio of bound dye to DNA base pair, and C is the concentration of free dye. All experiments were performed in 10 mM Tris, pH = 8.0, 0.1 mM EDTA at 30°C. The core particle concentration ranged from 1.0×10^5 M bp to 7.5×10^5 M bp.

Figure V.1

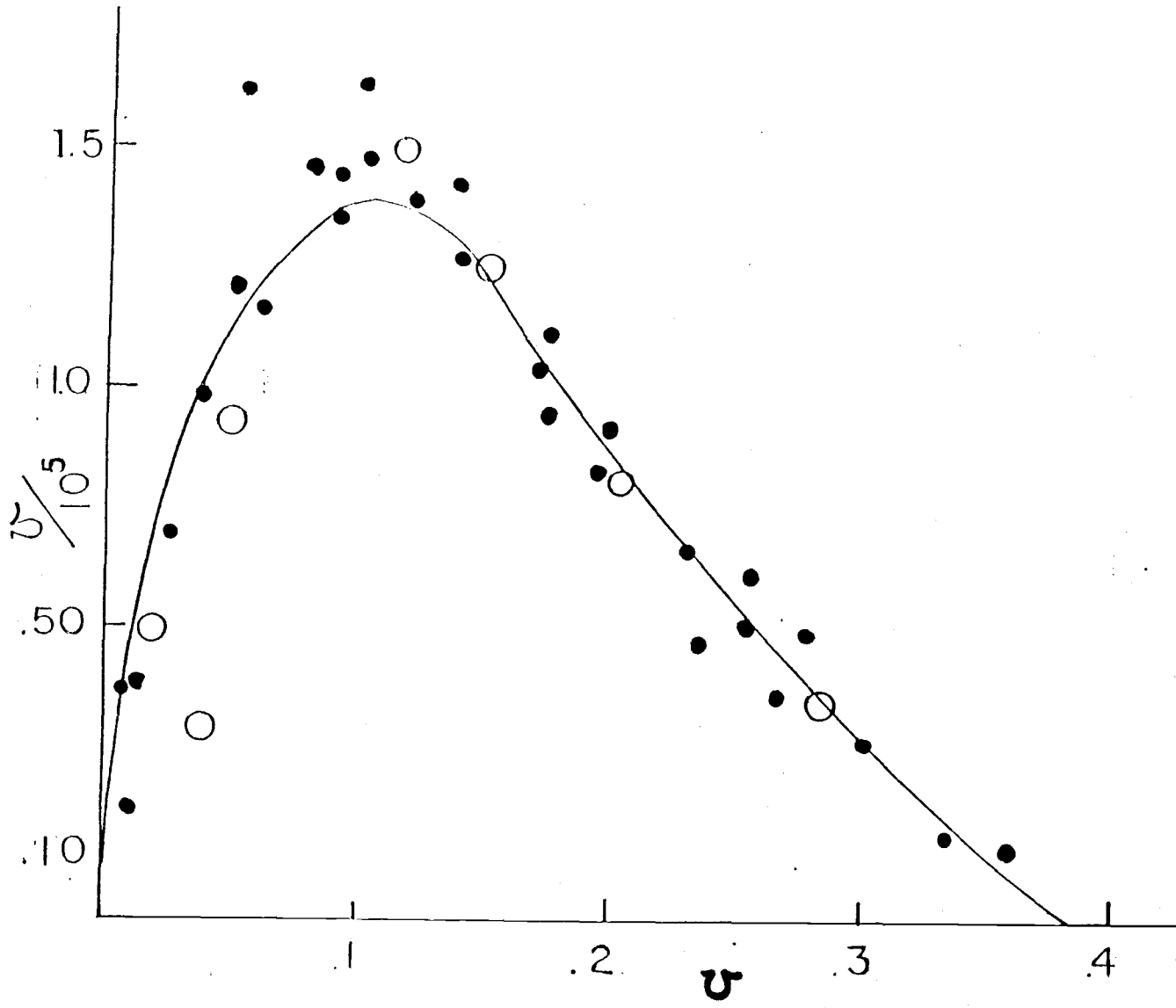


Figure V.2A. Schematic representation of the method used to determine v_{core} .

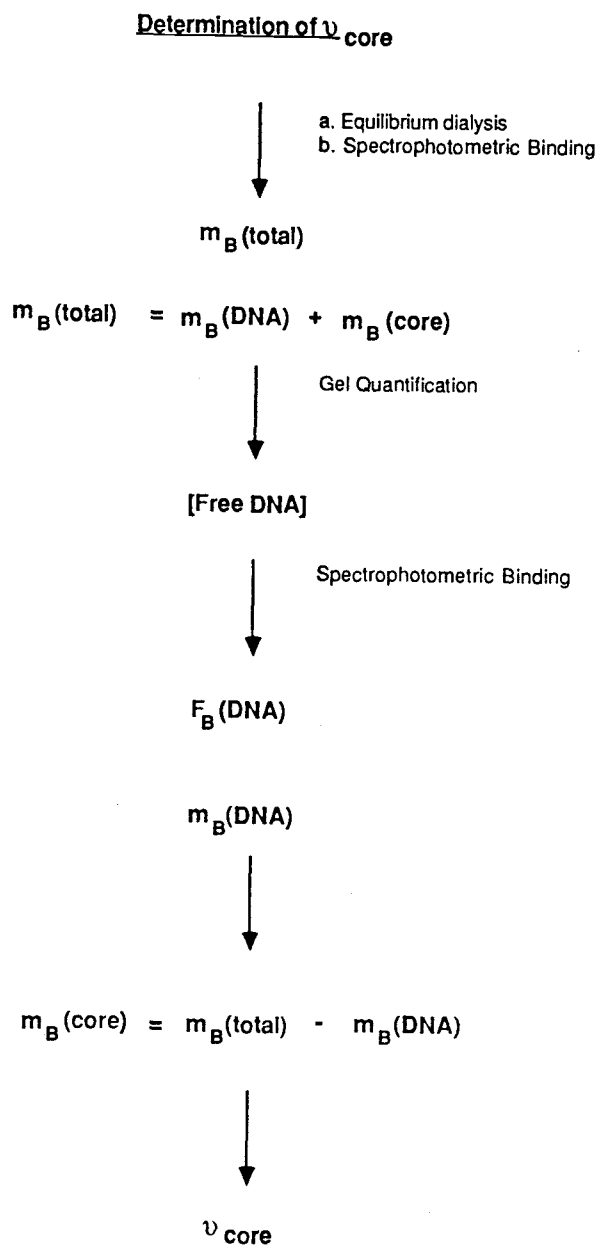


Figure V.2A

Figure V.2B. The plot of % dissociation versus v_{core} . The ratio of dye bound to the core particle was corrected for the amount of dye which was bound to free, dissociated DNA by the method described in Figure V.2A. The level of free DNA was quantified by the gel electrophoretic method described in (McMurray and van Holde, 1986). The buffer used in all experiments was 10 mM Tris, pH = 8.0, 0.1 mM EDTA and the core particle concentration was 3.8×10^{-5} M bp.

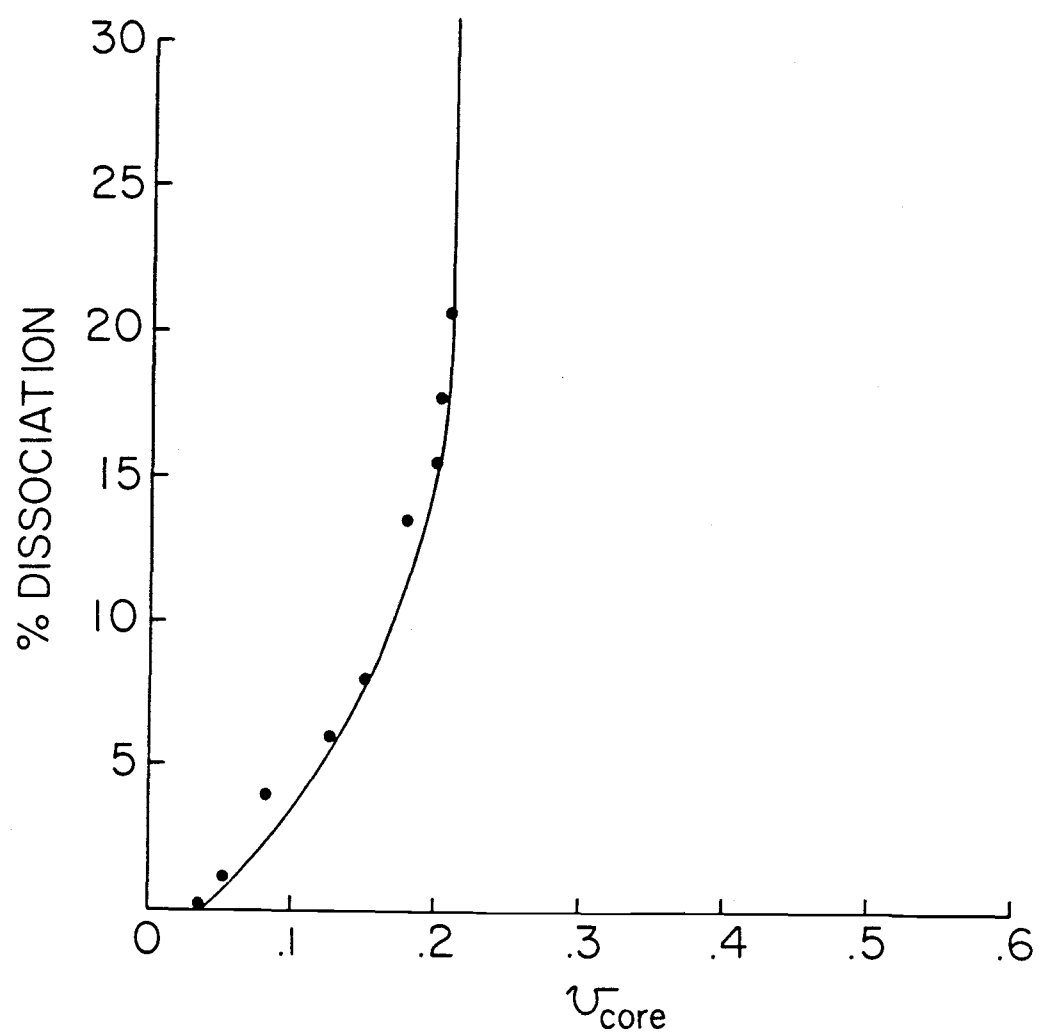


Figure V.2B

Figure V.3. The corrected Scatchard plot for the binding of ethidium to the nucleosome core particle at 30°C. The (●) represent the points calculated from the v_{core} values in Figure V.2B. The (●) represent the results from the spectrophotometric titration and (●) represent the results from equilibrium dialysis measurements. v/C is the observed binding constant, v is the ratio of bound dye to DNA base pair, and C is the concentration of free dye. All experiments were performed in 10 mM Tris, pH = 8.0, 0.1 mM EDTA at 30°C. The core particle concentration ranged from 1.0×10^5 M bp to 7.5×10^5 M bp.

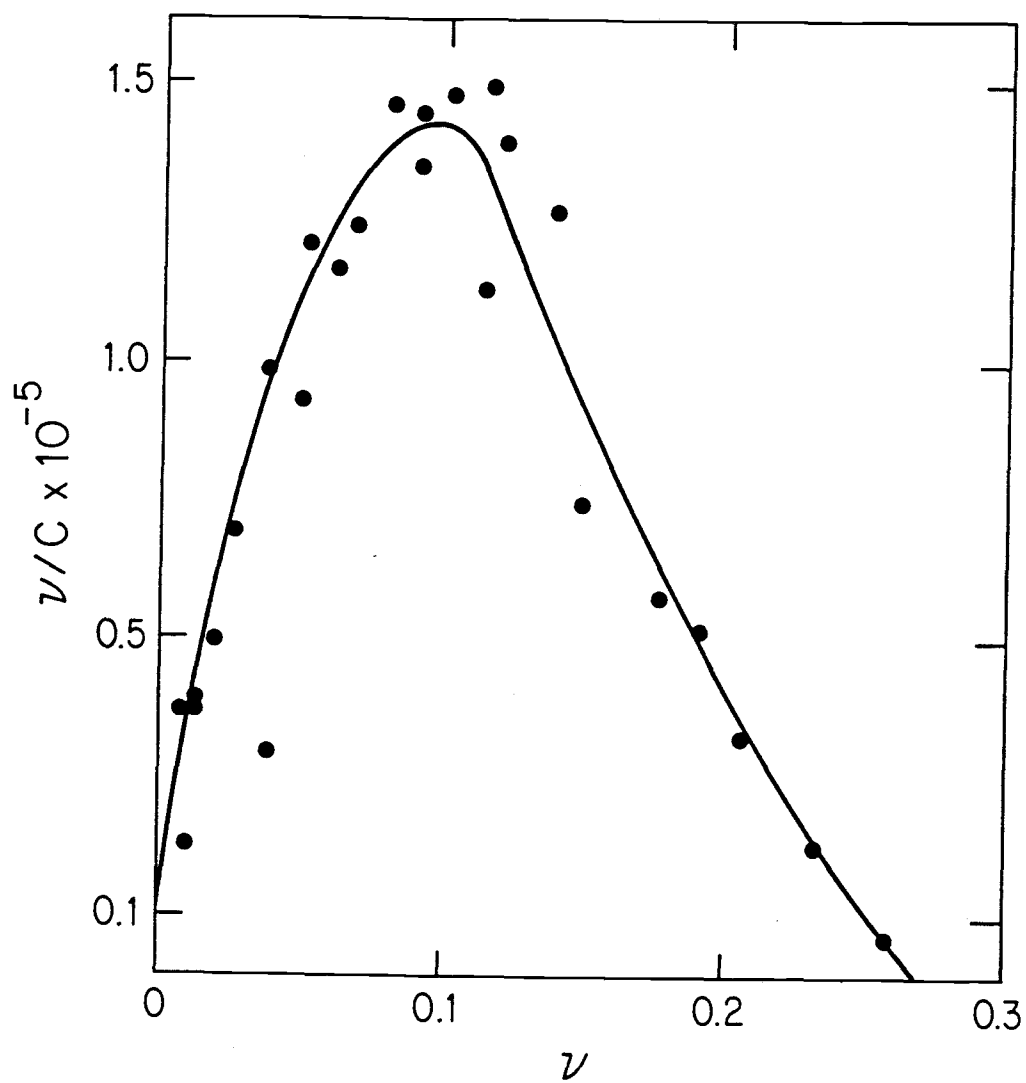


Figure V.3

Figure V.4A. The Scatchard plot for the binding of ethidium to the core particle and to free DNA at 30°C. The (●) represent the binding curve for free DNA; (▲) the uncorrected binding curve for the core particle. The free DNA curve (●) represent the results from the spectrophotometric titration and (▲) represent the results from equilibrium dialysis measurements. All data were analyzed by the McGhee and von Hippel conditional probability binding model (McGhee and van Hippel, 1974). v/C is the observed binding constant, v is the ratio of bound dye to DNA base pair, and C is the concentration of free dye. All experiments were performed in 10 mM Tris, pH = 8.0, 0.1 mM EDTA at 30°C. The core particle and free DNA concentration ranged from 1.0×10^5 M bp to 7.5×10^5 M bp.

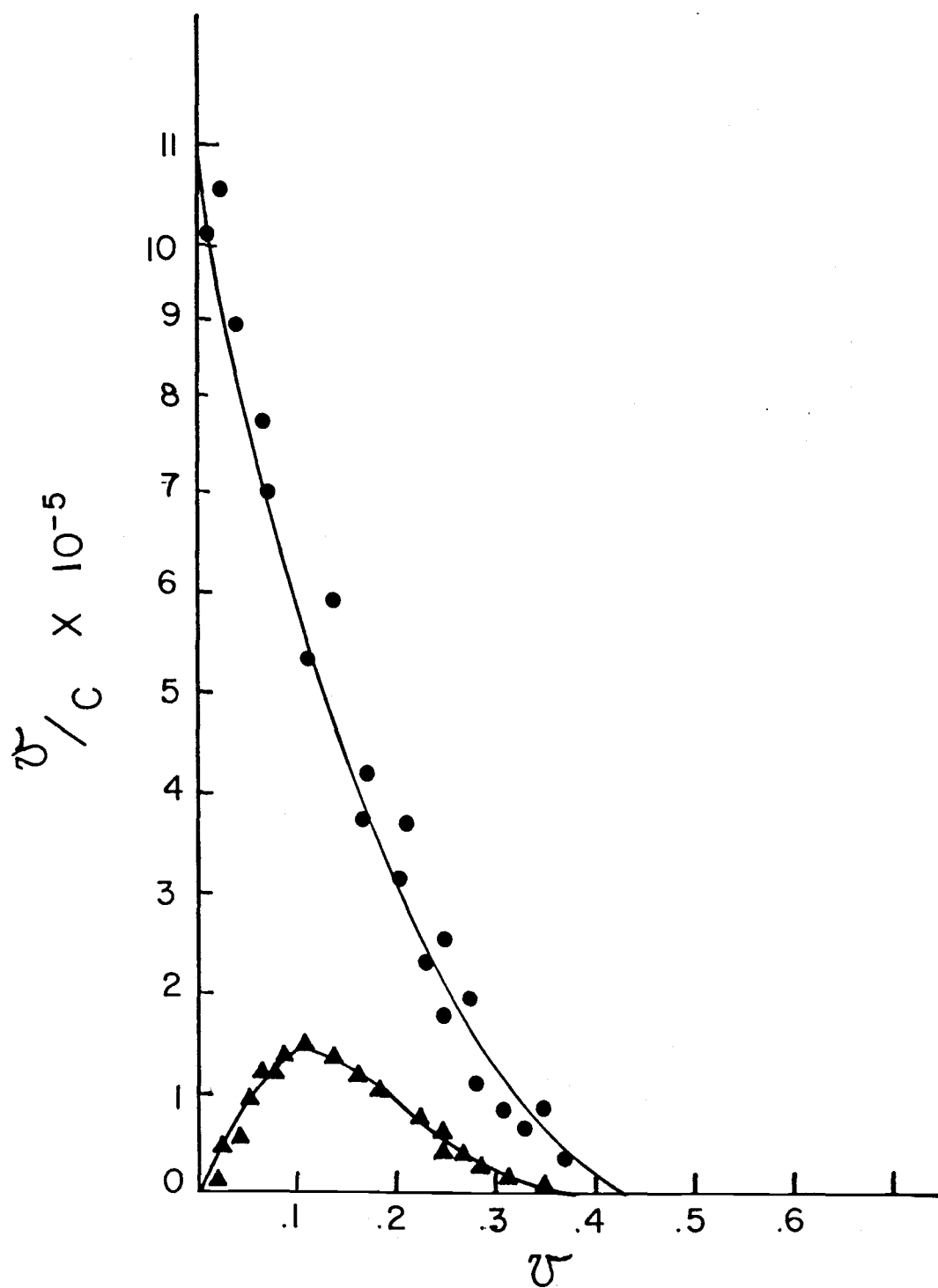


Figure V.4A

Figure V.4B. The plot of the free energy difference between the binding ethidium to free DNA and to the core particle at 30°C. The plot was generated by subtracting the ΔG° for the observed binding constants in Figure V.4A.

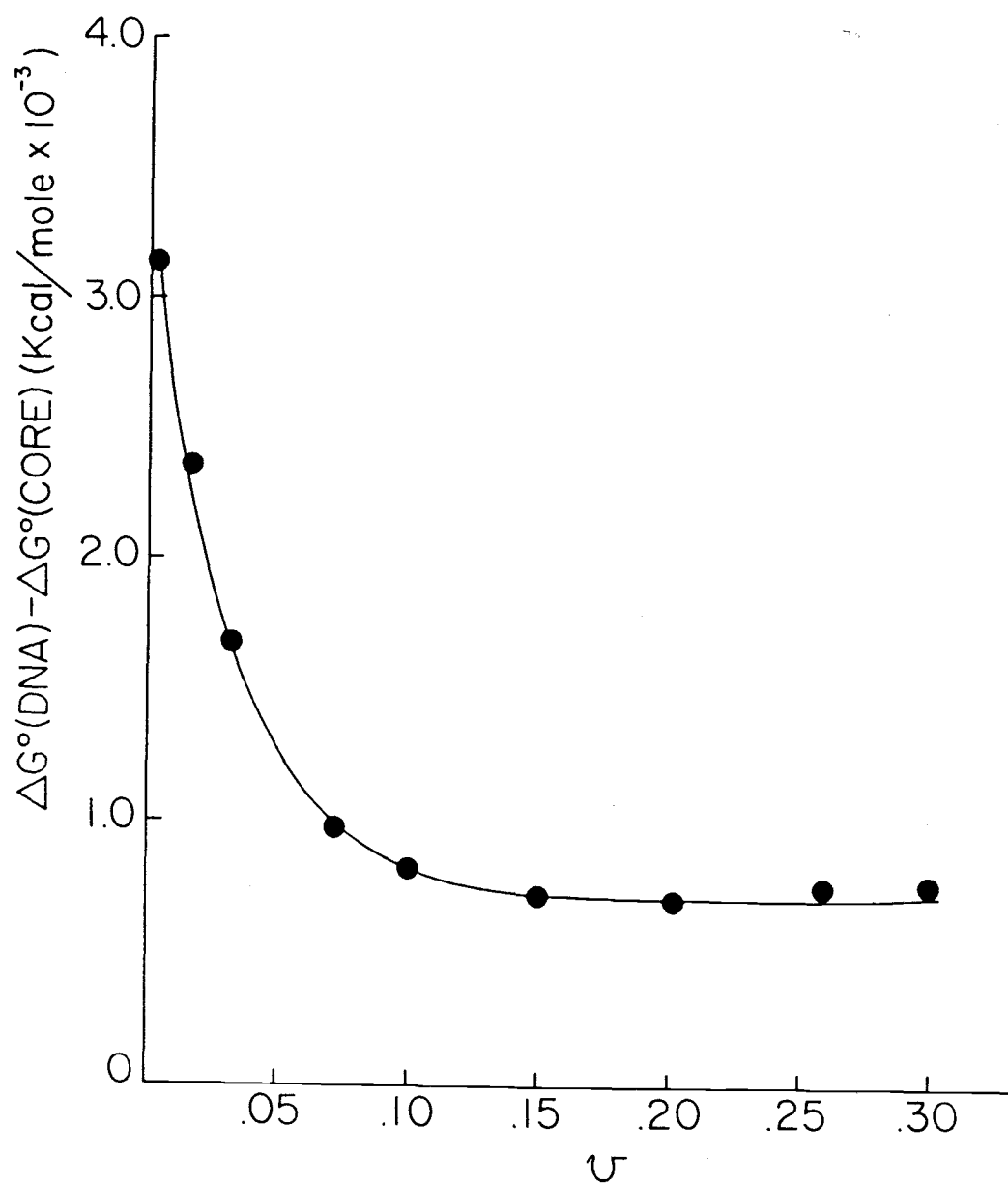


Figure V.4B

Figure V.5. Schematic design of the experimental procedure for determination of the location of ethidium binding sites on the nucleosome core particle. The structure at the top is methidiumpropyl- FE-EDTA , an ethidium derivative which can cleave the DNA where it binds. The ladders represent the DNA lattice and the stars represent the ^{32}P -end label at the 5'-termini. The S1 indicates cleavage by S1 nuclease at single breaks in the phosphodiester backbone.

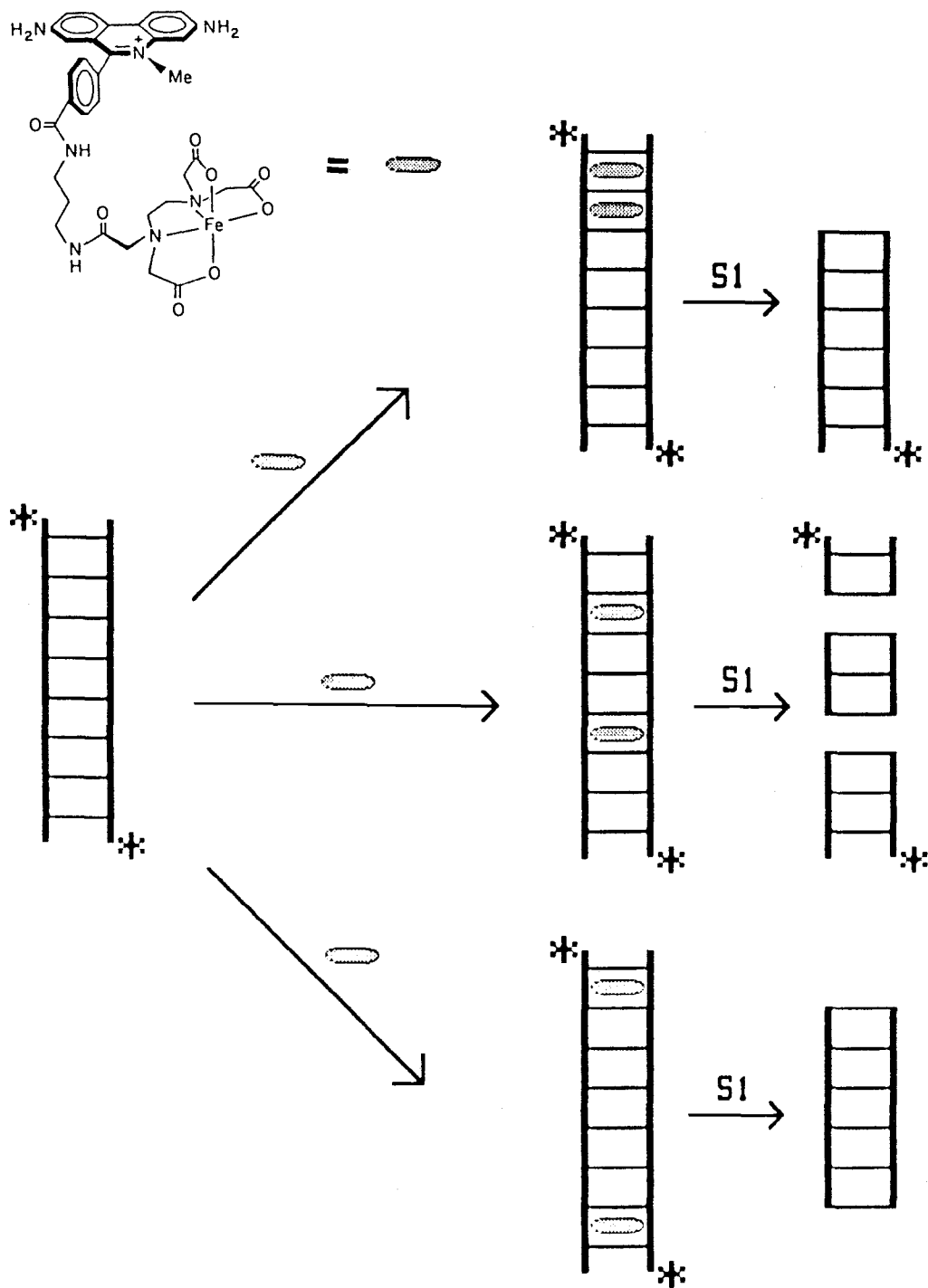


Figure V.5

Figure V.6. The results of the MPE cleavage reaction with the nucleosome core particle. (A) The analysis of the MPE cleavage fragments generated from the complex of MPE with the core particle and the corresponding free DNA. Lane (1) free DNA, $R = 0$; (2) free DNA, $R = 0$ mock; (3) free DNA, $R = .02$; (4) free DNA, $R = .06$ (M) DNA molecular weight markers generated from PBr322 cut with Hpa-II; (5) core particle, $R = 0$; (6) core particle, $R = 0$ mock; (7) core particle, $R = .02$; (8) core particle, $R = .06$; (9) core particle, $R = .10$; (10) core particle, $R = .20$. (B) The laser densitometer trace of the bands in (A). The length of the DNA molecular weight markers are indicated. Arrows indicate the presence of a peak for a prominent cleavage product. The bands were analyzed on 5.0% polyacrylamide minigels which were 1.0 mm thick.

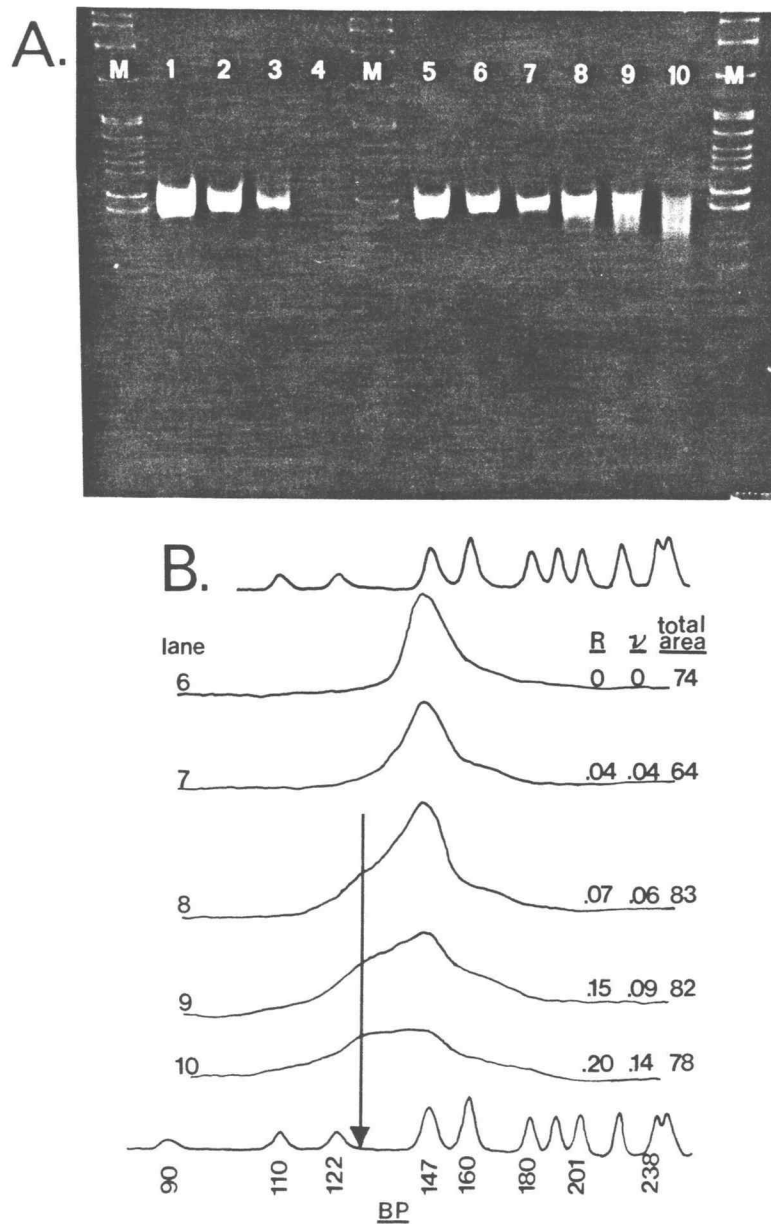


Figure V.6

Figure V.7. The results of the cleavage reaction of MPE with the ^{32}P -5'-end-labeled core particles and the corresponding free DNA. (A) The results of the MPE cleavage reaction visualized by ethidium staining on 7% polyacrylamide gels: DNA molecular weight markers generated from PBr322 cut with Hpa-II (1) core particle, $R = 0$; (2) core particle, $R = 0$ mock; (3) core particle, $R = .02$; (4) core particle, $R = .06$; (5) core particle, $R = .10$; (6) core particle, $R = .20$. (B) Autoradiography results of the MPE cleavage reaction of ^{32}P -5'-end-labeled core particles: DNA molecular weight markers generated from PBr322 cut with Hpa-II (1) core particle, $R = 0$; (2) core particle, $R = 0$ mock; (3) core particle, $R = .02$; (4) core particle, $R = .06$; (5) core particle, $R = .10$; (6) core particle, $R = .20$. (C) The laser densitometer trace of the bands in (B). The length of the DNA molecular weight markers are indicated. The bands were analyzed on 7.0% polyacrylamide minigels which were 1.0 mm thick.

Figure V.7

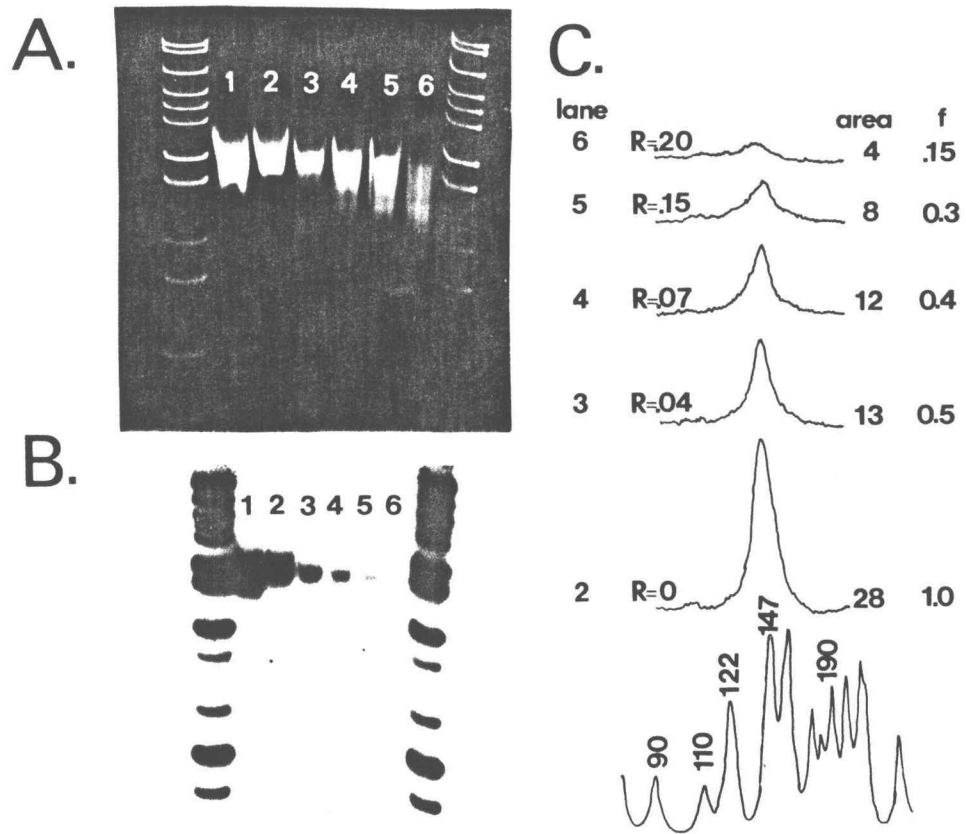


Figure 8. The temperature dependence of the ethidium binding to the core particle. (Δ) 20°C; (\bullet) 30°C; (\blacksquare) 32°C; (\blacktriangle) 37°C; (\bigcirc) 50°C. All binding curves were generated from equilibrium dialysis measurements and plotted as a Scatchard plot. All data were analyzed by the McGhee and von Hippel conditional probability binding model (McGhee and van Hippel, 1974). v/C is the observed binding constant, v is the ratio of bound dye to DNA base pair, and C is the concentration of free dye. All experiments were performed in 10 mM Tris, pH = 8.0, 0.1 mM EDTA at 30°C. The core particle concentration ranged from 1.0×10^5 M bp to 7.5×10^5 M bp.

Figure V.8

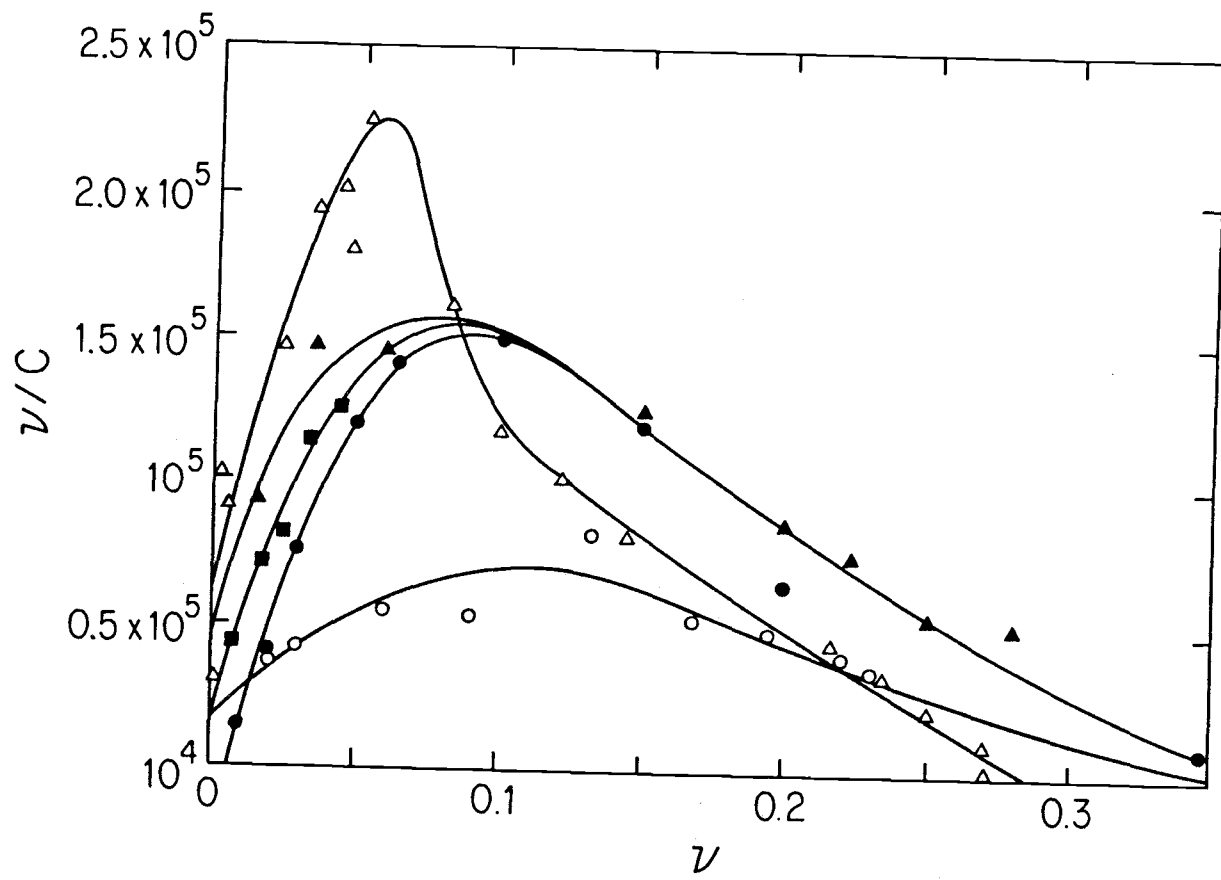


Figure V.9. The van't Hoff plot for the binding of ethidium to the nucleosome core particle. The plotted data were taken from Figure V.8 and Table V.2.

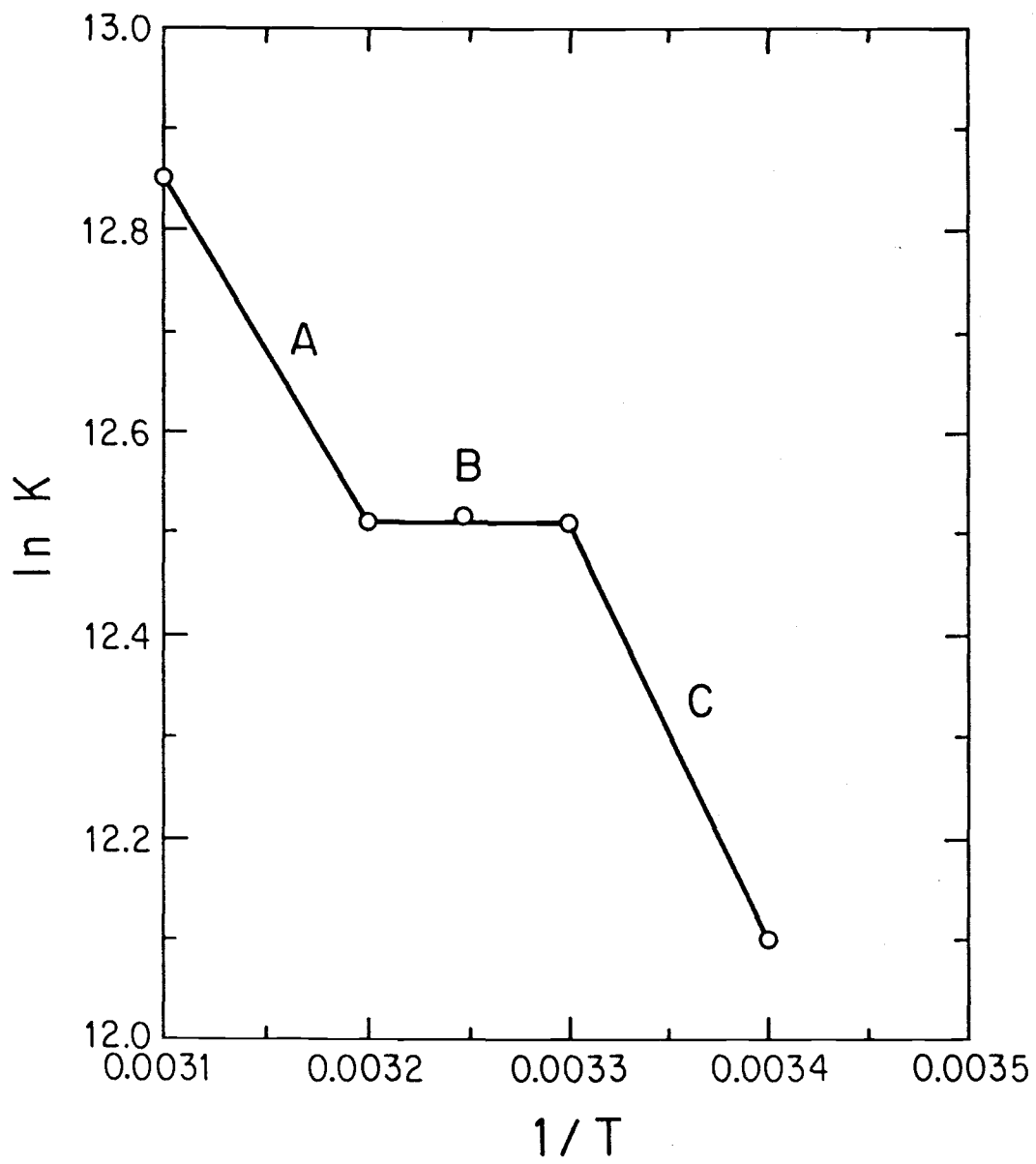


Figure V.9

Figure V.10. The Scatchard plot of the $[\text{Na}^+]$ dependence of ethidium binding to the nucleosome core particle at 30°C . (\blacklozenge) $[\text{Na}^+] = .005$; (\square) $[\text{Na}^+] = .01$; (\triangle) $[\text{Na}^+] = .02$; $[\text{Na}^+] = .055$. The open symbols represent the results from equilibrium dialysis measurements and the closed symbols represent the results from spectrophotometric measurements. All data were analyzed by the McGhee and von Hippel conditional probability binding model (McGhee and van Hippel, 1974). v/C is the observed binding constant, v is the ratio of bound dye to DNA base pair, and C is the concentration of free dye. All experiments were performed in 10 mM Tris, pH = 8.0, 0.1 mM EDTA at 30°C . The core particle concentration ranged from 1.0×10^5 M bp to 7.5×10^5 M bp.

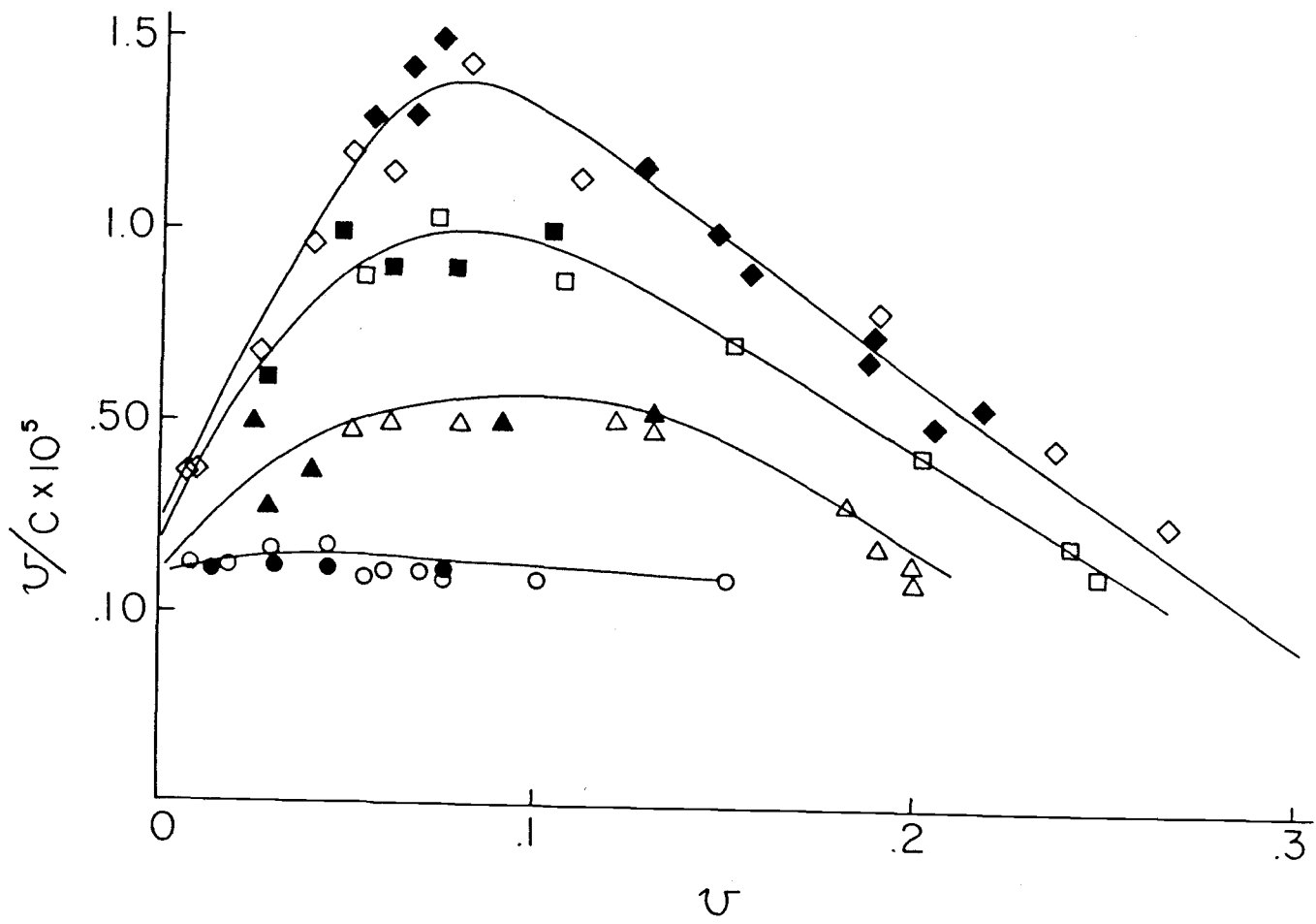


Figure V.10

Figure V.11. The $[Na^+]$ dependence of the intrinsic equilibrium constants for the binding of ethidium to the core particle and to free DNA at 30°C. (\bigcirc) the $[Na^+]$ dependence of ethidium binding to the core particle, region B fitting results; (\blacktriangle) the $[Na^+]$ dependence of the intrinsic equilibrium constant for the core particle fit to region A points (\bullet) the $[Na^+]$ dependence of the intrinsic equilibrium constant for ethidium binding to free DNA. The values used for the plot were taken from Figure V.10 and Table V.3. The data for the $[Na^+]$ dependence of the ethidium binding to free DNA were taken from Wilson et al., 1985.

Figure V.11

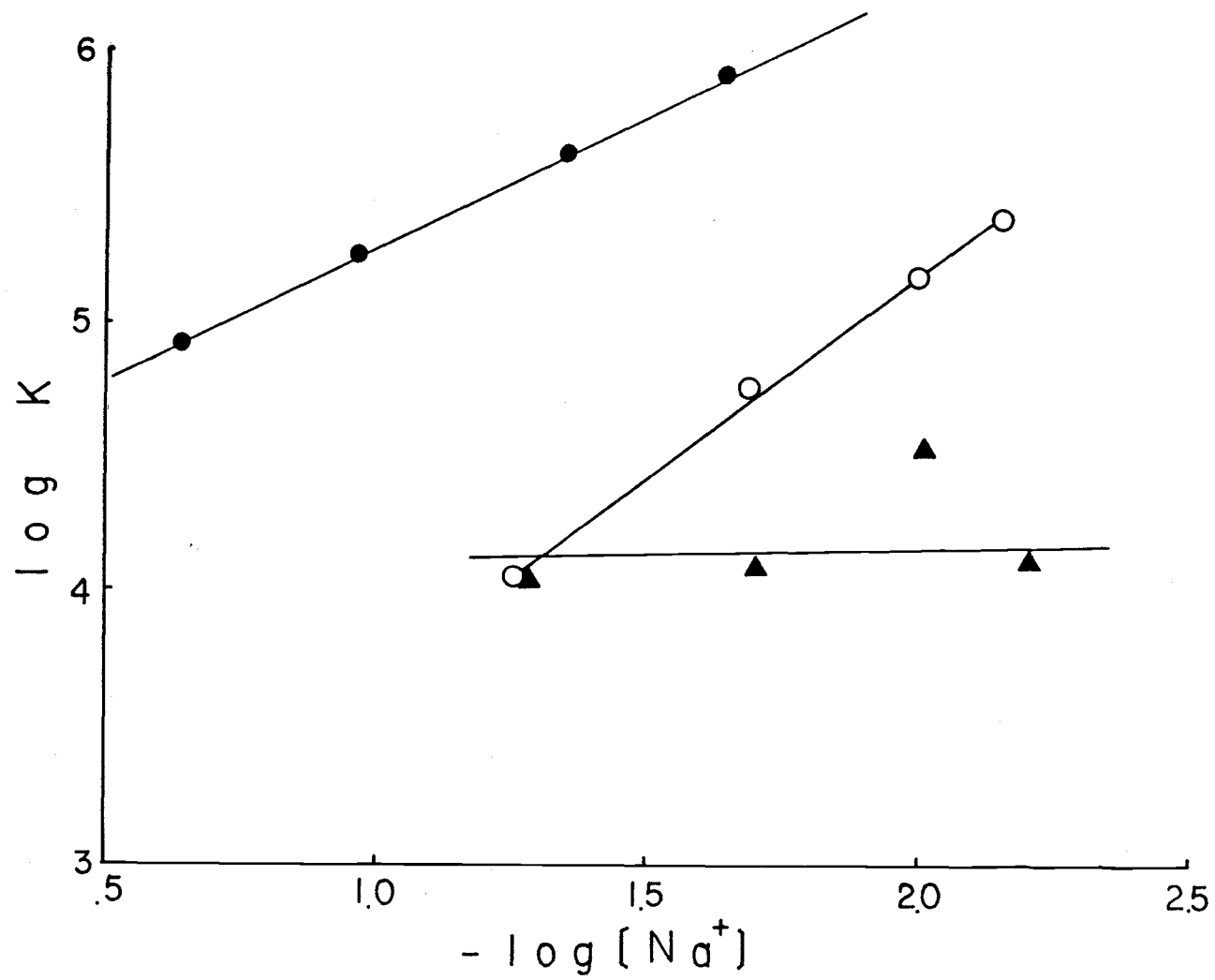


Figure V.12. (A) The results of the polyacrylamide gel electrophoretic analysis of the core particle/ethidium complexes used in the diffusion constant measurements. (A) $R = .03$; (B) $R = .06$; (C) $R = .09$; (D) $R = .12$; (E) $R = .15$. Band-1, 2 and 3 indicate the intact octamer, the hexamer and free DNA respectively. (B) The laser densitometer traces of lanes A-E in (A). The quantified composition of the samples is listed in Table V.4.

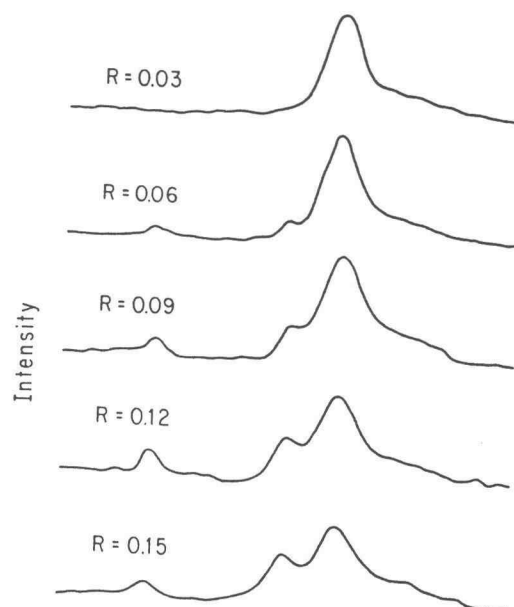
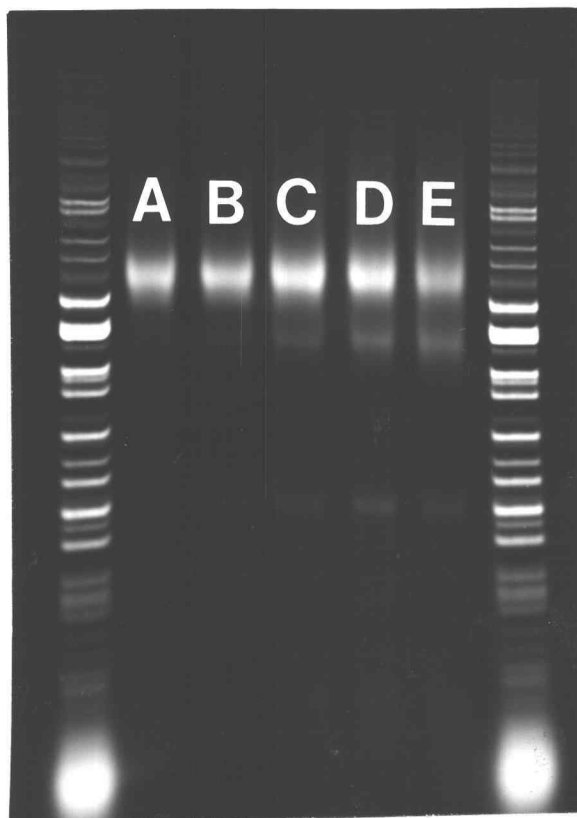


Figure V.12

Figure V.13. The plot of fluorescence anisotropy versus input ratio of complexes of ethidium with the nucleosome core particle and for the corresponding free DNA in 10 mM Tris, pH = 8.0, 0.1 mM EDTA at 20°C. The anisotropy is defined as the $I_F(\text{parallel}) - I_F(\text{perpendicular}) / I_F(\text{parallel}) + 2I_F(\text{perpendicular})$. The excitation wavelength was 550 nm and the excitation was monitored at 593 nm input ratio is defined as moles added dye/mole DNA bp. The inset corresponds to the dashed box in the main part of the figure. The core particle concentration was 3.5×10^{-5} M bp and the DNA concentration was 7.8×10^{-5} M bp.

Figure V.13

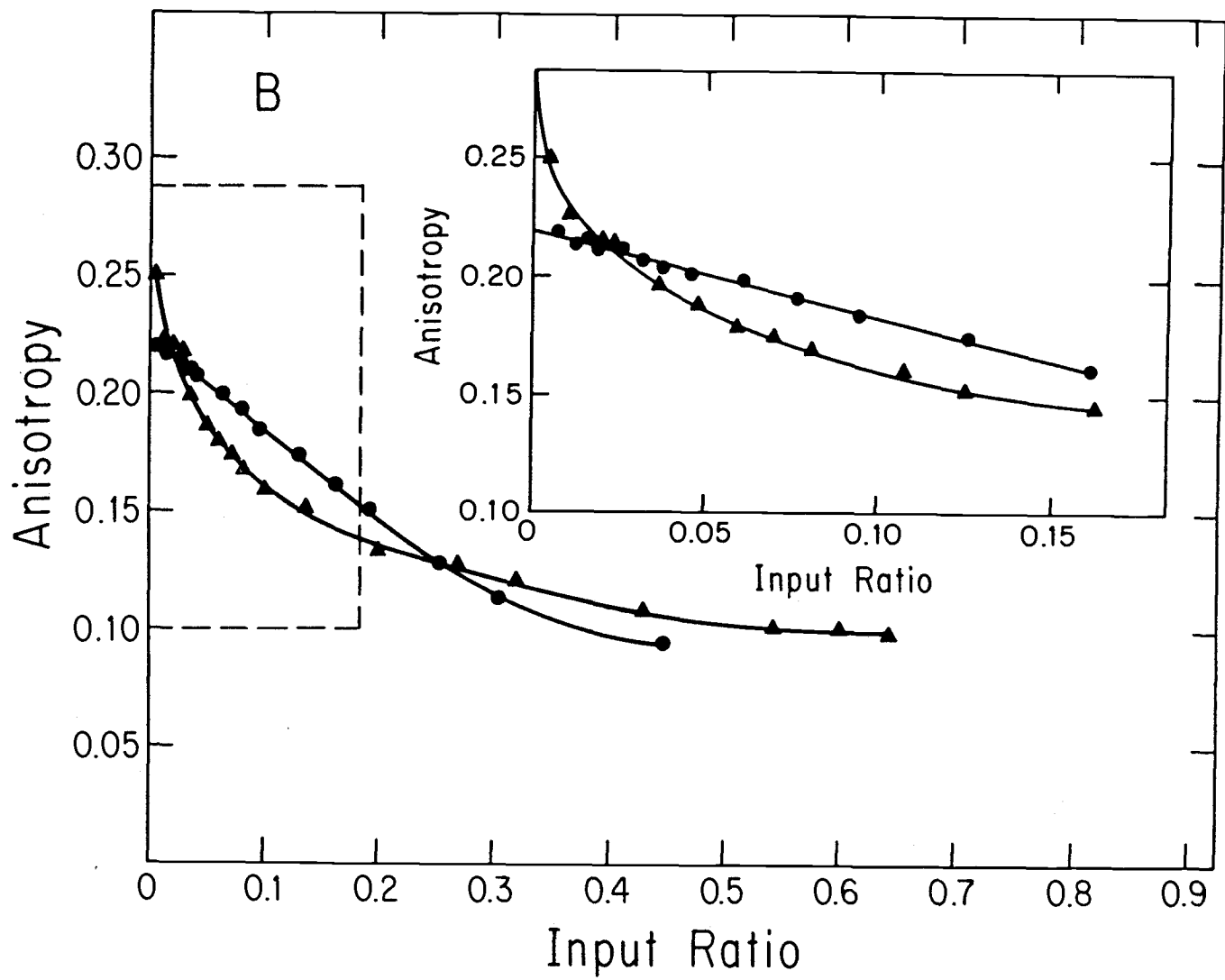


Figure V.14. The plot of fluorescence anisotropy versus viscosity for the ethidium complexes with the nucleosome core particle in 10 mM Tris, pH = 8.0, 0.1 mM EDTA at 20°C. (\blacktriangle) $R = .02$; (\triangle) $R = .04$; (\bullet) $R = .06$; (\circ) $R = .10$; (\square) $R = .15$. The viscosity was increased by the addition of sucrose from 10, 20, 30, 40 to 50%. The anisotropy is defined as the $I_F(\text{parallel}) - I_F(\text{perpendicular}) / I_F(\text{parallel} + 2I_F(\text{perpendicular}))$. The excitation wavelength was 550 nm and the excitation was monitored at 593 nm. Input ratio is defined as moles added dye/mole DNA bp. The core particle concentration was 3.5×10^{-5} M bp and the DNA concentration was 7.8×10^{-5} M bp.

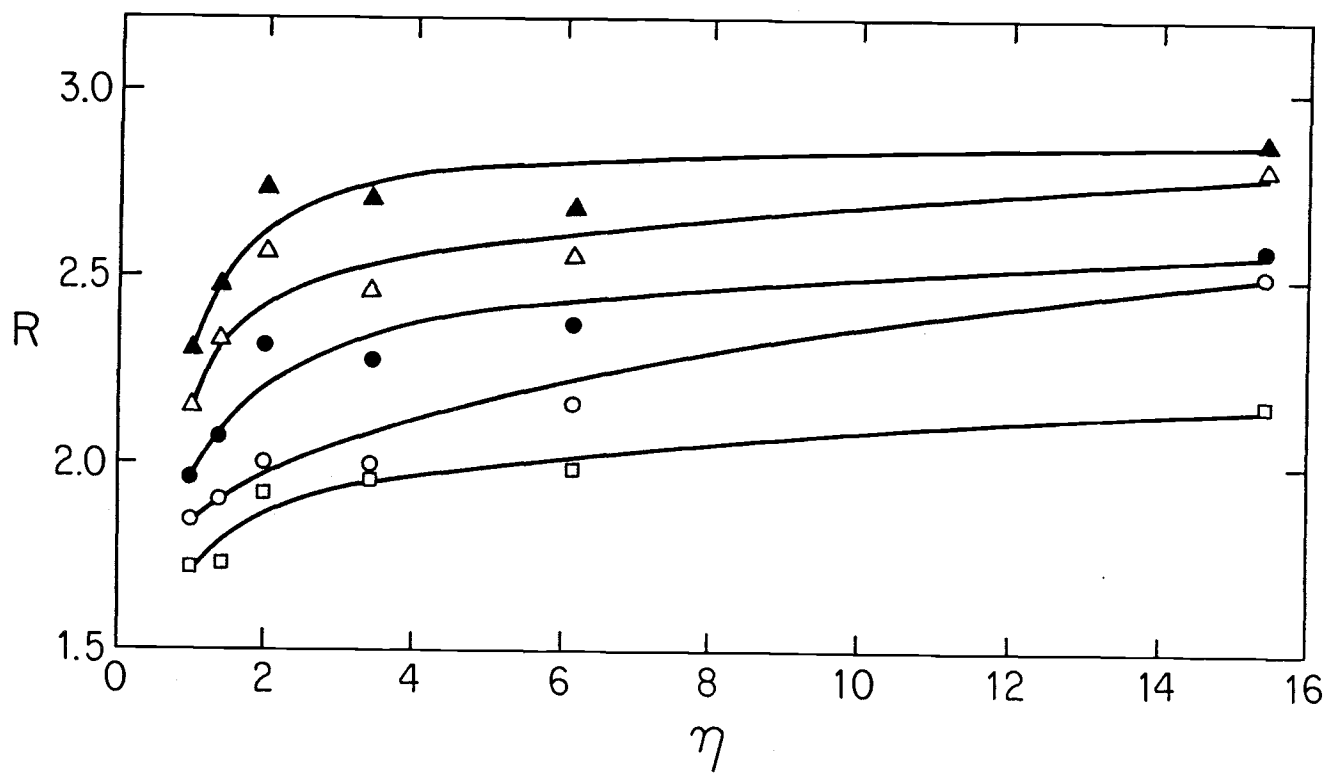


Figure V.14

Figure V.15. The Perrin plot for several complexes of ethidium with the nucleosome core particle. The data from Figure V.14 were used to construct the plot. T = temperature, π = viscosity, $1/A$ is the inverse of the anisotropy for the complex. (\blacktriangle) $R = .02$; (\triangle) $R = .04$; (\bullet) $R = .06$; (\circ) $R = .10$; (\square) $R = .15$. The slope is equal to $t_{Fk}/v_M A_0$. All other conditions are stated in Figure V.14.

Figure V.15

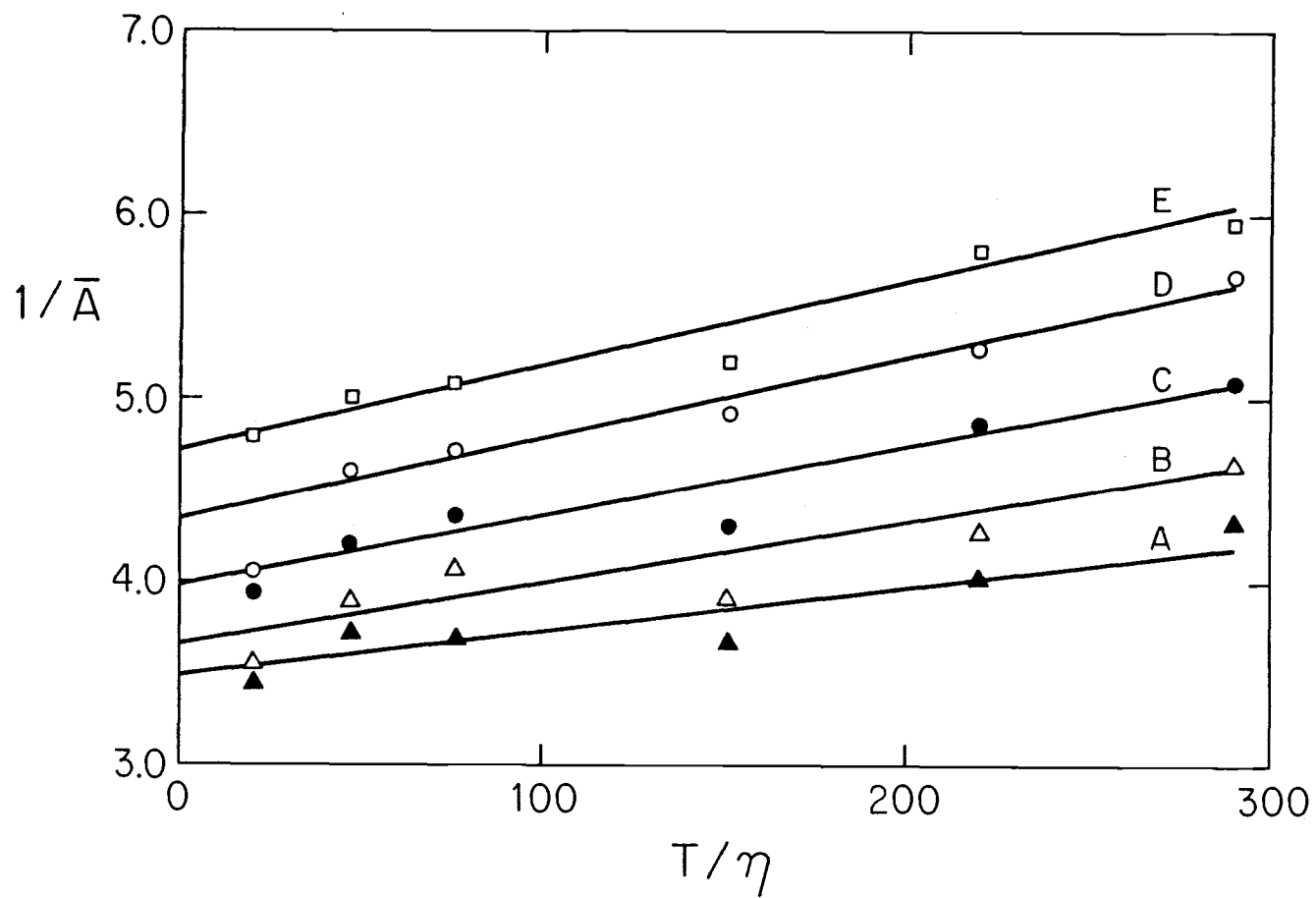


Figure V.16. The scans of the fluorescence anisotropy decay for three ethidium/core particle complexes. (A) $R = .06$; (B) $R = .15$; (C) $R = .25$. $R(t)$ is the anisotropy at time t . T is time in nanoseconds. All other conditions are as stated in Figure V.13 and Figure V.14.

Figure V.16

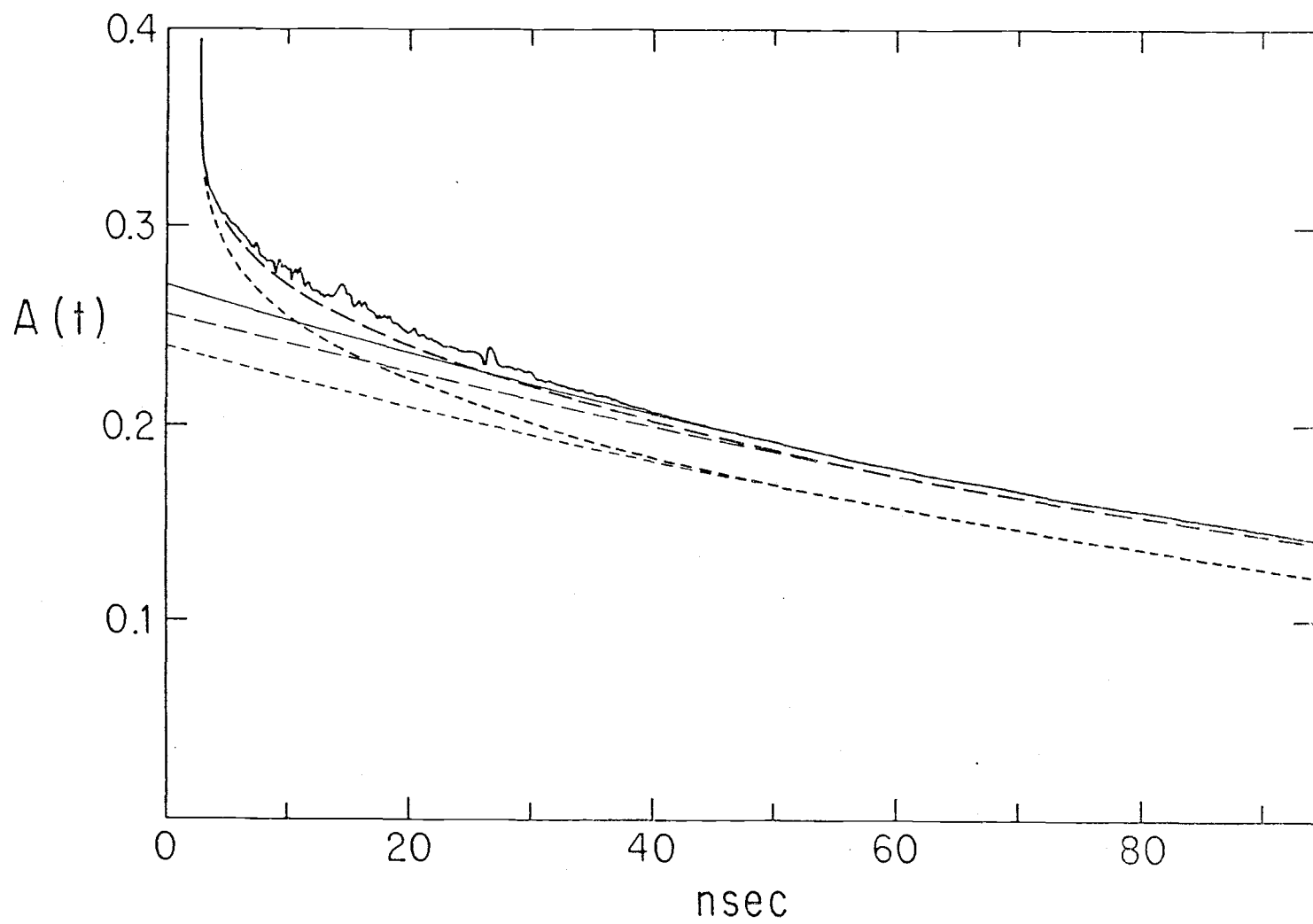


Figure V.17. Schematic representation of the model for ethidium binding to the core particle. Step 1 is the initial end-binding reaction of ethidium to the core particle. Step 2 is the loss of one copy each of H2A, H2B. Step 3 is a slight conformational change due to the peeling of one ethidium-bound DNA end from the core particle, resulting in a 2-4Å radius change. Step 4 is the complete dissociation of the core particle/ethidium complex. Step 5 is the reassociation reaction.

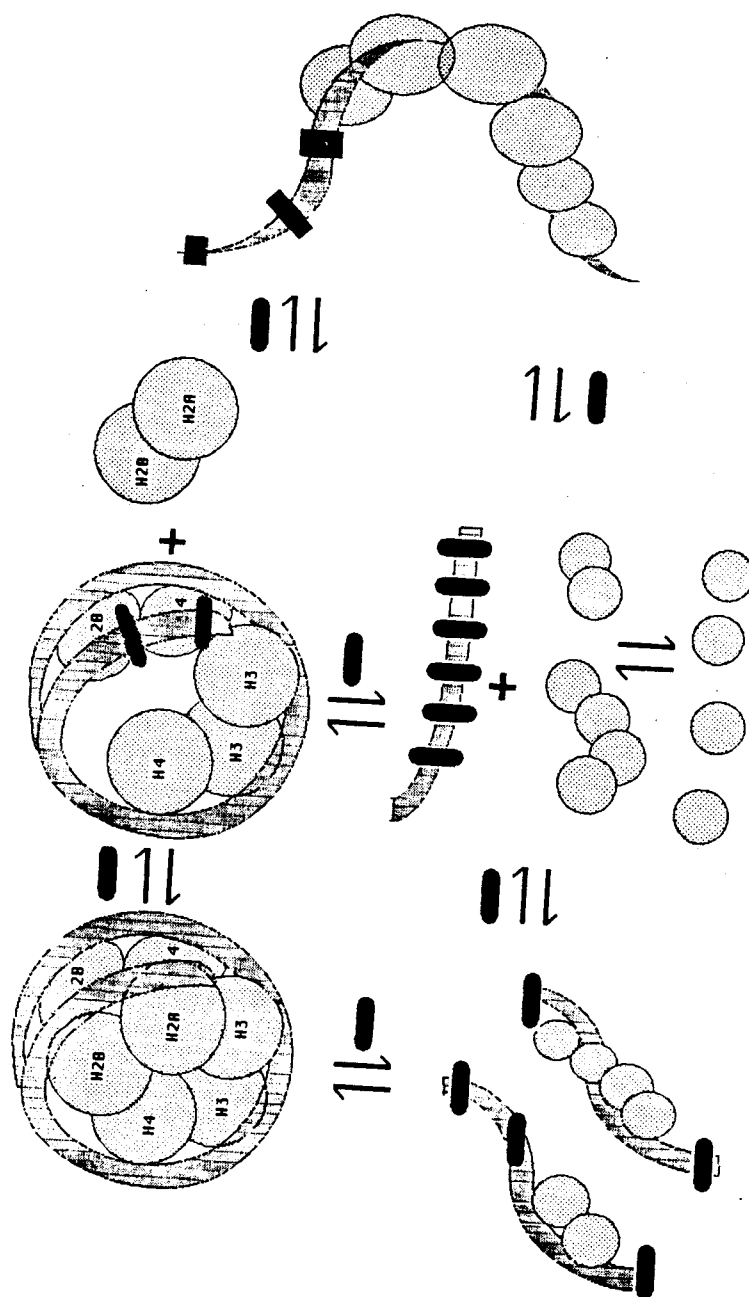


Figure V.17

Figure V.18. A schematic diagram for the passing of a polymerase through a nucleosome. All steps are as described in Figure V.17.

CHAPTER VI. THE BINDING OF ETHIDIUM BROMIDE TO THE NUCLEOSOME

CORE PARTICLE I. THE DISSOCIATION REACTION

ABSTRACT

We have examined the ethidium-induced dissociation reaction of the core particle as a function of ionic strength and temperature. We find that at a constant ratio of bound ethidium, $R = .23$, the dissociation of the core particle is independent of ionic strength from 5 mM $[Na^+]$. The slope of the $\log K$ versus $\log [Na^+]$ plot indicates that ~20 tight electrostatic contacts are broken upon dissociation by ethidium. The temperature dependence of the ethidium-induced process at $R = .13$ indicates that the overall ΔH° for the dissociation reaction is +6.83 Kcal/mole. Combining the binding reaction data with the dissociation data, we have calculated that the overall stabilization of the core particle occurs with a net release of 3.5 Kcal/mole of base pair. The free energy change comprises a significant enthalpic contribution as well as a significant entropic contribution. An overall model for the nature of these contributions is presented.

INTRODUCTION

The function of the nucleosome is multi-fold. First, the formation of the core particle results in a 8:1 compaction of the DNA (Lewin, 1980, 1983). Thus, the formation of the nucleosome structure has an important role in the level of DNA folding. The level of folding of the DNA into higher order structures has been linked to its ability to act as a template for transcription (Reeves, 1984). The presence of H1-containing 30 nm fibers have been correlated with inactive states of the DNA while the extended 11 nm fiber is associated with the more active regions. Since the nucleosome structure is associated with both these orders of chromatin folding, the formation of nucleosomes must play an important dual role in gene activation mechanisms. In other words, the forces which stabilize the nucleosome structure in higher order chromatin forms are the same forces which must be broken in order for DNA to be made a template for transcription. While much structural knowledge about the nucleosome has become available with the solution to the 7Å crystal structure, the forces which stabilize the formation of the particle remain a mystery.

We have recently reported that binding of ethidium bromide to the core particles induces a step-wise dissociation of the core particle structure. We have further demonstrated that the dissociation is produced by the intercalation of the dye molecules and not by alternative binding modes or binding to the histone proteins. The binding properties of the dye, corrected for the presence of free DNA, have indicated that dissociation is induced by a critical ratio of dye

which binds cooperatively to one side of the core particle. In this report, we have examined in detail the dissociation reaction induced by ethidium. We have examined the reversibility, the salt dependence and the temperature dependence of the dissociation reaction. In combination with the details of the binding reaction, we have attempted to utilize the properties of the ethidium-induced dissociation process to gain insight into the forces which stabilize the association state of the native core particle.

RESULTS

I. Characterization of Dissociation.

We have previously reported that the binding of ethidium bromide to the nucleosome core particle results in a step-wise dissociation of the structure which involves the initial release of one copy each of H2A and H2B (McMurray and van Holde, 1986). Under low ionic strength conditions, the initiation of core particle dissociation requires the binding of approximately 8-9 ethidium molecules, called the critical values. Above this "critical" level of dye binding, dissociation increases rapidly with increasing input of ethidium. The products of the dissociation are schematically diagrammed in Figure VI.1 Steps 1, 2 and 3 represent each step of the ethidium-induced dissociation process: the intact core particle, the hexamer and free DNA, respectively.

The ethidium-induced dissociation of the core particle was also shown to be time dependent (McMurray and van Holde, 1986). If the level of free DNA present at various times after addition of the dye is quantified by the gel electrophoretic method reported in Chapter 3, the results depicted in Figure VI.2 are obtained. Under low ionic strength conditions, the kinetics of dissociation were slow and occurred on the order of hours. Despite the slow dissociation rate, low levels of free DNA were detected as soon as 2 minutes after addition of the dye. Two minutes represented the time limit of the technique, i.e., the time required for addition of the dye, mixing, loading and application of the current for separation. Consequently,

we are unable to determine with confidence the kinetic order of the dissociation process using electrophoresis as the detection method. Under low ionic strength conditions, most of the dissociation occurred within the first 5 hours for all ratios measured. Dissociation was complete in ~25 hours.

To demonstrate that the dissociation of the core particles represented an equilibrium process, we measured the extent of reassociation of ethidium-dissociated ^{32}P -end-labeled-core particles at 30°C under identical buffer conditions. We dissociated the ^{32}P -labeled core particles with the addition of a high input ratio of ethidium bromide, $R_I = 4.0$. After mixing, the sample was allowed to equilibrate at 30°C for 24 hours until dissociation was complete. After equilibration, an aliquot of the $R_I = 4.0$ sample was diluted with an equal volume of ^{32}P -labeled, intact core particles (no ethidium bromide added) such that the final concentration of core particles and the amount of labeled material remained constant, but the dye/bp ratio was reduced by a factor of two. Successive dilutions of each sample were made so that the final ratio was $R_I = .03$. The samples were allowed to equilibrate for 24 hours, separated on a 3.5% polyacrylamide gel and the gel was exposed to autoradiographic film. Figure VI.3 shows the laser densitometer trace of ^{32}P -end labeled bands from the reversibility experiment. As can be seen in Figure VI.3, at 30°C under low ionic strength conditions, successive reduction in the ratio of ethidium bromide resulted in complete reassociation of the core particles. (A small amount of free DNA is seen in the control ($R = 0$) lane due to the Mg^{++} required for the end-labeling process). The resulting core particle band, after reassociation, was

identical in shape and position on polyacrylamide gels as the intact particles before dissociation. Upon reassociation, the level of free DNA ranged from 0-67% (see Figure VI.3), in good agreement with the level of DNA quantified in the forward reaction (McMurray and van Holde, 1986). However, we observed less of the hexamer band intermediate. At all ratios measured, we observed no loss of signal intensity, i.e., the integrated area of the DNA bands in each lane remained constant (Figure VI.2). Complete reassociation was observed only at input ratios below the critical ratio $V_c = .06$. In a parallel reversibility experiment (not shown), the sample volume loaded onto the gel, corresponding to successive dilutions of the original complex, were multiplied by the dilution factor. Thus, if any of the original dissociated DNA were only diluted, instead of reassociated, then we could detect its presence. In all cases, complete reassociation of the core particles was obtained below the critical value.

We concluded from these experiments that the dissociation of the core particle structure represented a reversible equilibrium process, induced by the binding of ethidium bromide.

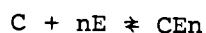
II. Temperature and Ionic Strength Dependence of Dissociation

A. Temperature Dependence

The temperature dependence of the ethidium-induced dissociation of the core particle is shown in Figure VI.4. Free DNA bands were quantified by the gel electrophoretic method described in McMurray and

van Holde (1986). At both 10° and 20°C, only low levels of core particle dissociation were observed. For both temperature points, we measured 5% core particle dissociated upon ethidium binding at $v = .35$ and $v = .31$, respectively. As previously described (McMurray and van Holde, 1986), extrapolation of the dissociation curve to zero % dissociation revealed the existence of a critical value, v_C , below which no dissociation occurred. The critical ratio was found to be $v_C = .06$, as previously reported for the $T = 30^\circ\text{C}$ dissociation curve. The critical ratio corresponds to the binding of 8-9 ethidium molecules and, assuming dye binding follows the neighbor exclusion principle, ~18 bp of DNA are excluded by the critical level of dye. Above 20°C, the ethidium-induced dissociation process became more sensitive to increases in temperature. At 30°C, the dissociation versus bound ratio plot described a non-linear, monotonically increasing function, and, above $v = .25$, the dissociation curve appeared to approach a limiting value near $v = .35$. Further increases in temperature to 37°C or 50°C resulted in curves which were quite similar in shape to the $T = 30^\circ\text{C}$ curve, however, each successive curve approached a limiting value at lower ratios relative to lower temperature curves. Increasing temperature resulted in no change in the critical value at any temperature point measured under our buffer conditions.

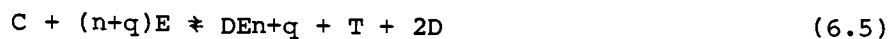
For the ethidium-induced dissociation reaction, the overall reaction can be expressed as the sum of four individual reactions:



(6.1)



where n represents the number of dyes molecules below the critical value and q represents any number of additional bound dye. Summing these 4 equilibria, we obtain an expression for the overall reaction:



and the overall equilibrium constant can be written as:

$$K_T = \frac{[DE]^{n+q} [T] [D]^2}{[C] [E]^{n+q}} \quad (6.6)$$

We have measured the temperature of the dissociation reaction, K' , expressed by:

$$K' = \frac{[DE]^{n+q} [T] [D]^2}{[C]} \quad (6.7)$$

Rewriting Eq. 6.6 in terms of K' , we obtain

$$K_T = \frac{K'}{[E]^{n+q}} \quad (6.8)$$

and

$$\log K' = \log K_T + n+q \log E \quad (6.9)$$

Therefore

$$\frac{\alpha \log K'}{\alpha 1/T} = \frac{\alpha \log K_T}{\alpha 1/T} \quad (6.10)$$

and the ΔH° which we measure from ethidium-induced dissociation equilibrium constants will be the ΔH for the overall reaction.

Therefore, we used the % dissociation values at $v = .23$ to calculate the observed equilibrium constant as a function of temperature. The equilibrium constants were plotted in Figure VI.5 according to the van't Hoff equation

$$\ln K = \frac{\Delta H^\circ}{RT} + \frac{\Delta S^\circ}{R} \quad (6.11)$$

where ΔH° and ΔS° are the observed enthalpy and entropy changes, respectively, for the ethidium-induced dissociation reaction. The values for ΔG° , K_{obs} , ΔS° and the critical value for the dissociation reaction at $R = .23$ for each temperature point is listed in Table VI.1.

The observed enthalpy value for the ethidium-induced dissociation reaction, calculated from the slope of the $\ln K$ versus $1/T$ plot, was found to be +6.8 kcal/mole of core particle. In order to accept the validity of the ΔH° value, we have assumed that the heat capacity of

the individual histone/DNA interactions is similar. The observed entropy values ranged from -32.3 eu at 10°C to -23 eu at 50°C.

B. Ionic Strength Dependence

The effect of [Na⁺] on the ethidium-induced dissociation of the core particle is illustrated in Figure VI.6. At $R = .25$, increasing the [Na⁺] from 5 mM to .2 M results in increasing amounts of free DNA (band-3, Figure VI.6) and a concomitant decrease in the amount of the intact core particles (band-1, Figure VI.6) and the hexamer form (band-2, Figure VI.6). Quantification of the level of ethidium-induced dissociated DNA, as a function of ionic strength, led to the construction of the % dissociation versus bound ratio plot, shown in Figure VI.7. Increasing the ionic strength from 5 mM to .2 M resulted in curves which asymptotically approached a limiting ratio of bound ethidium, similar in shape to the temperature-dependent plots. Increases in the [Na⁺] corresponded to a smaller limiting ratio relative to the lower salt points. At all ionic strengths measured, we found the existence of a critical level of dye which was required to be bound before dissociation began, however, in contrast to the temperature data, the apparent critical value did not remain constant. In 10 mM Tris, pH 8.0, 0.1 mM EDTA, the critical value was found to be $v = .06$. At both 50 mM and .2 M, the critical value was determined to be $v = .03$. We can interpret the reduced $v_{C(app)}$ value in one of two ways. First, at higher ionic strengths, dissociation requires the binding of only 8-9 dye molecules. In this case, we assume that the increase in ionic strength loosens the interaction between the

histones and the DNA, and, consequently, dissociation requires less energy input from the binding of ethidium. Alternatively, since $v_C = v_C(\text{app})/f$ (Chapter II and IV), at higher ionic strengths, the critical value could remain constant at $v_C = .06$, however, the fraction of core particles which bind the dye increases to 1.0. Examination of the ionic strength dependence of the ethidium binding curves (see Table V.2 in Chapter V) reveals that w , the cooperativity parameter, decreases with increasing ionic strength. Since w represents the equilibrium constant which describes the affinity for dye molecules to bind next to a singly bound site, the fact that w decreases with increasing ionic strength suggests that it becomes increasingly less favorable for dyes to bind in the same region at higher salt concentrations. Calculations (Schellman, 1980) indicate that if w decreases, the population of cores which initially bind the dye should increase. Consequently, we favor the idea that at .05 - .2 M ionic strength, all the core particles bind dye at their ends before any of the cores dissociate, i.e., $f = 1.0$. The ionic strength dependence of ΔK_{obs} , $\Delta G^{\circ}_{\text{obs}}$, $v_C(\text{app})$ and f for a core particle/ethidium complex, $R = .13$ are listed in Table VI.2. We concluded that the critical value or 17-18 bp of DNA, must reflect a true structural feature of the core particle DNA.

The % dissociation curves in Figure VI.7 were used to calculate an observed equilibrium constant for the ionic strength dependence of the ethidium-induced dissociation reaction, i.e., $K_{\text{obs}} = f/(1-f)$, where $f = \% \text{ dissociation} \times 100$. For the simple interaction of a ligand with a charged polymer, the dependence of the observed equilibrium constants on counter-ion concentration (Record et al., 1978) is described by

$$\frac{\partial \log K_{\text{obs}}}{\partial \log [\text{Na}^+]} = -m'\psi \quad (6.12)$$

where m' depends on the number of ion pairs found in the DNA/ligand complex and ψ is the number of thermodynamically associated counterions per phosphate charge, found to be 0.88 for free B-form DNA (Record et al., 1976; 1978). Thus, from the slope of a $\log K$ versus $\log [\text{Na}^+]$ plot, it should be possible to determine the number of electrostatic contact points made between the histones and DNA, in the nucleosome, called C , by solving for m' .

To determine m' for our complex reaction, we must first establish an expression for the Na^+ dependence of the observed ethidium-induced dissociation reaction. The overall reaction can be expressed by



where C = core particle, E = ethidium, CE = core particle/ethidium complex, DE = DNA/ethidium complex, m^* is the net change in Na^+ condensed from the initial to the final state and ψ is defined as above, the number of thermodynamically associated counterions per phosphate in both the condensation and screening layers (Record, 1978). The release of condensed Na^+ ions by the binding of ethidium and the dissociation of the core particle is schematically depicted in Figure VI.9.

Because dissociation of the core particle was induced by the binding of n ethidium molecules, the net change in Na^+ ions calculated from the slope of the $\log K$ versus $\log \text{Na}^+$ plot will be due not only

to contacts made between the histone DNA complex, but also depends on the ratio of bound ethidium. Thus, the dissociation reaction in terms of $[Na^+]$ is more precisely written as the sum of four equilibria.

The first reaction involves the initial binding of n ethidium molecules, expressed by



The value for $m_1\psi$ is the net Na^+ condensed during the first step of the dissociation process, the binding of n molecules of ethidium, when $n = v$ (145 bp). The following evidence suggests that $m_1\psi$ is itself the result of a two-step process. The ^{31}P -NMR spectra for core particle/ethidium complex (unpublished results) clearly indicate that the binding of ethidium results in a region of DNA within the core particle, at the ethidium binding site, which has lost its contact with the histones. Thus, even under pre-dissociation conditions, dye binding disrupts some number of DNA/histone interactions. Since the ethidium appears to follow neighbor exclusion principle (Bauer and Vinograd, 1970; Bresloff and Crothers, 1975), the number of sites excluded by the dye is ~ 2.0 . Consequently, the binding of n molecules of dye would release $2n$ bp of DNA. We will refer to $2n$ as m . Additionally, the association of the ethidium cation (Wilson et al., 1985), and other charged intercalators (Wilson and Lopp, 1979; Chaires et al., 1983), with the phosphodiester backbone of DNA forms a tight contact which displaces condensed Na^+ ions. For the ethidium monocation, the value for m' has been found to be 1.2, a value which includes the conformational change induced by the intercalation itself

(Wilson and Lopp, 1979; Wilson et al., 1985). Thus, $m_1\psi$ comprises the following two-steps process: 1) the condensation of Na^+ from the release of m bp of DNA from the constraints of histone binding and 2) the release of Na^+ from the formation of the ethidium/phosphate ion-pair. Eq. 6.4 can now be rewritten as

$$C + nE + m\psi[\text{Na}^+] \rightleftharpoons CEn + n\psi[\text{Na}^+] \quad (6.15)$$

and

$$m_1\psi = (n-m)\psi \quad (6.16)$$

The next reaction involves the dissociation of the CEn complex to free DNA and histones, written as

$$CEn \rightleftharpoons DEn + m_2\psi[\text{Na}^+] \quad (6.17)$$

where CEn , DEn and ψ are defined as before, 0 is the histone octamer and m_2 is the net $[\text{Na}^+]$ produced in the dissociation step.

Since dissociation of the histones from the DNA induces the condensation of counterions to replace p histone contacts, Equation 6.17 may be rewritten as

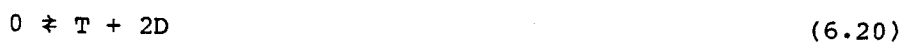
$$CEn + p\psi[\text{Na}^+] \rightleftharpoons DEn + 0 \quad (6.18)$$

where $m_2\psi = (-p)\psi$. Once dissociation has occurred, DEn , a DNA/ethidium complex containing n bound ethidium molecules, becomes a

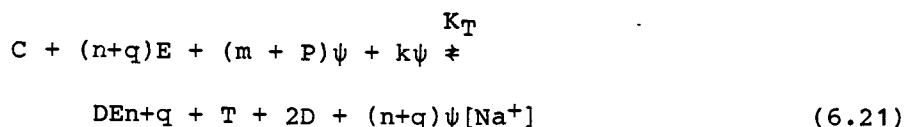
new participant in the binding reaction. Thus, C, CEn and DEn must be in equilibrium with each other, and we can include DEn in the equilibrium expression by



Finally, the histone octamer, itself, is subject to a dissociation equilibrium expressed by



Summing the reactions in 6.15, 6.18, 6.19 and 6.20, the overall expression for the ethidium-induced dissociation of the core particle in terms of $[\text{Na}^+]$ is



and the overall equilibrium constant can be expressed by

$$K_T = \frac{[\text{DEn}+q][\text{T}][\text{D}]^2[\text{Na}^+]^{(m+P)\psi}}{[\text{C}][\text{E}]^{n+q}[\text{Na}^+]^{(n+q)\psi}} \quad (6.22)$$

Since we have measured the equilibrium constant for only the dissociation reaction, called K'

$$\frac{[\text{DEn}+q][\text{T}][0]^2}{[\text{C}]} = K' \quad (6.23)$$

Eq. 6.22, can be rewritten in terms of K' where

$$K_T = \frac{K' [Na^+]^{(m+p)\psi}}{[E]^{n+q} [Na^+]^{(n+q)\psi}} \quad (6.24)$$

At equilibrium, under constant temperature and pressure conditions,

$$\begin{aligned} \log K' &= \log K_T + (n+q) \log [E] + (n+q)\psi \log [Na^+] \\ &\quad - (m+p)\psi \log [Na^+] \end{aligned} \quad (6.25)$$

Collecting terms, we can now express K' in terms of $[Na^+]$ by

$$\begin{aligned} \log K' &= \log K_T + (n+q) \log [E] + (n+q)\psi_D [Na^+] \\ &\quad - (m+p)\psi_C [Na^+] \end{aligned} \quad (6.26)$$

If we vary only the Na^+ ,

$$\frac{\alpha \log K'}{\alpha \log Na^+} = (n+q)\psi_D [Na^+] - (m+p)\psi_C [Na^+] \quad (6.27)$$

and the slope of the $\log K$ versus $\log [Na^+]$ plot should depend on both Na^+ , reflected in n , q , m and p and the bound ratio of dye, reflected in $n+q$.

We now consider ψ , the number of ions thermodynamically associated with both the condensation and screening layers of the polymer. In the $(m+p)$ term, ψ_C represents the number of ion associated with the core particle thermodynamic condensation layer. In the $(n+q)$ term, ψ_D

represents the ions associated with the free DNA thermodynamic condensation layer. Since the core particle DNA is underwound relative to free DNA, and the 7A° resolution crystal structure for the core particle (Richmond et al., 1984) reveals an increased groove size relative to free DNA, the interphosphate distances in the core particle DNA may be increased, thereby reducing the requirement for counterion condensation. Consequently, we cannot assume that ψ is the same for free DNA and the core particle, and we cannot combine the expression in terms of a common ψ .

The Na^+ -dependence of the dissociation reaction may be complicated by the possibility that the dissociation of the core particle results in a change in the number of condensed anions by the octamer. If the histones condense k anions upon dissociation, then

$$\frac{-\partial \ln K}{\partial \ln [\text{Na}^+]} = (n+q)\psi_D[\text{Na}^+] - (m+p)\psi_C[\text{Na}^+] + K \quad (6.28)$$

Similarly, if a change in ionic strength results in a significant change in the hydration state of the products, then Eq. 6.28 becomes

$$\frac{-\partial \ln K}{\partial \ln [\text{Na}^+]} = (n+q)\psi_D[\text{Na}^+] - (m+p)\psi_C + K + h \quad (6.29)$$

letting $(n+q)\psi_D - (m+p)\psi_C[\text{Na}^+] = m^*$,

$$\frac{\alpha \log K}{\alpha \log \text{Na}^+} = m^* + K + h \quad (6.30)$$

Thus, in order to determine $m+p$, the number of histone-DNA contacts made in the nucleosome, from the slope of the $\log K$ versus $\log Na^+$ plot we must first evaluate m^* , K and h .

We can simplify m^* by noting that $n+q$ must be equal to the total number of bound ethidium molecules, E_B ; n represents any level of bound dye below the critical level and q is any additional bound dye. Additionally, ψ_0 is known to be 0.88 for B-form DNA (Record, 1976, 1978). Therefore m^* reduces to

$$m^* = 0.88 E_B - [m+p]\psi_C \quad (6.31)$$

We also know that $m = 2n$ and that $m+p$ must be equal to the total number of histone/DNA contact points over the entire core particle, which we will call C . Therefore

$$m^* = 0.88 E_B - C\psi_C \quad (6.32)$$

and

$$\frac{\alpha \log K'}{\alpha \log Na^+} = 0.88 E_B - C\psi_C + k + h \quad (6.33)$$

The k term in Eq. 6.23 relates the dependence of the equilibrium constant on the number of counterions produced by the binding of the anion to the histones. Although we cannot rule out a possible anion effect, two lines of evidence suggest that it may not be important in the formation of the DNA/histone complex. First, McGhee and

Felsenfeld (1980) reported that thermal denaturation of core particles in a range of Na⁺ salts associated with anions of differing protein binding affinities, resulted in no differences among the melting curves. Second, the binding properties of oligolysine with free DNA (Lohman and Record, 1980) displayed no anion dependence. Assuming the interaction of oligolysine is a good model for the histone interaction, we will assume the most simple case where $k = 0$. Thus, Eq. 6.24 becomes

$$\frac{\alpha \log K}{\alpha \log \text{Na}^+} = .88 E_B - C\psi_C + h \quad (6.34)$$

We have no data with which to quantify hydration changes in the core particle which accompany changes in ionic strength. However, hydration terms are only included in equilibrium expressions when the salt conditions are very high. Since our buffer conditions never exceeded 50 mM [Na⁺], we will neglect the h term. Equation 6.34 can now be used to calculate C , the total number of C histone contacts.

The results of the $\log K$ versus $\log [\text{Na}^+]$ plot for several ratios are shown in Figure VI.8. Inspection of Figure VI.8 reveals that the dependence of $\log K$ on the $\log [\text{Na}^+]$ is non-linear, suggesting that ethidium-induced dissociation of the core particle is not accompanied by a constant net change of condensed Na⁺ at all ionic strengths. The tangent to the curve was calculated for two regions (low and high salt points) for four different complexes of ethidium with core particle. Additionally, we calculated the slope from a linear fit to all the data points. The results are listed in Table VI.3. Inserting these

slope into Equation 6.34, we found that $p\psi_C$ was always the difference between the calculated slope and the bound ratio of dye. As the bound ratio increased, the slope also increased, but the difference remained fairly constant. Since $C\psi_C$ was constant, we could not extract a value for ψ_C from the expression, and we are forced to estimate its value. Taking the average of the ψ for B-form DNA (.88) and single-stranded DNA ($\psi = .73$), we used a $\psi_C = .80$ to calculate C for the core particle. The results of the calculations are shown in Table VI.3. Consequently, we estimate that no more than 15-20 tight electrostatic interaction stabilize the DNA/histone complex in the core particle. At present, we cannot explain the curvature of the log K versus log $[Na^+]$ plot. However, the presence of the curvature indicates that either anion binding or some significant hydration change accompanies dissociation. We note that if this is the case C will be underestimated at high ratios.

DISCUSSION

We had previously demonstrated that the dissociation of the core particle occurs as the result of binding ethidium bromide (McMurray and van Holde, 1986). The kinetics and reversibility of the ethidium-induced dissociation reaction reveal that the process is a time-dependent equilibrium. Kinetic measurements demonstrated that under our low ionic strength conditions, dissociation is slow, taking 15-24 hours to reach completion. Although we have not systematically measured ethidium-induced dissociation at higher ionic strengths, we have observed that the rate of dissociation is increased with increasing ionic strength. Increases in both temperature and ionic strength result in increased levels of free DNA. We used the data from the temperature and ionic strength dependence of the ethidium-induced dissociation reaction to gain more insight into the forces which stabilize the association of the native nucleosome structure.

Thermodynamic Analysis of Dissociation

We have envisioned the ethidium-induced dissociation as a thermodynamic cycle, schematically represented in Figure IV.10, where ΔG°_1 is the Gibbs free energy for the association reaction of ethidium with the core particle, ΔG°_2 is the Gibbs free energy for the association reaction of ethidium with free DNA, ΔG°_3 is the Gibbs free energy for the difference in energy of the core particle/ethidium complex and a DNA/ethidium complex, and ΔG°_4 is the dissociation

energy of the core particle. The value used in the calculation for ΔG°_3 was determined from the difference in binding energy between free DNA and the core particle, plotted in Figure V.3. Since ΔG° is a state function, independent of the pathway, the following must be true:

$$\sum_i \Delta G_i^\circ = 0 \quad (6.25)$$

Substituting the experimentally determined values from the binding data in Chapter 5 ($\Delta G^\circ_1 = -6.0$ kcal/mole, $\Delta G^\circ_2 = +8.8$ kcal/mole) and $\Delta G^\circ_3 = +3.0$ kcal/mole, we can calculate ΔG°_4 by

$$\Delta G^\circ_4 = -(\Delta G^\circ_1 + \Delta G^\circ_2 + \Delta G^\circ_3) \quad (6.26)$$

Thus, the energy of dissociation for the DNA and the histones complex, ΔG°_4 , is +5.8 kcal/mole of core particle, i.e., the energy of nucleosome formation is -5.8 kcal/mole. Since ΔH° is also a state function, we can use the same cycle to determine ΔH° for each step of the process. Using the $\Delta H^\circ_1 = -7.5$ kcal/mole, the average enthalpy change for binding ethidium to the core particle (from Chapter 5), a value of -6.2 kcal/mole (Quadrifoglio et al., 1974) for the association of ethidium with DNA and a value of +.05 kcal/mole from the van't Hoff plot in Figure IV.8 for the ethidium-induced dissociation of the core particle, equal to (6.86 kcal/mole core

particle)/(145 bp/core particle), we calculated the ΔH° for the formation of the core particle to be -1.3 kcal/mole core particle. Taking the ΔG° and the ΔH° for the formation of the nucleosome, at 30°C, the ΔS° value for the association of the DNA and the histones to form the core particle is 14 eu.

Thus, the formation of the core particle is a spontaneous reaction stabilized by the release of 5.8 kcal/mole of core particle. At 30°C, the free energy change comprises a significant enthalpy term of -1.3 kcal/mole bp and a large entropy term of 11.5 eu. The results suggest that core particle stabilization is almost entirely entropy driven, in agreement with others (Stein, 1980; Mirzabekov, 1980), and the values of ΔH° and ΔS° for formation are consistent with the small number of electrostatic interactions calculated from the salt analysis. We calculate that, maximally, 15-20.0 tight electrostatic interactions are broken per core particle dissociation event. This number is far less than previously predicted, even by the analysis of McGhee and Felsenfeld (1980). Since electrostatic interactions give rise to little or no change in ΔH° , 15-20 electrostatic interactions would lead to the prediction that association should be accompanied by a small enthalpy change, as observed. Since electrostatic interactions are entropically stabilized, the entropy values are also consistent with the calculated number of interactions. Knowledge of the ΔG_F° , ΔH_F° and ΔS_F° allows a more detailed analysis of the forces which contribute to the overall stabilization of the core particle. We will consider three possible candidates for such forces: conformational changes in the histones, conformational changes in the DNA, hydration changes in the histones and/or the DNA and, finally, hydrogen bonding

between amino acid residues in the histones to the phosphates or bases in the DNA.

1. Conformational Changes.

Weischet et al. (1978) have measured the circular dichroism (CD) spectra at 230 nm for the histone octamer, folded within the core particle, as a function of temperature. The authors observed no change in molar ellipticity at 230 nm for the octamer below the second phase of melting. Similarly, no changes have been observed in core particle molar ellipticity value at 230 nm between 10 mM to 50 mM ionic strength (McMurray, unpublished results). Thus, under our buffer and temperature conditions (10-50°C), no evidence supports the existence of a conformational change in the histones. In contrast, we have previously reported the existence of a histone-induced conformational change in the DNA which involves alterations in hydrogen bonding within the core particle (McMurray et al., 1985). The altered hydrogen bonding is observed as a population of ^1H -NMR signals from exchangeable protons which are found upfield relative to the normal protons observed for linear, B-form DNA. We find that the number of bases involved in the altered hydrogen-bonding increases with increasing temperature, and involves 5-25 bp of DNA between 15-55°C. From the integrated area of the ^1H -NMR peaks listed in Table I of (McMurray et al., 1985), we calculated the K_{obs} for the temperature-induced conformational change. The data were plotted according to the van't Hoff equation, and are shown in Figure IV.13. We have calculated the ΔH° for this transition, $\Delta H_{\text{B}}^\circ$, from the slope

in Figure IV.13, to be +9 kcal/mole bp. The entropy calculated for this conformational transition is +40 eu. Since, at 30°C, the number of base pairs of DNA involved in the conformational change is ~8, and ΔH_B° expressed per mole of core particle is +72 kcal. Thus, core particle formation is accompanied by a conformational change with $\Delta G^\circ = -24$ kcal/mole of core particle. The free energy comprises a highly unfavorable enthalpy, but occurs due to entropic stabilization. Since, we interpret our unusual ^1H -NMR resonances to be the result of a DNA binding, we refine our analysis to suggest that the conformational change which occurs during the formation of the nucleosome is the formation of DNA bends. The energetics of DNA bending which we calculate are in excellent agreement with previously reported values (Camerini-Otero and Felsenfeld, 1977; Levitt, 1978).

2. Changes in Hydration

Calculations from sedimentation velocity experiments (McMurray; unpublished results), using a $s = 10.8$ for the native core particle (Yager and van Holde, 1984), reveal that the core particle is a highly hydrated particle, attaining a hydrated volume 2.5 times the anhydrous volume. However, the crystal structure for the histone octamer at 3.3 Å resolution (Burlingame et al., 1985) in high salt reveals that the octamer itself is highly hydrated with solvent channels 4-14 Å in radius separating the H2A-H2B dimers from the H3-H4 tetramer. Thus, it is possible that association of the DNA with the histones does not result in a large bulk change in hydration. However, several lines of evidence suggest that significant hydration changes may occur in the

core particle structure. First, we have measured the sedimentation coefficient of the core particle under a variety of ionic strength conditions (Yager et al., submitted). In the ionic strength range from 5 mM to .1 M, we have observed a slight increase in the sedimentation coefficient from 10.8s to 10.9s. Further increases in ionic strength result in a decrease in s from 10.9 to 9.2s. The decrease in s occurs in the same salt range as a loosening of the histone tails (Walker, 1984), but the salt increase results in no change in the R_G , concomitantly measured by neutron scattering (Yager et al., submitted). Since R_G is constant in this salt range, we cannot explain the decreased s value on the basis of increased frictional coefficient due to a large change in shape. But, assuming all other parameters are not changed, the results can be explained by increased hydration. The 7Å crystal structure of the core particle (Richmond et al., 1984) indicates that both the major and minor grooves of the folded DNA are quite different relative to free DNA. The minor groove on the inside of the nucleosome (7Å) is compressed by 2Å relative to free DNA. The groove on the outside of the nucleosome (14Å) is larger by 5Å relative to free DNA. Although not directly measured, one would predict that these large differences in the groove size within the core particle could have dramatic effects on the interphosphate distance and the hydration state of the DNA, especially in the minor groove. Drew and Dickerson (1981) have postulated that the highly ordered water spine of hydration in the minor groove of B-form DNA is a major determinant of the conformation of the DNA. Thus, disruption of the water spine in free DNA upon core particle formation, and the re-formation of the water spine during

dissociation, could account for a number of unexplained observations: the slightly altered conformation in the nucleosome core particle (Cowman and Fasman, 1977), a decrease in the sedimentation coefficient of the core particle under moderate, pre-dissociation conditions (Yager et al., submitted; Ausio et al., 1984), an increase in the molar ellipticity value at 282 nm under moderate, pre-dissociation ionic strength conditions (Yager et al., submitted), and the curvature in the log K versus log $[Na^+]$ plot.

3. Hydrogen Bonding Between the Histones and DNA.

It should be reemphasized that 30% of the positive charge found in the histone proteins resides in the N-terminal tails. Weintraub and van Lente (1974) demonstrated that core particles maintain a normal folded state, with only minor differences, after removal of these charges by trypsinization. Additionally, trypsinization and maximum acetylation of the histone tails do not result in any detectable destabilization of the core particle (Ausio and van Holde, 1986). Thus, these data suggest the possibility that interactions other than electrostatic ones are important in stabilizing the core particle. Results from model peptide studies in several laboratories (Brown, 1970; Helene et al., 1971; Gabbay et al., 1972, 1973; Dimicoli and Helene, 1974; Kapicak and Gabbay, 1975) have led to the proposal that aromatic amino acid residues, tyrosine or phenylalanine, within the histones might intercalate into the DNA. Other workers have suggested that the histone/DNA interaction is stabilized by the hydrogen bonding of arginines or histidines to either the DNA phosphates or to a DNA

base (Helene and Lancelot, 1982). However, despite the existence for bonding of specific amino acids to core particle DNA, there exists no direct evidence of such associations. Since the average value for ΔH° for hydrogen-bonding in water is -4.5 kcal/mole bonds, the presence of even a few such bonds should result in a significant contribution to the overall enthalpy.

From the preceding discussion, we have evaluated three possible contributions to the stabilization of core particle formation in addition to electrostatic interactions. If we define ΔG_F° as the overall free energy of formation of the core particle, ΔG_B° as the free energy of bending, ΔG_O° as the free energy due to other forces we can estimate (ΔG_O°) by

$$\Delta G_F^\circ = \Delta G_B^\circ + \Delta G_O^\circ \quad (6.27)$$

$$\Delta G_O^\circ = \Delta G_F^\circ - \Delta G_B^\circ \quad (6.28)$$

Thus, (ΔG_O°) = + 18.2 kcal/mole, (ΔH_O°) = -73 kcal/mole and (ΔS_O°) = -306 eu/mole of core particles. A summary of the energetics of all components is listed in Table IV.4. Thus forces, other than bending of the DNA, are very important in stabilizing the core particles. The sum of these "other" forces comprises a large favorable enthalpy term and a large unfavorable entropy term. If we assume that these "other" forces are the sum of electrostatic, hydrogen-bonding and hydration changes, then the sum of these forces must be consistent with the energetic analysis.

We know the electrostatic interaction stabilize the core particle

with favorable entropy and negligible enthalpy. If we allow the existence of hydrogen bonding, then some of the favorable enthalpy in the ΔG_0° is accounted for. Camerini-Otero and Felsenfeld (1977) have shown that only histones H3 and H4, the arginine rich histones, are required in the folding of the nucleosome. Whereas, the binding of oligolysine is chiefly electrostatic in nature (Klump, 1976), binding studies of oligoarginine to DNA indicate that there is a considerable non-electrostatic component to the binding free energy (Felsenfeld, G., unpublished results).

Thus, if DNA/oligoarginines are a good model for DNA/histone interactions, it is reasonable to assume that hydrogen bonding may play a role in the association of the histones to DNA. However since the ΔH_H° for formation of hydrogen-bonding is a -4.5 kcal/mole, 17-18 interactions of the type would be required to account for all the observed enthalpy change in ΔG_0° . Since most of the arginine amino acid residues reside in the histone tails and histone tails are not required for folding the DNA, it does not appear likely that 17-18 hydrogen-bonded interactions occur upon core particle formation. Thus, we favor the idea that hydration changes may also be important. Changes in hydration would contribute to the enthalpic stabilization of the core particle. If hydrogen bonding and hydration changes are both important, then the sum of these two forces gives rise to a very large unfavorable entropy. Since we know that loss of structured water, if it occurs, is entropically favorable, the disfavorable entropy of forming hydrogen bonds between the DNA and the histones must be large.

We propose the following model for core particle stabilization.

The enthalpic contribution to the core particle association energy is the competition among three forces: 1) the formation of non-specific hydrogen bonding, a highly favorable reaction, 2) the necessary consequence of hydrogen bond formation, the formation of DNA bends, a highly unfavorable reaction, and changes in groove hydration which accompany each process. The formation/dissociation of the core particle is entropically stabilized by hydration changes and any electrostatic interactions made between the histones and the DNA. Since we have shown that the bending of DNA results in large positive entropy change, we can speculate that the bending the DNA is favored because it reduces the need to form a highly ordered water spine due to the alterations in the groove geometry. At the same time, the loss of hydrogen-bonding between the DNA base and the water molecules accounts for the unfavorable enthalpy.

Thus, conditions which affect hydrogen bond formation, DNA bending or the formation of the hydration spine will have large effects on the association state of the core particle. If our slope of the $\log K$ versus $\log \text{Na}^+$ plot has underestimated the number of electrostatic interactions, we take this as evidence that hydration is important. Our model can explain both ethidium-induced dissociation under low ionic strength conditions and salt-induced dissociation of the core particle in the absence of a large number of electrostatic interactions. The binding of ethidium results in a stiffening and straightening of the DNA at the ethidium binding site, thereby, reducing the ability of the DNA and histones to form contacts which require a specific geometry. Ionic strength-induced dissociation is a more complicated process, but can be viewed as the sum of three

affects. First, the electrostatic interactions made by the association of the histones with the DNA are loosened, thereby, initially decreasing the strength of the DNA histone interaction. The loosened interaction tends to decrease the ability of the DNA to bend around the histone octamer. Since DNA bending is enthalpically unfavorable, the loosened structure results in a tendency for the DNA to straighten and return to a normal B-form winding angle of 10.4 bp/turn. The decrease in bending and the return to a normal groove geometry necessitates the formation of the water spine. Finally, all these changes in the DNA combined with small changes in the state of the histones may affect the ability to form hydrogen bonds.

Finally, through a thermodynamic analysis of core particle melting, McGhee and Felsenfeld (1980) have pointed out that the core particle is stabilized by far fewer (~44) electrostatic interactions than was previously thought based on the histone/DNA charge ratio. Our thermodynamic analysis reveals a more extreme limit of this point of view. We conclude that the core particle is stabilized by far fewer electrostatic interactions, a maximum of 15-20. However, the authors did observe a much larger ionic strength dependence associated with the core particle structure relative to our results. Since their analysis is conceptually correct, we can only explain the differences between their results and our results to involve the their use of ΔH° for the thermal denaturation process. It is quite reasonable to suspect that there are many electrostatic, and other interactions, which stabilize the double helical structure of DNA within the core particle, but which do not result in the release of condensed Na^+ ions. Our analysis is insensitive to the presence of such

electrostatic interactions. In contrast, the ΔH° for thermal denaturation of the core particle, but not the DNA, must include stabilization from these sources. Taking the difference in the slopes of the $\log K$ versus $1/T$ plot between the core particle and DNA will lead to an underestimation of y in their analysis and, consequently, an overestimation of x .

Table VI.1

Temperature Dependence of the K_{Obs} , ΔG° and ΔS° for the
Ethidium-Induced Dissociation of the Nucleosome
Core Particle R = .23 Complex

$T^\circ\text{C}^a$	% D ^b	K_{Obs}^c	$\Delta G^\circ (\text{Kcal/mole})^d$	$\Delta S^\circ (\text{cal/deg})^e$
10	2.0	.02	-2.21	32.3
20	3.0	.03	-2.10	30
30	10.0	.11	-1.33	27
37	12.5	.14	-1.21	26
50	28	.39	- .60	23

a. Core particle concentration was 3.8×10^{-5} M bp. The buffer for all samples was 10 mM Tris, pH 8.0, 0.1 mM EDTA. Temperature was held constant as indicated by equilibrium in a constant temperature incubator.

b. %D = percent dissociation. Dissociation values were determined by gel quantification method (McMurray and van Holde, 1986). Samples used in the analysis were taken from the sample well of an equilibrium dialysis apparatus and the v values were determined from the absorbance of the buffer chamber.

c. $K_{\text{Obs}} = \frac{f}{1-f}$ where $f = \%D \div 100$.

d. $\Delta G^\circ = \ln K_{\text{Obs}}$.

e. $\Delta S^\circ = R \ln K - \frac{\Delta H^\circ}{T}$

Table VI.2

Ionic Strength Dependence of K_{obs} , ΔG° and v_c for the
Ethidium-Induced Association of the Nucleosome
Core Particle R = .13 Complex at 30°C

$[Na^+]^a$	% D ^b	K_{obs}^d	ΔG° (Kcal/mole) ^c	v_c (app) ^e	BP _C (app) ^f
5 mM	40	0.42	-1.90	.06	17 ± 1 bp
10 mM	5	0.52	-1.80	.05	14 ± bp
20 mM	11	.12	-1.3	.04	11 ± 1 bp
55 mM	37.5	.60	-0.3	.03	8 ± 1
200 mM	--	--	--	.03	8 ± 1

a. Core particle concentration was 3.8×10^{-5} M bp. The buffer for all samples has 10 mM Tris, pH 8.0, 0.1 mM EDTA with NaCl added as indicated.

b. %D = percent dissociation. The level of dissociated DNA was determined by quantitative gel electrophoresis (McMurray and van Holde, 1986). The v_c values were determined by equilibrium dialysis.

c. $\Delta G^\circ = - \ln K_{obs}$

d. $K_{obs} = \frac{f}{1-f}$ where $f = \%D \div 100$

e. v_c was determined by extrapolation of the % dissociation curve to zero % dissociation.

f. BP_C = the number of base pairs excluded by the critical level of dye = $(v_c)(145 \text{ bp})$.

Table VI.3

Values for $C\psi_C$ and C Calculated from the Slope of the $[\text{Na}^+]$ -Dependence of the Observed Equilibrium Constant for the Ethidium-Induced Dissociation Reaction of the Nucleosome Core Particle

Data ^a	Slope	E_B^b	$C\psi_C^c$	C (for $\psi_C=.80$) ^d
<u>Average</u>				
.10	1.00	14.5	11.8	15
.13	1.04	18.9	15.6	21
.14	1.17	20.3	16.7	21
.15	2.0	21.8	17.2	21
<u>Region A</u>				
.10	.60	14.5	12.2	15
.13	.30	18.9	16.3	20
.14	.33	20.3	17.5	22
.15	.47	21.8	18.7	23
<u>Region B</u>				
.10	1.47	14.5	11.3	14
.13	1.41	18.9	15.2	19
.14	2.60	20.3	15.3	19
.15	5.0	21.8	14.2	18

- a. Data refers to the region of the $\log K$ versus $\log [\text{Na}^+]$ plot where the slope was calculated. Region A was the slope calculated from the low salt points and Region B was calculated from the high salt points. Average refers to the slope calculated from a linear fit to all the data points.
- b. E_B = the number of bound ethidium molecules = $v_B \times 145$ bp, where v_B is the total ratio of bound ethidium/DNA base pair.
- c. $C\psi_C$ is defined as the product of the number of DNA/histone contact points, C, times ψ_C , the number of Na^+ thermodynamically associated with each charge on the polymer.
- d. C is the number of DNA/histone contacts made as a result of nucleosome formation.

Table VI.4

Summary of Thermodynamic Parameters^a which Govern the
Association/Dissociation of the Nucleosome Core Particle at 30°C

Process	ΔG° (Kcal/mole)	ΔH° (Kcal/mole)	ΔS° (eu/mole)
Ethidium-Induced Dissociation	+1.3	+6.9	27
Overall Formation	-5.8	-1.3	14
Bending	-24.0	+72.0	+320
Other	+18	-73	-306

- a. All values and methods for determining these parameters are described in the text. All values are reported as Kcal/mole of core particle under low ionic strength conditions.

Figure VI.1. Schematic representation of the step-wise dissociation of the nucleosome core particle. Step 1. The binding of ethidium results in the loss of one copy each of H2A and H2B. Step 2. The binding of a critical ratio of dye results in the production of free DNA and histones.

Figure V I.1

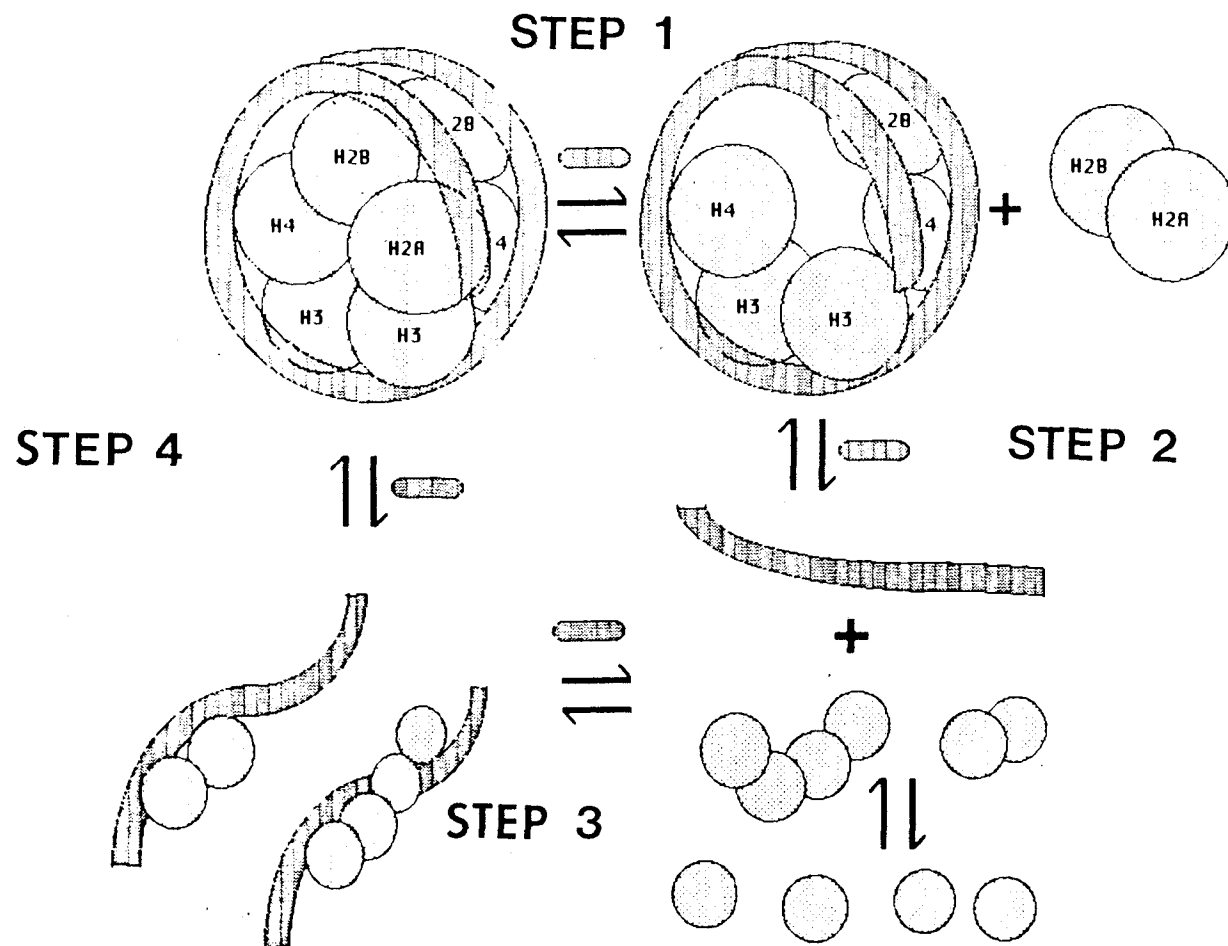


Figure VI.2. Time dependence of the ethidium-induced dissociation of the chicken erythrocyte core particle at 30°C in 10 mM Tris, pH 8.0, 0.1 mM EDTA. (●) Input ratio, $R = 0.15$; (○) Input ratio, $R = 0.35$. The buffer used in all experiments was 10 mM Tris, pH = 8.0, 0.1 mM EDTA and the core particle DNA concentration was $3.0 - 7.5 \times 10^{-5}$ M BP. The core particles were added to solutions of ethidium bromide to yield the indicated ratios of dye to BP. At the indicated times after addition of the dye, the complexes were separated on 3.5% native polyacrylamide, 1.0 mm minigels. The gels were stained with ethidium bromide and dissociation was detected by monitoring mobility of free DNA bands. The amount of dissociation was quantified by the gel electrophoretic method described in (McMurray and van Holde, 1986, Chapter 3).

Figure VI.2

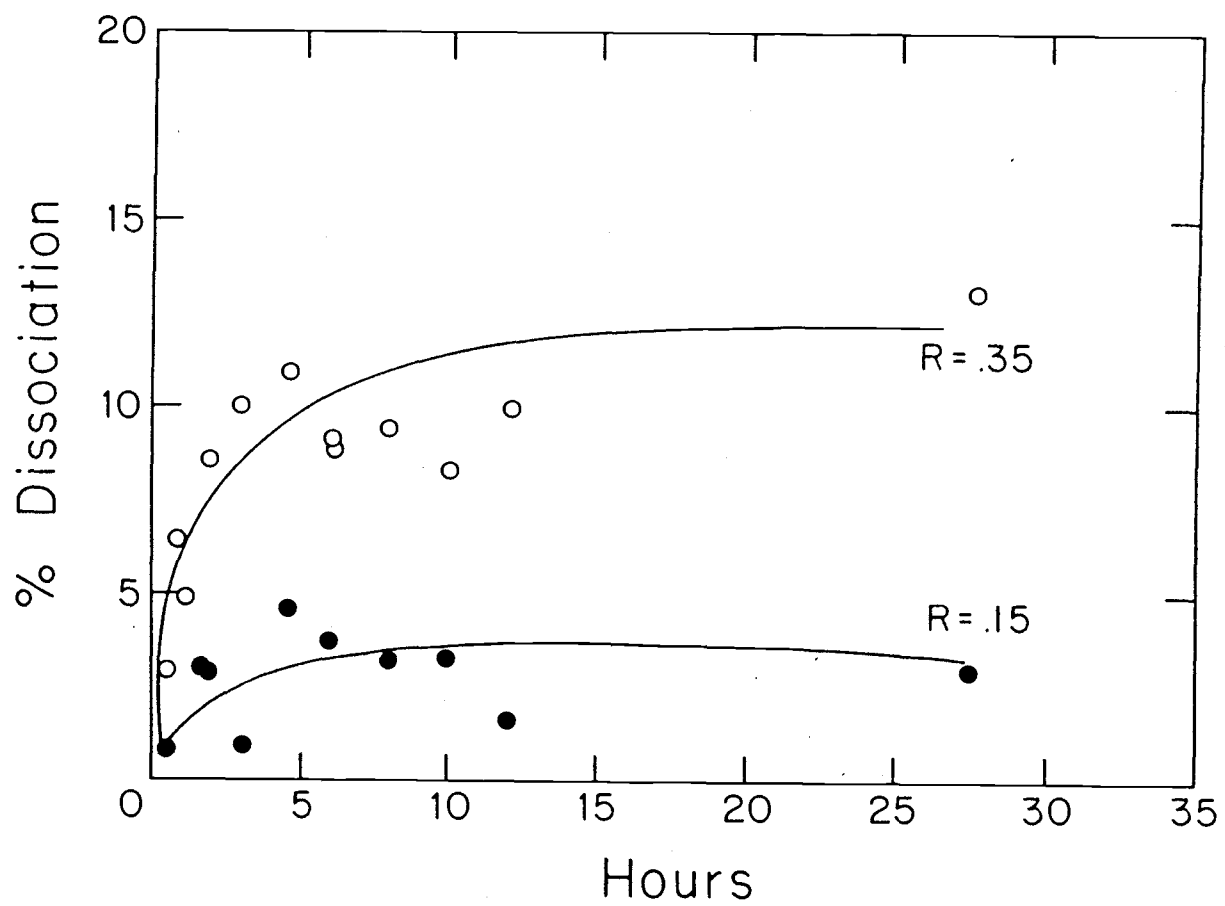


Figure VI.3. Reversibility of the ethidium-induced dissociation of ^{32}P -5'-end-labeled core particles in 10 mM Tris, pH 8.0, 0.1 mM EDTA at 30°C. A core particle/EB complex, $R = 4.0$, was equilibrated for 24 hours until complete dissociation had occurred. The sample was successively diluted with equal volumes of intact ^{32}P -5'-end labeled core particles such that the ratio was reduced by a factor of two, but the concentration and the amount of label remained constant. The samples were analyzed and separated by 3.5% native polyacrylamide gel electrophoresis after equilibrium. The arrow indicates the direction of migration. Each scan represents the laser densitometer trace of each successive dilution of the $R = 4.0$ sample, as indicated. Arrows labeled 1, 2 and 3 represent the positions of the intact octamer (1), the hexamer (2) and free DNA (3) found in the forward reaction. The gel picture at the right side of scans depicts the products of the forward dissociation reaction, $R = .30$. The total area of each peak was integrated by cutting and weighing the traces, and the values for the total area and the % dissociation are listed. Core particle concentration was always 3.8×10^{-5} M bp.

Figure VI.3

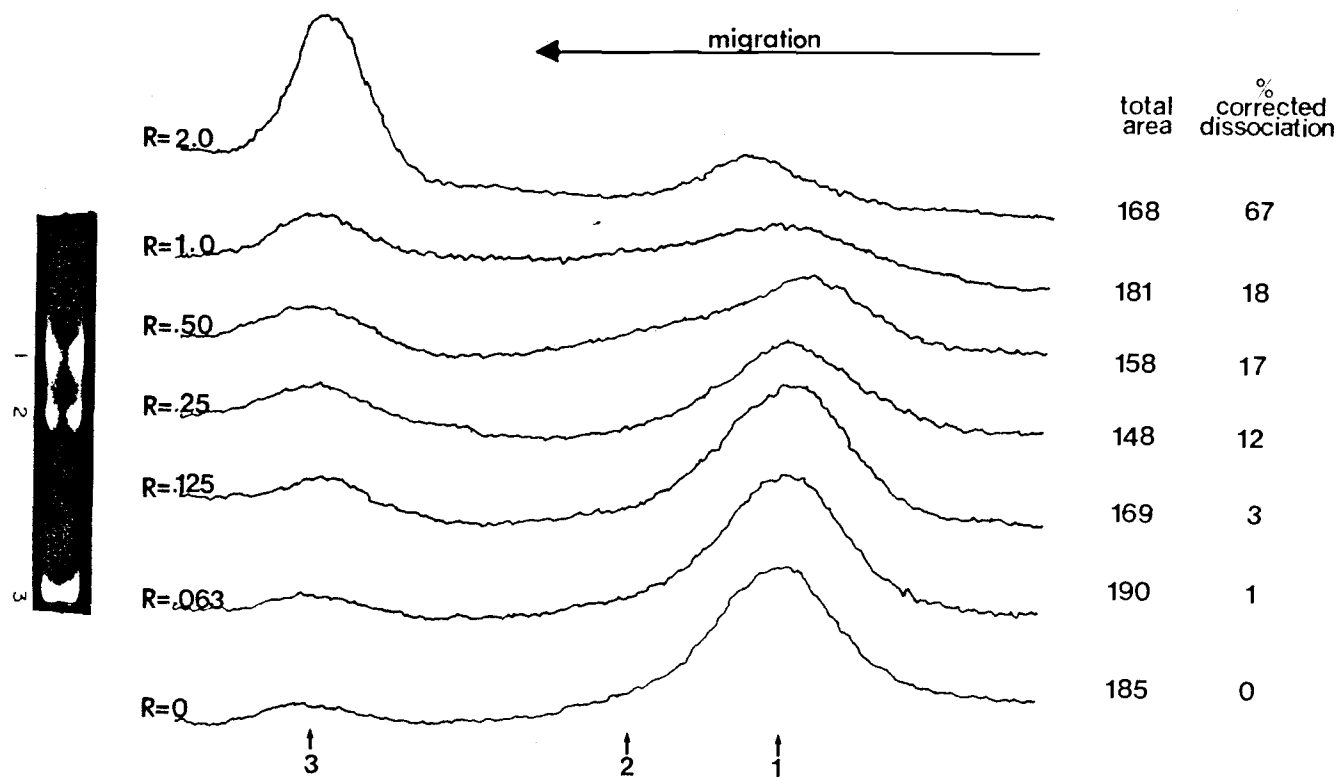


Figure VI.4. The % dissociation versus bound ratio plots for the dissociation of the chicken erythrocyte core particle as a function of temperature. (A) $T = 50^{\circ}\text{C}$, (B) $T = 37^{\circ}\text{C}$, (C) $T = 30^{\circ}\text{C}$, (D) $T = 20^{\circ}\text{C}$, (E) $T = 10^{\circ}\text{C}$. All free DNA was quantified by the gel electrophoretic method described in (McMurray and van Holde, 1986, and in Chapter 3). The core particle concentration used in all experiments was 3.8×10^{-5} M bp. The buffer used in all experiments was 10 mM Tris, pH = 8.0, 0.1 mM EDTA.

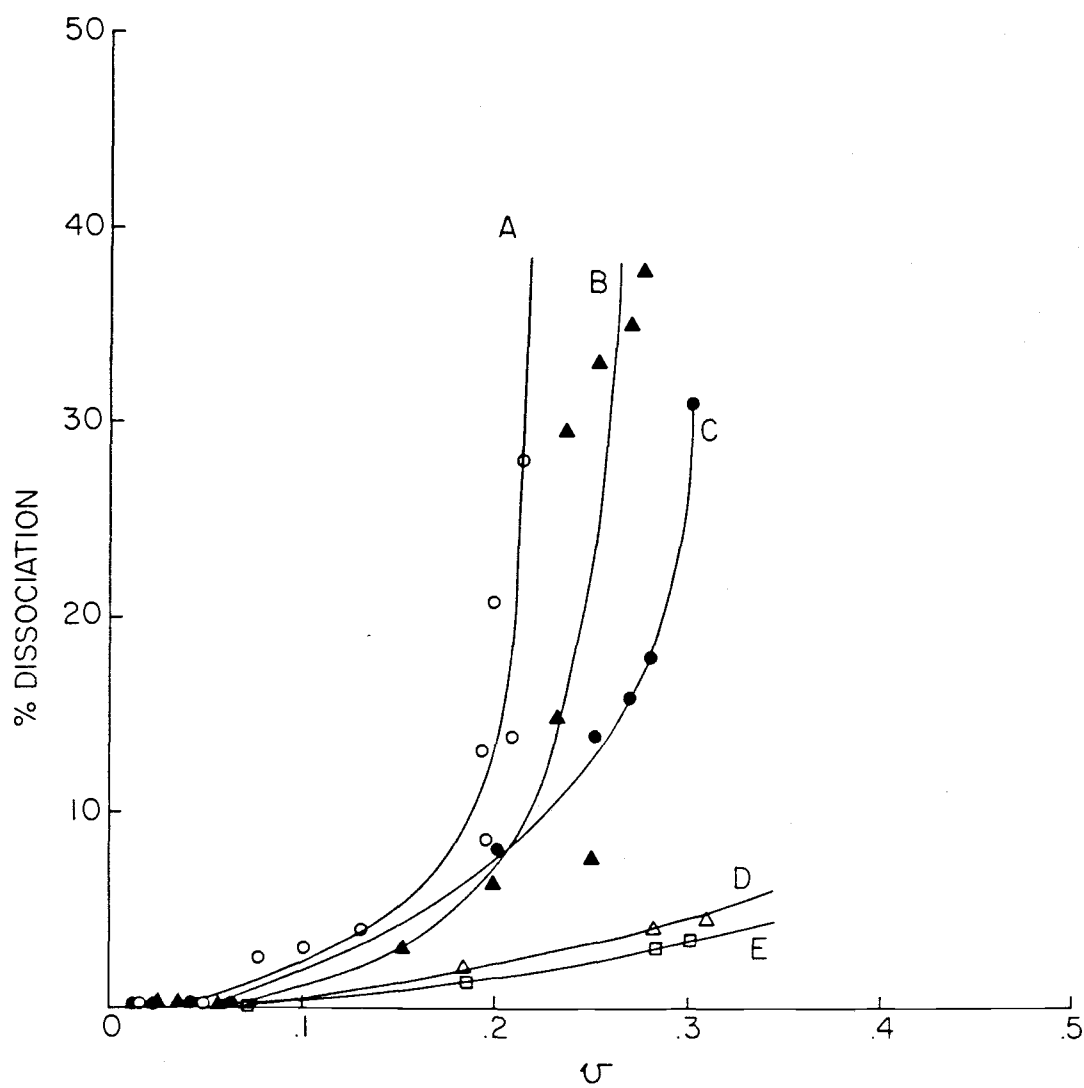


Figure VI.4

Figure VI.5. van't Hoff plot of the ethidium-induced dissociation reaction of the nucleosome core particle in 10 mM Tris, pH 8.0, 0.1 mM EDTA. The plotted values for the equilibrium constants were calculated from the dissociation curves at $R = .23$ in Figure IV.8 and listed in Table IV.6. The experimental details are described in Figure IV.8.

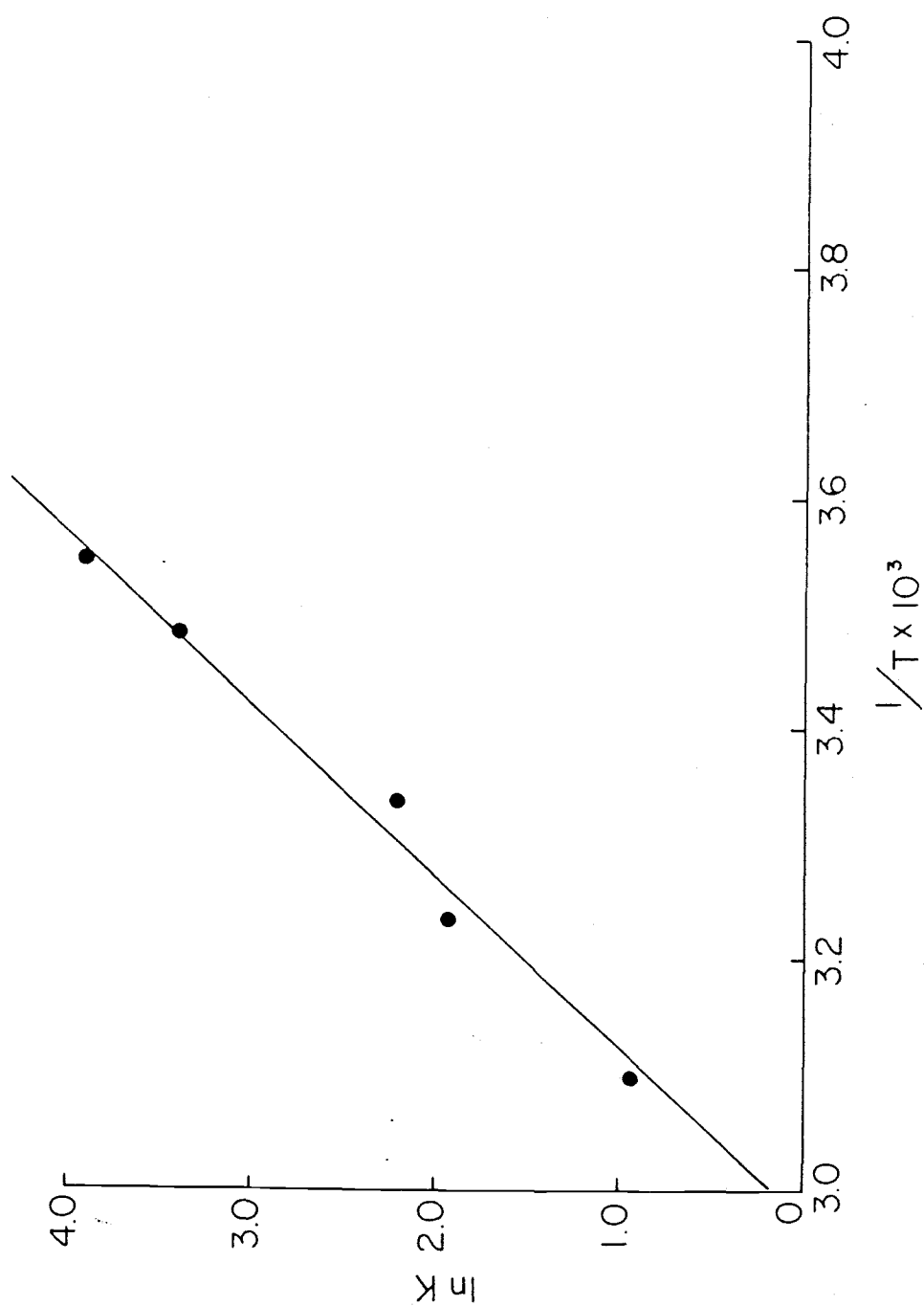


Figure VI.5

Figure VI.6. Laser densitometer trace of the ^{32}P -end-labeled-core particle/ethidium complexes, $R = .25$, at various ionic strengths. (A) $[\text{Na}^+] = .005 \text{ M}$, (B) $[\text{Na}^+] = .01 \text{ M}$, (C) $[\text{Na}^+] = .02 \text{ M}$, (D) $[\text{Na}^+] = .055 \text{ M}$, (E) $[\text{Na}^+] = .20 \text{ M}$. The R = the input ratio of ethidium = moles dye added/DNA base pair. The complexes were equilibrated for 24 hours at $T = 30^\circ\text{C}$ before separated on a 3.5% native, polyacrylamide gel with a low crosslinking ratio. The gel was dried and exposed to audioradiographic film for 20 hours before scanning.

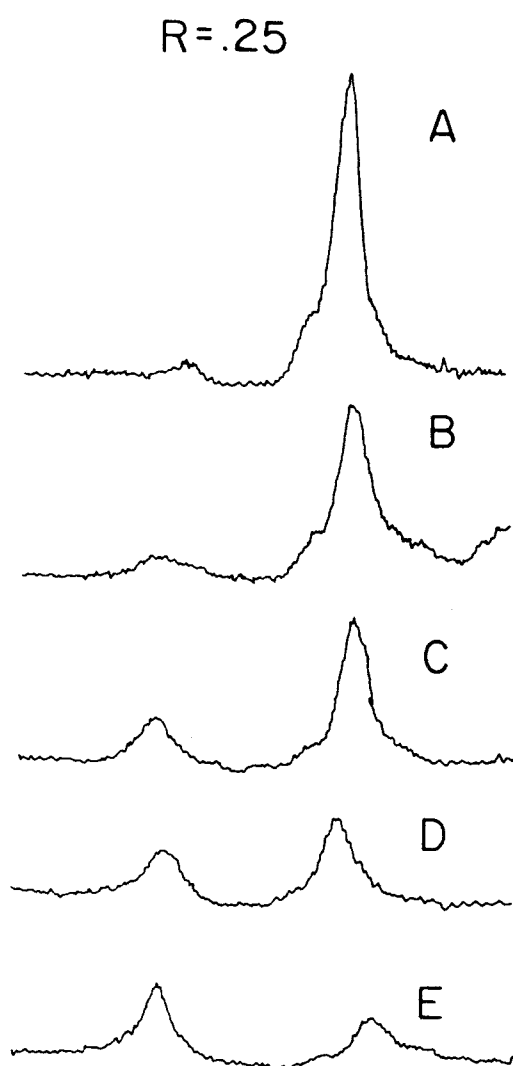


Figure VI.6

Figure VI.7. The % dissociation versus bound ratio plot for the dissociation of the chicken erythrocyte core particle as a function of ionic strength at $T = 30^{\circ}\text{C}$. (A) $[\text{Na}^+] = .2 \text{ M}$, (B) $[\text{Na}^+] = .055 \text{ M}$, (C) $[\text{Na}^+] = .02 \text{ M}$, (D) $[\text{Na}^+] = .01 \text{ M}$ and (E) $[\text{Na}^+] = .005 \text{ M}$. The free DNA was quantified by the gel electrophoretic method described in (McMurray and van Holde, 1986 and in Chapter 3). The core particle concentration used in all experiments was 10 mM Tris, $\text{pH} = 8.0$, 0.1 mM EDTA. The buffer used in all experiments was 10 mM Tris, $\text{pH} = 8.0$, 0.1 mM EDTA.

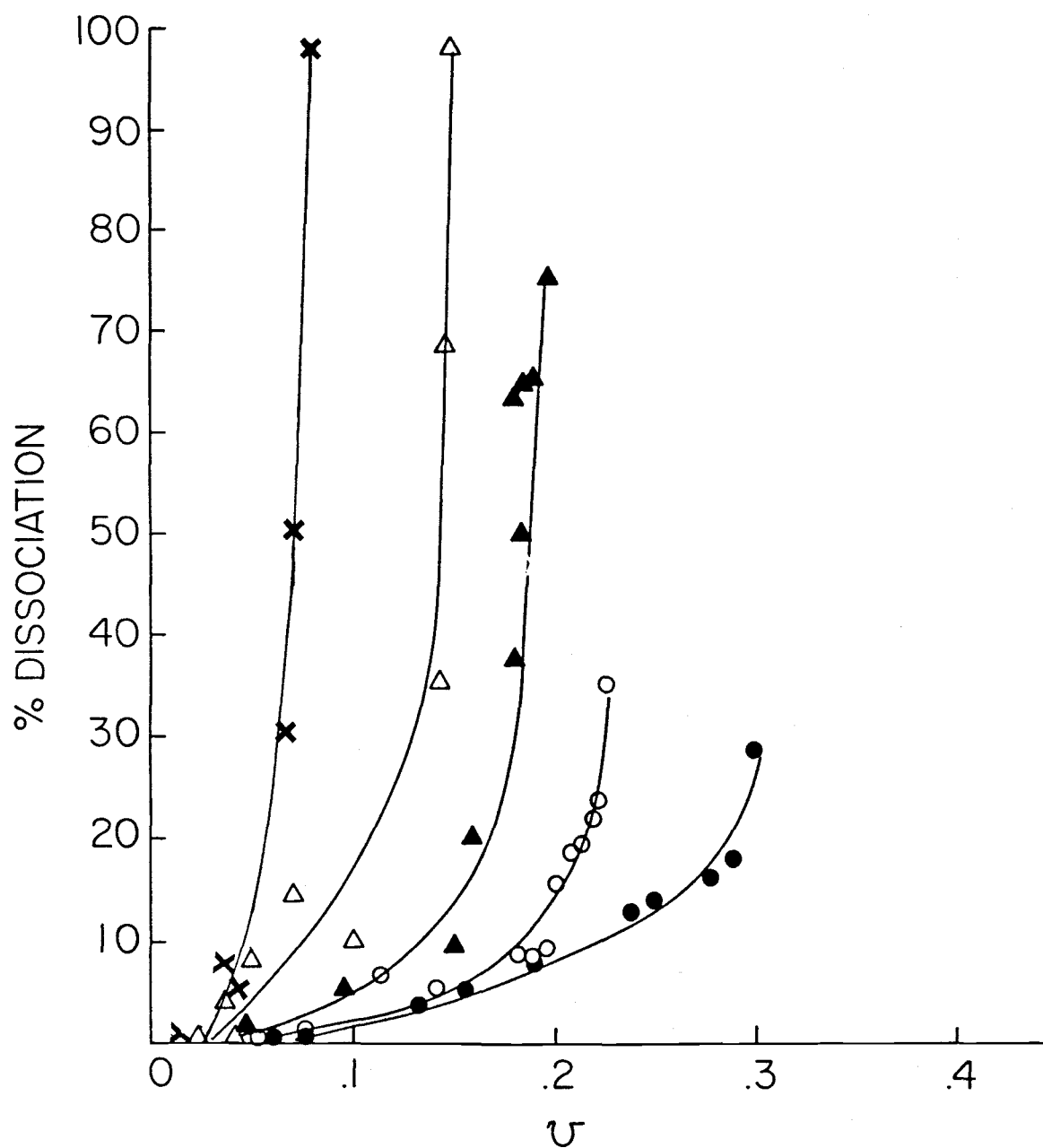


Figure VI.7

Figure VI.8. The Log K versus Log [Na⁺] plot for the dissociation of the chicken erythrocyte core particle several bound ratios. The equilibrium constants were calculated from the % dissociation curves in Figure IV.7 and listed in Table IV.7. (□) R = .10; (◆) R = .13; (■) R = .14; (○) R = .145; (⊙) R = .15. All other conditions are as stated in Figure VI.7.

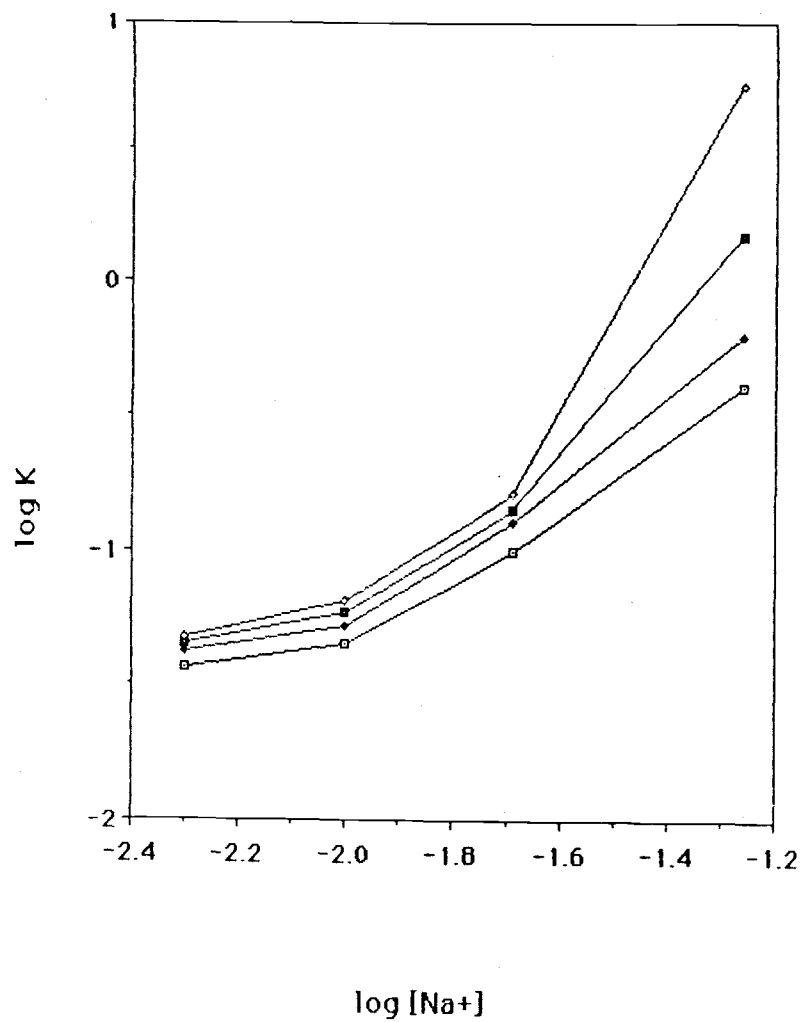
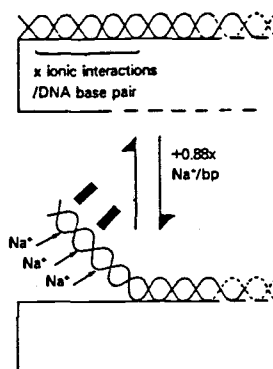


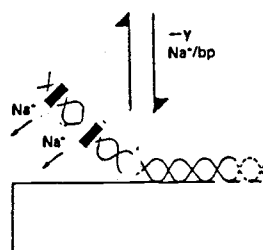
Figure VI.8

Figure VI.9. Schematic mechanism for the condensation Na^+ upon ethidium-induced dissociation. Step 1. The condensation of $m_1''\psi \text{ Na}^+$ upon the release of 38 bp of DNA from the constraints of the histones, where $m_1''\psi$ is the number of tight contacts broken in the reaction. Step 2. The release of $m_1'\psi \text{ Na}^+$ by the intercalation of ethidium into 38 bp, $m_1' = 1.2$. Step 3. The condensation of $m_2'\psi \text{ Na}^+$ due to the dissociation of the histones from the DNA.

STEP 1: The condensation of $.88x$ Na^+ due to the dissociation of 38bp of DNA from the core particle.



STEP 2: The release of $.88y$ Na^+ due to the binding of ethidium.



STEP 3: The condensation of $m'y$ Na^+ due to the dissociation of the remaining DNA from the histone octamer.

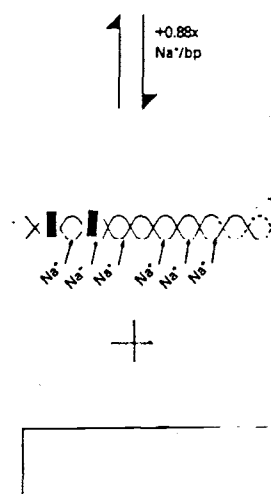


Figure VI.9

Figure VI.10. Schematic diagram for a thermodynamic cycle which describes both ethidium-induced dissociation and the formation of the core particle.

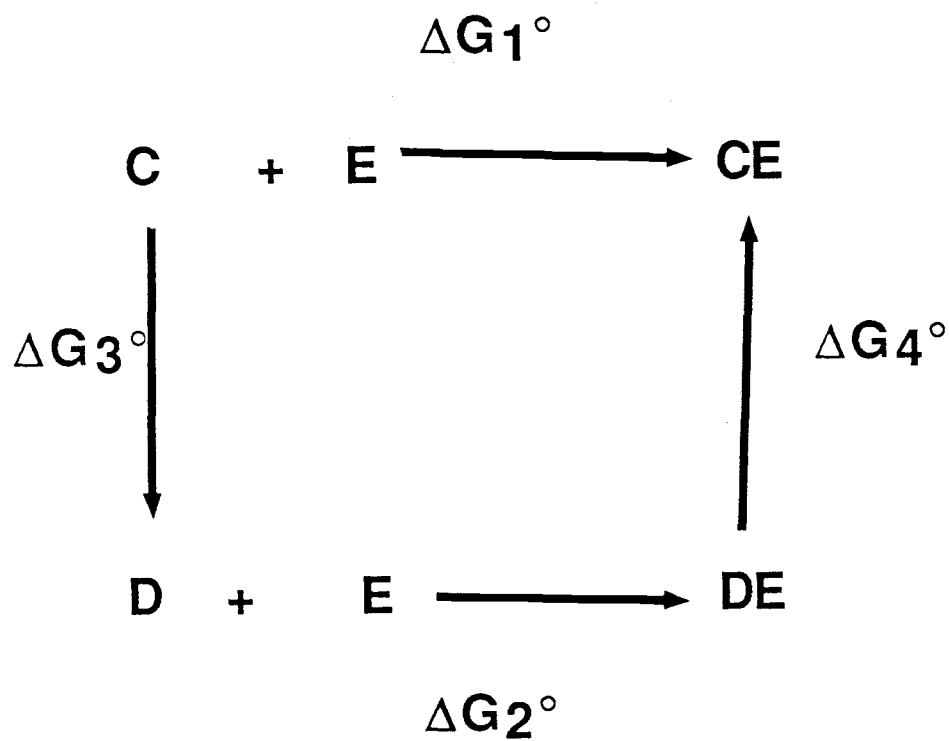


Figure VI.10

Figure VI.11. The van't Hoff plot of the DNA conformational change of the nucleosome core particle in 10 mM Tris, pH = 8.0, 0.1 m EDTA. The equilibrium constants were calculated from the integrated area of the ^1H -NMR spectra described in Table 1 in McMurray et al., 1985.

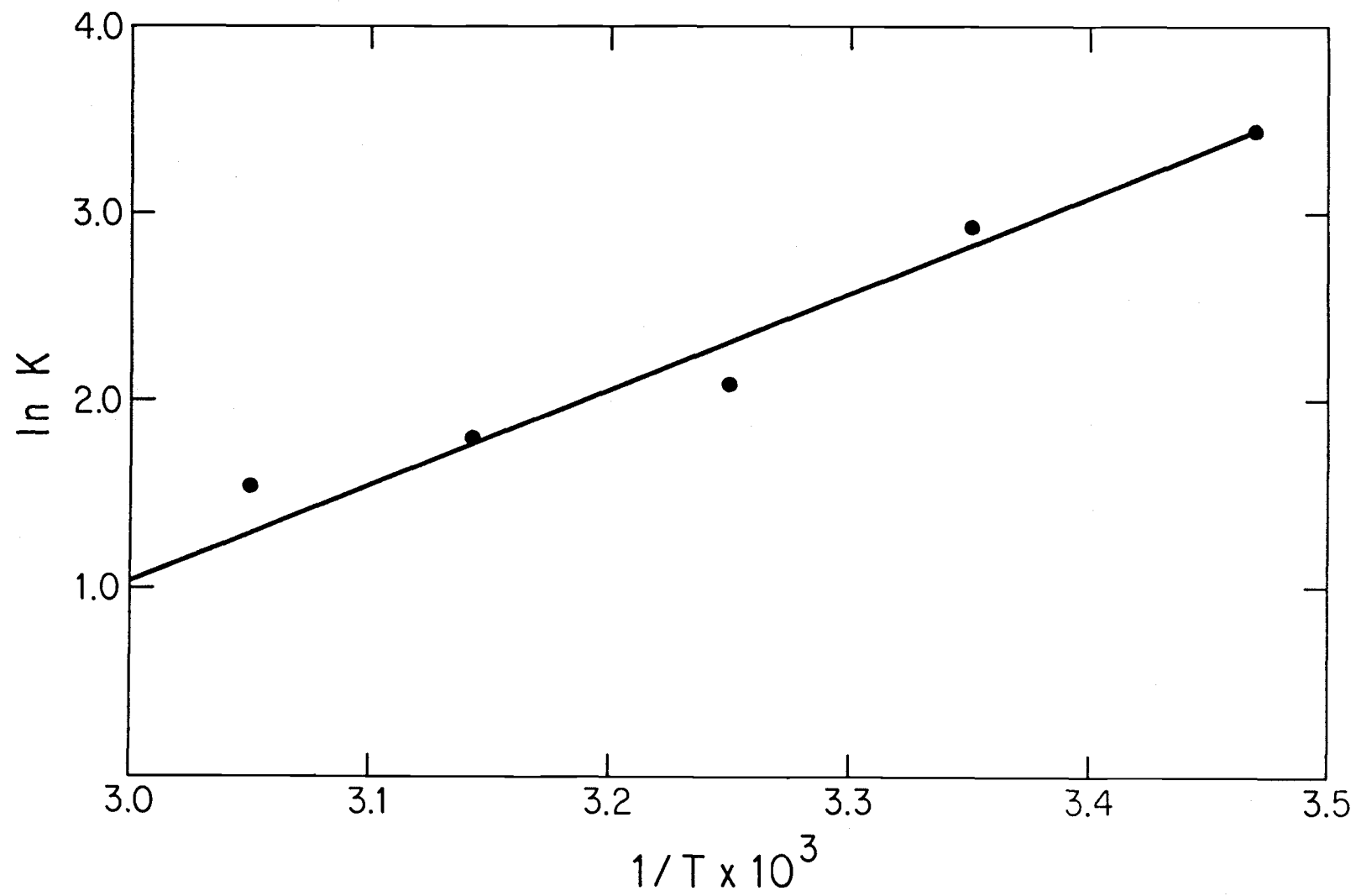


Figure VI.11

Chapter VII. HIGHER ORDER STRUCTURE AND CONCLUSION

ABSTRACT

The binding of ethidium bromide to long chromatin forms which represent the 11 nm and 30 nm fiber have been measured. In the absence of H1 and H5, the binding of the ethidium to the linker portions of the DNA occurs with an affinity similar to free DNA. The dyes tend to not be clustered, but instead seek isolated sites. In the presence of H1 and H5 in low ionic strength, conditions under which the chromatin is in the helical 11 nm fiber form, the binding of ethidium is inhibited nearly 10-fold relative to free DNA. The binding sites available to the dye are only 50 bp out of 60 bp within the linker region. Under these conditions, circular dichroism studies indicate that H1 and H5 bind 15 bp of DNA within the linker. Increasing the ionic strength for the H1 and H5 containing chromatin, and inducing the 11 nm to 30 nm transition, results in another 3-fold decrease in the ability of ethidium to bind. Thus, ethidium binding is decreased 30-fold relative to free DNA when chromatin is folded into the 30 nm fiber form. We conclude that both protein-binding and folding events inhibit the likelihood of carcinogen binding events. The results were used to construct a probability model for predicting the frequency of carcinogen binding to nucleic acids in vivo.

INTRODUCTION

The process of intercalation to DNA has been associated with a range of biologically important processes (Hajduk, S.L., 1978; Waring, 1981). First, the binding of planar aromatic compounds, such as aflatoxin B₁, has been directly shown to induce cancer in mouse liver cells (Wogan, 1986). The carcinogenic response in these cells has been shown to be the result from a mutation in the mouse c-ras protein at the aflatoxin G-specific binding site (Wogan, 1986). Since the base sequence specificity of aflatoxin is abolished if the dye cannot bind by intercalation (Misra et al., 1983; Meunch et al., 1983), the carcinogenic response has been directly linked to the intercalation mechanism. Additionally, the binding of ethidium bromide has been shown to induce frame-shift mutagenesis in *Salmonella typhimurium* (McCann et al., 1975) and petite mutants in yeast. Another class of biological responses which result from intercalation is the ability of intercalating molecules to target and kill cancer cells in preference to normal cells. Intercalating molecules, such as daunomycin and adriamycin, are currently used as effective chemotherapeutic agents in the treatment of a wide range of cancers (Wilson and Jones, 1981; Waring, 1972). Finally, intercalation and/or stacking of aromatic amino acid residues is implicated in the binding mechanism for proteins involved in transcription and replication, such as GP-5 and GP-32 in T4 phage (Shine and James, 1985; Kowlaczykowski et al., 1981; Coleman and Oakley, 1980; Coleman and Armitage, 1978) and DNA-dependent-RNA polymerase (Siebenlist, 1979; Siebelist et al., 1980). Thus, some aspect of DNA conformation which governs the

binding ability of intercalating molecules preceeds, and is common to, such diverse processes as carcinogenesis, mutagenesis, transcription and replication. We believe this aspect is at the level of DNA packaging.

Very early studies demonstrated that the intercalation mode of binding was extremely sensitive to the tertiary structure of the nucleic acid substrate. Vinograd and Bauer (1968, 1970) first showed that the ethidium bromide displays higher affinity to supercoiled regions relative to linear, B-form DNA. Removal of the supercoils in the DNA via intercalation binding was accompanied by a negative free energy change which increased the association of the dye. Terrence et al. (1985) reported that equilibrium binding of ethidium to poly d(m⁵GC) at physiological ionic strength, conditions under which the copolymer was known to be in the B-form, was non-cooperative with intermediate binding constants. When the ionic strength was increased to 4.4 M, conditions under which the copolymer flips to the left-handed Z-form conformation, the highly cooperative ethidium binding was correlated with circular dichroism data to indicate a sequential Z to B-form transition wherever the dye bound. Since the dye was found clustered in only the B-form regions, the authors concluded that ethidium bromide binding was unfavorable to Z-form DNA. Finally, Le Pecq and Paoletti (1967) demonstrated that the binding of ethidium bromide to RNA, a single-stranded nucleic acid, was greatly diminished relative to linear, duplex DNA or double stranded-RNA. Since both electrostatic and hydrophobic components comprise the total binding free energy of intercalated ethidium, denaturation of the double helix removed the hydrophobic pocket provided by the base

pairs, eliminating the free energy due to the hydrophobic interaction.

Thus, the binding of intercalating molecules is quite sensitive to the structure of DNA, and the differential binding affinity of intercalating ligands to the different conformations of DNA in vitro can be used as a starting point to predict the DNA binding site of intercalating ligands in vivo. But in eukaryotes, little, of any, free DNA actually exists in the cell. Instead the DNA is found folded into various levels of packaged structures, the most basic level being the formation of regularly repeating nucleo-protein units called nucleosomes (Richmond et al., 1984; van Holde, 1974; Olins and Olins, 1974; Noll, 1974; Hewish and Burgoyne, 1973). Each core particle unit is connected to adjacent particles by a variable length of free, linker DNA, usually 50-60 bp (Lewin, 1980). Under low ionic strength conditions, the polymerized chain of the core particles and linker DNA form the 11 nm fiber known as the "beads-on-a-string" form of chromatin. However, the bulk of chromatin in the interphase nucleus is found in association with a fifth class of histone protein, H1. In the presence of 0.2 - 0.3 mM Mg⁺⁺ or 5-70 mM monovalent cation concentration, H1 mediates the condensation of the loosely helical 11 nm fiber to the highly condensed 30 nm form (Thoma et al., 1979).

Thus, in vivo, the DNA is condensed into various levels of packaged structures, the most "simple" being a length of DNA associated with eight proteins. How, then, can we extrapolate the site preference for dye binding in simple systems to the complexities of the eukaryotic genome? Does the presence of chromatin structure and associated proteins alter the distribution of the dye? In this report, we have carefully studied the binding properties of a model

intercalator, ethidium bromide, to various forms of chromatin. We have used the measured binding constants, in combination with certain assumptions concerning the activity state of the interphase nucleus, to construct a simple model which predicts the distribution of intercalators within the interphase nucleus. The results of the model are discussed with respect to biological function.

RESULTS

I. The Number of Base Pairs Protected by H1 and H5.

Long whole chromatin (LC+H1,5) was prepared by nuclease digestion of chicken erythrocyte nucleic, followed by column fractionation to isolate purified chromatin of 20-30 nucleosomes in length. The chromatin was further purified by the extraction of H1 and H5 proteins by CM-Sephadex anion exchange to yield long chromatin stripped of all but the four histone proteins (LC-H1,5). Analysis of the protein component for both chromatin forms is shown in Figure VII.1. The protein component for LC+H1,5 (lane 1) shows the presence of H2A, H2B, H3 and H4 in equal molar quantities, and the presence of H1 and H5 with only minor contamination (< 1%) with non-histone proteins. The protein component chromatin of LC-H1,5 displays only the four histone proteins in equal molar ratio with no trace of H1, H5 or other non-histone contamination.

To characterize the role of H1 and H5 in the packaging step, we attempted to determine using circular dichroism how many base pairs were protected or bound by these proteins in forming the 30 nm fiber. The circular dichroism spectra of the long chromatin forms, the core particle and the dimer are shown in Figure VII.2. Cowman and Fasman (1977) have shown that the difference spectrum between free DNA and the core particle has a maximum at 272 nm. Therefore, the molar ellipticity at this wavelength is inversely related to the amount of free DNA present in the chromatin form. Assuming that the ellipticity was a linear combination of the free DNA and core particle content,

$$[O_{270}]_{\text{Total}} = [O_{270}]_{\text{core}} + [O_{270}]_{\text{DNA}} \text{ and} \quad (7.1)$$

$$[O_{270}]_{\text{total}} - [O_{270}]_{\text{core}} = [O_{270}]_{\text{DNA}} \quad (7.2)$$

we plotted the difference between the ellipticity of the sample and the core particle at 270 nm versus the % free DNA content of the sample. Ellipticity values and % free DNA used in the plot are listed in Table VII.1. Since LC+H1,5 was the "unknown", we interpolated the measured ellipticity difference from the standard curve to the % free DNA in the H1, H5 containing chromatin. The results of the plot are shown in Figure VII.3. All chromatin forms displayed a linear relationship between the % free DNA and the measured molar ellipticities. Interpolation of the ellipticity for H1, H5 containing chromatin indicated that 22% of the DNA in the 30 nm chromatin fiber has the ellipticity of free-DNA. Since the repeat of the core particle plus the linker is 210 bp, the 22% corresponds to 46 bp of DNA. Since the linker length in chicken chromatin is 64 bp, the results indicated that 18 bp of DNA in the linker was bound by histones H1 and H5 in the low salt form of form of the 30 nm fiber.

II. Binding Studies

The absorbance spectrum for ethidium bromide fully bound to both free DNA in 10 mM Tris, pH = 8.0, 0.1 mM EDTA (TE) resulted in a reduced extinction coefficient $2300 \text{ M}^{-1}\text{cm}^{-1}$. The measured extinction coefficients for the free and fully bound dye were used to generate Scatchard plots (Scatchard, 1949) for the binding of ethidium bromide

to the long chromatin, complexed with H1 and H5 in the 30 nm fiber and long chromatin stripped of these proteins in the 11 nm fiber form. The results for the binding of ethidium bromide to the chicken erythrocyte 11 nm fiber long chromatin at 30°C in TE are shown in Figure VII.4. The closed circles represents the observed binding constants generated from a spectrophotometric titration. Assuming that the extinction coefficient in the presence of nucleic acid, E_{app} , was a linear function of the bound dye, the absorbance for the complex was measured at 480 nm (where the maximum change occurred) and the extinction coefficients for the free ($5750 \text{ M}^{-1}\text{cm}^{-1}$) and the bound ($2300 \text{ M}^{-1}\text{cm}^{-1}$) forms of the dye were used to convert the absorbance measurements to Scatchard plots. In this case, the fraction of bound dye is calculated by

$$F_{bound} = E_{free} - E_{app} / E_{free} - E_{bound} \quad (7.3)$$

The concentration of bound and free dye, as well as the ratio of bound dye were calculated by

$$C_{bound} = F_{bound} \times C_{total} \quad (7.4)$$

$$C_{free} = C_{total} - C_{bound} \quad \text{and} \quad (7.5)$$

$$V_{bound} = C_{bound} / [\text{DNA}] \quad (7.6)$$

The data from Figure VII.4 were fitted to theoretical expressions for the McGhee and von Hippel (1974) conditional probability model of

excluded site binding. The intrinsic binding constant K , was determined from the apparent (observed) binding constant, v/C , using

$$v/C = K (1 - nv) \times \frac{(2w - 1)(1 - nv) + (v - R)}{2(w - 1)(1 - nv)}^{n-1} \frac{1 - (n + 1)v + R}{2(1 - nv)}^2 \quad (7.7)$$

$$R = [(1 - (n + 1)v)^2 + 4wv(1 - nv)]^{1/2}$$

where v is the moles of dye bound per polymer base pair, C is the free dye concentration, n is the number of base pairs excluded per dye molecule upon binding and w is the cooperativity parameter, which represents the equilibrium constant for the transfer of a dye molecule from an isolated site to a singly contiguous site. The values for K , n and w were calculated from Eq. 7.7 from a non-linear least squares fitting program by minimizing the sum of the root mean square for all experimental points. The results of the best fit to the points are listed in Table VII.2. The values for free DNA and the core particle under similar conditions are also listed in Table VII.2 for comparison. The best fit to the LC-H1,5 curve indicated that LC-H1,5 chromatin exhibited a binding constant of $9.3 \times 10^{-5} \text{ M}^{-1}$, quite close to that found for free DNA. Ethidium molecules tended to seek isolated sites as evidenced by the low w value of .3. The number of sites excluded by the dye, $n = 3.1$, was intermediate between the value found for free DNA and the value found for the core particle (see Table VII.2).

The binding isotherm of ethidium to LC+H1,5 at low ionic strength

is shown in Figure VII.5A. Unlike the LC-H1,5 curve, the LC+H1,5 curve in low ionic strength indicated the presence of two distinct classes of binding sites which differed in binding affinity. In order to determine the best fit, we divided the curve into two regions where region A was designated as the set of points below a bound ratio (v) of 0.1, and region B points were designated as a set of points after $v = .1$. For region A points, the best fit to the binding data indicated that ethidium bound to a portion of the DNA within the H1,5 containing chromatin with an affinity of $1.43 \times 10^5 \text{ M}^{-1}$. The binding affinity to this region was significantly lower than the affinity of ethidium for either LC-H1 or for free DNA. However, if Region A corresponds the dye binding to only a limited region of the linker DNA in the polynucleosome repeat, the binding affinity will be higher than we measure. We concluded that the presence of H1 inhibited the binding of the dye. The tendency of the dye to seek an isolated site remained unchanged relative to the LC-H1 or for free DNA. We concluded that the presence of H1 inhibited the binding of the dye. The tendency of the dye to seek an isolated site remained unchanged relative to the LC-H1,5 chromatin form or free DNA. Finally, the K_A value corresponds to the binding of ethidium to roughly 20% of the DNA in the polynucleosome structure. In region B, the binding of ethidium shows less affinity than for region A points. The binding curve is characterized by a $K_B = 1.15 \times 10^5 \text{ M}^{-1}$, an $w = .7$ and a $n = 2.6$. The results indicate that the rest of the DNA binds ethidium with lower affinity and with less preference for isolated binding sites than observed for the Region A points.

We attempted to compact the long chromatin into the solenoidal

form or 30 nm fiber by the addition of NaCl to 0.08 M. These results are shown in Figure VII.5B. The chromatin tended to aggregate upon addition of salt, but this aggregation was removed by centrifugation. We bound ethidium to the remaining unaggregated chromatin, but, again, aggregation prevented the completion of the binding curve. The analysis of the first points in this titration indicated that the binding constant was lowered 30-fold to $3.1 \times 10^4 \text{ M}^{-1}$ relative to the 11 nm extended, H1-containing chromatin. We did not attempt analysis of n or w .

DISCUSSION

The binding curves for free DNA, LC-H1,5, LC+H1,5 and the core particle are plotted on the same scale for comparison in Figure VII.6. From comparing the ethidium binding curves for all four nucleic acid forms, one notices immediately that the binding constant is directly related to the amount of free DNA present in each. If the % of free DNA decreases, the binding constant decreases. Thus, the first conclusion we can draw is that the presence of protein does not enhance, but most definitely, inhibits the binding of intercalating dyes. The core particle may be thought to have no free DNA and consequently, the binding affinity is very low until it can undergo the conformational transition of dissociation. Adding a portion of free linker DNA in the LC-H1,5 form, results in a nearly 50-fold increase in the observed binding constant. Footprinting of the ethidium binding sites (Cartwright et al., 1983), monitored by the binding of an ethidium derivative, MPE, has directly shown that the binding of ethidium occurs within the linker DNA and that binding is not favored within the folded nucleosome structures. Similarly, adding H1 and H5, decreased the affinity of ethidium for long chromatin. The n value for the LC+H1,5 Region A points indicates that only 20% of the DNA within the LC-H1,5 form binds ethidium with high affinity. Thus, the binding data predicts that 41 bp of DNA are involved with the high affinity binding of ethidium, while the remaining base pairs are somewhat inhibited from binding the dye. Our circular dichroism analysis also indicated that the number of bp of free DNA within the H1, H5 containing chromatin was 45. Thus, both

measurements suggest that 15 bp of DNA are excluded by the association of H1 and H5 in the low ionic strength, 11 nm fiber.

The second conclusion which can be gained from the analysis is that, in addition to the presence of protein, the folding of chromatin into the 30 nm fiber also has a dramatic impact on the ability of intercalating dyes to bind. Thus, our results suggest that supercoiling of the chromatin fibers into higher order structures does not enhance, but inhibit by 30-fold the ability for intercalation binding. Since superhelical stress would tend to enhance intercalation binding, we conclude that one of two cases must be true. Either supercoiling of the chromatin in solution is not accompanied by superhelical stress or the combined effect of folding and binding of cations is energetically more favorable than the alleviation of superhelical stress which might accompany ethidium binding. The results of the binding analysis has been used to predict the probability of dye binding in vivo.

CONCLUSION

Ethidium molecules, when introduced into the nucleus, have the potential to bind to DNA folded into one or several forms of chromatin. The binding of ethidium to any packaged form of chromatin within a single phase, j , of the cell cycle can be described by a series of individual binding reactions expressed as



where N_i represents any i form of nucleic acid, E represents free ethidium bromide and N_iE represents the complex of ethidium to the i^{th} form of nucleic acid. Consequently, the equilibrium constant for such an interaction can be expressed by

$$K_{ij} = \frac{[N_iE]_j}{[N] [E]} \quad (7.9)$$

If we know the equilibrium constant of an individual binding reaction, then the concentration of any complex can be expressed by

$$[N_iE] = K_{ij} [N] [E] \quad (7.10)$$

Since the probability of forming a particular type of nucleic acid/ethidium complex within a particular cell-cycle is, by definition, the mole fraction of the complex, the probability (p) is defined by

$$p = \frac{K_{ij}[N_i][E]}{\sum_i K_{ij}[N_i][E]} \quad (7.11)$$

We can further simplify the expression by noting that

$$N_i = f_{ij} N_T \quad (7.12)$$

where f is the fraction of total nucleic acid found in the i^{th} state and N_T is the total concentration of nucleic acid. Therefore Eq. 7.5 reduces to

$$p = \frac{K_{ij}f_{ij}[N_T]}{\sum_i K_{ij}f_{ij}[N_T]} \quad (7.13)$$

or

$$p = \frac{K_{ij}f_{ij}}{\sum_i K_{ij}f_{ij}} \quad (7.14)$$

The expression is complete if we sum over the entire cell cycle.

Thus, the complete expression for the distribution of dye binding over j cycle phases is

$$p = \frac{\sum_j K_{ij}f_{ij}}{\sum_j \sum_i K_{ij}f_{ij}} \quad (7.15)$$

To account for cooperative binding, we can insert for K_i the expression for v/C in the McGhee and von Hippel (1974) conditional

probability model in Equation 7.7. Thus, the expression for the probability for dye binding to multiple components can be completely expressed by

$$P_i = \sum_j f_i K_i (1 - n_i v) X \quad (7.16)$$

$$\frac{(2w_i - 1)(1 - n_i v) + (v - R_i)^{n-1}}{2(w - 1)(1 - n_i v)} \frac{1 - (n_i + 1)v + R_i^2}{2(1 - n_i v)}$$

$$\sum_j \sum_i f_i K_i (1 - n_i v) X$$

$$\frac{(2w_i - 1)(1 - n_i v) + (v - R_i)^{n-1}}{2(w_i - 1)(1 - n_i v)} \frac{1 - (n_i + 1)v + R_i^2}{2(1 - n_i v)}$$

$$R = [(1 - (n_i + 1)v)^2 + 4w_i v(1 - n_i v)]^{1/2}$$

The limit of Eq. 7.16 as $v \rightarrow 0$ is simply Eq. 7.15. Thus, the prediction of the binding distribution is independent of the total DNA concentration and only depends on knowledge of the binding constant of a particular nucleic acid configuration, an estimate of the fraction of DNA which is in the particular configuration during a particular phase of the cell cycle and the cell cycle during the binding event. The binding constants, calculated from the conditional probability model of McGhee and von Hippel and summarized in Table VII.2, were used to construct the probability of finding an ethidium within a particular type of chromatin structure for two different biological models. The results of the calculations for both models are presented

in Table VII.3. Model I assumes that a low level of dye is allowed to bind only during G1 phase. During G1 phase, we assume that 90% of the DNA is in the inactive configuration and 10% of the genes are in the active configuration (Lewin, 1980, 1983; Reeves, 1984). Additionally, we assume that nucleosome structure is maintained during transcription. Inserting $f = .9$ and $f = .1$ for the inactive and active forms of chromatin and the binding constants from Table VII.3, we predict that 83% of the total dye will be bound to the 30 nm fiber form, that 15.5% of the dye will be found within the linker DNA in the 11 nm fiber and that only 1.5% of the dye will be found bound to the nucleosomal DNA within the 11 nm fiber. Thus, for Model I, a total of 17.0% of the dye will be found associated with "active" DNA. In Model II, we again assume that the cell cycle phase is G1 and that the respective fractions of inactive and active DNA are the same. However, this time we assume that nucleosome structure is not maintained in the active chromatin, and that the transcribing region is equivalent to free DNA. In this case, the probability of finding the dye in the active region is increased to 47% while the probability of finding the dye in the inactive region is decreased to 53%.

Although the actual association state of histones, at the moment of polymerase passing, may be in question, the presence of histones within active genes has been repeatedly demonstrated (Richards et al., 1977; Weintraub and Goudine, 1976; Reeves, 1984; Cartwright et al., 1982). Thus, Model I appears to most closely describe the in vivo state of the nucleus. If our simple model is correct, the calculations reveal that the large majority of the dye is distributed in the inactive regions of the genome, despite their 100-fold lower

binding constants. Assuming that 100 molecules of ethidium are introduced in the nucleus of a cell, 83 molecules will bind to the inactive chromatin form in the 30 nm fiber form, 16 molecules will bind within the linker portion of active chromatin and 1-2 will cluster in the nucleosomal portion of active chromatin. While more dye binds in the inactive regions, the frequency of hitting "active" chromatin versus inactive is ~2:1, schematically represented in Figure VII.7. Assuming that there are a total of eukaryotic 100,000 genes (Lewin, 1983), the frequency of hitting a particular active genes is $2/10,000$, i.e., 2.0×10^{-4} , while the frequency of hitting a particular inactive gene is 1.1×10^{-5} . Thus, based on the simple model presented here, we calculate that the chance of hitting a particular active gene is 20 times more likely event relative to hitting a particular inactive gene. The probability results for Model I are tabulated and correlated with the biological function in Figure VII.8. Thus, carcinogens and mutagens can produce their effects in one of two ways. First, the molecules have an enhanced frequency of binding to an active gene versus an inactive one. Thus, the straightforward effect of dye binding in such regions would be to increase the chance of a mutation by causing misreading events at the dye binding site which escape the eukaryotic repair mechanisms. Since the active genes are required by the cell at any particular time in development to maintain normal metabolism, mutations in these genes can have large and immediate effects. The other way in which mutagens and carcinogens can induce their effects is by causing structural perturbations in the 30 nm fiber, which might result in the premature or incorrect 30 nm to 11 nm transition. Since opening of the 30 nm

fiber has been postulated to be a signal for the gene transcriptional competency (Labhart and Koller, 1982; Andersson et al., 1982; Kimura et al., 1983), the binding of intercalating carcinogens might mimic the signal for a domain-opening event.

It is also reasonable to assume that Model I binding can be used to predict the behavior of carcinogen binding in G2. Since the model is independent of the amount of nucleic acid, multiple copies of replicated DNA should have no effect on the results. The model could also be used to predict the distribution of dye in S phase, as long as the replicated DNA did not change f to a large extent. The model does not include, at present, the effects of particular structural features, such as the eukaryotic replication fork or the transcription complex formation. Not enough information is available to include these features into a simple model. However, if such structures are particularly sensitive to intercalation binding and the dye distribution is altered, any such feature can easily be incorporated into the probability expression.

Table VII.1

Empirical Relationship Between % Free DNA and Molar
Ellipticity Values at 272 nm for Core Particles,
Dimers, Long Chromatin -H and Long Chromatin +H₁

Sample ^a	[θ] ^b 272 nm	Difference Value for [θ] at 272 nm	Calc. % DNA
CORE	250	0	0
Dimer	2028	1778	17
L.C.-H ₁	3611	3361	27
L.C.+H ₁	2480	2230	x
DNA	8450	8200	100

a. The buffer used for all experiments was 10 mM Tris, pH 8.0, 0.1 mM EDTA. The DNA concentration was 7.0×10^{-5} M bp. The ellipticity was measured in a 1 cm cylindrical quartz cell at 270 nm using a 700 M slit width.

b. The molar ellipticity value measured at 272 nm. $[\theta]_{272} = \frac{\Delta E}{Cl} \times 100$.

Table VII.2

The Results of the Best Fit for K, n and w for the Binding of Ethidium Bromide to the Nucleosome Core Particle, Free DNA, Long Chromatin +H₁ and Long Chromatin-H1 at 30°C

Sample ^a	Region ^b	K ^c	n ^d	w ^e
DNA ^f	-	1.1×10^6	2.6	.3
LC-H1 ^g (11 nm form)	-	9.3×10^5	2.3 3.1	.3
LC+H1 ^h (11 nm form)	A	1.43×10^5	4.9	.3
	B	1.15×10^5	2.6	.7
LC+H1 ⁱ (30 nm form)	-	3.1×10^4	-	-
Core Particle ^j	A	2.2×10^4	7.4	143
	B	2.7×10^5	2.7	.7

- a. All nucleic acid samples were buffered with 10 mM Tris, pH 8.0, 0.1 mM EDTA. The concentration range for all experiments was 9.0×10^{-6} bp - 9.0×10^{-4} M bp. T = 30°C.
- b. Region A = points below bound ratio = 0.1; Region B = points after bound ratio = 0.1.
- c. K defined by Eq. 7.7.
- d. n = number of sites excluded by the binding of one ligand.
- e. w = equilibrium constant for the transfer of an isolated ligand to a singly bound site.
- f. DNA = $145 \pm$ nucleosome-sized DNA from chicken erythrocytes.
- g. LC-H = long chromatin stripped of all histones and non-histone proteins other than H2A, H2B, H3 and H4.
- h. LC+H = whole purified chromatin containing H1, H5.
- i. LC+H1 (30 nm form) = same as LC+H, except the ionic strength = .08 M. In this ionic strength the 11 nm - 30 nm transition has occurred.
- j. Core particle = 145 bp of DNA wrapped around the inner core histones: H2A, H2B, H3 and H4.

Table VII.3

The calculated probability of finding intercalating dyes
associated with various folded forms of chromatin
according to biological models

	K	f	p
<u>Model I^a</u>			
Solenoid (30 nm fiber)	1.4×10^5	.9	.83
Linker (11 nm fiber)	9.3×10^5	.027	.165
Core (11 nm fiber)	2.2×10^4	.073	.015
<u>Model II^b</u>			
DNA	1.1×10^6	.10	.47
Solenoid	1.4×10^5	.90	.53

- a. Model I assumes that 10% of the genes are in the active configuration, but maintain nucleosome structure
- b. Model II assumes that 10% of the genes are active but nucleosome structure is lost in the active regions, i.e., like free DNA

Figure VII.1. Results of the CM-sephadex removal of H1 and H5 and non-histone proteins from whole chicken erythrocyte chromatin.

Laemmli SDS - 15% polyacrylamide gel electrophoresis results of the CM-Sephadex treated chromatin (lane 2) and untreated chicken erythrocyte chromatin (lane 1). Polyacrylamide gels were 0.8 mm thick containing 15% polyacrylamide (acrylamide: bisacrylamide 30:.8) in the separating gel and 6% acrylamide in the stacking gel. Lane 2 contains 1.0 μ g of total protein from our preparation. Lane 1 represented 3.12 μ g of chicken erythrocyte whole chromatin.

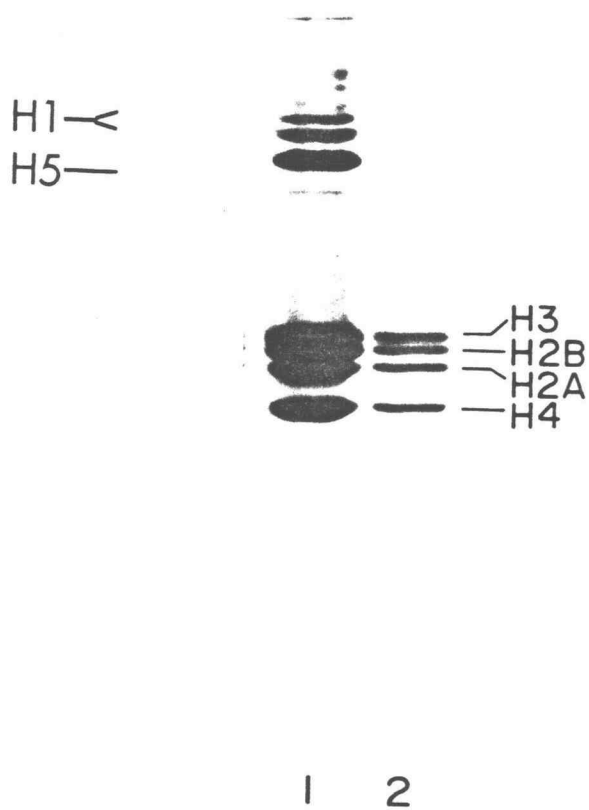


Figure VII.1

Figure VII.2. The circular dichroism spectra from 250 - 300 nm for the core particle, a nucleosome dimer, long chromatin +H1 and long chromatin -H1. The nucleic acid concentration was always 7.0×10^{-5} M bp. All experiments were performed at 23°C in 10 mM Tris, pH 8.0, 0.1 mM EDTA.

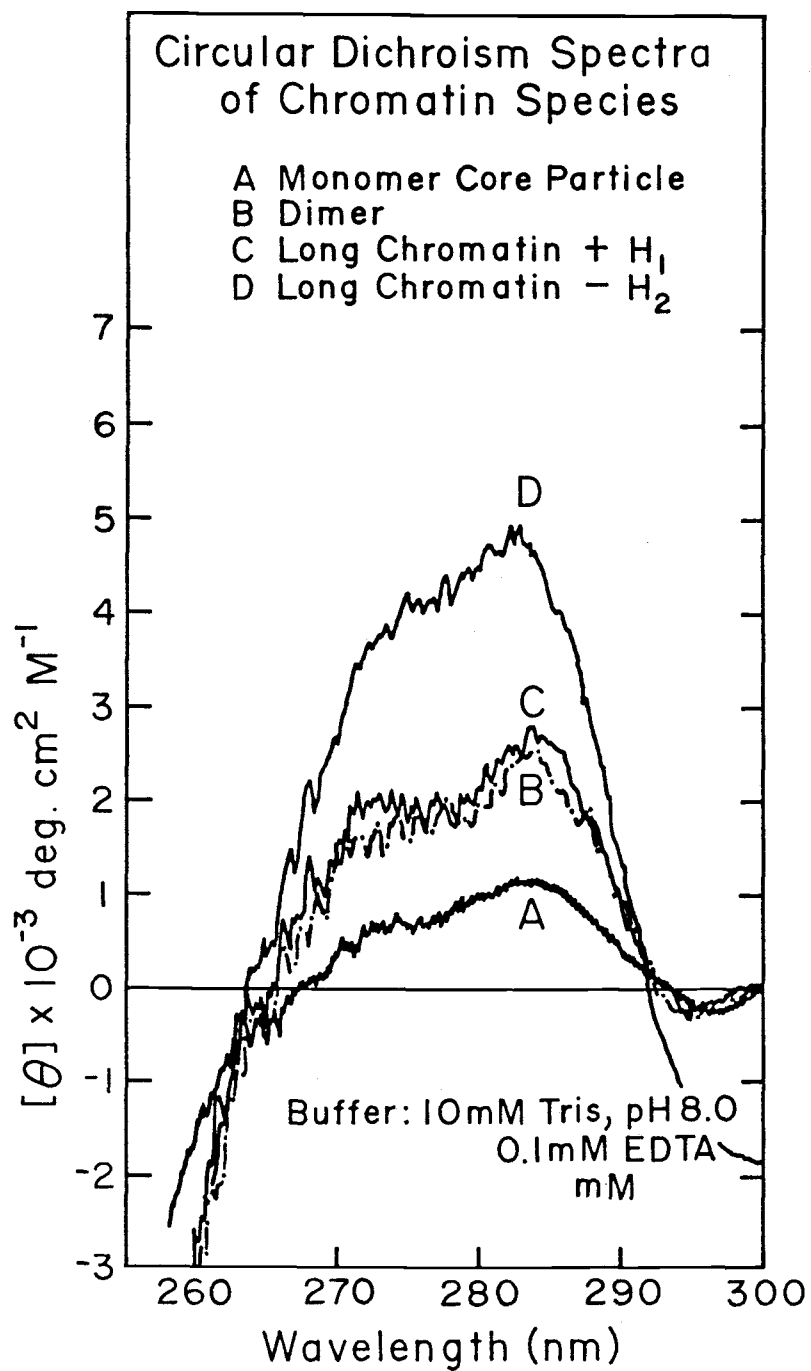


Figure VII.2

Figure VII.3. The plot of molar ellipticity versus % free DNA from the various chromatin forms. The molar ellipticity was measured at 270 nm and the values plotted were taken from Table VII.1. The dashed line indicates the ellipticity value for long chromatin +H1 extrapolated to the % free DNA contained in that chromatin form.

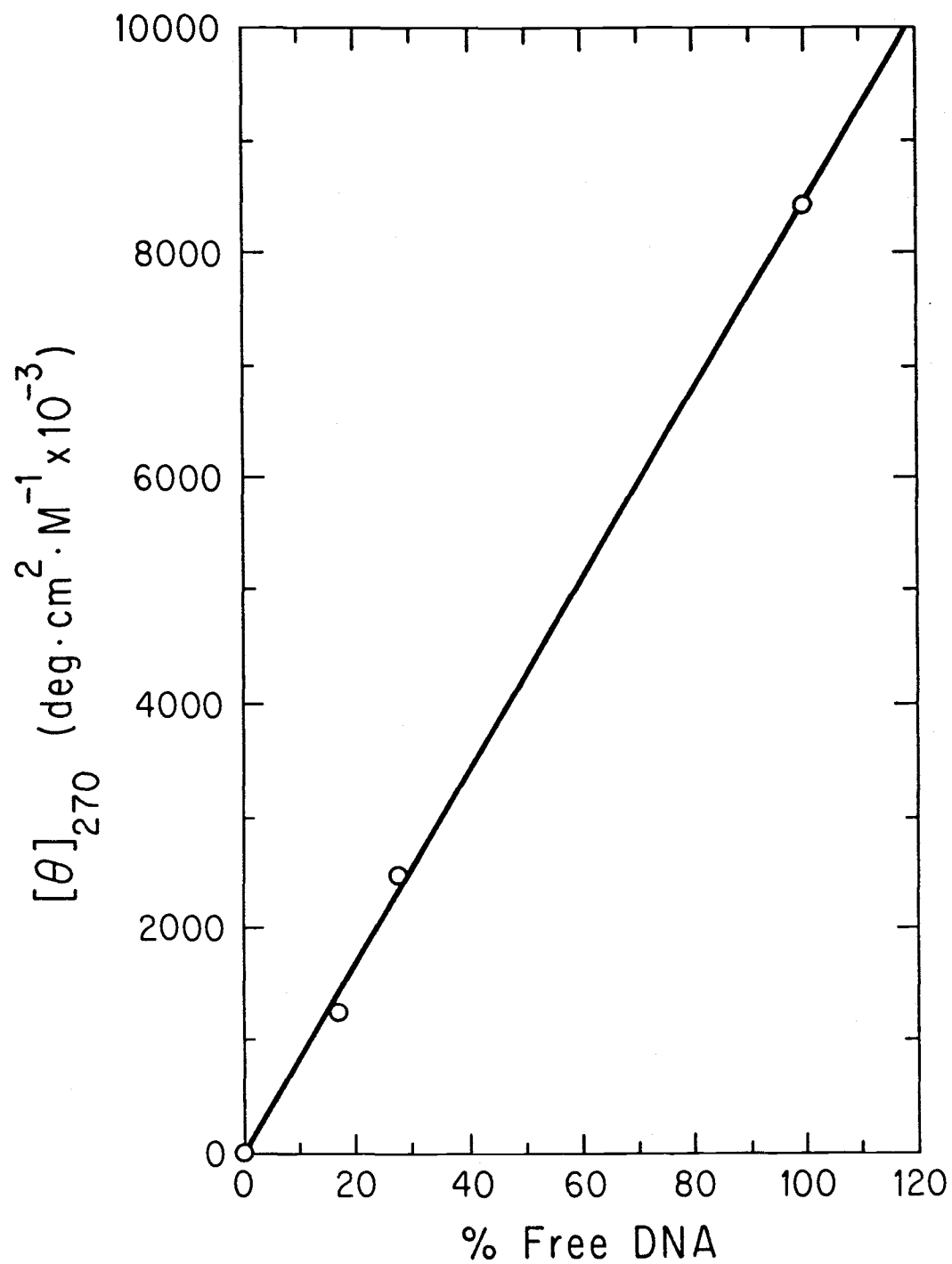


Figure VII.3

Figure VII.4. The Scatchard plot for the binding of ethidium to long chromatin -H1 generated from a spectrophotometric titration method. The v/C indicates the observed binding constants and v is the ratio of dye bound per DNA base pair. The concentration of the long chromatin ranged from $2.0 - 9.0 \times 10^{-5}$ M. The buffer used in all experiments was 10 mM Tris, pH 8.0, .1 mM EDTA. The temperature was 30°C. Absorbance was monitored at 480 nm in a 10 cm quartz cylindrical cell.

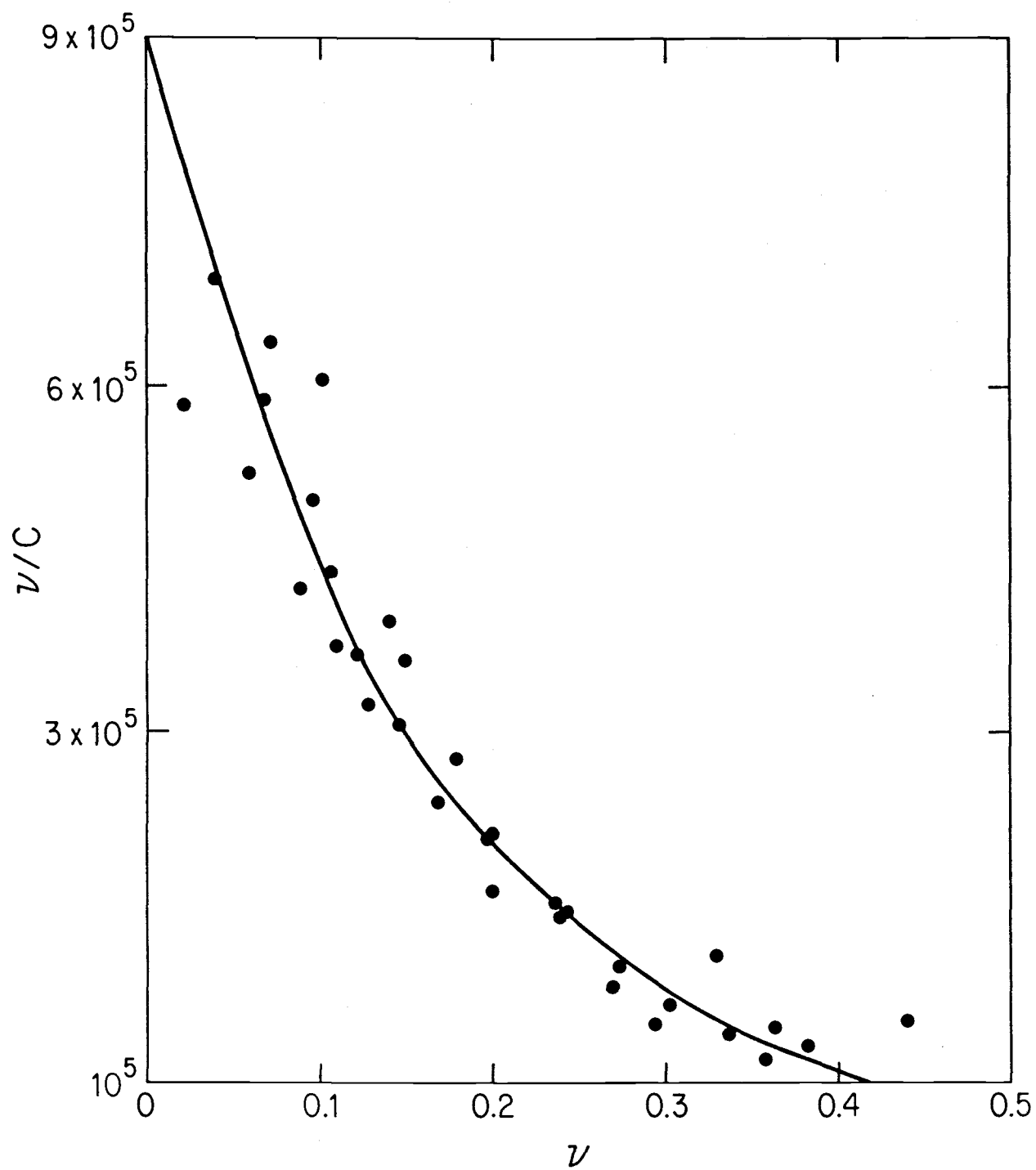


Figure VII.4

Figure VII.5. The Scatchard plot for the binding of ethidium to long chromatin +H1 (LC+H1) generated from a spectrophotometric titration method. (A) The binding curve for LC+H1 in the low salt 11 nm helical fiber. (B) The binding curve for LC+H1 in .08 M NaCl where the chromatin is folded into the 30 nm fiber form. The v/C indicates the observed binding constants and v is the ratio of dye bound per DNA base pair. The concentration of the long chromatin ranged from $2.0 - 9.0 \times 10^5$ M. The buffer used in all experiments was 10 mM Tris, pH 8.0, .1 mM EDTA. The temperature was 30°C. Absorbance was monitored at 480 nm in a 10 cm quartz cylindrical cell.

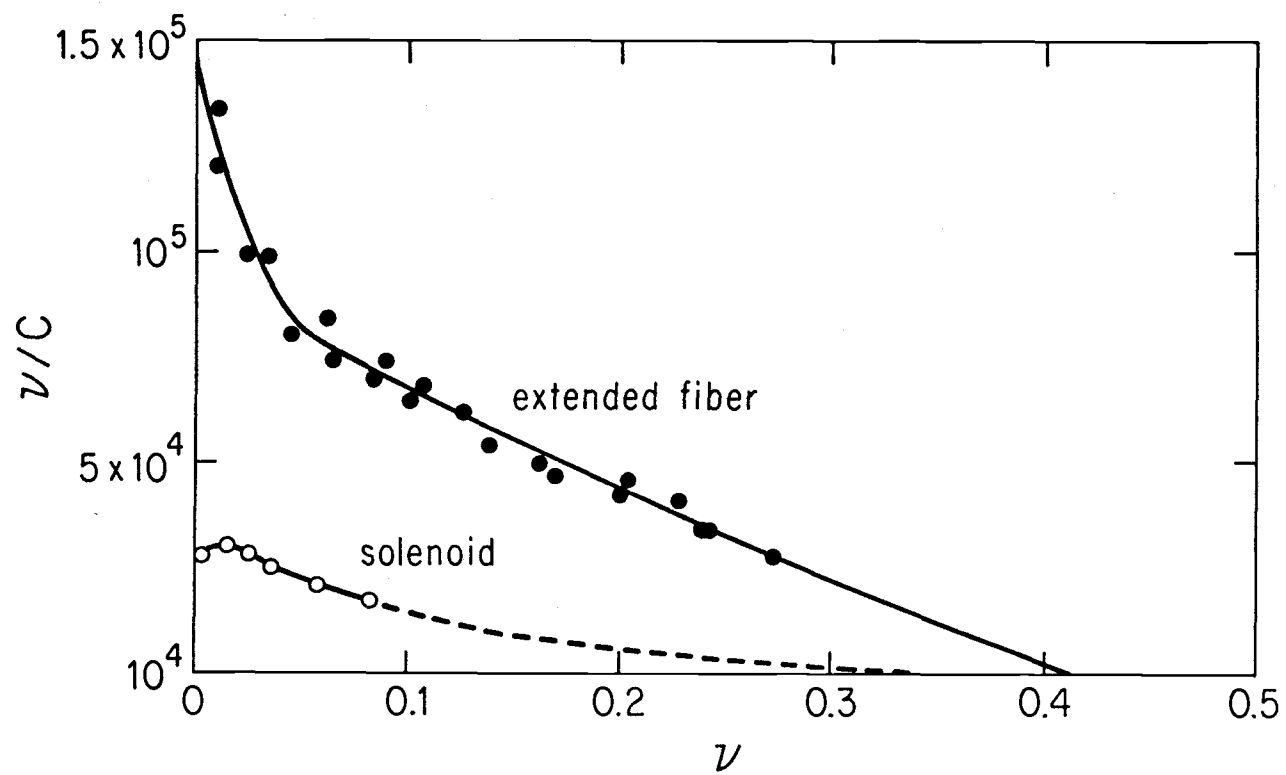


Figure VII.5

Figure VII.6. The Scatchard plot for the binding of ethidium to the chicken erythrocyte free DNA, the core particle, long chromatin +H1 (LC+H1) and long chromatin -H1 generated from a spectrophotometric titration method. (A) The binding curve for free 145 bp DNA. (C) The binding curve for the core particle. (D) The binding curve for LC+H1 in the low salt 11 nm helical fiber. (E) The binding curve for LC+H1 in .08 M NaCl where the chromatin is folded into the 30 nm fiber form. The v/C indicates the observed binding constants and v is the ratio of dye bound per DNA base pair. The concentration of the long chromatin ranged from $2.0 - 9.0 \times 10^5$ M. The buffer used in all experiments was 10 mM Tris, pH 8.0, .1 mM EDTA and the temperature was 30°C. Absorbance was monitored at 480 nm in a 10 cm quartz cylindrical cell.

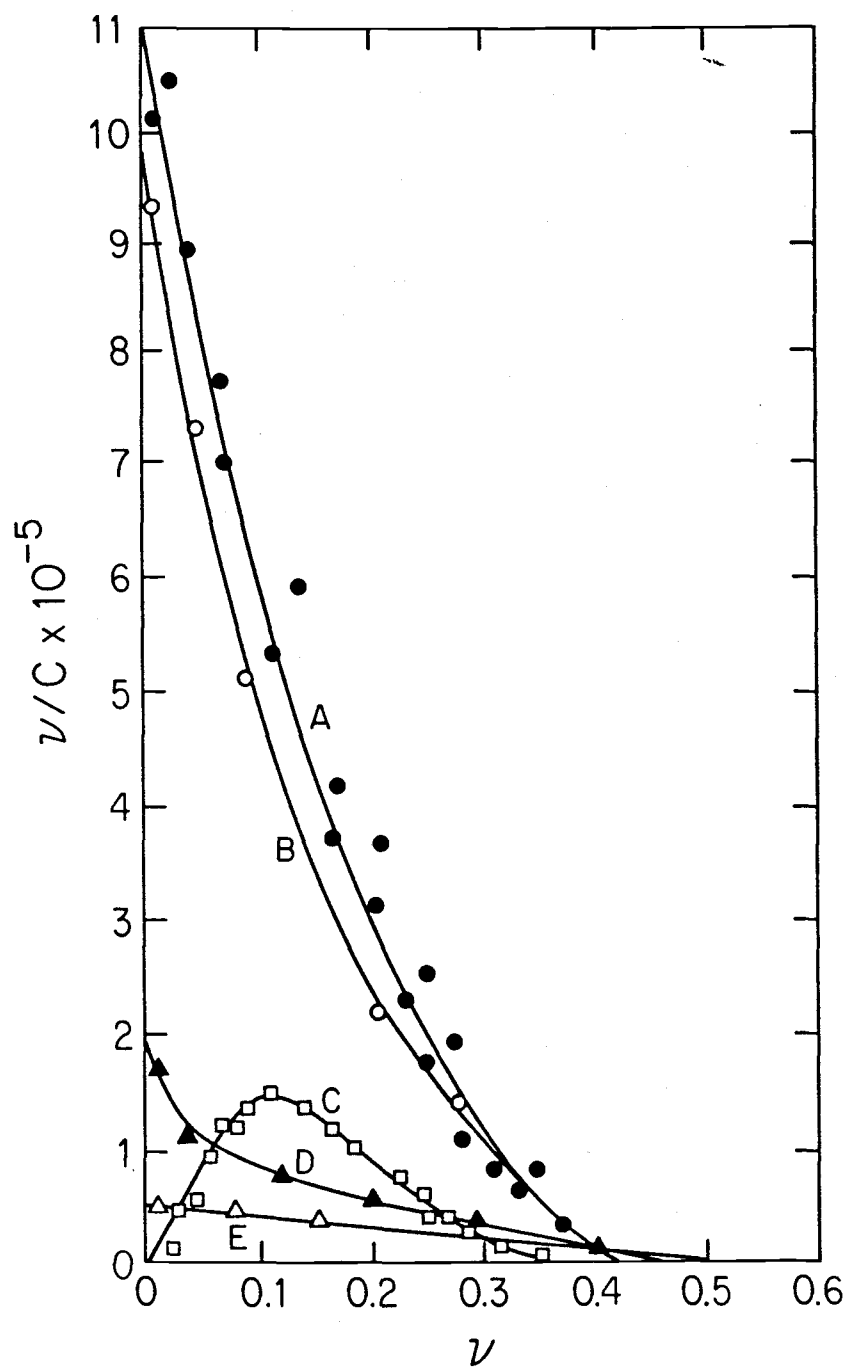


Figure VII.6

Figure VII.7. Schematic representation of the looped chromatin domains in the interphase nucleus. The loops represent the inactive 30 nm fibers attached to the nuclear membrane by some hypothetical anchorage protein. The extended "beads-on-a-string" structure is a chromatin domain which has undergone a 30 nm to 11 nm unfolding transition and is presumably in the active state. The schematic shows the predicted distribution of ten dye molecules bound according to the model described in the text.

Figure VII.7

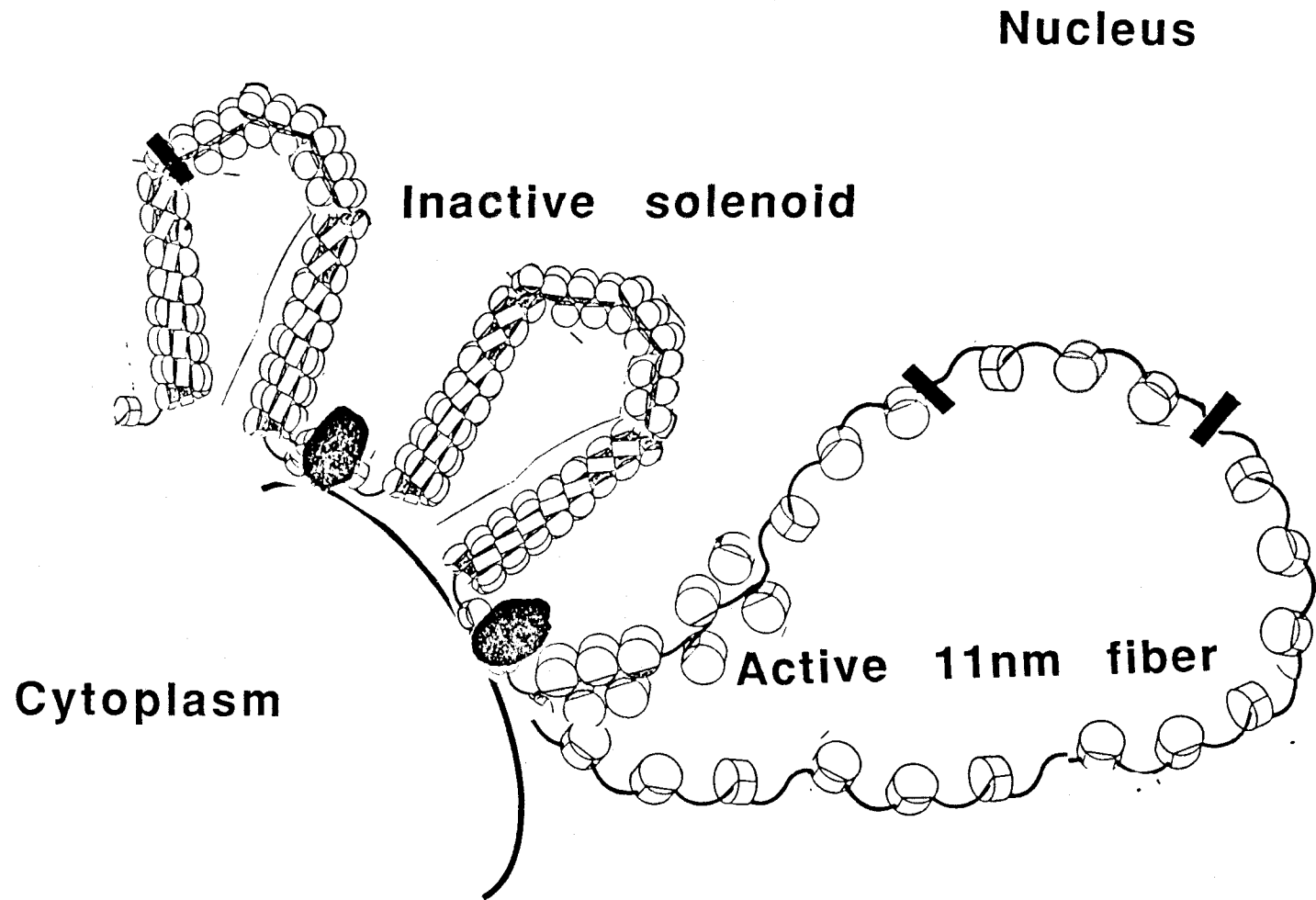


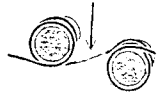
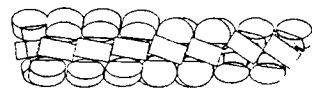


Figure VII.8. The tabulated probabilities of finding the dye molecules bound within different folded structures within the interphase nucleus. The biological function of each of the structures is indicated. P is the calculated probability of finding the dye in various folded chromatin forms. F is the fraction total interphase DNA which is in the pictured form. K is the intrinsic binding constant and the dye to the particular nucleic acid form.

Figure VII.8

form	function	$(m^{-1})K$	f	p
Free DNA				
	Not found in eucaryotes	1.1×10^6	—	
Core particle				
	<ol style="list-style-type: none"> 1. Associated with active 11nm fiber 2. Associated with inactive 30nm fiber 	2.2×10^4	.027	.015
Linker DNA				
	<ol style="list-style-type: none"> 1. Free in active 11nm fiber 2. Bound in solenoid in 30nm fiber 	9.3×10^5	.073	.155
Solenoid				
	Inactive 30nm fiber form	3.0×10^4	.90	.83

BIBLIOGRAPHY

- Abraham, R.J., Loftus, P., Proton and Carbon-13 NMR Spectroscopy: An Integrated Approach, Heyden and Sons, 1979.
- Abraham, J., Feidman, J., Nasmyth, K.A., Strathern, J.N., Klar, A.J., Broach, J.R., Hicks, J.B., 1983, Cold Spring Harbor Symp. Quant. Biol., 47, 989-996.
- Akasaka, K., Yamada, A., Hatano, H., 1975, FEBS Lett., 53, 339-341.
- Albright, S.C., Wiseman, J.M., Lange, R.A., Garrard, W.T., 1980, J. Biol. Chem. 255, 3673-3684.
- Alewood, Kazmaier, Rank, 1973, J. Am. Chem. Soc., 95, 5466.
- Angerer, L.M., Moudrianakis, E.N., 1972, J. Mol. Biol., 63, 505-521.
- Angerer, L.M., Georghion, S., Moudrianakis, E.N., 1974, Biochem., 13, 1075-1082.
- Angerer, L.M., Georghiou, S. and Moudrianakis, E.N., 1972, J. Mol. Biol., 63, 505.
- Arnott, S., Selsing, E., 1974, J. Mol. Biol., 509-521.
- Arnott, S., Bond, R., 1980, Nature, 287, 561-563.
- Arnott, S., Chandrasekaran, R., Selsing, E., Structure and Conformation of Nucleic Acids and Proteins-Nucleic Acid Interactions, 1975, University Park Press, Baltimore, MD, 577-4.
- Ausio, J., Seeger, D., Eisenberg, H., 1984, J. Mol. Biol., 176, 77-104.
- Ausio, J. and van Holde, K.E., 1985, Biochemistry,
- Ausio, J., Ramakrishnen, S. and Fasman, G.D., 1986, Biochemistry, 25, 1981-1988.
- Baase, W.A., Johnson, C.W. Jr., 1979, Nucleic Acids Res., 6, 797.
- Bak, P., Bak, A.L., Zeuthen, J., 1979, Chromosoma, 73, 301-315.
- Bakayev, V.V., Bakayeva, T.G. and Varshavsky, A.J., 1976, Cell, 11, 619-629.
- Bates, D.L., Thomas, J.O., 1981, Nuc. Acids Res., 9, 5883.
- Bauer, W.R., Vinograd, J., 1968, J. Mol. Biol., 33, 141-171.

- Bauer, W. and Vinograd, J., 1970, *J. Mol. Biol.* 47, 419.
- Bauer, W.R., 1978, *Ann. Rev. Biophys. Bioeng.*, 7, 287-313.
- Beaudette, N.V., Fulmer, A.W., Okabayshi, H., Fasman, G.D., 1981, *Biochemistry*, 20, 6526-6535.
- Bejayati, C. and Warcel, A., 1976, *Cell*, 9, 393-407.
- Benezra, R., Cantor, C.R. & Axel, R., 1986, *Cell* 44, 697-704.
- Bentley, G.A., Lewit-Bentley, A., Finch, J.T., Podjarny, A.D., Roth, M., 1984, *J. Mol. Biol.*, 176, 55-76.
- Berezney, R. and Coffey, D.S., 1977, *J. Cell. Biol.*, 73, 616-637.
- Berry, S. in *Nitrenes* (W. Luorski, ed.), John Wiley & Sons, New York, p. (1970).
- Birnie, G.D., 1972, Subcellular Components Preparation and Fractionation, Butterworths, London.
- Blake, A. and Peacocke, A.R., 1968, *Biopolymers*, 6, 1225.
- Bloomfield, V.A., Crothers, D.M., Tinoco, I., Jr., "Physical Chemistry of Nucleic Acids", Chap. 7, Harper and Row, New York, 1974.
- Bodner, J.W., Jones, C.J., Coombs, D.H., Pearson, G.D., Ward, D.C., 1983, *Mol. Cell. Biol.*, 3, 1567-1579.
- Bolton, P.H. and Kearns, D.R., 1978, *Nucleic Acids Res.* 5(12), 4891.
- Bolton, P.H., James, T.L., 1979, *J. Phys. Chem.*, 83, 26, 3359-3366.
- Bonner, J. Dahmus, M.E. Fambrough, D., Huang, R.C., Marishuge, K., Tuan, D.Y.H., 1969, *Science*, 159, 47-56.
- Bonner, J., Chalkley, G.R., Dahmus, M.E., Fambrough, D., Fujimura, F., Huang, R.C., Huberman, J., Jensen, R., Marishuge, K., Ohlenbusch, H., Ohuera, B., and Widohm, J., Methods in Enzymology, "Isolation and Characterization of Chromosomal Nucleoprotein", 1213, 3-64, 1968.
- Bonner, J.T. and Stedman, J.D., 1979, *Proc. Natl. Acad. Sci.*, 76, 190-194.
- Bradley, D.F. and Wolf, M.K., 1969, *Proc. Natl. Acad. Sci. USA*, 45, 944.
- Bresloff, J. and Crothers, D.M., 1975, *J. Mol. Biol.*, 95, 103.
- Brown, P.E., 1970, *Biochem. Biophys. Acta*, 213, 282.

- Burlingame, R.W., Love, W.E., Wang, B-C., Hamlin, R., Xuong, N.H. and Moudrianakis, E.N., 1985, *Science*, 228, 546-553.
- Burton, D.R., and Reimarsson, R., *FEBS Lett.*, 1978, 89, 183-186.
- Bush, C.A., "U. V. Spectroscopy, C. D., and ORD." Basic Principles in Nucleic Acid Chemistry, 1974, Academic Press, New York.
- Cary, P.T., Moss, T., and Bradbury, E.M., 1978, *Eur. J. Biochem.*, 89, 475-482.
- Camerini-Otero, R.D., and Felsenfeld, G., 1977, *Nuc. Acids Res.*, 4, 1159-81.
- Campbell, A.M., Cotter, R.D., and Pardon, J.F., 1978, *Nuc. Acids Res.*, 5, 1571-1580.
- Cannon, B., Polnaszek, C.F., Butler, K.W., Erikson, L.C.G. and Smith, L., 1975, *Arch. Biochem. Biophys.*, 167, 505.
- Cantor, C.R., Schimmel, P.R., Biophysical Chemistry Part II: Techniques for the Study of Biological Structure and Function, W.H. Freeman, 1980, San Francisco.
- Cartwright, I.L., Hertzberg, R.P., Dervan, P.B., and Elgin, S.C.R., 1983, *Proc. Natl. Acad. Sci. USA*, 80, 3213-3217.
- Chaires, J.B., Dattagupta, N., and Crothers, D.M., 1982, *Biochemistry*, 21, 3927-3932.
- Chaires, J.B., Dattagupta, N., and Crothers, D.M., 1983, *Biochemistry*, 22, 284-292.
- Cheng, S.W., and Eisenfeld, J., "A direct computational method for estimating the parameters of a nonlinear model" in Applied Non-Linear Analysis, V. Lakshmikantham, Ed., Academic Press, 1979, New York, pp. 485-487.
- Church, G., Sussman, J.L., and Kim, Surg-Hiu, 1971, *Proc. Natl. Acad. Sci.*, 74, 1458-1462.
- Clore, G.M., and Gronenborn, A.M., 1984, *Eur. J. Biochem.*, 141, 119-129.
- Cotter, R.I., and Lilley, D.M.J., 1977, *FEBS Lett.*, 82, 63-68.
- Cotton, F.A., and Hazen, E.E., Jr., 1971, *The Enzymes*, 4, 153-75.
- Cotton, R.W. and Hamkalo, B.A., 1981, *Nucleic Acids Res.*, 9, 445-457.
- Cowman, M.K., and Fasman, G.D., 1978, *Proc. Natl. Acad. Sci. USA*, 75, 4759-4763.

- Coupppez, M., Sautiere, P., Brachmachari, S.K., Brahms, J., Liquiere, J., and Taillandier, E., 1980, *Biochemistry*, 19, 3358-63.
- Crick, F.H.C., and Klug, A., 1975, *Nature (London)*, 255, 530-533.
- Crothers, D.M., 1968, *Biopolymers*, 6, 525.
- Crothers, D.M., 1968, *Biopolymers*, 6, 575-584.
- Davidson, M.W., Lopp, I., Alexander, S. and Wilson, W.D., 1977, *Nucleic Acids Res.*, 4, 2696.
- Davidson, M.W., Griggs, B.G., Boykin, W.D. and Wilson, W.D., 1977, *J. Med. Chem.*, 20, 1117.
- Dechter, J.J., "NMR of Nuclides", in Advances in Inorganic Chemistry, Academic Press, 1982, New York, pp. 283-320.
- de Murcia, G., Mazen, A., Erard, M., Povyet, O., Champagne, M., 1980, *Nuc-Acids Res.*, 8, 767-779.
- Dickerson, R.E., 1983, *Scientific American*, 249, 94-111.
- DiMarco, F., Arcamone, F., Zunio, R., Cockran, J., and Hahn, F.H., 1975, in Mechanisms of Action of Antimicrobial and Antitumor Agents, Springer Verlag, Berlin.
- Dimicola, J.L., and Helene, C., 1974, *Biochemistry*, 13, 714, 724-730.
- Doenecke, D., 1977, *Eur. J. Biochem.*, 76, 355-363.
- Early, T.A., Olmstead, III, J., Kearns, D.R., and Lezuis, A.G., 1978, *Nucleic Acids Res.*, 5, 1955.
- Edelstein, S.J., 1975, *Ann. Rev. Biochemistry*, 44, 209-230.
- Edmondson, S.P. and Johnson, W.C. Jr., 1985, *Biopolymers*, 24, 825-841.
- Elgin, S.C.R., and Weintraub, H.A., 1975, Ann. Rev. Biochem., 44, 725-774.
- Englander, S.W., Downer, N.W., and Teitelbaum, H., 1972, *Ann. Rev. Biochemistry*, 41, 903-924.
- Erard, M., Das, G.C., de Murcia, G., Mazen, A., Pouyet, J., Champagne, M., and Daune, M., 1979, *Nucleic Acid Research*, 6, 3231-3253.
- Fahrney, D.E., and Gold, A.M., 1963, *J. Am. Chem. Soc.*, 85, 997.
- Fasman, G.D., "Circular Dichroism of DNA, Protein and Chromatin", Chromatin Structure and Function., NATO Adv. Studies Institute Series, Plenum Press, 1979, New York, pp. 68-108.

- Fazakerley, G.V., van der Marel, G.A., van Boom, J.H., and Guschlbauer, W., 1984, *Nucleic Acids Res.*, 21, 8269-8279.
- Feigon, J., and Kearns, D.R., 1979, *Nucleic Acids Res.*, 6, 2327-2336.
- Felsenfeld, G. and McGhee, J.D., 1986, *Cell*, 44, 375-377.
- Fenske, H., Eichorn, I., Böttger, M., and Lindigkeit, R., 1975, *Nucleic Acids Res.*, 2, 1975-1985.
- Finch, J.T. and Klug, A., 1976, *Proc. Natl. Acad. Sci.*, 73, 1897-1901.
- Finch, J.T., Lutter, L.C., Rhodes, D., Brown, R.S., Rushton, B., Levitt, M., and Klug, A., 1977, *Nature*, 269, 29-36.
- Fritzsche, H., Triebel, H., Chaires, J.B., Dattagupta, N. and Crothers, D.M., 1982, *Biochemistry*, 21, 3940-3946.
- Fuller, W. and Waring, M.J., 1964, *Ber. Bunsenges, Phys. Chem.*, 68, 805-808.
- Gabbey, E.J., Sanford, K., and Baxter, C.S., 1972, *Biochemistry*, 11, 3429-3433.
- Gabbey, E.J., Sanford, K., Baxter, C.S. and Kapicak, L., 1973, *Biochemistry*, 12, 4021-4026.
- Gelin, B.R. and Karplus, M., 1977, *Proc. Natl. Acad. Sci.*, 74, 801-805.
- Genest, D., Sabeur, G., Wahl, P., and Auchet, P., 1981, *Biophysical Chem.*, 13, 77-87.
- Genest, D., and Wahl, P., 1981, *Biochimie*, 63, 561-564.
- Girardet, J.L., and Lawrence, J.J., 1979, *Nuc. Acids Res.*, 7, 2419-2429.
- Godfrey, J.E., Eickbush, T.H., and Mondrianakis, E.N., 1980, *Biochemistry*, 19, 1339-1346.
- Goodwin, D.C., and Brahms, J., 1978, *Nuc. Acid. Res.*, 5, 835-50.
- Goodwin, D.C., Vergne, J., Brahms, J., Defer, N., and Kruh, J., 1979, *Biochemistry*, 18, 2057-64.
- Gorenstein, D.G., 1975, *J. Am. Chem. Soc.*, 97, 898-900.
- Gorenstein, D.G., Kar, D., 1975, *Biochem. Biophys. Res. Commun.*, 65, 1073-80.
- Gorenstein, D.G., Findlay, J.B., Morrii, R.K., Luxom, B.A., Kar, D., 1976, *Biochemistry*, 15, 3796-3803.

- Gorenstein, D.G. et al., 1976, J. Am. Chem. Soc., 98, 1688-73.
- Gorenstein, D.G., and Kar, D., 1977, J. Am. Chem. Soc., 99, 672-77.
- Gorenstein, D.G., 1981, Ann. Rev. Biophys. Bioerg., 10, 355-86.
- Gorenstein, G.D., Luxon, B.A., Goldfield, E.M., Lai, K., and Vegeais, D., 1982, Biochemistry, 21, 580-589.
- Graves, D.E., Yielding, L.W., Watkins, C.I. and Yielding, K.L., 1977, Biochim. Biophys. Acta 479, 98.
- Graves, D.E., Watkins, C.I. and Yielding, L.W., 1981, Biochemistry, 20, 1837.
- Graves, D.E., Watkins, C.I., and Yielding, L.W., 1981, Biochemistry, 20, 1887.
- Haasnoot, C.A.G., den Hartog, J.H.T., de Rooij, J.F.M., van Boom, J.H., and Altona, C., 1979, Nature, 281, 253-236.
- Haasnoot, A.G.C., den Hartog, J.H.J., de Rooij, J.F.M., van Boom, J.H., and Altona, C., 1980, Nucleic Acids Res., 8, 169-180.
- Hajduk, S.L., 1978, Progress in Molecular and Subcellular Biology, F.E. Hahn, H. Kersten, W. Kersten, W. Szybalski, eds. (Springer-Verlag, Berlin) pp. 158-200.
- Hamkalo, B.A. and Rattner, J.B., 1980, Q. Rev. Biol., 55, 409-417.
- Hanlon, S., Glonek, T., and Chan, A., 1976, Biochemistry, 15, 3869-75.
- Hawkins, F., in Experimental Chemotherapy, R.J. Schnitzer and F. Hawkins, eds., Academic Press, New York, p. 129.
- Helene, C., Dimicola, J.L. and Brun, F., 1971, Biochemistry 10, 3802-3807.
- Helene, C. and Lancelot, G., 1982, Prog. Biophys. Molec. Biol., 39, 1-68.
- Hertzberg, R.P. and Dervan, P.B., 1984, Biochemistry, 23, 3934-3945.
- Hewish, D.R., and Burgoyne, L.A., 1973, Biochem. Biophys. Res. Commun., 52, 504-510.
- Hogan, M., and Jardetzky, O., 1979, Proc. Natl. Acad. Sci. USA, 77, 169.
- Hogan, M., and Jardetcky, O., 1980, Biochemistry, 19, 2079.
- Hollandt, H., Notbohm, H., Riedel, F., and Herbers, E., 1979, Nuc. Acids Res., 6, 2017-2027.

- Horner, L., Christmann, A. and Gross, A., 1922, *Chem. Ber.* 55, 2450.
- Hurley, I., Osei-Gyimah, P., Archer, S., Scholes, C.P. and Lerman, L.S., 1982, *Biochemistry*, 21, 4999-5009.
- Igo-kemenes, T., and Zacheu, H.G., 1978, *Cold Spring Harbor Symp. Quant. Biol.*, 42, 109-118.
- Isenberg, I. and Dyson, R.D., 1969, *Biophys. J.*, 9, 1337-1350.
- Isenberg, I., 1973, *J. Chem. Phys.*, 59, 5696-5707.
- Isenberg, I., 1979, *Ann. Rev. Biochem.*, 46, 159-191.
- Isenberg, I. and Small, E.W., 1982, *J. Chem. Phys.*, 77, 2799-2805.
- Jain, S.C., Tsai, C. and Sobell, H.M., 1977, *J. Mol. Biol.*, 114, 317-332.
- Jain, S.C., Tsai, C. and Sobell, H.M., 1979, *J. Mol. Biol.*, 135, 813.
- Jones, R.L. and Wilson, W.D., 1980, *J. Am. Chem. Soc.*, 102, 7776.
- Jones, R.L., Lanier, A.C., Keel, R.A. and Wilson, W.D., 1980, *Nuc. Acids Res.*, 8, 1613-1624.
- Jones, R.L., Lanier, A., Keel, R.A. and Wilson, W.D., 1980, *Nucleic Acids Res.* 9, 197.
- Kallenbach, N.R., Appleby, D.W., and Bradley, C.H., 1978, *Nature*, 272, 134.
- Kapicak, L. and Gabbay, E.J., 1975, *J. Am. Chem. Soc.*, 97, 403-406.
- Karplus, M., and Pople, J.A., 1963, *J. Chem. Phys.*, 38, 2803-7.
- Kastrup, R.V., Young, M.A. and Krugh, T.R., 1978, *Biochemistry*, 17, 4855-4865.
- Kearns, D.R., 1977, *Ann. Rev. Biophys. and Bioengineering*, 6, 477-523.
- Kearns, D.R., 1984, *Critical Reviews in Biochemistry*, Vol. 15, #3, 237-290.
- Klevan, L., Armitage, I.M., and Crothers, D.M., 1979, *Nucleic Acids Res.*, 5, 139-160.
- Komaiko, W. and Felsenfeld, G., 1985, *Biochemistry*, 24, 1186-1193.
- Kovacic, R.T., and van Holde, K.E., 1977, *Biochemistry*, 16, 1490-1498.
- Krugh, T.R., and Graves, D.E., 1983, *Biochemistry*, 22, 3941-3947.

- Laemmli, U.K., 1970, *Nature*, 227, 680-685.
- Langaa, P., Delbarre, A., LePecq, J.B. and Rogries, B.P., 1983, *Eur. J. Biochem.*, 134, 163.
- Langmore, J.P. and Paulson, U.K., 1983, *J. Cell. Biol.*, 96, 1120-1131.
- Langmore, J.P. and Paulson, U.K., 1983, *J. Cell. Biol.*, 96, 1132-1137.
- Lapeyre, J.N. and Bekhor, I., 1974, *J. Mol. Biol.*, 69, 139.
- Laskey, R.A., and Ernshaw, W.C., 1970, *Nature*, 286, 763-767.
- Lawrence, J.L. and Louis, M., 1972, *Biochim. Biophys. Acta*, 272, 231.
- Lawrence, J., Chan, D.C.F., and Piette, L.H., 1976, *NAR*, 11, 2879-2893.
- Lebkowski, J.S. and Laemmli, U.K., 1982, *J. Mol. Biol.*, 156, 309-324.
- Lebkowski, J.S. and Laemmli, U.K., 1982, *J. Mol. Biol.*, 156, 325-344.
- LePecq, J.B., Paoletti, C., 1967, *J. Mol. Biol.*, 27, 87-106.
- Lerman, L.S., 1961, *J. Mol. Biol.*, 3, 18-30.
- Lerman, L.S., 1963, *Proc. Natl. Acad. Sci. USA*, 49, 94-102.
- Lerman, L.S., 1964, *Proc. Natl. Cancer Conf.*, 5, 39-43.
- Lewin, B., Gene Expression 2 , 1980, John Wiley and Sons, Inc., New York., pp. 428-430.
- Lewin, B., 1983, Genes, John Wiley and Sons, Inc., New York.
- Lewin, B., 1985, Genes II, John Wiley and Sons, Inc., New York.
- Levitt, M., 1978, *Proc. Natl. Acad. Sci. (USA)*, 75, 640-644.
- Lewis, C.D. and Laemmli, U.K., 1982, *Cell*, 29, 171-181.
- Levinger, L., Barsoum, J. and Varshavsky, A., 1981, *J. Mol. Biol.*, 146, 287-304.
- Levitt, M., 1976, *Proc. Natl. Acad. Sci.*, 5, 2233-2252.
- Libertini, L. and Small, E., 1980, *Nuc. Acids Res.*, 8, 3517-3534.
- Lilley, D.M., and Tatchell, K., 1977, *Nuc. Acids Res.*, 4, 2039-55.
- Lilley, D.M. and Pardon, J.F., 1979, *Ann. Rev. Genet.*, 13, 197-233.
- Lilley, D.M.J., Jacobs, M.F., and Houghton, M., 1979, *Nucleic Acids Res.*, 7, 377-399.

- Liu, L.F., and Wang, J.C., 1978, *Cell*, 15, 979-84.
- Luchnik, A.N., Bakayev, V.V., Zbarsky, I.B. and Gorgiev, G.P., 1962, *EMBO J.*, 1, 1353-1356.
- Lurquin, P.R. and Seligy, V.L., 1972, *Biochem. Biophys. Res. Comm.*, 46, 1399.
- Lurquin, P.F., 1972, *Chem-Biol. Inter.*, 8, 303-313.
- Lutter, L.C., 1978, *J. Mol. Biol.*, 124, 391-420.
- Lynch, 1970, *J. Bio. Chem.*, 245, 3911.
- Lwowski, W., Nitrenes, John Wiley & Sons, New York (1970).
- Maniatis, T., Jeffrey, A., and van de Sande, H., 1975, *Biochemistry*, 14, 3787.
- Maniatis, T., and Fritsch, E.F., Sambrook, J., *Molecular Cloning*, 1982, Cold Spring Harbor, N.Y.
- Maniatis, T., Jeffrey, A., and van de Sande, H., 1975, *Biochemistry* 17, 3787.
- Maniatis, T., Fritsch, F., Laner, J. and Lawn, 1980, *Ann. Rev. Genetics*, 14, 145-178.
- Manning, G.S., 1978, *Quart. Rev. Biophysics* II, 1, 179-246.
- Mariani, Y.H. and Wilson, W.D., 1979, *Biochem. Biophys. Res. Commun.*, 88, 861.
- Marmur, J. and Doty, P., 1961, *J. Mol. Biol.*, 5, 109-118.
- Marishuge, K. and Bonner, J., 1966, *J. Mol. Biol.*, 15, 160-174.
- Maxam, A., and Gilbert, W., 1980, *Methods Enzymology*, 65, 499-560.
- McCann, J., Cai, E., Yamasaki, E. and Ames, B.N., 1975, *Proc. Natl. Acad. Sci. USA*, 72, 979.
- McCarthy, M.P., Steffan, P.K., Maxwell, N.M., Benedict, R.C., Mondrianakis, E.N., and Ackers, G.K., 1984, *Biochemistry*, 23, 2227-2230.
- McCready, S.J., Jackson, D.A. and Cook, P.R., 1982, *Prog. Mut. Res.*, 5, 113-130.
- McGhee, J.D. and von Hippel, P.H., 1974, *J. Mol. Biol.*, 86, 469-489.
- McGhee, J.D., and Felsenfeld, G., 1979, *Proc. Natl. Acad. Sci. USA*, 76, 2133-2137.

- McGhee, J.D., Felsenfeld, G., and Eisenberg, H., 1980, *Biophys. J.*, 32, 261-270.
- McGhee, J.D., and Felsenfeld, G., 1980, *Nucleic Acids Res.*, 8, 2751-2769.
- McGhee, J.D., and Felsenfeld, G., 1980, *Ann. Rev. Biochem.*, 49, 115-56.
- McGhee, J.D., and Felsenfeld, G., 1982, *J. Mol. Biol.*, 158, 685-698.
- McGhee, J.D., Nickol, J.M., Felsenfeld, G., and Rau, D.C., 1983, *Cell*, 33, 831-841.
- McMurray, C.T., van Holde, K.E., Jones, R.T., and Wilson, W.D., 1985, *Biochemistry*, 24, 7037-7044.
- McMurray, C.T. and van Holde, K.E., 1986, *Proc. Natl. Acad. Sci. USA*, 83, 8472-8476.
- Meienhofer, J. and Antherton, E., 1977, Structure-Activity Relationships Among the Semisynthetic Antibiotics, D. Perlman, ed. (Academic Press, N.Y.) pp. 427-529.
- Miller, O.L. and Beatty, B.R., 1969, *Science*, 164, 955.
- Miller, M. R., in The Operon, M. R. Miller and W. Reznikoff, W., eds., Cold Spring Harbor Laboratory, 1979, New York.
- Mirzabekov, A.D., and Melnikova, A.F., 1974, *Mol. Biol. Rep. I*, 385-390.
- Mirzabekov, A.D., Shick, V.V., Belyavsky, A.V., and Bavykin, S.G., 1978, *Proc. Natl. Acad. Sci. USA*, 75, 4184-4188.
- Mirzabekov, A.D., and Rich, A., 1979, *Proc. Natl. Acad. Sci., USA*, 76, 1113-1121.
- Mirzabekov, A.D., 1980, *Quart. Rev. Biophys.*, 13, 2, 255-295.
- Müller, W., Crothers, D.M. and Waring, M.J., 1973, *Eur. J. Biochem.*, 39, 223.
- Müller, W., Crothers, D.M. and Waring, M.J., 1975, *Eur. J. Biochem.*, 54, 267-277.
- Murray, A.B. and Davies, H.S., 1979, *J. Cell. Sci.*, 35, 59-66.
- Nelson, E., Tewey, K., Liu, L., 1984, *Proc. Natl. Acad. Sci. USA*, 81, 1361-1365.
- Nelson, P., Albright, S.C., Wiseman, J.M. and Garrard, W.T., *J. Biol. Chem.*, 254, 11751-11760.

- Newton, B.A., 1974, Trypanosomiasis and Lev, CIBA Foundation Symposium 20 (Elsevier, Excerpta Medica, North Holland Associated Scientific Pub., Amsterdam, pp. 285-334.
- Nicola, N.A., Fulmer, A.W., Schwartz, A.M., and Fasman, G.D., 1978, *Biochemistry*, 17, 1779-1785.
- Noll, M., 1974, *Nucleic Acids Research*, 1, 1573-78.
- Noll, M., 1974, *Nature*, 251, 249-251.
- Noll, M., Thomas, J.O., Kornberg, R.D., 1975, *Science*, 167, 1203.
- Nordheim, A. and Rich, A., 1983, *Nature*, 303, 674-678.
- O'Farrell, P.H., 1975, *J. Biol. Chem.*, 250, 4007-40021.
- Olins, A.L. and Olins, D.E., 1974, *Science*, 183, 330-332.
- Olins, D.E., Olins, A., (Personal communication).
- Olins, A.L., Carlson, R.D., Wright, E.B. and Olins, D.E., 1976, *Nuc. Acids Res.*, 3, 3271-3291.
- Olmsted, J. and Kearns, D., 1977, *Biochemistry*, 16, 3647-3654.
- Orkin, S.H. and Kazazian, H.H., 1984, *Ann. Rev. Genetics*, 18, 131-171.
- Pabo and Suau, 1984, *Ann. Rev. Biochemistry*,
- Paoletti, J., Magee, B.B., and Magee, P.T., 1977, *Biochemistry*, 16, 351.
- Paton, A.E., Wikinson-Singley, G., and Olins, D.E., 1983, *J. Biol. Chem.*, 258, 13221-13229.
- Patel, D.J., Kozlowski, S.A., Marky, L.A., Rice, J.A., Broka, C., Dallas, K., and Itakura, K.J., 1982, *Biochemistry*, 21, 437.
- Patel, D.J., 1976, *Biopolymers*, 15, 523-558.
- Paulson, J.R. and Laemmli, U.K., 1977, *Cell*, 12, 817-828.
- Perry, M. and Chalkley, R., 1982, *J. Biol. Chem.*, 257, 7338-7347.
- Perutz, P., 1970, *Nature*, 228(6), 92-95.
- Perutz, P., 1978, *Scientific American*, 239(6), 92-99.
- Pettijohn, D.E. and Pfenning, O., 1980, *Proc. Natl. Acad. Sci. USA*, 77, 1331-34.

- Quadrifoglio, V., Crescenzi, V. and Giancotti, G., 1974, *Biophys. Chem.*, 2(1), 64-69.
- Quigley, G.J., Wang, A.H.J., Ughetto, G., van der Marel, G., van Boom, J.H. and Rich, A., 1980, *Proc. Natl. Acad. Sci. USA*, 77, 7204-7208.
- Rattner, J.B. and Hamkalo, B.A., 1978, *Chromosoma*, 69, 363-379.
- Record, T., Lohman, T.M. and deHaseth, P., 1976, *J. Mol. Biol.*, 107, 145-158.
- Record, T., Anderson, C.F. and Lohman, T.M., 1978, *Q. Rev. Biophysics* II, 2, 103-178.
- Record, T.M. and Lohman, M.T., 1980, *Biochemistry*, 20, 3120-3125.
- Reddy, B.S., Seshadri, T.P., Sakore, T.D. and Sobell, H.M., 1979, *J. Mol. Biol.*, 135, 787.
- Redfield, A.G., and Kunz, S.D., 1979, *NMR and Biochemistry*, S.J. Opella and P. Lu, eds., Marcel Dekker, New York, pp. 225-239.
- Reeves, R., 1984, *Biochim. Biophys. Acta*, 782, 343-393.
- Reid, B.R., and Hurd, R.E., Transfer RNA: Structure, Properties and Recognition, 1979, Cold Spring Harbor Laboratory, Cold Spring Harbor Monograph Series, P. Schimmel, D. Söll, and J. Abelson, eds.
- Rein, R., Shebata, M., Gardund-Juarez, and Kieber-Emmons, T., 1983, Structure and Dynamics: Nucleic Acids and Proteins, Eds. Enrico Clementi and Ramaswamy, H. Sarma, Adenine Press, N.Y.
- Reinhardt, C.G. and Krugh, T.R., 1978, *Biochemistry*, 17, 4845-4854.
- Remers, W.A., 1979, The Chemistry of Antitumor Antibiotics, Wiley and Sons, N.Y.
- Reynolds, W.F. and Gottesfeld, J.M., 1983, *Proc. Natl. Acad. Sci. USA*, 60, 1862-1866.
- Richmond, T.J., Finch, J.T., Rushton, B., Rhodes, D., and Klug, A., 1984, *Nature*, 311, 532-537.
- Rickwood, D., Centrifugation, 1978, Retrieval Information, Washington, D.C.
- Robinson, B.H., Lerman, L.S., Beth, A.H. Frisch, H.L., Dalton, L.R., and Auer, C., 1980, *J. Mol. Biol.*, 139, 19-44.
- Ryoji, M. and Worcel, A., 1984, *Cell*, 37, 21-34.

- Saucier, J.M., Feety, B. and LePecq, J.B., 1971, *Biochimie*, 53, 973.
- Scatchard, G., 1949, *Annals. of N.Y. Acad. of Sci.*, 51, 660.
- Schlessinger, F.B., Dattagupta, N. and Crothers, D.M., 1982, *Biochemistry*, 21, 664-669.
- Schmidt, K.S., 1982, *J. Theor. Biol.*, 98, 29-43.
- Sedat, J. and Manuelidis, L., 1978, *Cold Spring Harbor Symp. Quant. Bio.*, 42, 331-350.
- Shaw, B.R., Herman, T.M., Kovacic, R.T., Beaudreau, G.S., van Holde, K.E., 1976, *Proc. Natl. Acad. Sci. USA*, 73, 505-509.
- Shindo, H., 1980, *Biopolymers*, 19, 509-522.
- Shindo, H., McGhee, J.D., Cohen, J.S., 1980, *Biopolymers*, 19, 523-537.
- Siebenlist, U., 1979, *Nature*, 279, 651-653.
- Simpson, R.T., 1978, *Biochemistry*, 17, 5524-5531.
- Simpson, R.T., Shindo, H., 1979, *Nucleic Acids Res.*, 7, 481-492.
- Simpson, R.T., 1979, *J. Biol. Chem.*, 254, 10123-10127.
- Simpson, R.T. and Stafford, D.W., 1983, *Proc. Natl. Acad. Sci. USA*, 80, 51-55.
- Sinden, R.R., Carlson, J.O. and Pettijohn, D.E., 1980, *Cell* 21, 773-83.
- Small, E.W., and Isenberg, I., 1976, *Biopolymers*, 15, 1093-1101.
- Small, E.W., and Isenberg, I., 1977, *J. Chem. Phys.*, 66, 3347-3351.
- Small, E.W., Libertini, L.J., and Isenberg, I., 1984, *Rev. Sci. Instrum.*, 55, 879-885.
- Smith, P. in Nitrenes (W. Luorski, ed.), John Wiley & Sons, New York, p. 106, 1970.
- Sobell, H.M., Tsai, C., Gelberg, S.G., Jain, S.C., and Sakore, T.D., 1976, *Proc. Natl. Acad. Sci. USA*, 73, 3068-3072.
- Sobell, H.M., Tsai, C., Jain, S.C., and Gilbert, S.G., 1977, *J. Mol. Biol.*, 114, 333-369.
- Sollner-Webb, B., Camerini-Otero, R.D., and Felsenfeld, G., 1976, *Cell*, 9, 179-194.

- Sakora, T.D., Reddy, B., and Sobell, H.M., 1977, *Proc. Natl. Acad. Sci. USA*, 74, 186.
- Sollner-Webb, B., Melchior, W.B. Jr., Felsenfeld, G., 1978, *Cell*, 14, 611-27.
- Stacks, P.C. and Schumaker, V.N., 1979, *Nucleic Acids Res.*, 7, 2457-2467.
- Stumph, W.E., Baez, M., Lawson, G.M., Tsai, M-J., and O'Malley, B.W., 1982, *U.C.L.A. Symp. Mol. Cell. Biol.*, 26, 87-104.
- Stumph, W.E., Baez, M., Beattie, W.G., Tsai, M-J., and O'Malley, B.W., 1983, *Biochemistry*, 22, 306-315.
- Suau, P., Bradbury, E.M. and Baldwin, J.P., 1979, *Eur. J. Biochem.*, 97, 593-602.
- Sundarlingham, M., 1969, *Biopolymers*, 7, 821-60.
- Sussman, J.L., and Trifanov, E.N., 1978, *Proc. Natl. Acad. Sci. USA*, 75, 3583-3587.
- Tatchell, K., 1977, Ph.D. Thesis, Oregon State University.
- Tatchell, K., and van Holde, K.E., 1978, *Proc. Natl. Acad. Sci. USA*, 75, 3583-3587.
- Terrance, W.G., Stone, M.P. and Krugh, T.R., 1985, *Biochemistry*, 24, 7462-7471.
- Theoligides, A., Yarbrow, J., and Kennedy, B.J., 1968, *Cancer*, 21, 16.
- Thoma, F., Koller, T.L. and Klug, A., 1979, *J. Cell. Biol.*, 83, 403-427.
- Thomas, G.J., Prescott, B., and Olins, D.E., 1977, *Science*, 197, 385-88.
- Thomas, J.O., and Burton, P.J.G., 1980, *J. Mol. Biol.*, 198, J. Mol. Biol., 144, 89-93.
- Thomas, J.C., and Schurr, 1983, *Biochemistry*, 22, 6194-6198.
- Todd, R.D., and Garrard, W.T., 1977, *J. Biol. Chem.*, 252, 4729-4738.
- Todd, R.D., and Garrard, W.T., 1978, *J. Biol. Chem.*, 254(8), 3074-3083.
- Tritton, T.F., and Lee, G., 1982, *Science*, 217, 248.
- Tsai, C., Jain, S.C., and Sobell, H.M., 1977, *J. Mol. Biol.*, 114, 301-315.

- Uberbacher, E.C., Ramakrishnan, V., Olins, D.E., and Bunick, G.J., 1983, *Biochemistry*, 22, 4916-4923.
- van Holde, K.E., Sahasrabudhe, C.G., and Shaw, B.R., 1974, *Nuc. Acids Res.*, 1, 1579-1586.
- van Holde, K.E., and Isenberg, I., 1975, *Acc. Chem. Res.* 8, 327-335.
- van Holde, K.E., and Weischet, W.O., 1978, *Biopolymers*, 17, 1382.
- van Holde, K.E., Allen, J.R., Tatchell, K., Weischet, W.O., and Lohr, D., 1980, *Biophys. J.*, 32, 271-282.
- van Wazen, Topics in Phosphorus Chemistry, Vol. 5, 1967.
- Varshavsky, A.J., Bakeyev, V.V., and Gorgiev, G.P., 1976, *Nuc. Acids Res.*, 3, 477-492.
- Varshavsky, A.J., Nedospasov, S.A., Schmatchenko, V.V., Bakeyev, V.V., Chumachov, P.M., and Gorgiev, G.P., 1977, *Nuc. Acids Res.*, 4, 3303-3325.
- Villponteau, B., Lundell, M., and Martinson, H., 1984, *Cell*, 39, 469-478.
- Wahl, P., Paoletti, J., and LePecq, J.B., 1970, *Proc. Natl. Acad. Sci. USA*, 65(2), 417.
- Wahl, P., Paoletti, J., and LePecq, J.B., 1980, *Proc. N. Acad. Sci. USA*, 65, 417-421.
- Walker, I.O., 1984, *Biochemistry*, 23, 5622-5628.
- Wang, J.C., 1974, *J. Mol. Biol.*, 89, 783.
- Wang, J., Hogan, M., and Austin, R.H., 1982, *Proc. Natl. Acad. Sci. USA*, 79, 5896-5900.
- Waring, M.J., 1970, *J. Mol. Biol.*, 54, 247-279.
- Waring, J.J., 1972, Molecular Basis for Antibiotic Action, E.F. Gale, E. Cundliffe, P.E. Reynolds, H.M. Richmond & Waring, M.J., eds., John Wiley & Sons, N.Y., pp. 173-277.
- Waring, M.J., 1981, *Ann. Rev. Biochem.*, 50, 159-191.
- Waring, M.J., 1982, in Molecular Basis for Antibiotic Action, Gale, E.F., Cundliffe, E., Reynolds, P.F., Richmond, M.H., and Waring, M.J., eds., pp. 173-277, John Wiley & Sons, London.
- Watanabe, K., Iso, K., 1981, *J. Mol. Biol.*, 151, 143-163.
- Weber, K., and Osborn, M., 1969, *J. Biol. Chem.*, 244, 4406-4412.

- Weintraub, H., and van Lente, F., 1974, *Proc. Natl. Acad. Sci.*, 71, 4249-4253.
- Weischet, W.O., Tatchell, K., van Holde, K.E., and Klump, H., 1978, *Nucleic Acids Res.*, 5, 139-160.
- Whitlock, J.P., and Simpson, R.T., 1976, *Biochemistry*, 15, 3307-3314.
- Whitlock, J.P., and Stein, A., 1978, *J. Bio. Chem.*, 253, 3857-61.
- Widom, J., and Klug, A., 1985, *Cell*, 43, 207-213.
- Williams, R.E., Lurquin, P.F., and Seligy, V.L., 1972, *Eur. J. Biochem.*, 29, 426.
- Wilson, W.D., and Lopp, I., 1979, *Biopolymers*, 18, 3025.
- Wilson, W.D., and Jones, R.L., 1980, *J. Am. Chem. Soc.*, 102, 7776.
- Wilson, W.D., and Jones, R.L., 1981, Advances in Pharmacology and Chemotherapy, Vol. 18, F. Hawking, ed., Academic Press, N.Y., pp. 117-222.
- Wilson, W.D., and Jones, L.R., 1982, *Nuc. Acids Res.*, 10, 1399-1410.
- Wilson, W.D., Keel, R.A., and Marian, Y.H., 1981, *J. Am. Chem. Soc.*, 103, 6267-6269.
- Wilson, W.D., and Jones, R.L., 1982, Intercalation Chemistry, M.S. Whittingham and A.J. Jacobsen, eds., Academic Press, New York, pp. 445-501.
- Wilson, W.D., Krishnamoorthy, C.R., Wang, Y.H. and Smith, J.C., 1985, *Biopolymers*, 1941-1961.
- Wilson, W.D., Wang, Y.H., Krishnamoorthy, C.R. and Smith, W.D., 1985, *Biochemistry*, 3991-3999.
- Winkle, S.A., Rosenberg, L.S., and Krugh, T.R., 1982, *NAR*, 10, 8211-8223.
- Wong, Y.P., Kearns, D.R., Reid, B.R., and Shulman, B.G., 1972, *J. Mol. Biol.*, 72, 725-740.
- Wray, W., Boulikas, T., Wray, V., and Hancock, P., 1981, *Anal. Biochem.*, 118, 197-203.
- Wu, H., Dattagupth, Hogan, M., and Crothers, D.M., 1980, *Biochemistry*, 19, 626-634.
- Yager, T.D., McMurray, C.T., Ramakrishnan, V. and van Holde, K.E., 1987, *Biochemistry*, submitted.